Discovery and Characterization of Ultracool Dwarfs in Large Scale Surveys

April 2013

ZengHua Zhang

A report submitted to the University of Hertfordshire in partial fulfilment of the requirements of the degree of Doctor of Philosophy

Abstract

Ultracool dwarfs including the lowest mass stars and substellar dwarfs (or brown dwarfs) is a rapidly evolving and very active field. In this thesis I present the discovery and characterization of ultracool dwarfs and their binary systems with solar and subsolar abundances and try to answer a few scientific questions related to these ultracool objects.

I use different techniques based on photometric and astrometric data of modern large scale surveys to identify ultracool dwarfs and their binaries. I identify around 1000 ultracool dwarfs from SDSS, 2MASS and UKIDSS surveys, including 82 L dwarfs and 129 L dwarf candidates (Chapter 2 and 4). This work largely increases the known number of ultracool dwarfs and aid the statistic study of these objects. Eighteen ultracool dwarfs in my sample are found to be in wide binary systems by common proper motion (Chapter 4 and 5). Wide binary systems are often used to test formation theories of low mass stars and brown dwarfs, which have different predictions of separations and binary fractions. One of these binary systems is the first L dwarf companion to a giant star η Cancri. The η Cancri B is clearly a useful benchmark object, with constrained distance, age, and metallicity. Further more, the L3.5 dwarf companion η Cancri B is found to be a potential L4 + T4 binary.

I focus on the studies of low mass stars and brown dwarfs with subsolar abundance referred as red and ultracool subdwarfs. They belong to the older Population II of the Galactic halo contain more information of the formation, early evolution and structure of the Milky Way. Using the most extensive optical survey, the Sloan Digital Sky Survey (SDSS), to select low mass stars with subsolar abundance, referred as red subdwarfs with spectral types of late K and M. I identify about 1800 M subdwarfs including 30 new $\geq$M6 subdwarfs and five M ultra subdwarfs with very high gravity as well as 14 carbon enhanced red subdwarfs. I also identify 45 red subdwarf binary systems from my red subdwarf sample. Thirty of them are in wide binary systems identified by common proper motion. Fifteen binaries are partially resolved in SDSS and UKIDSS. I estimate the M subdwarf binary fraction. I fit the relationships of spectral types and absolute magnitudes of optical and near infrared bands for M and L subdwarfs. I also measure UVW space velocities of the my M subdwarf sample (Chapter 5).

Our studies of the lowest mass stars and brown dwarfs of the Galactic halo are limited by the lack of known objects. There are only seven L subdwarfs published in the literature. I search for ultracool subdwarfs by a combine use of the most extensive optical and near infrared surveys, the SDSS and the UKIRT Infrared Deep Sky Survey. I identify three new L subdwarfs with spectral types of sdL3, sdL7 and esdL6. I re-examine the spectral types and metal classes of all known L subdwarfs and propose to use 2.3 μm CO line as an indicator of L subdwarfs. Two of my new L subdwarfs are found to be candidates of halo brown dwarfs (or substellar subdwarfs). I find four of these known ten L subdwarfs could be halo brown dwarfs. I propose a new name "purple dwarf" for lowest-mass stars and brown dwarfs with subsolar abundance (Chapter 3).

Finally I summarize and discuss the thesis project in Chapter 6 and describe future research plans in Chapter 7.

Acknowledgements

I would like to extend a thank you to all the people who have provided help and support throughout my Ph.D. no matter how large or small, your help was always appreciated.

I firstly need to thank my supervisors for their constant support and help with every aspect of the Ph.D, for their patience and understanding and for teaching me the knowledge and skills needed to succeed. Prof. David Pinfield is a kind and reliable supervisor. When ever I have problems to solve or hard decision to make related to my research, I would go to talk with him, and he always give very useful comments based on his wisdom and wide knowledge. I would thank my supervisor Prof. Hugh Jones, who had guided my research since 2006 when I was a MSc student and is also lighting my future research career. He has the capability to raise curiosity of young researcher and encourage them to carry on their research. My research projects would not be going so well without help from Dr. Ben Burningham who is a talented and experienced researcher. I also thank my supervision team for their respect to my research interests and help me to find and conduct the most interested research projects to me.

I could also not have done this Ph.D. without the support, both emotionally and financially from all of my parents Sheng Ming ZHANG and Xu Cun YIN. I would also like to thank my extended family, particularly my uncle Gen Yang DONG and aunt Ai Xin YIN, for their support.

I would like to thank the Ph.D. candidate interview panel of the Centre for Astrophysics Research for offering me a position in 2008.

I would also like to thank my fellow students, postdocs and staff of the Centre for Astrophysics Research for their help and support. I owe many thanks to Prof. James Hough and Prof. Janet Drew, the director of the Centre for Astrophysics Research before and after 2010 for their signatures on my claim forms and reference letters. A particular thank you to Dr. Mark Thompson who was my progression examiner and agreed to be the internal examiner of my viva. I would also like to thank Dr. Nicolas Lodieu from the Instituto de Astrofísica de Canarias who agreed to be my external examiner.

I also thank these young astronomers who reside and ever resided at 13 Horsa Gardens. I had a lot of good times together with these housemates from 2009 to 2012. They are Roberto Riddi, Kieran Forde, Hugo Ledo, Federico Marocco and Hywel Farnhill. All of them will be honored the title of "Dr." soon.

I would like to take this opportunity to thank my M.Sc. supervisors. I would not have started my Ph.D. without their help and support during my M.Sc. study. They are Prof. Zhanwen Han and Dr. Richard Pokorny from the Yunnan Astronomical Observatory of the Chinese Academy of Sciences.

Thank You to you all!

Contents

List of Figures

List of Tables

Chapter 1

Background

This chapter describe the background knowledge relevant to the later chapters. In brief the main topics here include an introduction of brown dwarfs and ultracool dwarfs, followed by introduction of properties of ultracool dwarfs with solar to sub-solar metallicity. Then I introduce the observational techniques for ultracool dwarfs and their binaries and major science topics related to ultracool dwarfs. I describe the motivation of the thesis in the end.

1.1 Introduction

The Hertzsprung-Russell Diagram (HRD; Figure 1.1) is a scatter graph of stars showing the relationship between the absolute magnitudes or luminosities of stars versus their spectral types or effective temperatures. It was created a century ago (Hertzsprung 1911; Russell 1913) is the most important diagram in stellar astronomy. It is a guide map of stellar populations and stellar evolutions. I was fascinated by two special populations, subdwarfs and substellar dwarfs which are the oldest and newest populations in the HRD respectively.

The subdwarf population was discovered because they appears less luminous than the stellar main sequence in the HRD (Kuiper 1939). Subdwarfs normally referred as cool subdwarfs to distinguish from hot subdwarfs. These objects are in fact not sub-luminous but rather hotter than equivalent-mass main sequence dwarfs, a consequence of their reduced metal opacity (Chamberlain & Aller 1951; Sandage & Eggen 1959) thus have bluer colours (Burgasser et al. 2003a). The discovery of cool subdwarfs also represents

the discovery of the second generation stars (Population II; Baade 1944). These objects associated with the Galactic spheroid are presumably relics of the early Galaxy, with ages of 10-15 Gyr. Cool subdwarfs were formed during the early stage of the Galaxy and have much less heavy elements (Roman 1950; Roman 1952; Roman 1954) than Population I stars (or the 3rd generation stars; e.g. the Sun) and are important tracers of early Galaxy. Understanding the first generations of stellar formation, Galactic chemical history and ultracool metal-poor atmospheres become the driving forces to discover extreme metal-poor and ultracool subdwarfs.

The substellar dwarf population is the newest population predicted by Kumar (1963a) and discovered by Rebolo, Zapatero Osorio & Martín (1995) firstly. Substellar dwarfs normally referred as brown dwarfs (BDs; Section 1.1.1) are substellar mass objects with masses between lowest mass stars and most massive planets. Massive BDs have similar properties to lowest mass stars while cool BDs are similar to gaseous planets. BDs appear at the low temperature and low luminosity corner on the HRD. BDs contribute very little of their mass into the interstellar medium and never even have a period of substantive hydrogen burning, the material from which they formed is never further enriched. BDs represent fossilized records of star formation at all Galactic epochs and preserve information on Galactic metallicity enrichment at the time of their births. However, most of the known BDs are in the Galactic disk younger than a few Gyr (Figure 1.19). Only one BD of the Galactic halo ($>$ 10 Gyr) is published in the literature (Burgasser et al. 2003a). BDs show what ultracool atmospheres look like. However, metal-poor ultracool atmospheres have not been well studied. We still do not know what halo BDs look like. Halo BDs are rare and faint. We don't know if we can find a sample of halo BDs with different temperatures and metallicities even with current most extensive optical and near infrared (NIR) large scale surveys. The halo substellar MF has not been studied due to the lack of known halo brown dwarfs (see Section 1.3).

Ultracool atmospheric models (Section 1.2.3) for lowest mass stars and BDs have been established but have not been well calibrated particular in the low metallicity region. Luminosities and effective temperatures ($T_{\rm eff}$) predicted from atmospheric and evolutionary do not agree with each other. Thus benchmark BDs are needed to test both atmospheric and evolutionary models (Section 1.2.4). Measurements of substellar MF rely on well calibrated atmospheric and evolutionary models. Meanwhile, since BDs are evolving throughout their life time thus their luminosities depends on both masses and ages, so reliable theoretical models are needed to convert from a substellar luminosity function to

a MF. The key for all these problems would be to identify a sample of lowest mass stars and BDs, particular BD binary systems which can be used as benchmarks to calibrate models. More and more solar abundance BD benchmarks are being discovered. But we still don't know if we can we find halo BD binaries with current sky surveys. Without examples of lowest mass stars and BDs of the halo, the binary fraction can not be measured and thus we lack information about star formation at low masses and metallicities.

This thesis is concerned with the identification, and subsequent analysis and follow-up of a substantial new populations of lowest mass stars and BDs and their binaries. I focused on the identification of lowest mass stars and BDs of solar and subsolar abundances during the first and the second half of the programme respectively. I identify these populations in searches of new and existing large astronomical databases including 2MASS, SDSS, UKIDSS and VISTA (see Section 1.4.3), in ways that combine the sensitivities/capabilities of these surveys. A variety of criteria are assessed while implementing selections, including optical-infrared colours, proper motions, and spectroscopy. Additional follow-up observations also form part of the process of confirmation and initial characterization of new objects, using deeper photometry and spectroscopy.

1.1.1 Brown dwarfs

Numerical simulations show that low mass stars with $M < 0.1\ M_{\odot}$ could form within a period much shorter than a Hubble time, and thus should exist. Stars having a mass less than a certain limiting mass (0.07-0.09 $M_{\odot}$, depending on different metallicity) will became degenerate objects or "black" dwarfs without going through the normal stellar evolution (Kumar 1963a). Hayashi & Nakano (1963) also found that the stars less massive than 0.08 $M_{\odot}$ will contract toward configurations of high electron-degeneracy without hydrogen burning. Tarter (1975) suggested to use the name "brown dwarfs" for these substellar objects and this has become widely accepted.

BDs occupy the mass range between the lowest mass stars and the highest mass planets. The central temperature of a BD is not high enough to achieve stable hydrogen burning like a main sequence star, but all BDs should have undergone short periods of primordial deuterium burning very early during their evolution. When the deuterium burning shuts down shortly after birth, BDs simply cool down throughout their life time. Spectral types of BDs gradually evolve though their life time as they cool. Warmer BDs have observational properties that overlap with the lowest mass stars, while cooler BDs

have atmospheric temperatures similar to giant planets. The minimum mass for stable hydrogen burning is $\sim 0.0744\ M_{\odot}$ for solar abundance ($Z = Z_{\odot}$ or $\log\ (Z/Z_{\odot}) = 0$ = [M/H], where $Z_{\odot} = 0.019$) according to theoretical models (Burrows et al. 2001). Chemical abundance is the second intrinsic property of BDs. Lower metallicity leads to smaller atmospheric opacities, which in turn produces shallower temperature gradients and higher luminosities, and correspondingly lower core temperature. Thus decreasing metallicity leads to increased minimum mass for hydrogen burning. Model predicted hydrogen burning minimum mass is $\sim 0.0835\ M_{\odot}$ for lower metallicity ($Z = 0.01\ Z_{\odot}$ or [M/H] $= -2$) and could be as high as $\sim 0.092\ M_{\odot}$ for zero metallicity (Burrows et al. 2001).

The minimum mass limit for deuterium burning is $\sim 0.012\ M_{\odot}$ or $\sim 13\ M_{\rm Jup}$ (for solar abundance) adopted as the distinction between the BD and giant planet. The distinction between BD and giant planet is in a debate based on the existence of young objects with masses of a few $M_{\rm Jup}$ isolated (Béjar et al. 2001) and wide binaries (Jayawardhana & Ivanov 2006). Formation scenarios are suggested to be used on the distinction of BDs and planets. Objects below hydrogen burning minimum mass formed either in systems or as isolated objects from the collapse of a cloud are BDs. In this case BDs could have mass less than the deuterium burning minimum mass. Objects formed in a protoplanetary disk around a parent stars, with a high mass ratio and enhanced average abundances of heavy elements are planets (e.g. Chabrier et al. 2005).

There are several brown dwarfs (BDs) formation scenarios been proposed based on numerical simulation. It is hard to say which scenario is dominating. Low-mass objects are difficult to form by gravitational fragmentation of unstable gas, as for masses in the BD region, a high density ($\gtrsim 10^{-16}$g cm^{-3}) is required for the gas to be Jeans unstable. Padoan & Nordlund (2004) and Hennebelle & Chabrier (2008) suggest that these high density cores can be formed by colliding flows in a turbulent magnetic medium. However, this model requires a large amount of turbulence, and has difficulty in explaining the binary properties of BDs. Additionally, the large number of brown-dwarf mass cores that the theory predicts have not been observed. Another way to reach the high densities required for the formation of BDs and low-mass stars is in gravitationally unstable discs (e.g. Whitworth & Stamatellos 2006; Whitworth et al. 2007; Stamatellos & Whitworth 2009). These discs form around newly born stars and grow quickly in mass by accreting material from the infalling envelope. They become unstable if the mass accreted onto them cannot efficiently redistribute its angular momentum outwards in order to accrete

onto the central star (Attwood et al. 2009). BDs are also thought to form as ejected embryos from star forming regions, i.e. as a by-product of the star formation process (e.g. Reipurth & Clarke 2001; Bate, Bonnell & Bromm 2003; Bate 2012). In this model BDs form the same way as low-mass stars, i.e. in collapsing molecular cores, but shortly after their formation they are ejected from their parental core and stop accreting any further material. Hence, they do not realise their potential to become hydrogen-burning stars. A hybrid scenario is also proposed for the formation of BDs and low mass stars (Basu & Vorobyov 2012). This model suggests gaseous clumps are ejected from protostellar disk during the early stage of evolution could form BDs. Whitworth & Zinnecker (2004) discussed the possibility that, in the vicinity of an OB stars, a prestellar core which would otherwise have formed an intermediate or low mass stas may form from a free floating BD or planetary mass object, because the outer layers of the core are eroded by the ionizing radiation from the OB star before they can accrete onto the protostar at the centre of the core. However, the effectiveness of photo-erosion also implies that that any intermediate-mass protostars which have formed in the vicinity of a group of OB stars must already have been well on the way to formation before the OB stars switched on their ionizing radiation; otherwise these protostars would have been stripped down to extremely low mass.

1.1.2 Ultracool dwarfs

It is difficult to distinguish lowest mass stars and massive BDs without knowing their ages. While spectral type is an observational parameter which is more directly related to effective temperature or luminosity thus is often used to name lowest mass stars and BDs, such as M dwarfs, L dwarfs, T dwarfs, Y dwarfs (e.g. Kirkpatrick 2005; Kirkpatrick et al. 2012).

Ultracool dwarf (UCD) was first used to describe stars with spectral type of $\leq$M7 by Kirkpatrick, Henry & Irwin (1997). The UCD population contains a mixture of low mass stars and brown dwarfs based on physical and observational characteristics. The spectral type versus mass relation (Kirkpatrick & McCarthy 1994; Baraffe & Chabrier 1996) and temperature versus mass relation (Mohanty, Jayawardhana & Basri 2004) suggests that objects at the theoretical brown dwarfs upper limit of 0.074-0.080 $M_{\odot}$ could have spectral types around M7 when young (e.g. young brown dwarfs in the Pleiades open cluster; Martin, Rebolo & Zapatero-Osorio 1996; Stauffer, Schultz & Kirkpatrick 1998). Dust

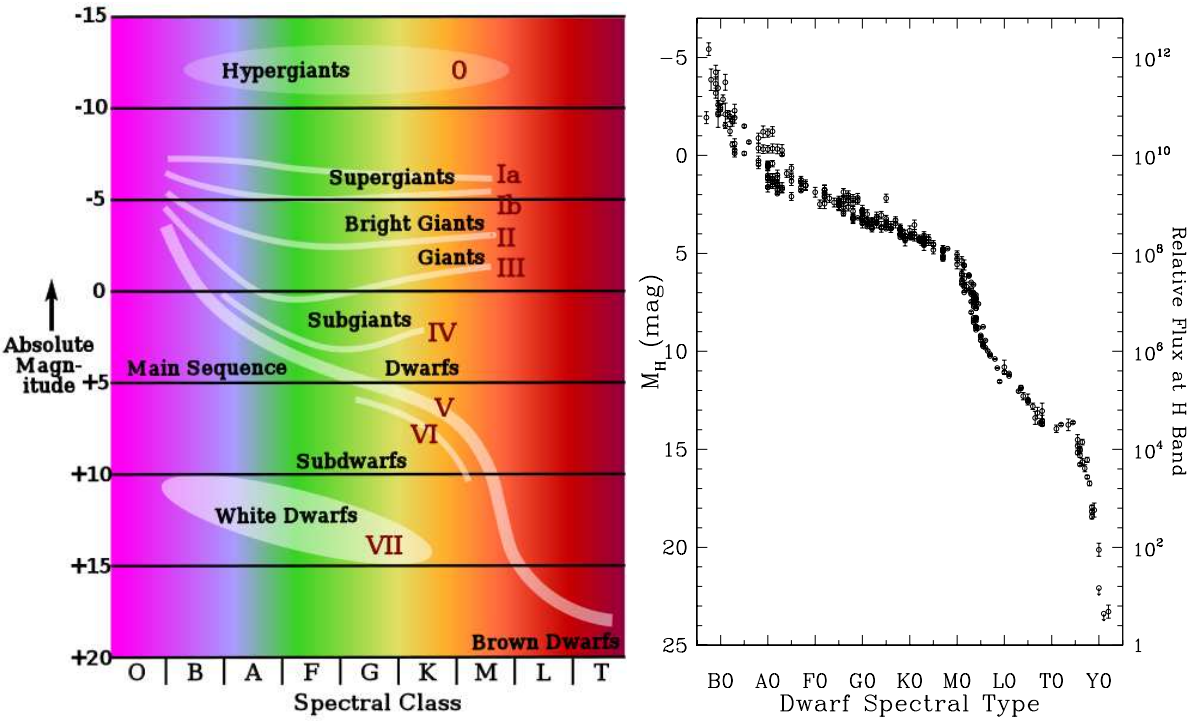

Figure 1.1: Hertzsprung-Russell diagrams. Brown dwarfs are located at the bottom-right corner. The figures are from http://commons.wikimedia.org/wiki/File:HR-diag-w-text.svg (left) and Kirkpatrick et al. (2012) (right).

starts to form in the atmosphere of M7 dwarfs (Jones & Tsuji 1997; Burrows & Sharp 1999) with effective temperature of ∼2800 K (Burrows et al. 2001) and is changing their spectral features away from warmer mid M dwarfs. UCDs have mass below $\sim 0.1\ M_{\odot}$, temperature below $\sim 2800\pm200$K (Burrows et al. 2001) and radius of $\sim 0.1\ R_{\odot}$ or $\sim R_{\rm Jup}$ (López-Morales 2007; Burrows, Heng & Nampaisarn 2011).

Cool subdwarfs with spectral types of late-type M and L are referred as ultracool subdwarfs (UCSDs) following the definition of UCDs, T type subdwarf has not been discovered so far. A UCSD is a UCD with strongly sub-solar abundance, or the halo counterpart of a disk UCD. To-date, about 70 late-type M type UCSDs have been discovered (Gizis 1997; Gizis & Harvin 2006; Schweitzer et al. 1999; Lépine, Shara & Rich 2003b; Lépine, Rich & Shara 2003; Lépine, Shara & Rich 2004; Lépine, Rich & Shara 2007; Lépine & Scholz 2008; Scholz et al. 2004; Scholz, Lodieu & McCaughrean 2004; Burgasser et al. 2003a; Burgasser 2004b; Burgasser & Kirkpatrick 2006; Burgasser, Cruz & Kirkpatrick 2007; Marshall 2008; Jao et al. 2008; Sivarani et al. 2009; Cushing et al. 2009; Lodieu et al. 2010; Lodieu et al. 2012c; Kirkpatrick et al. 2010).

1.2 Characteristics of UCDs and UCSDs

Low mass stars and BDs with solar abundance are cool dwarfs. Low mass stars and BDs with subsolar abundance ($Z \lesssim 0.13\ Z_{\odot}$ or [M/H] $\lesssim -0.9$) are cool subdwarfs. Cool dwarfs and cool subdwarfs are different observationally and kinematically. Cool dwarfs kinematically associated with the Galactic disk are the third generation objects and belong to the so-called Population I. Cool subdwarfs kinematically associated with the Galactic halo are the second generation of objects (Population II). The concept of stellar populations originated with Baade (1944). The Population I stars comprised the stars of the Galactic disk, whereas Population II included stars in the Galactic halo. Population II stars have high velocity and are substantially older than Population I stars. The connection between population II stars and metallicity was first made by Roman (1950); Roman (1952); Roman (1954), who showed that the the old, high-velocity Population II stars were also had weak metal lines. Figure 1.2 shows the structure and distribution of star populations in the Milky Way.

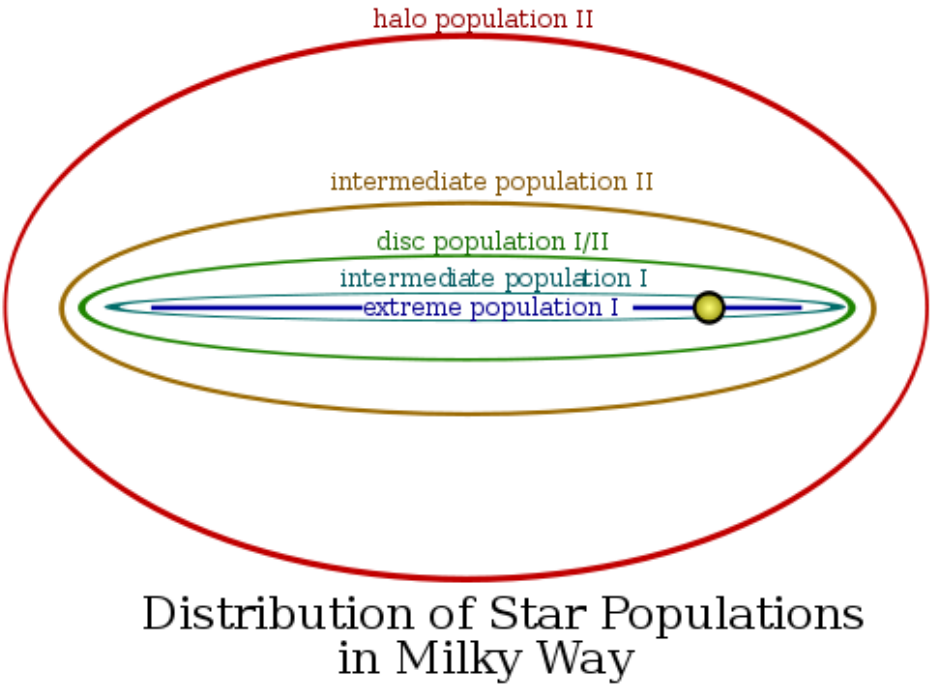

Figure 1.2: Distribution of star populations in the Milky Way (edge on). The population II is the halo. The thick disk are between intermediate population II and disc population I/II. The thin disk are the intermediate and extreme population I (e.g. Majewski 1993). A circle filled with yellow indicates the location of the Sun. The figure is from http://en.wikipedia.org/wiki/File:Starpop.svg.

1.2.1 Spectral types

As a BD ages and cools, the spectral energy distribution changes significantly. As the effective surface temperature ($T_{\rm eff}$) of a BD decreases its spectral type will evolve from late-type type M to L to T and Y. Figure 1.3 shows theoretical evolution tracks of luminosity and $T_{\rm eff}$ of low-mass stars and substellar objects (Burrows et al. 2001). In summary BDs start with $T_{\rm eff}$ around 3100-2600 K corresponding to late-type M dwarfs, whose spectra are dominated by metal oxide (TiO, VO) and metal hydride (CaH, MgH) absorption at optical wavelengths, and water bands in the NIR. When $T_{\rm eff}$ falls bellow $\sim$2500 K, silicate dust particles condense in the atmosphere, removing TiO and VO. Metal hydrides (MgH, CaH and FeH) and alkaline absorption lines (Na, K, Cs, and Rb) become the most prominent features in the optical and far-red wavelength and BDs become L dwarfs (Kirkpatrick et al. 1999b). Figure 1.4 shows optical spectra of M9, L3 and L8 dwarfs. As the $T_{\rm eff}$ cools below $\sim$ 1700 K, methane forms in the outer atmosphere, and becomes a prominent source of NIR absorption at $T_{\rm eff} \lesssim$ 1300 K, which corresponds to T type dwarfs (Burgasser et al. 2002). Figure 1.5 shows the 0.6 to 4.2 μm spectral sequence of M, L and T dwarfs. At $T_{\rm eff} \lesssim$ 500 K, ammonia (NH_3) becomes a prominent source of NIR absorption and the J band region suffers from a Wien tail collapse leading to redder $J-W2$ colours and the onset of the Y band spectral class (Cushing et al. 2011; Kirkpatrick et al. 2012).

Thus a late-type M dwarf could either be a very low mass star or a young BD. Early-type L dwarfs can be very old stars (e.g. $\sim$ 10 Gyr) or field brown dwarfs or very young planetary mass objects. Spectral types of very old BDs of the Galactic halo start from mid L type. A T or Y dwarf is could be either a BD or a planetary mass object depending on its age. BDs in open clusters are young and have spectral types of late-type M and mid L (Lodieu, Dobbie & Hambly 2011; Mužić et al. 2012; Alves de Oliveira et al. 2013). BDs in the Galactic disk have spectral types of L, T and Y. BDs in the Galactic halo have spectral types of $\gtrsim$esdL6 or $\gtrsim$sdL5 (Chapter 3).

M dwarfs

Kirkpatrick, Henry & McCarthy (1991) published the entire M dwarf sequence at red optical wavelength 6000 - 9000 Å and established spectral standards. Kirkpatrick et al. (1993) and Jones et al. (1994) published the first NIR spectral sequences of M dwarfs. Kirkpatrick et al. (2010) published an standard dwarf spectral sequence covers 0.7 to 2.5 μm wavelength for M dwarfs. The bottom panel of Figure 1.6 shows an optical spectral

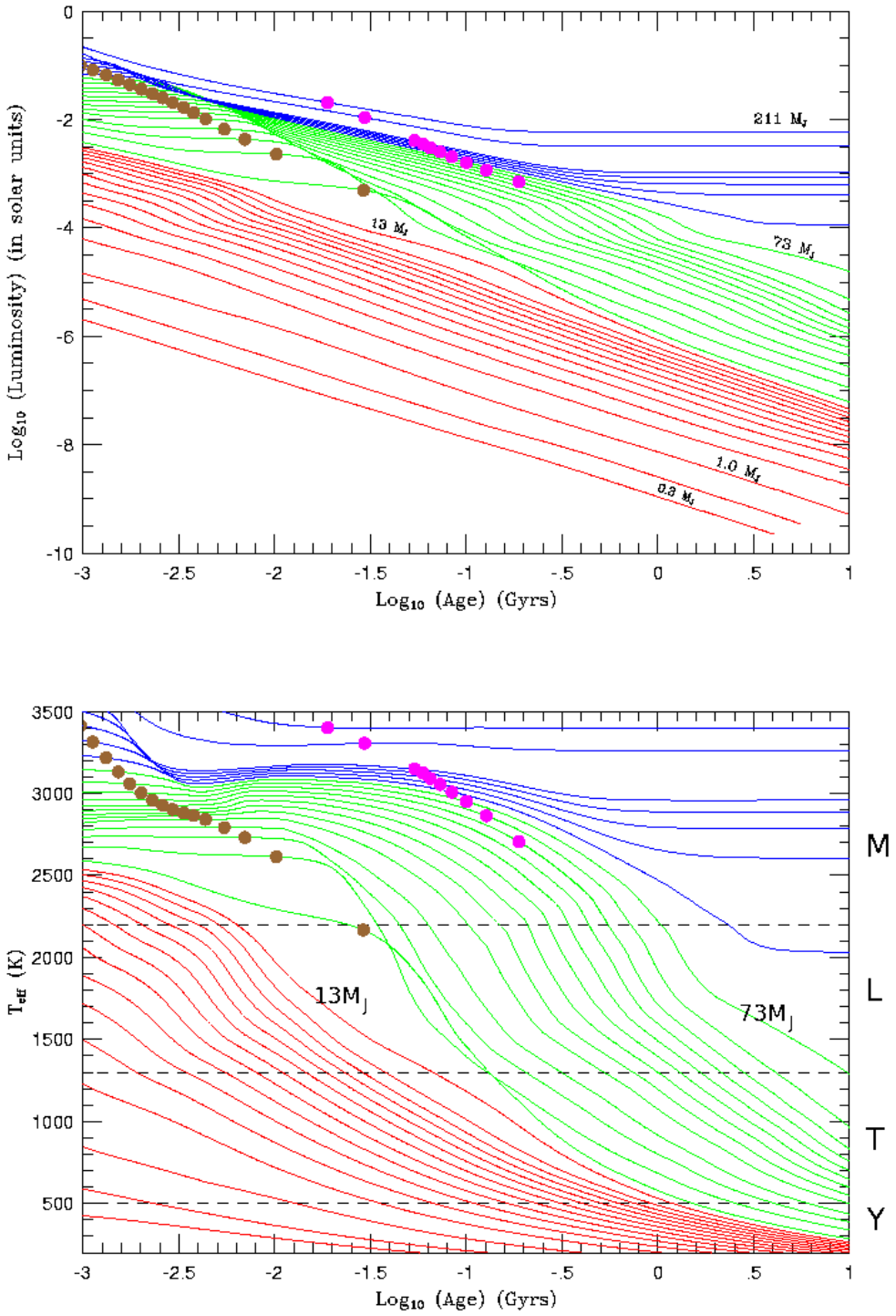

Figure 1.3: Evolution of the luminosity (top panel) and effective temperature (bottom panel) of isolated solar-metallicity red dwarf stars and substellar-mass objects versus age. Dots mark ages at which 50% of deuterium (gold) and lithium (magenta) have been burned via fusion. Approximate realms for the M, L, T and Y dwarfs are indicated with the dashed horizontal lines. Almost all brown dwarfs evolve from M to L to T spectral types. The figures are from Burrows et al. (2001).

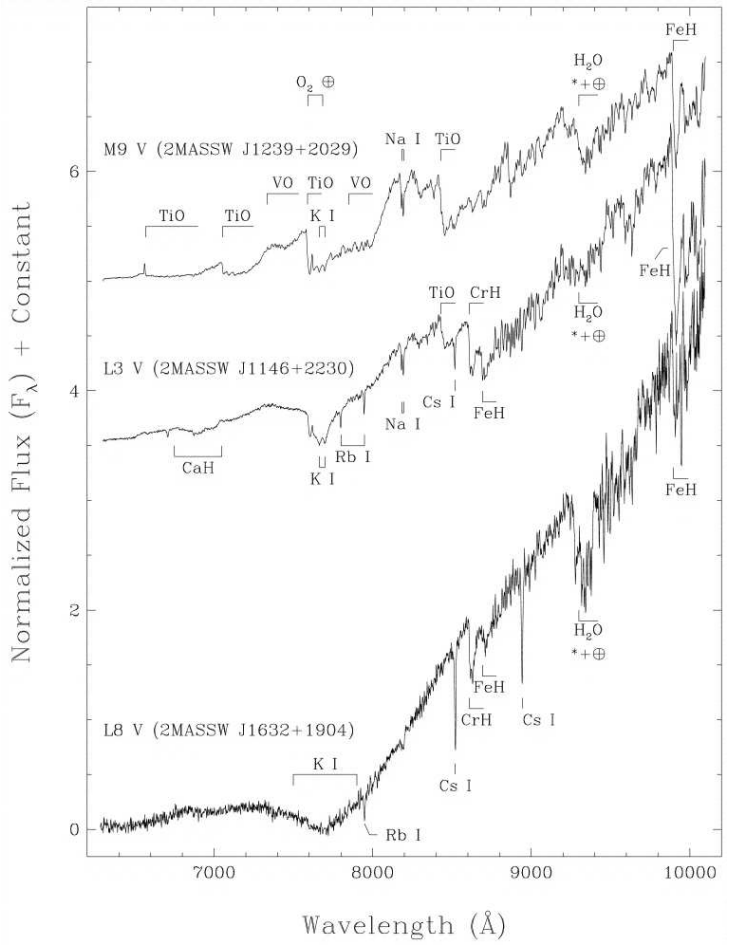

Figure 1.4: Spectra of M9, L3 and L8 dwarfs. The figure is from Kirkpatrick et al. (1999b).

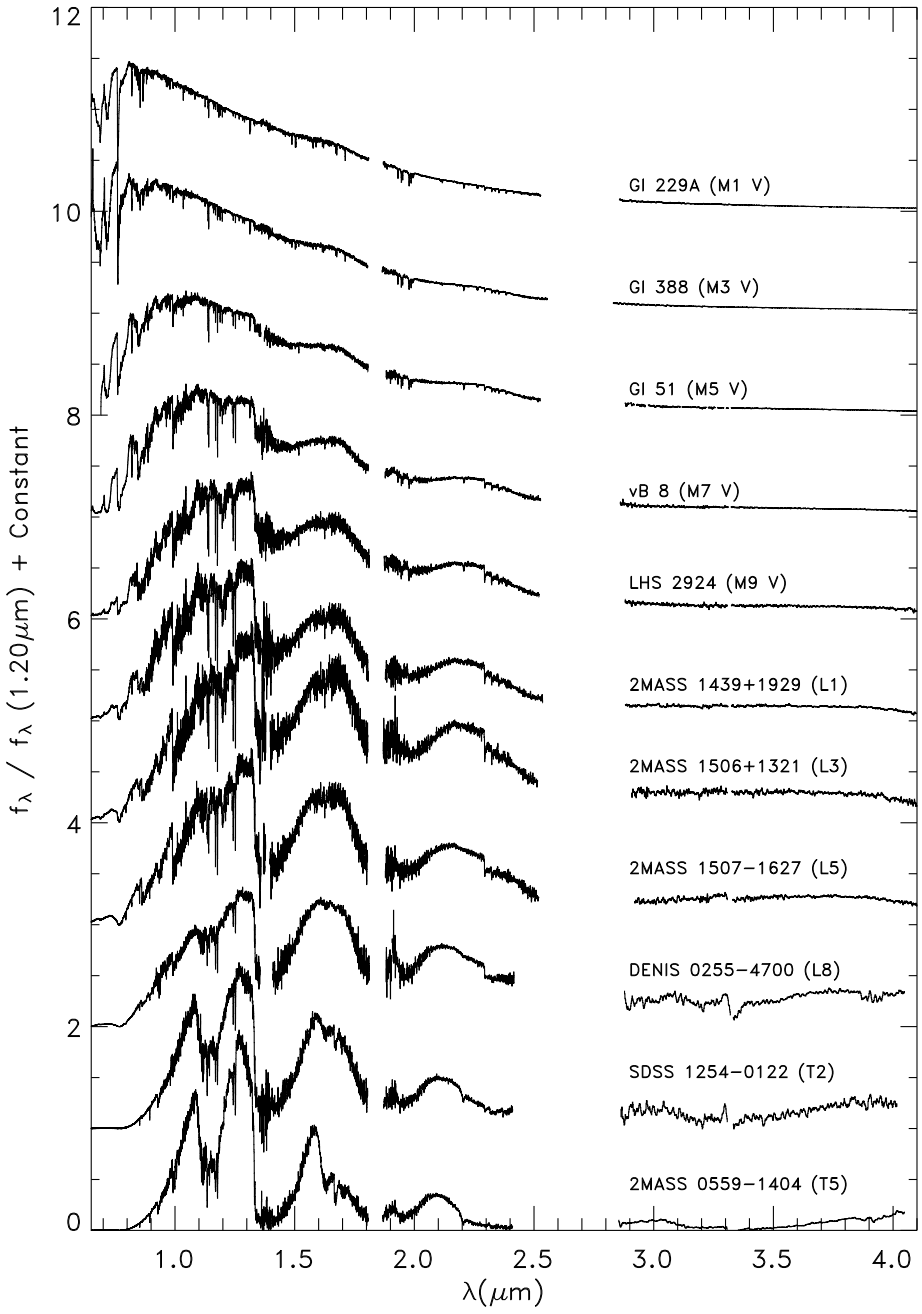

Figure 1.5: 0.6 to 4.2 μm spectral sequence of M, L and T dwarfs. In the optical wavelength, dwarfs become redder and redder from M to L to T types, while in the NIR wavelength, they become redder until late-type L types then become bluer from early-type T types. The figure is from Cushing, Rayner & Vacca (2005).

sequence of M dwarfs. Note that the TiO bands strengthen from M0 to M6, and the VO bands strengthen after M6. Top panel of Figure 1.6 shows a NIR standard sequence. The peak flux is shifting to longer wavelength from M0 to L0. Broad H_2O bands around 1.45 and 1.9 μm appeared and strengthen from M4.

Spectra of M dwarfs and subdwarfs are dominated by molecular absorption bands of metal oxides and hydrides. TiO and CaH near 7000Å are the most prominently bands (Bessell 1991). The ratio between the strength of the oxide and hydride bands is a metallicity diagnostic (Bessell 1982). Atmospheric models show that optical spectra of M subdwarfs are dramatically affected by metallicity variations. Thus low-resolution spectroscopy is sufficient for measuring effective temperature, metallicity and gravity effects (Allard & Hauschildt 1995). M dwarfs are generally associated with the Galactic disk population and show strong bands of TiO and CaH, while most M subdwarfs are kinematically associated with the Galactic halo and show relatively weaker TiO band and strong CaH bands.

M subdwarfs

M subdwarf classification is an fast developing field. The first M subdwarf classification system was established by Gizis (1997). M type dwarf stars are classify into three metal classes based on measurements of the four spectroscopic indices (CaH1, CaH2, CaH3 and TiO5) defined by Reid, Hawley & Gizis (1995). These three metal classes are M dwarf (dM), M subdwarf (sdM), and extreme subdwarf (esdM), and correspond to metallicity of [M/H] $\approx$0.0, –1.2$\pm$0.3, –2.0$\pm$0.5 respectively. Lépine, Rich & Shara (2007) revised the classification system and classified M type dwarf stars into four metal classes: dM, sdM, esdM and usdM for ultra subdwarf. But the metallicity range of each metal class was not mentioned. In this thesis, I assume [M/H] > -0.3 for dwarfs, $-0.3 \geq$ [M/H] > -0.9 for mild subdwarfs (or thick disk dwarfs), ≥ -0.9 [M/H] > -1.2 for subdwarfs, $-1.2 \geq$ [M/H] > -1.8 for extreme subdwarfs and $-1.8 \geq$ [M/H] for ultra subdwarfs under the four classes classification systems proposed by Lépine, Rich & Shara (2007). Figure 1.7 shows the new spectroscopic sequences of subdwarfs, extreme subdwarfs and ultra subdwarfs. Bottom panel of Figure 1.10 shows the spectral comparison of a normal M7 dwarf and an esdM7 subdwarf. The NIR band spectrum of the esdM7 is suppressed and the flux peaks at shorter wavelength compared to the M7 spectrum.

Apart from effective temperature and metallicity, a third parameter gravity also has effects on the spectra of M subdwarfs. It has not been considered in the current

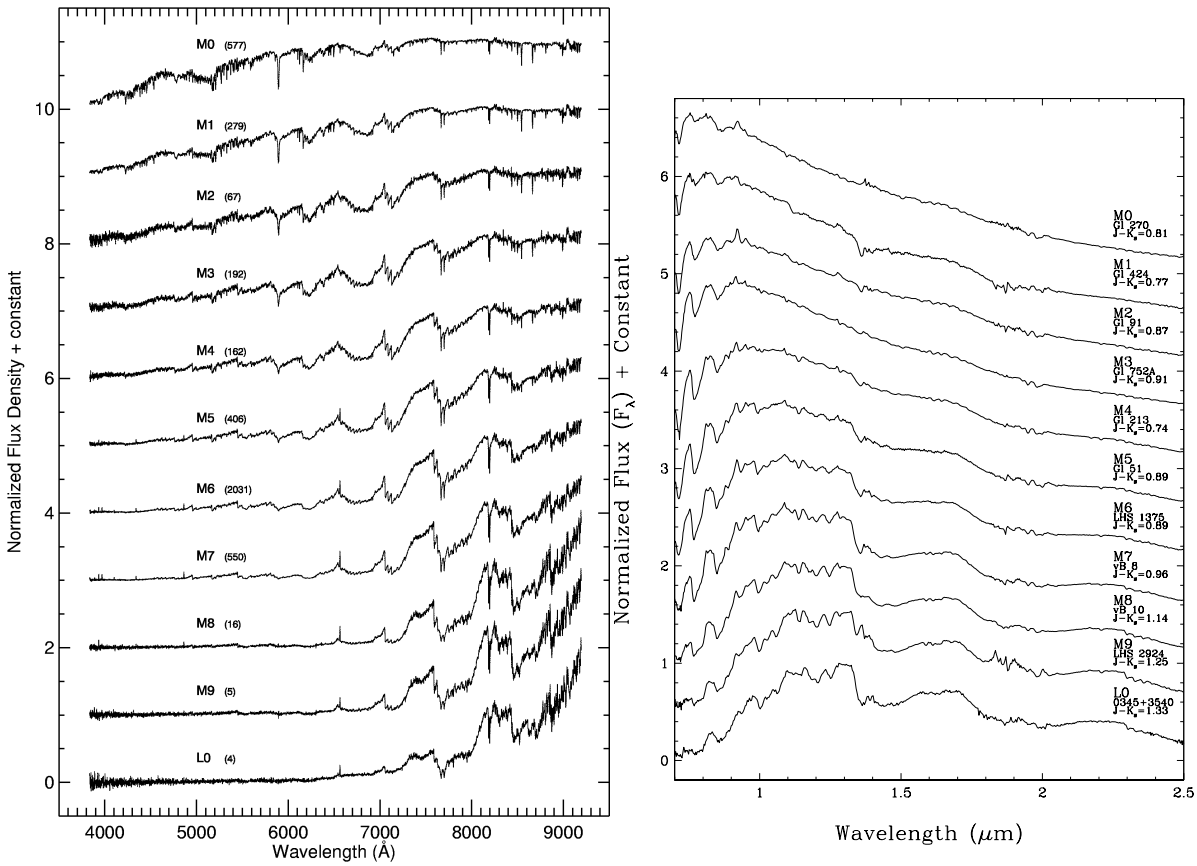

Figure 1.6: Bottom panel: SDSS optical spectral sequence of M0-L0 dwarfs. Spectra have been normalized at 8350 Å. The figure is from Bochanski et al. (2007). Top panel: SpeX NIR standard spectral sequence of M0-L0 dwarfs. Spectra have been normalized at 1.28 μm. The figure is from Kirkpatrick et al. (2010).

classification of M subdwarfs (e.g. Jao et al. 2008). I will discuss gravity affects on spectra of M subdwarfs in Section 7.2.3. Jao et al. (2008) proposed to use the luminosity class of "VI" for the classification of cool subdwarfs, especially for K and K types, following the classification (Figure 1.1) of hypergiant (I), supergiant (II), giant (III), subgiant (IV), dwarf (V). He argued that "sd" has been used for hot subdwarfs, in order to separate the OB subdwarfs from the cool subdwarfs, "sd" prefix should not be used for low-metallicity subdwarfs.

L dwarfs

The first L dwarf discovered was GD 165B, a very red companion to a WD GD 165 (Becklin & Zuckerman 1988). Kirkpatrick, Henry & Liebert (1993) obtained the first L dwarf spectrum of GD 165B. Now there are $\sim$ 1000 L dwarfs identified (e.g. http://DwarfArchives.org) thanks to the the large scale surveys DENIS (Epchtein 1997), 2MASS (Skrutskie et al. 2006) and SDSS (York et al. 2000).

Early-type L dwarfs show both atomic and molecular bands in the optical. The neutral alkali lines (Na I, K I, Rb I, Cs I, and Li I), oxide bands TiO and VO, hydride bands CrH and FeH, and CaOH are the most prominent ones. By mid-L the Na I, K I lines, and hydrides MgH, CaH, CrH, and FeH lines have strengthened, while the oxides TiO and VO have largely disappeared. By late-L H_2O has increased in strength, the neutral alkali lines are still strong, and the hydrides are much reduced (see, Figure 1.4). Kirkpatrick et al. (1999b) established the optical classifications for L dwarfs. The bottom panel of Figure 1.8 shows an optical spectral sequence of L dwarfs. The top panel of Figure 1.8 shows a NIR spectral sequence of L dwarfs. L dwarfs are characterized by strong H_2O, FeH and CO bands and neutral atomic lines of Na, Fe, and K.

L subdwarfs

L subdwarfs exhibit characteristic spectral signatures of strong metal hydrides (CaH, MgH, AlH and FeH), weak or absent metal oxides (TiO, VO and CO), and enhanced collision-induced H_2 absorption (CIA). Only seven L subdwarfs have been reported in the literature (see Table 3.1, Burgasser et al. 2003a; Burgasser 2004b; Cushing et al. 2009; Sivarani et al. 2009; Lodieu et al. 2010; Lodieu et al. 2012c). In this thesis I report another three new L subdwarfs (esdL6, sdL7, sdL3), confirmed with X-Shooter on VLT, and by SDSS spectroscopy (see Chapter 3). A spectral classification system has

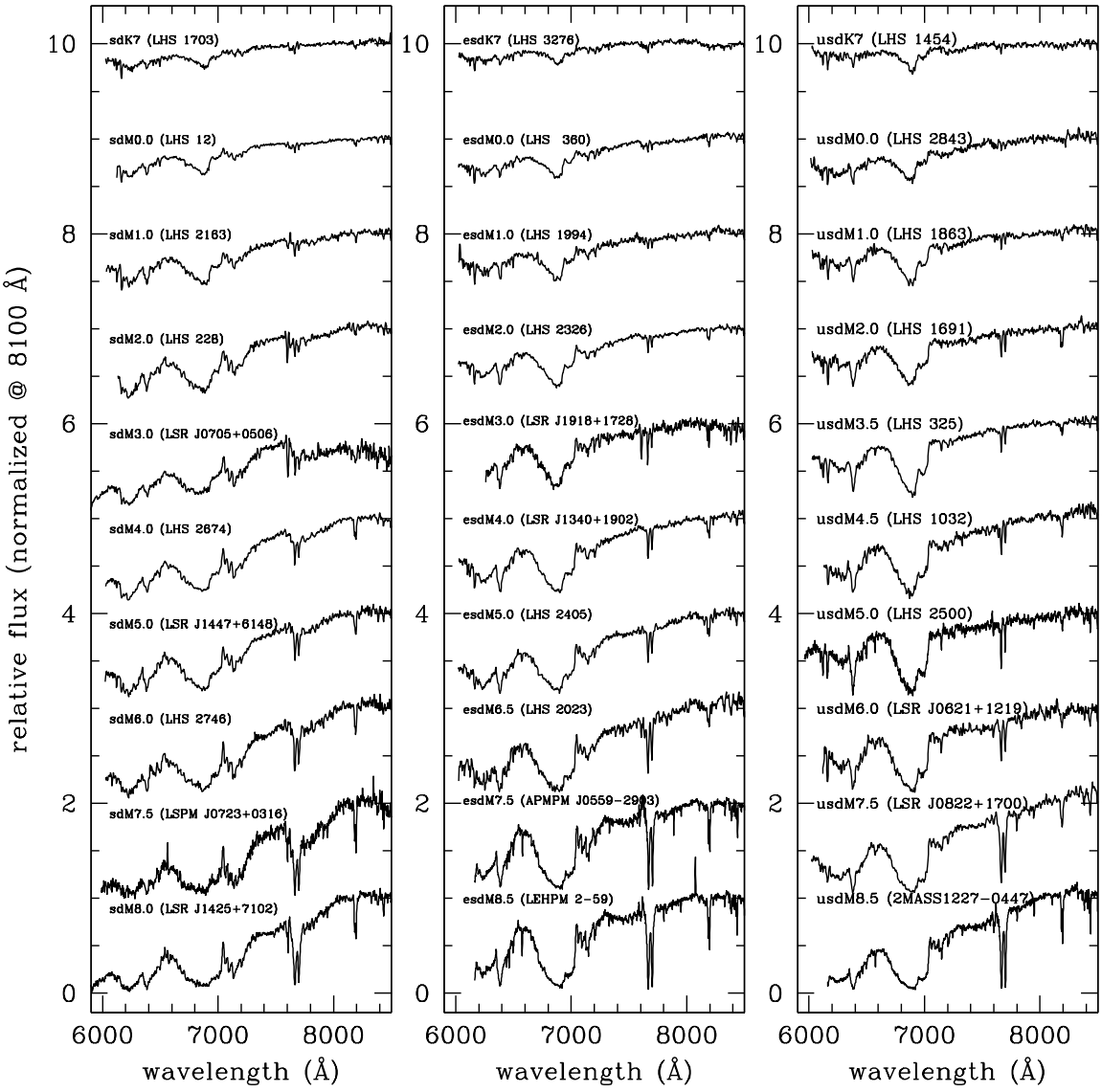

Figure 1.7: Sequences of classification standards for red subdwarfs (left), extreme subdwarfs (center), and ultra subdwarfs (right). Metallicity classes (sd, esd, usd) are based on the ratio of the TiO band head blueward of 7000Å to the CaH band head redward of 7000Å. The figure is from Lépine, Rich & Shara (2007).

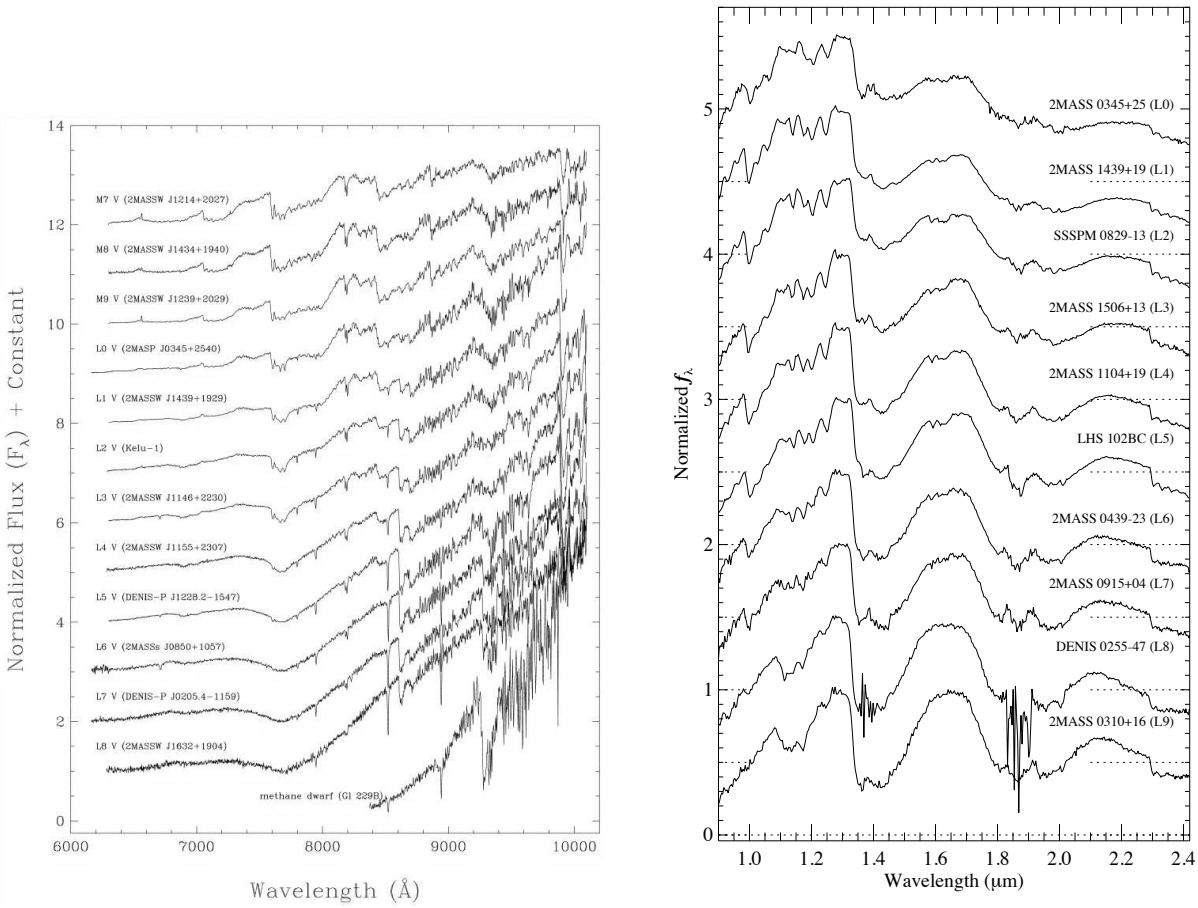

Figure 1.8: Bottom panel: Optical spectral sequence of L dwarfs. Spectra have been normalized at 8250 Å. The figure is from Kirkpatrick et al. (1999b). Top panel: NIR spectral templates of L dwarfs. Spectra are normalized in the $1.1 - 1.3\mu$m region. The figure is from Burgasser (2007).

not been established due to the lack of known L subdwarfs and our poor understanding of metal-poor ultracool atmospheres. Current spectral types of L subdwarfs are assigned by comparing their red optical spectra with those of L dwarfs. Figure 1.9 shows optical spectra of four L subdwarfs and one mild L subdwarfs. Spectral indices centred on CaH and TiO can not be used to classify the metal classes of L subdwarfs. NIR spectra must be considered to characterize L subdwarfs properly. The top plot of Figure 1.10 shows the spectral comparison of a normal L7 dwarf and an esdL7 subdwarf. Strong CIA H_2 shows up in the NIR bands. Figure 1.11 shows model NIR spectral sequences of L dwarfs with different temperature (2000 K $\sim$ L4; 2500 K $\sim$ L0), metallicity and gravity. Both low metallicity and high gravity suppress the flux in the NIR bands, and shift the flux peak to shorter wavelength.

It is critical to discover a sample of L subdwarfs with different temperature and metallicity. L subdwarfs not only help us to understand metal-poor ultracool atmospheres but also the formation and structure of the Galactic halo through study of the luminosity function and kinematics. I will discuss the discovery and characterization of L subdwarfs in Chapter 3.

T dwarfs

Approximately 500 T dwarfs have been discovered since the first one, Gliese 229B (Nakajima et al. 1995; Oppenheimer et al. 1995). Figure 1.12 shows optical and NIR spectra of two T dwarfs, ε Indi Ba and Bb (T1, T6; Scholz et al. 2003; McCaughrean et al. 2004). The primary distinguishing spectral features of T dwarfs are the NIR CH_4 absorption bands centred at 1.15, 1.35, 1.65, 2.2, 3.3 μm. T dwarfs have stronger H_2O bands at 1.15, 1.4, and 1.8 μm than M and L dwarfs. CO absorption at 4.7 μm has been identified in T dwarf spectra (King et al. 2009).

Atomic line absorption in the NIR is largely limited to the K I line in the 1.1 - 1.25 μm region, which disappears in the spectra of latest T dwarfs. The red optical spectra of T dwarfs are dominated by the pressure broadened wings of the K I resonance doublet, at 0.7665 and 0.7699 μm. Alkali lines of Rb I (0.78 and 0.7948 μm) and Cs I (0.8521 and 0.8943 μm) are superimposed on the red wing of K I. Molecular H_2O absorption over 0.925 - 0.98 μm is present in the spectra of all T dwarfs, while the 0.99 μm FeH, prominent in mid L dwarf spectra, is weakly present in the mid T dwarf spectra. CH_4 absorption at 0.89 μm presents in late-type T dwarf spectra.

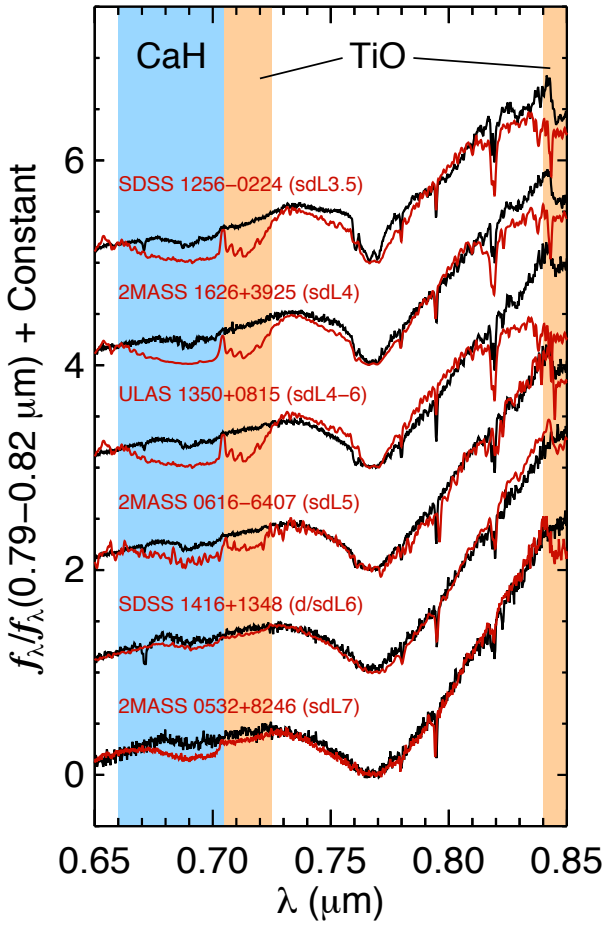

Figure 1.9: Optical spectra of four L subdwarfs and one mild subdwarf(red). The most notable differences in metal-poor L dwarfs compared to ordinary field objects are the stronger CaH absorption band at 6800 Å and stronger TiO absorption bands at 7100 Å and 8400 Å. The spectra are normalized between 7900 Å and 8200 Å and are offset by a constant. Note that the spectrum labeled as ULAS 1350 is actually of SDSS 1256. The optical spectrum of ULAS 1350 is shown in Figure 3.10. The figure is from Witte et al. (West et al. 2011).

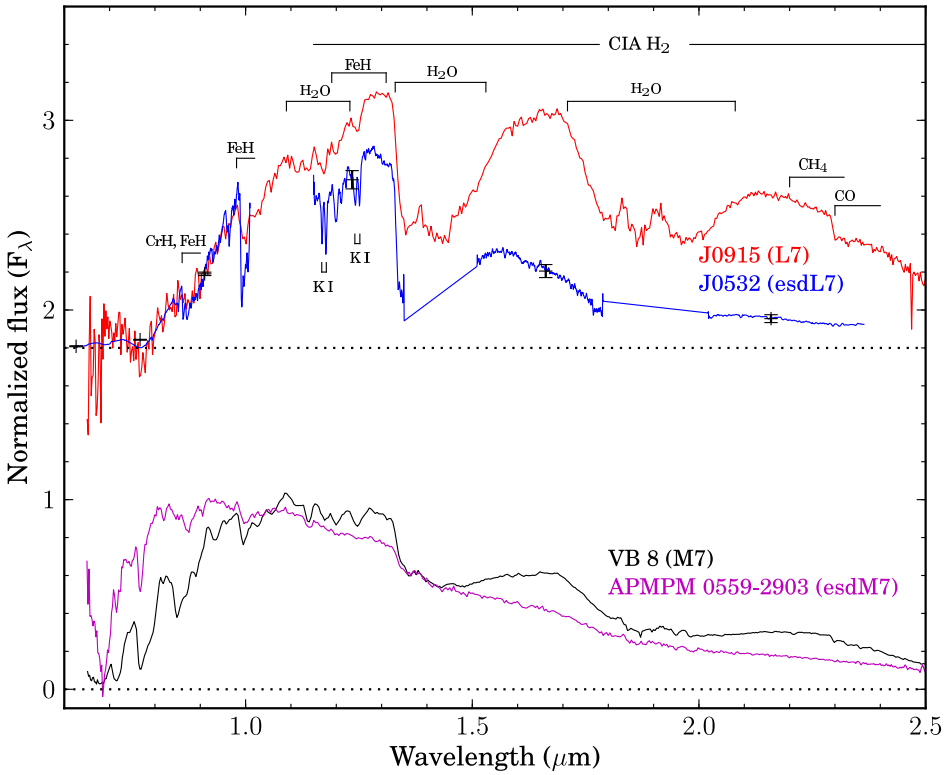

Figure 1.10: NIR spectra of an esdL7 2MASS J05325346+8246465 (Burgasser et al. 2003a) and an esdM7 APMPM 0559-2903 (Burgasser & Kirkpatrick 2006). Black pluses are SEDs of 2MASS J0532. Spectra of the dL7 2MASS J09153413+0422045 (Burgasser et al. 2010), and the dM7 VB 8 (Burgasser et al. 2008a) are also plotted for comparison.

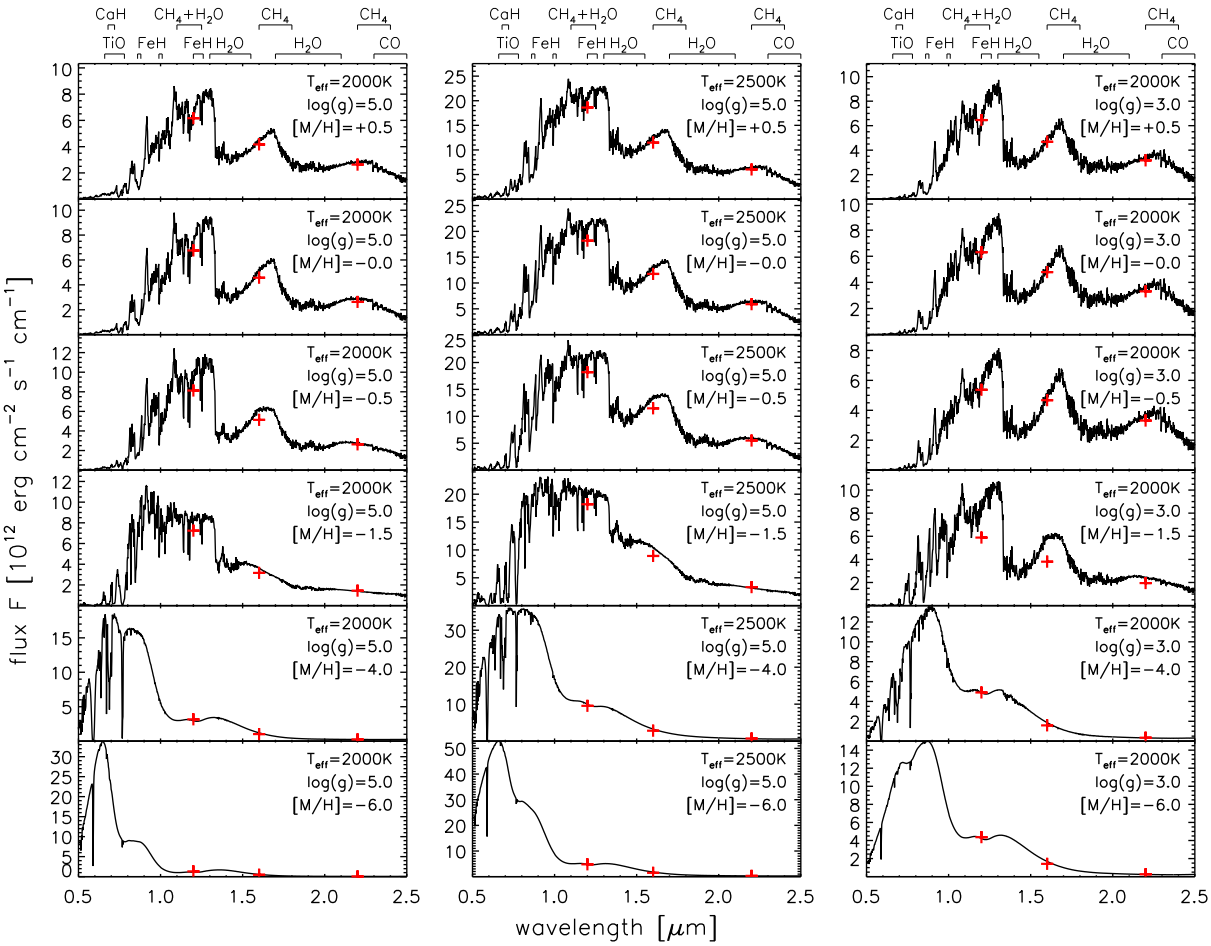

Figure 1.11: Model NIR spectral sequences of L dwarfs with different temperature (2000 K $\sim$ L4; 2500 K $\sim$ L0) and metallicity. The red crosses indicate the photometric fluxes in the J, H and K bands as they would be observed by 2MASS. The figure is from Witte, Helling & Hauschildt (2009).

Burgasser et al. (2002) and Burgasser et al. (2003b) developed and proposed a T dwarf standard spectral sequences in NIR and red optical wavelength. Figure 1.13 shows updated optical and NIR standard sequences of T dwarfs from Kirkpatrick et al. (2011) and Burgasser (2007).

At lower metallicity there are a few mildly metal-poor disk T dwarfs that have been reported (Burningham et al. 2010a; Murray et al. 2011; Pinfield et al. 2012) with suppressed K band flux (e.g, Figure 3.11). No unambiguous T type subdwarf with lower metallicity has not been discovered so far.

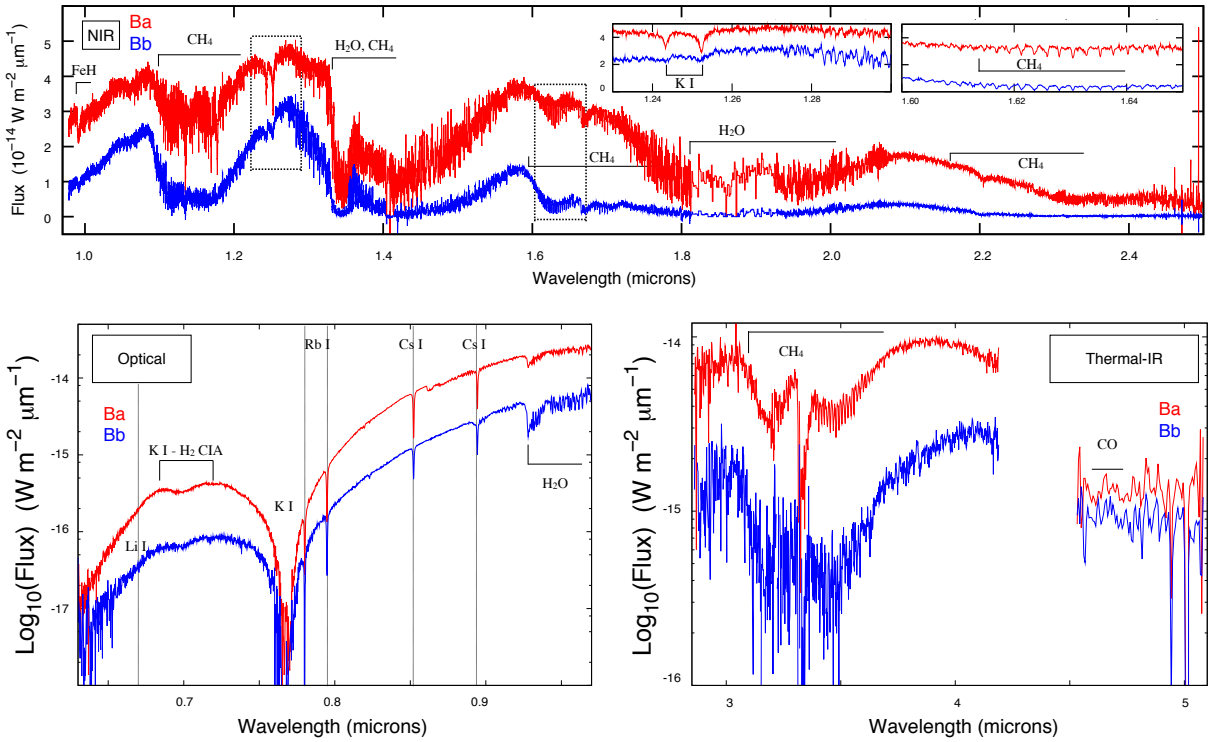

Figure 1.12: The optical and NIR spectra of ε Indi Ba and Bb. The figures are from King et al. (2009).

Y dwarfs

Fourteen Y dwarfs have been discovered and confirmed with spectra recently (Cushing et al. 2011; Kirkpatrick et al. 2012; Tinney et al. 2012). Figure 1.14 shows the NIR spectra and model spectra of Y dwarfs. This distinguishing features of Y dwarfs is the NH_3 line around 1.5 μm. All Y dwarf spectra exhibit deep H_2O and CH_4 absorption bands characteristic of late-type T dwarfs but the J and H band peaks of Y dwarfs

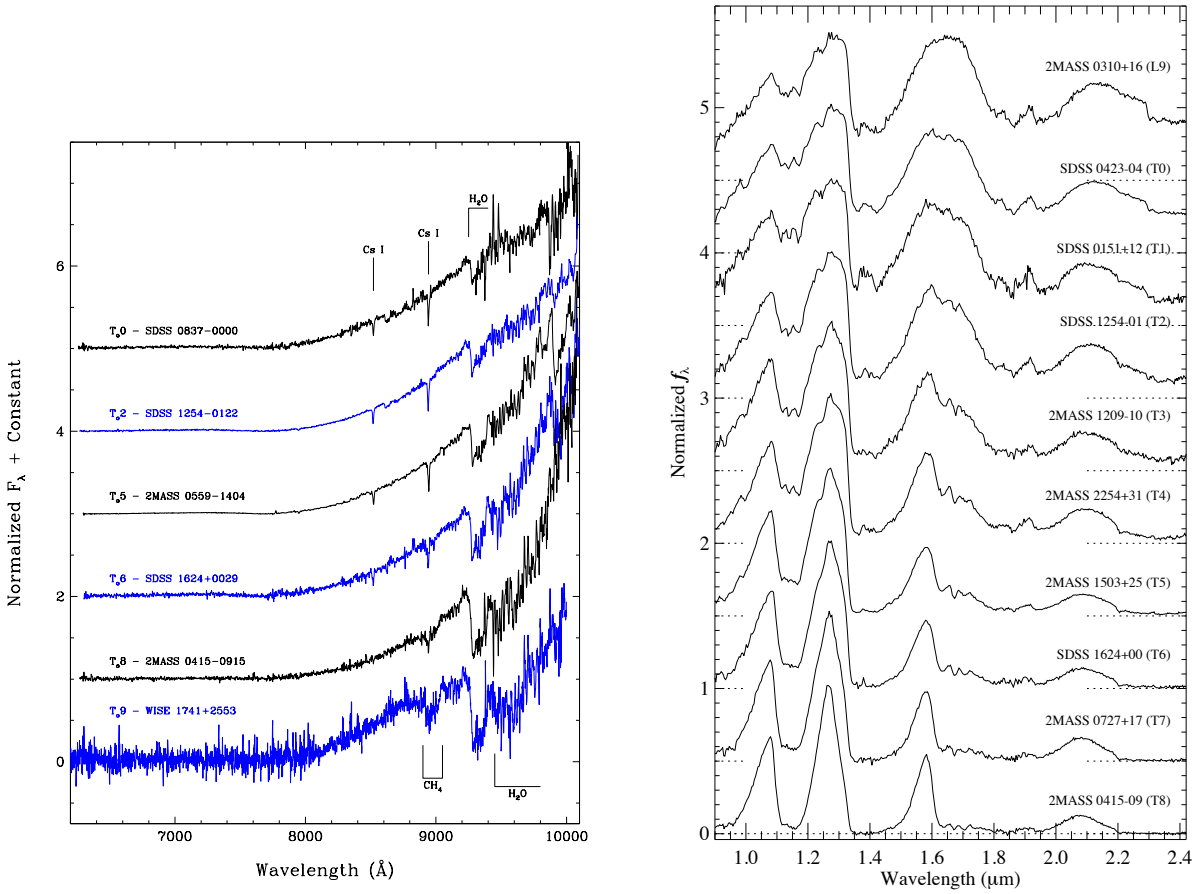

Figure 1.13: Bottom panel: Optical spectral of T dwarfs. Spectra have been normalized at 9200 Å. Figure is from Kirkpatrick et al. (2011). Top panel: NIR spectral templates for T dwarfs. Spectra are normalized in the $1.1 - 1.3\mu$m region. Figure is from Burgasser (2007).

are narrower than the corresponding peak in the spectrum of the latest T dwarf, UGPS 0722-05 (Lucas et al. 2010). $J - H$ colour of Y dwarfs becomes redder than that of late-type T dwarfs. WD 0806-661B is a Y dwarf candidate as a wide companion to a white dwarf WD 0806-661 discovered recently (Luhman, Burgasser & Bochanski 2011; Luhman et al. 2012) using data from a Spitzer program led by M. Burleigh. CFBDSIR J1458+1013B is another Y dwarf candidate that is a close companion to a T9.5 dwarf CFBDSIR J1458+1013 discovered by Liu et al. (2011b). But both of them are too faint to be observed spectroscopically with currently available technology.

Figure 1.15 shows the 8pc sample of celestial objects as a function of spectral type. T and Y dwarf bins are believed to suffer from significant incompleteness. It is likely that a small number of T dwarfs, and a larger number of Y dwarfs, have yet to be identified along with T and Y companions to higher-mass objects already known within the 8 pc volume (Kirkpatrick et al. 2012).

1.2.2 Absolute magnitudes

The relationship of absolute magnitudes and spectra types of BDs is useful because it can be used directly to compare with model predictions, and estimate BD distances. Parallaxes are required to measure absolute magnitudes. A lot of work have been done on parallax measurements of UCDs (e.g. Tinney, Burgasser & Kirkpatrick 2003; Vrba et al. 2004; Costa et al. 2005; Costa et al. 2006; Gizis et al. 2007; Burgasser et al. 2008b; Schilbach, Röser & Scholz 2009; Marocco et al. 2010; Faherty et al. 2012; Dupuy & Liu 2012).

The onset of methane absorption has a significant affect on the luminosities of cool dwarfs at NIR wavelengths. The impact at H and K bands is obvious, but the J band is also affected, in the opposite sense. Figure 1.16 shows plots of J, H and K band absolute magnitudes with spectral types for ultracool dwarfs with parallax measurements. Cool subdwarfs, likely unresolved binaries and very low gravity objects are excluded from the plot. It is clear that L6-T5 dwarfs have similar M_J. T3-T5 dwarfs are even a bit brighter than L8-T2 dwarfs in J band. This J band brightening is partly due to the presence of higher opacities at longer and shorter wavelengths in T dwarfs, which force a higher proportion of the total flux into the relatively transparent 1.2 μm window. The effect is also present to a lesser extent in the K passband, which includes strong CH_4 absorption. The absolute magnitude and spectral type relationships are often used to

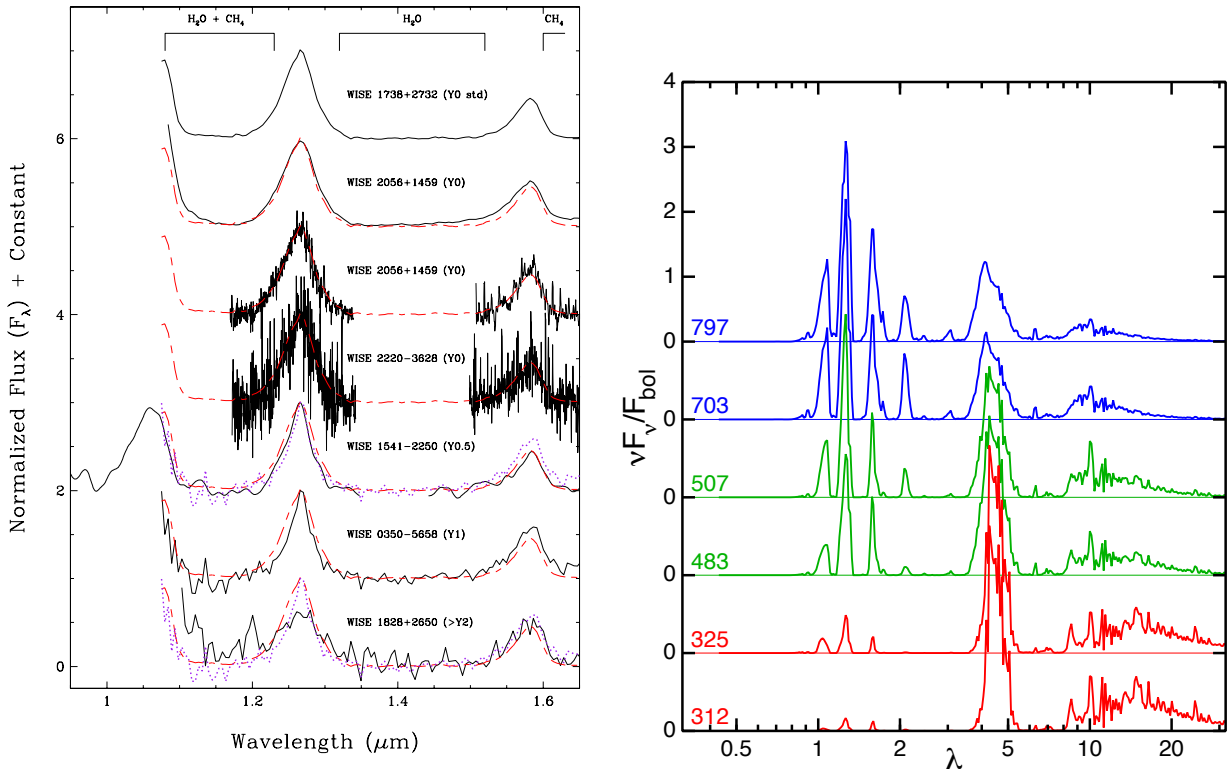

Figure 1.14: Bottom panel: The NIR spectra of Y dwarfs. The spectrum of the Y1 standard, WISE 0350-5658, is shown by the purple dotted line and is normalized to 1.0 at the J-band peak. The figure is from Kirkpatrick et al. (2012). Top panel: Model spectra (Burrows, Sudarsky & Lunine 2003) of late-type T and Y (red) dwarfs. Effective temperatures are labeled from 797 K to 312 K. The figure is from Wright et al. (2010).

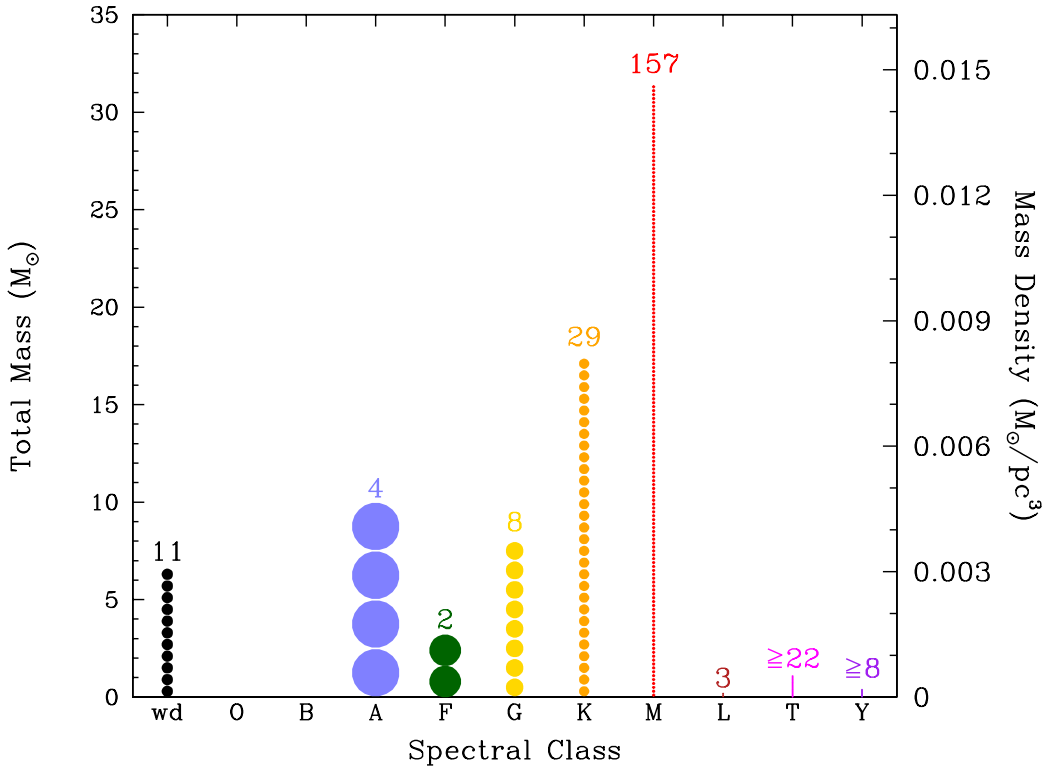

Figure 1.15: The 8pc sample of celestial objects as a function of spectral type plotted in three ways; as total mass (left axis), mass density (right axis), and histogram (numbers above each star stack). The figure is from Kirkpatrick et al. (2012).

estimate distances of ultracool dwarfs. Figure 1.17 shows J, H and K band absolute magnitudes vs spectral types of ultracool dwarfs and subdwarfs. L subdwarfs are brighter than L dwarfs in the J band and have similar magnitudes to L dwarfs in the H and K bands. The L subdwarf classification system has not been established. Known L subdwarfs have not been classified properly (see Chapter 3), thus Figure 1.17 might will be adjusted when an L subdwarf classification system is established.

1.2.3 Ultracool atmosphere models

The atmospheres of substellar objects contain clouds of oxides, iron, silicates and other refractory condensates. Water clouds are expected in the coolest objects. The opacity of these 'dust' clouds strongly affects both the atmospheric temperature-pressure profile and the emergent flux. Thus, any attempt to model the spectra of these atmospheres must incorporate a cloud model. However, the diversity of cloud models in atmospheric simulations is large and it is not always clear how the underlying physics of the various models compare. Likewise, the observational consequences of different modelling approaches can be masked by other model differences, making objective comparisons challenging (Helling et al. 2008a). Spectra of UCDs are determined by the physics and properties of their atmospheres. Successful ultracool atmosphere models can help us to understand and accurately predict properties of UCDs. Several models have been built to explain observational properties of of UCDs. These models can have very different predictions of spectra and colours of UCDs depending on how they treat dust in the atmosphere. Dust in UCDs has a significant role in the underlying physics, affecting molecular and scattering opacity, as well as the temperature profile. I will new describe three commonly used model atmospheres.

Lyon (PHOENIX) models

PHOENIX is a general-purpose model atmosphere code, using plane-parallel geometry, thermochemical equilibrium calculations, and opacity sampling to self-consistently solve for the temperature-pressure profile, chemical abundances, and radiative/convective energy transfer through the atmosphere. Several implementations of Phoenix have been used to study late-type dwarfs, incorporating various assumptions on elemental abundances, atomic and molecular opacities, line profiles, condensate formation, and convective overshoot (e.g. Hauschildt, Allard & Baron 1999; Allard et al. 2001; Johnas et al. 2008; Helling, Woitke & Thi 2008; Witte, Helling & Hauschildt 2009; Witte et al. 2011).

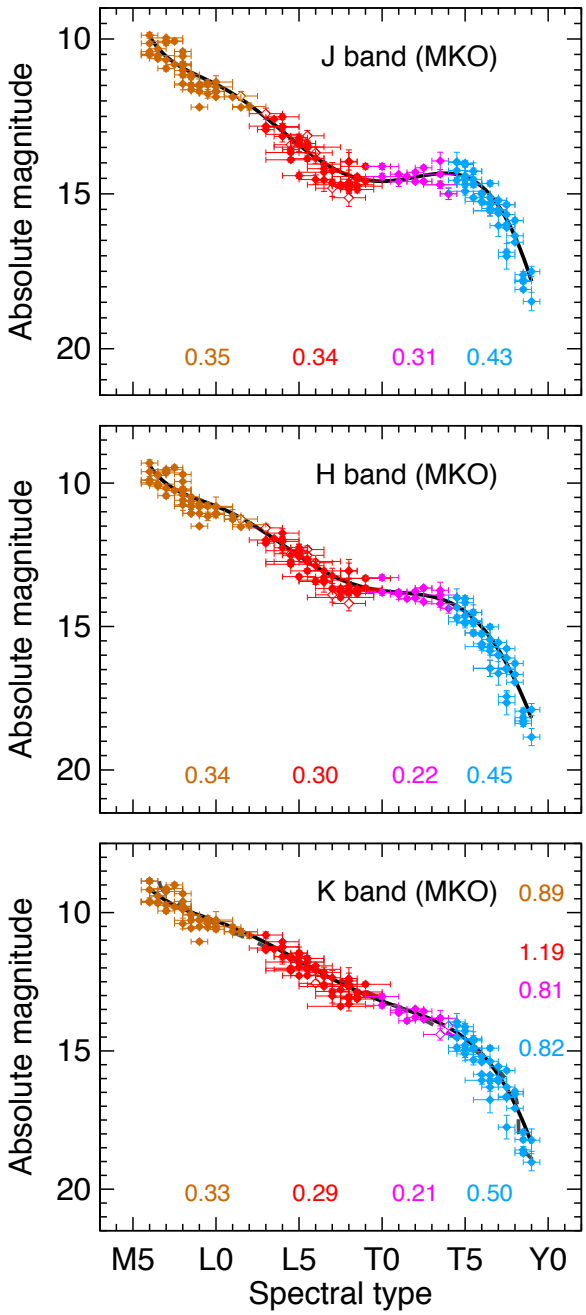

Figure 1.16: NIR absolute magnitude as a function of spectral type for ultracool dwarfs with parallaxes. Thick solid lines are polynomial fits to the data. At the bottom of each panel the root mean square (rms) about the fit is given, broken down by spectral type range: M6–L2 (brown), L2.5–L9 (red), L9.5–T4 (purple), and ≥T4.5 (blue). The rms about these fits for the same spectral type ranges as listed above are given along the right side of the respective panels. The figures are from Dupuy & Liu (2012).

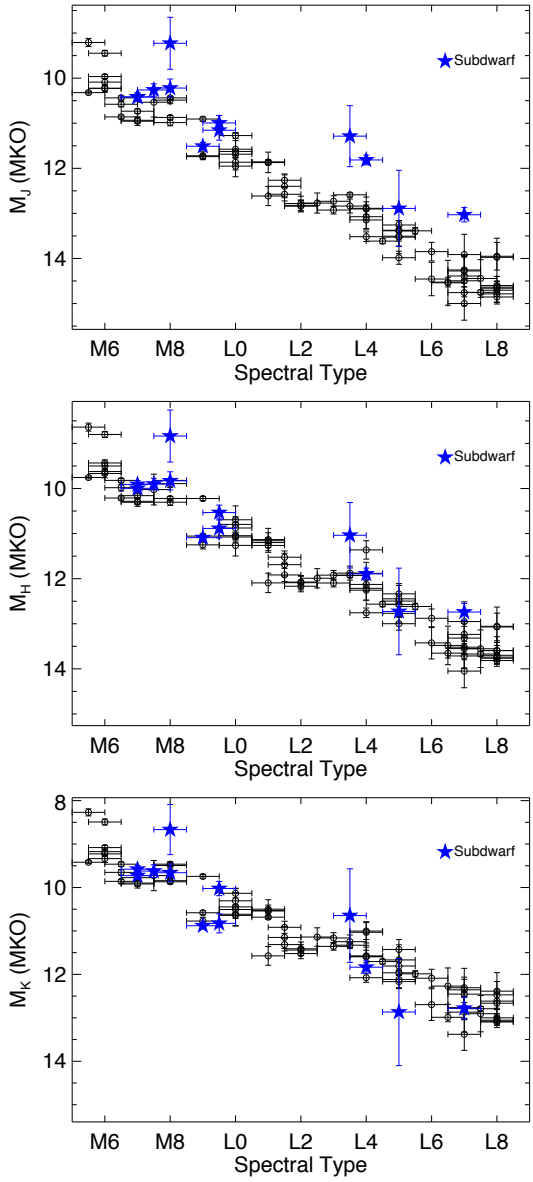

Figure 1.17: NIR absolute magnitude of ultracool subdwarfs

Spectral type v.s. absolute magnitude in the MKO JHK filters for late-type M and L dwarfs. Black circles are normal dwarfs. Blue five point stars are subdwarfs. The figures are from Faherty et al. (2012).

PHOENIX has a few implementations depending on the treatment of the dust cloud layers. From the older versions of Dusty-PHOENIX (1300 K $\leq T_{\rm eff} \leq$2700 K; Chabrier et al. 2000; Allard et al. 2001; Baraffe et al. 2002) and Cond-PHOENIX (700 K $\leq T_{\rm eff} \leq$ 1300 K; Allard et al. 2001; Baraffe et al. 2003) to newer BT-Settl (Allard, Homeier & Freytag 2011); Gaia-Cond/Dusty (Hauschildt et al. 2003; Rice et al. 2010) and Drift-PHOENIX (Dehn et al. 2007; Helling, Woitke & Thi 2008; Witte, Helling & Hauschildt 2009).

The Cond/Dusty-PHOENIX models are used to understand the two limiting cases of brown dwarf atmospheres that are either covered by thick cloud layers (Dusty), and where these clouds are located beneath an optically thick gaseous atmosphere (Cond). Both assume a phase equilibrium between gas and dust. While the Dusty approach fully considered the opacity of the dust itself, the dust opacity was neglected for the Cond model, where the dust was assumed to have settled completely below the photosphere.

The Gaia-Cond model is most similar to the Cond-PHOENIX model, in which condensate species are treated as element sinks only and phase equilibrium is assumed. Gaia-Dusty and BT-Settle models have superseded the Dusty models with improved treatments of abundances and line lists. The Drift-PHOENIX model applies an advanced model of non-equilibrium grain formation, and convective up-mixing to simulate the size distribution, abundances, and vertical distribution of grains and their material composition (e.g. Helling, Woitke & Thi 2008; Witte et al. 2011).

Gaia-Cond does not track well with the mean $i - J$ versus $J - K$ colours of M0-L0 field dwarfs (see, Figure 1.18). It also do not predicted the right colour trend for L subdwarfs in Figure 1.18. Drift-PHOENIX performed better in tracking the $i - J$ versus $J - K$ colours of M0-L0 dwarfs, but failed to reproduce colours of L subdwarfs because i band magnitudes are highly sensitive to the strong molecular opacity present at these wavelengths.

Tuscon models

(Burrows, Sudarsky & Hubeny 2006) use a model of refractory clouds, coupled with the latest gas-phase molecular opacities for dust molecules, similar to those used by the Lyon group. They also look at the effects of gravity and metallicity and vary grain size, cloud scale height and cloud distribution, applicable over a $T_{\rm eff}$ = 2200-700K range. They show generally good agreement with the observed spectra of IR colours for early-mid L and

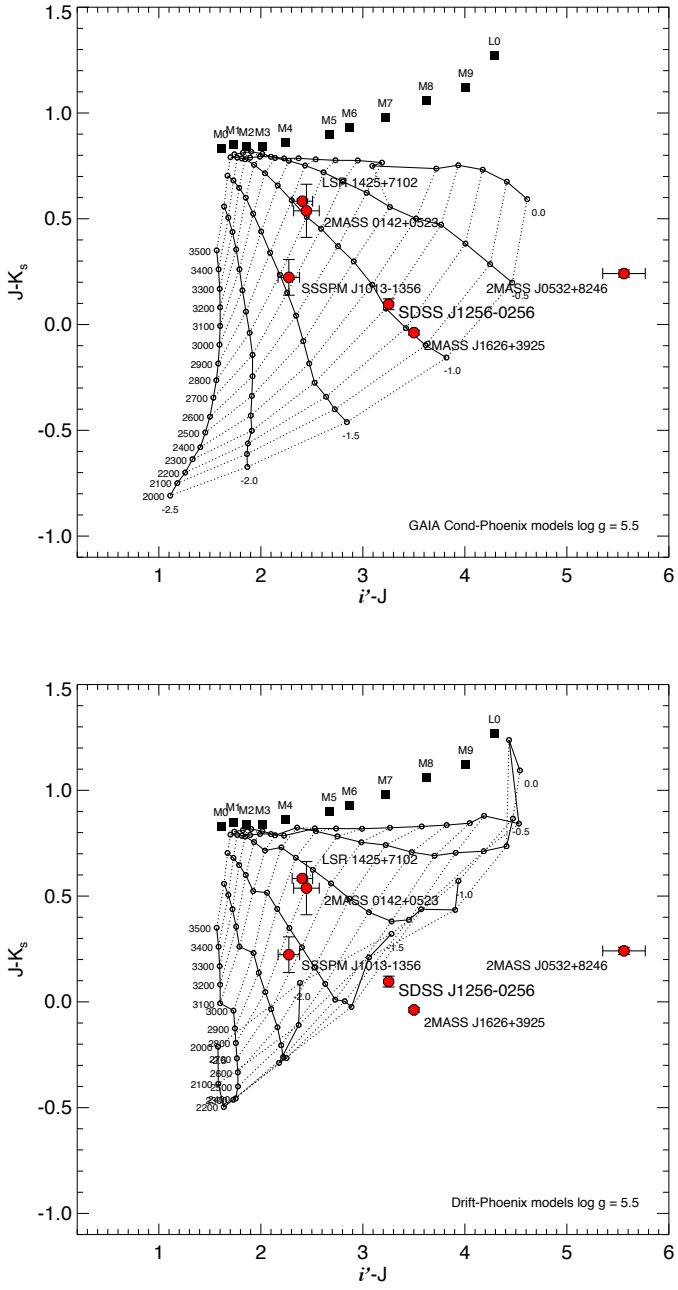

Figure 1.18: SDSS-2MASS $i' - J$ versus $J - K_s$ colours for the late-type subdwarfs 2MASS J0142+0523 (sdM8.5), LSR 1424+7102 (sdM8), SSSPM J1013-1356 (sdM9.5), SDSS J1256-0224 (sdL3.5), 2MASS J1626+3925 (sdL4) and 2MASS J0532+8246 (sdL7) as compared to GAIA COND-PHOENIX (top) and DRIFT-PHOENIX (bottom) atmospheric model predictions. Models are shown for log$g$ = 5.5, 2000 K $\leq T_{eff} \leq$ 3500 K in steps of 100 K (along solid lines) and –3.0 $\leq$ [M/H] $\leq$ 0 in steps of 0.5 dex (along dotted lines). Also shown are mean SDSS-2MASS colours of M0–L0 dwarfs from West et al. (2008). The figures are from Burgasser et al. (2009).

mid-late T dwarfs and by varying gravity parameters get a closer fit to the L/T transition than other models. However they do not reproduce the apparent brightening seen in the J-band at the transition, nor the dimming at very late-type T. They suggest that the L/T transition is likely related to gravity and possibly metallicity, though this needs further investigation.

Ames models

The Ames model was developed by Ackerman & Marley (2001), Marley et al. (2002), Saumon & Marley (2008) and Freedman, Marley & Lodders (2008), uses a self-consistent treatment of cloud formation. They suggest that $i - z$ colour is extremely sensitive to chemical equilibrium assumptions, having an effect of up to ~ 2 magnitudes on colour. They consider not only the sedimentation of condensates but also the efficiency of the process to help explain both L and T dwarfs and the L/T transition with the same model, for solar metallicity. As such they attempt to represent an intermediate case between the DUSTY and COND extremes. In this case the cloud decks are confined to a fraction of the pressure scale height and the models assume that it is sedimentation that controls vertical mixing in the clouds, causing the observed turnover in $J - K$ colour with decreasing $T_{\rm eff}$. They also take into account grain sizes between 10-100 μm and assume that if the grain size is less than the observed wavelength of light, Rayleigh scattering dominates and has little affect on opacity. The problems with this model are that while it predicts the overall trend seen by observations, the finer details are not matched, e.g. the peak of the model value in $J - K$ is not as red as that observed, and the models predict a move to bluer colours that is much slower than is actually seen.

As yet no self-consistent model has been presented that can reproduce the observed characteristics of L and T dwarfs and how they evolve from one type to the other in both optical and NIR colours and spectra. It seems evident that the treatment of dust plays a vital part in fully understanding the underlying physical processes at work. Different vertical cloud extension is suggested by different simulations: the BT-Settl model (Allard et al. 2001; Allard et al. 2007) produces a vertically less extended cloud layer than Ames model (Ackerman & Marley 2001; Freedman, Marley & Lodders 2008), and the Drift-PHOENIX model (Helling, Woitke & Thi 2008; Helling et al. 2008b), which will have consequence for the emergent spectrum of such an atmosphere (Helling et al. 2008a).

1.2.4 Benchmark ultracool dwarfs

Theoretical models are good tools to help us to understand the ultracool atmospheres and evolution of red and brown dwarfs well. Our knowledge of ultracool atmospheres and evolution of low mass objects is a tool to help us to understand brown dwarfs observationally and physically. This in turn allow us to better understand the initial mass function and stellar/substellar formation history of our Galaxy. Ultracool atmospheric models (see Section 1.2.3) have difficult to reproduce observed spectra particular in the low metallicity region. Effective temperature and luminosity of UCDs predicted from evolutionary models (Baraffe et al. 1997; Baraffe et al. 2003; Montalbán, D'Antona & Mazzitelli 2000) and atmospheric models (Burrows et al. 2001; Marley et al. 2002; Helling, Woitke & Thi 2008) are not agree well. Thus we need benchmark objects to calibrate our models.

In order for an UCD to be considered as a benchmark it must have one or more properties (e.g. distance, age, metallicity, mass, radius) that can be constrained relatively independently of UCD models. Benchmark objects are used for calibration of both ultracool atmospheric and evolutionary models which have difficulty in accurately reproducing observations. The overall usefulness of an object as a benchmark is also dependent on the accuracy of the measured properties and the number of assumptions that have to be made if some degree of referencing to models is required. Companions in a binary system are generally sharing the same age, metallicity and distance (Pinfield et al. 2006 and references there in). Good benchmark companions to other stars include subgiant/giant stars and white dwarfs (WD), along with the more common main sequence stars which can provide useful constraints on age, metallicity and distance.

UCD companions to subgiant/giant stars and WD are ideal age benchmarks but they are very rare (e.g. Zhang et al. 2010; Day-Jones et al. 2011a). UCD companions to bright stars with good measurements are also good benchmarks (e.g. Scholz et al. 2003; Pinfield et al. 2012). UCDs in open clusters (Bouvier et al. 2008; Hogan et al. 2008) and moving groups (Clarke et al. 2010) are also good benchmarks for age, metallicity and distance. They generally have very young age (<1 Gyr) and solar metallicity, so they cover a narrow age and metallicity parameter ranges. Clusters are mostly at distance of >100pc, thus require more telescope time to observe. Young isolated UCDs in the field that have Lithium in their atmospheres, such as Kelu1 (Ruiz, Leggett & Allard 1997), are also benchmarks, where the Lithium test can be used to constrain age. Close binaries of UCD + UCD or UCD + low mass star with orbital period less than a few decades could provide accurate dynamical measurements (Dupuy, Liu & Ireland 2009;

Luhman 2013). Eclipsing UCDs could provide radius measurement, thus can be radius benchmarks (Stassun, Mathieu & Valenti 2006). Figure 1.19 shows the current population of age benchmark UCDs (Day-Jones et al. 2011b). At subsolar metallicity, there is only one ultracool benchmark, a d/sdM9 subdwarf companions to an d/sdF9 [M/H] = –0.7 (Bowler, Liu & Cushing 2009). The small separation (3.3 arcsec) from the primary star makes it an challenge for detailed observation of the faint secondary.

The multiplicity system, ε Indi A, Ba and Bb is an ideal benchmark. ε Indi B was found to be an wide companion to the K5V (ε Indi A) by Scholz et al. (2003), and later found contain two companions (ε Indi Ba and Bb) by McCaughrean et al. (2004). ε Indi A is 3.626 pc away from the Sun (Perryman & ESA 1997), and have proper motion of 4.7 arcsec/yr and age of $0.8 - 2$ Gyr (Lachaume et al. 1999). The ε Indi B subsystem is separated from the primary by 402.3 arcsec corresponding to a projected spatial separation of 1459 au (Scholz et al. 2003). ε Indi Ba and Bb is the nearest binary BD containing a T1 and a T6 dwarf separated by 0.732 arcsec or 2.65 au (McCaughrean et al. 2004). Cardoso et al. (2009) obtained the preliminary system mass of 121 ± 1 $M_{\rm Jup}$. King et al. (2010) estimated the mass of $67.6 - 69.1$ $M_{\rm Jup}$ for ε Ba, $50.0 - 54.5$ $M_{\rm Jup}$ for ε Bb, and age of $\sim 3.7 - 4.3$ Gyr based on observations and evolutionary models (Baraffe et al. 2003). Figure 1.12 shows spectra of ε Ba and Bb from King et al. (2009).

To establish a fully comprehensive benchmark population we would need to identify a sample of UCD benchmarks which cover inclusive parameter-space regions of age, mass and metallicity in current and future large scale surveys (Section 1.4.3). Such a population could then be used to calibrate evolutionary and atmospheric models. Since the luminosity of BDs are evolving all the life-time, thus to convert the observed substellar luminosity function to the present-day mass function we would need help of well calibrated evolutionary and atmospheric models.

1.3 The initial mass function

The distribution of stellar masses that form in one star formation event in a given volume of space is called the initial mass function (IMF). The IMF is a fundamental cornerstone of star formation and Galactic evolution (Corbelli, Palla & Zinnecker 2005). The form of the substellar IMF has key implications for both Galactic and stellar astronomy. The MF influences most observable properties of stellar populations and thus galaxies, and variations in the MF provide deep insights into the star formation process. The IMF of

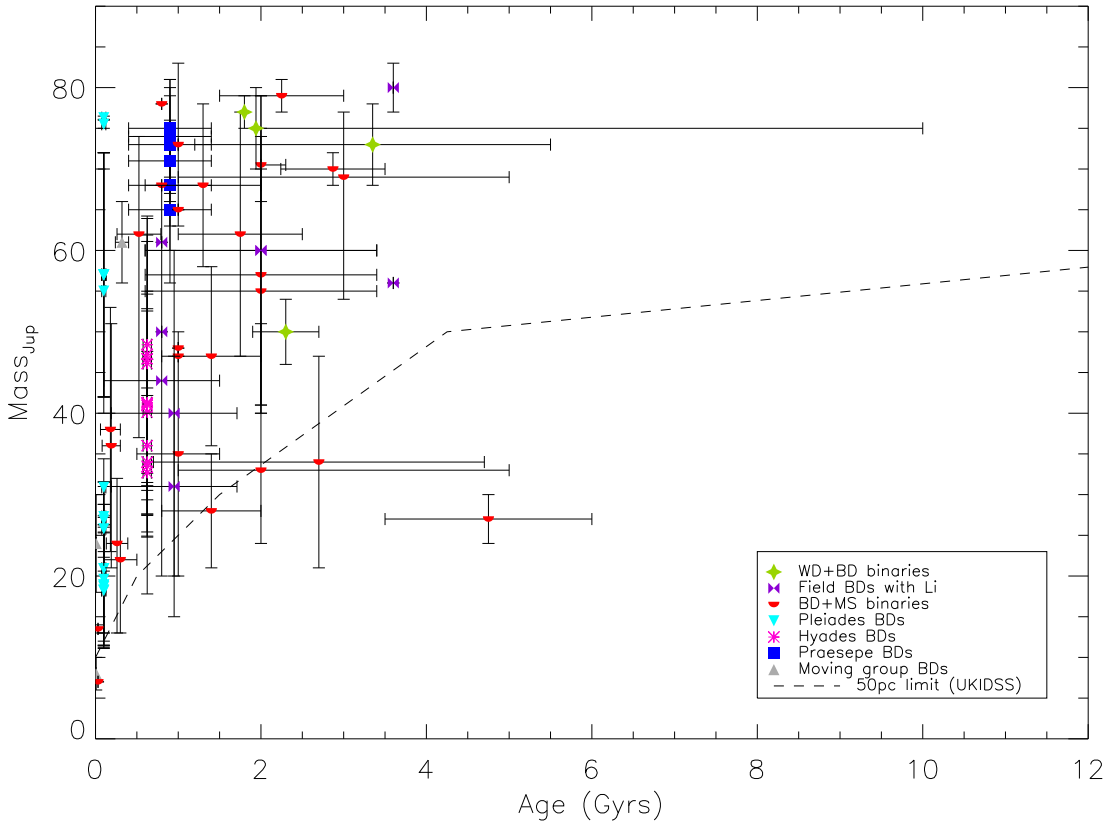

Figure 1.19: The mass-age distribution of benchmark brown dwarfs. The figure is from Day-Jones et al. (2011b).

stars with mass larger than one solar mass has been well studied and has not changed much for half a century (Salpeter 1955). Evidence for uniformity of IMF in different regions has been found (Kroupa 2002). And no overwhelming evidence for large systematic variations in the IMF as a function of the initial conditions of star formation was found (Bastian, Covey & Meyer 2010). A lot works on substellar MF have been done (e.g. Chabrier 2003; Kirkpatrick et al. 2012; Lodieu et al. 2012b).

While, the halo substellar MF also has important implications for our understanding of stellar and substellar formation and evolution as a function of metallicity and time, and reveals the conditions in which the different populations of stars formed.

1.3.1 The disk brown dwarf mass function

Brown dwarfs are thought to form in the same way as stars, so in this sense can be considered as a continuity of stellar formation. The stellar IMF is reasonably well constrained in the disk of the Galaxy but the substellar MF still under investigation and large uncertainties remain (e.g. Bastian, Covey & Meyer 2010) especially at the low temperature ($<$ 1000 K, T and Y types) regions (e.g. Burningham et al. 2010b; Kirkpatrick et al. 2012).

The IMF is usually converted from a luminosity function (LF) via a mass-luminosity relation. Deriving the likely form of the mass function below the hydrogen-burning limit is more complicated. The nature of BD evolution (cooling and fading with time) means that the mass-luminosity relation depends strongly on age, and one can not determine either mass or age from a BD's luminosity alone. The usual approach to this problem is to fit synthesized $T_{\rm eff}$ and luminosity functions (constructed with different IMFs and formation histories) to observed BD populations (Allen et al. 2005; Deacon & Hambly 2006). However, this method is sensitive only to quite drastically different formation histories and then only if one assumes a non evolving IMF (Burgasser 2004a). This method also has little chance of constraining the BD metallicity distribution (Pinfield et al. 2006).

1.3.2 The mass function of open clusters

In principle, young clusters (age $\sim$ 10-200 Myr, e.g. Pleiades) are particularly favourable targets to determine the IMF. Indeed, all objects in a cluster are likely form at the similar time which can be comparable with the age of the cluster; young objects are brighter and

less dynamically evolved. Membership of objects to the cluster can be confirmed with accurate spectroscopic observations or proper motion measurements.

The study of substellar IMF has been conducted based on nearby open clusters, e.g. Pleiades (e.g. Hambly et al. 1999; Moraux et al. 2003; Lodieu et al. 2007b; Lodieu, Deacon & Hambly 2012); Praesepe (e.g. Wang et al. 2011; Boudreault et al. 2012); Hyades (e.g. Bouvier et al. 2008); IC 4665 (e.g. Lodieu et al. 2011); Upper Scorpius (e.g. Lodieu, Dobbie & Hambly 2011); IC 348(e.g. Muench et al. 2003; Alves de Oliveira et al. 2013; σ Orionis (e.g. Béjar et al. 2001; Caballero et al. 2007; Peña Ramírez et al. 2012); ϱ Ophiuchi (e.g. Stamatellos, Whitworth & Ward-Thompson 2007; Mužić et al. 2012; Alves de Oliveira et al. 2012). Open clusters likely to have similar IMF with the Galactic field, extending below the substellar limit. Suggesting a universal, dominant process in star formation both in young cluster and in the Galactic field. Differences are likely to arise from unresolved binaries and from uncertainties in the mass determination of BDs, due to uncertainties in the theoretical models at young age (Baraffe et al. 2002) and in the treatment of dust formation (Chabrier et al. 2000). There are some evidence that the characteristic mass of a log-normal IMF in the Upper Sco Region is significantly lower than that found in the field or other regions (e.g. Lodieu, Hambly & Jameson 2006; Lodieu et al. 2007b; Slesnick, Hillenbrand & Carpenter 2008). If confirmed, Upper Scorpius would contain more brown dwarfs than other regions (like Orion). There are several attempts to look at the low-mass end of the IMF in IC 348 (Alves de Oliveira et al. 2013), Pleiades (Lodieu, Deacon & Hambly 2012), ϱ Ophiuchi (Mužić et al. 2012; Alves de Oliveira et al. 2012), Upper Scorpius (Lodieu, Dobbie & Hambly 2011), σ Orion (Peña Ramírez et al. 2012).

1.3.3 The halo low-mass mass function

The substellar halo MF also has important implications for our understanding of stellar and substellar formation and evolution as a function of metallicity and time, and reveals the conditions in which the different populations of stars formed. The most recent work on the subdwarf LF and MF extended down to masses of 0.11 $M_{\odot}$ (e.g. de Marchi & Paresce 1995; Richer et al. 2002; Digby et al. 2003; Gould 2003; Chabrier 2003), but the ultracool halo LF and MF across the substellar limit has not been measured. Figure 1.20 shows the LF and MF of subdwarfs with mass between 0.11 - 0.70 $M_{\odot}$ from Chabrier (2003). The form of the substellar mass distribution in the halo is currently

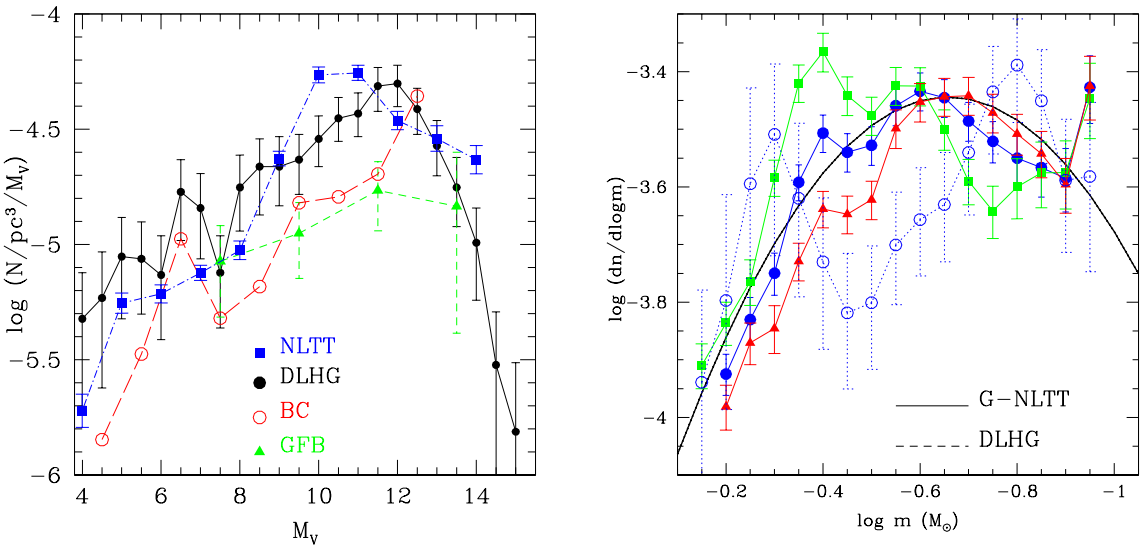

Figure 1.20: The subdwarf luminosity (left) and mass (right) function. Solid dots (solid line): Dahn et al. (1995); solid squares (dash-dot line): NLTT survey Gould (2003); open circles (long-dash line): Bahcall & Casertano (1986); triangles (short-dash line): HST Gould, Flynn & Bahcall (1998). All LFs have been recalculated with a completion factor based on the Casertano, Ratnatunga & Bahcall (1990) kinematic model. Mass function of the Galactic spheroid, based on the NLTT (Gould 2003) LF (solid lines) and the Baraffe et al. (1997) mass-M_V relationship, for three metallicities: [M/H] $= -1.5$ (triangles), -1.0 (circles) and -0.5 (squares), respectively. Dotted line: same calculation based on Dahn et al. (1995) LF and [M/H] $= -1.0$ models. Solid line: parameterization given by equation: $\xi(\log m) = 3.6 \times 10^{-4} \exp\{-\frac{[\log m - \log(0.22 \pm 0.05)]^2}{2 \times 0.33^2}\}$, $m \leq 0.7\ M_\odot$. The figures are from Chabrier (2003).

an unknown. No evidence for large population of BD in the halo has been found so far (Alcock et al. 2000). Tisserand et al. (2007); Wyrzykowski et al. (2009) conclude that less than 10% of the mass of Galactic halo could be in the form of compact objects with likely masses between 0.15 and 0.9 $M_{\odot}$. It can be integrated to estimate the number density of subdwarfs in the spheroid and hence determine the contribution of low-mass objects to the baryonic "dark" mass fraction of the Galaxy.

The direct determination of the halo LF is very difficult, since the halo population is much sparser within the disk (than disk stars), and must be separated kinematically. Proper motions surveys (Salim & Gould 2003; Munn et al. 2004; Pokorny et al. 2004; Lodieu et al. 2012c) supply a powerful tools to identify the halo population. It is an even bigger challenge to measure the halo BD MF. Halo BDs will be very old and very faint, so difficult to detect out to large distances. There are only one halo BD know so far, and the new population is not been understood well both observationally and theoretically.

1.4 Observational techniques

After the theoretical prediction of brown dwarf by Kumar (1963b), people searched for BDs for more than 30 years until first discoveries in 1995, after NIR detector developments in the late 1980s. GD 165B is the first BD presented as a candidate by Becklin & Zuckerman (1988). Its spectrum was first observed in 1991 by Kirkpatrick, Henry & Liebert (1993). Then confirmed as a BD by Kirkpatrick et al. (1999a). The first announced BD, Teide 1 was discovered in the Pleiades open cluster by Rebolo, Zapatero Osorio & Martín (1995) and is an M8 type young BD. The first methane BD found was the T6.5 type Gliese 229 B by Nakajima et al. (1995); Oppenheimer et al. (1995). Current, around 1500 L and T type BDs been discovered thanks to modern larger scale optical and infrared surveys (see Section 1.4.3).

1.4.1 Identification of field ultracool dwarfs

In this section I will talk about observational techniques used to identify UCDs and UCD binary systems. These techniques are developed through an appreciation of the observational properties of UCDs. More details of identification techniques used in the thesis are described in Chapters 2, 3 and Zhang et al. (2011).

Optical drop-out

UCDs emitted most of their light in infrared bands, thus they have late spectral types and appear very red in the HRD (Figure 1.1). Figure 1.21 shows the optical and NIR colours of M, L and T type dwarfs. Optical-NIR colours generally get redder as spectral type changes from M to L to T. The $r-i$ colour reverses at M9 due to weakening of TiO absorption. The $z-K$ and $J-K$ colours turn around at L8 due to increasing strength of methane absorption band in the K band. The $i-z, i-J$ and $z-J$ sequences are all close to monotonic with spectral type. Optical-NIR colours are the most effective method to select UCDs in large scale surveys like 2MASS (e.g. Kirkpatrick et al. 1999b; Burgasser et al. 2003c; Cruz et al. 2003), SDSS (e.g. Chiu et al. 2006; Zhang et al. 2009; Zhang et al. 2010), UKIDSS (e.g. Lodieu et al. 2007b; Burningham et al. 2010b; Day-Jones et al. 2013) and WISE (e.g. Kirkpatrick et al. 2011).

Proper motion

Proper motion (PM) of a star is its angular change in position over time as seen from the center of mass of the solar system. Intrinsically faint objects must be close by to be detected and thus have high PM. BDs are are numerous objects formed in the same way as stars, they have similar space velocity but much fainter than stars (Figure 1.1). Thus observable BDs are closer and have larger PMs than stars. PM is a powerful method to distinguish BDs from distance stars and galaxies. Various PM surveys (e.g. Luyten 1979a; Luyten 1979b; Pokorny, Jones & Hambly 2003; Pokorny et al. 2004; Munn et al. 2004) have been used to search for cool stars and BDs (e.g. Lépine, Shara & Rich 2003a; Lépine 2005; Lépine & Shara 2005; Lépine 2008; Lodieu et al. 2005; Deacon et al. 2011; Reid & Cruz 2002; Ruiz et al. 2001; Scholz, Meusinger & Jahreiß 2005; Scholz et al. 2009; Scholz et al. 2011; Zhang et al. 2009; Liu et al. 2011b; Luhman 2013).

1.4.2 Identification of ultracool binaries

A variety of observational techniques have been employed to search for UCD companions to main sequence and evolved stars separated closely and widely. More details of optical drop-out technique used in the thesis are described in Chapters 4, 5.

Direct imaging

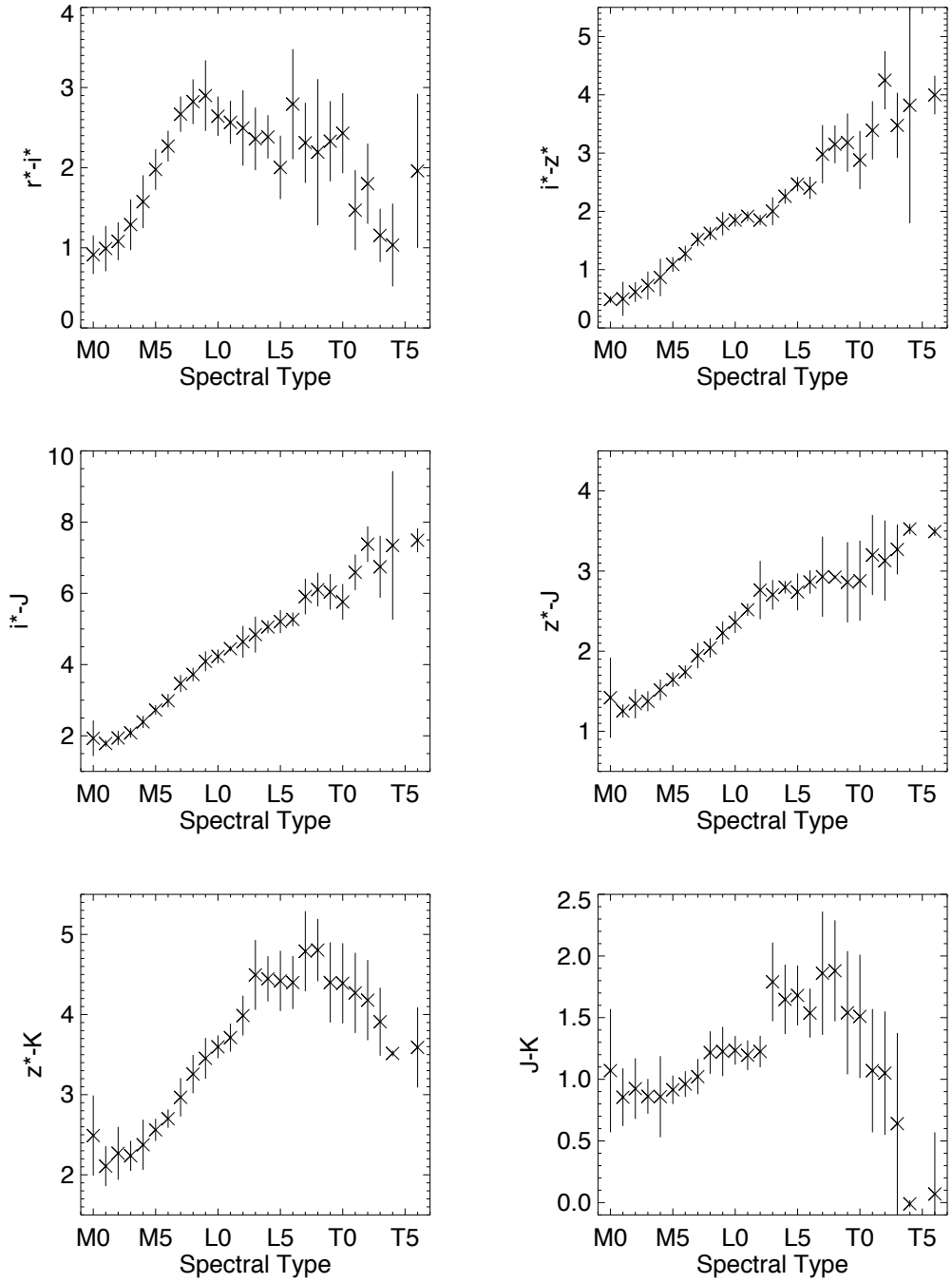

Figure 1.21: Red and NIR colours of M, L and T type dwarfs. The figures are from Hawley et al. (2002).

William Herschel was the first to observe secular motions of close star pairs consistent with orbital motion, and refer to these physically associated stars as "binary systems" (Herschel 1803). The search for low-mass substellar companions to stars, received new impetus in the early 1990's with the introduction of large-area digital detectors that were sensitive in the NIR. Adaptive Optics (AO) has been used in astronomy since the 1990's. The technique dramatically sharpens images blurred by the turbulent atmosphere, reducing apparent angular sizes of point sources. Additional scattered light suppression and contrast enhancement may be achieved with the use of a coronagraph which can block light from the primary star. These techniques were used to discover Gliese 229B (Nakajima et al. 1995). High resolution and contrast imaging has been widely used in the search for UCD binaries and exoplanets (e.g. McCaughrean et al. 2004; Chauvin et al. 2004; Chauvin et al. 2012; Marois et al. 2008; Marois et al. 2010; Currie et al. 2010; Labadie et al. 2011; Liu et al. 2011b; Dupuy & Liu 2012). High-spatial resolution imaging with Hubble Space Telescope has also been used to find ultracool binaries (e.g. Burgasser et al. 2003d; Burgasser et al. 2006b; Kalas et al. 2008; Burgasser, Bardalez-Gagliuffi & Gizis 2011; Song et al. 2006). Lucky imaging also provide a effective method to identify ultracool binaries (e.g. Lodieu, Zapatero Osorio & Martín 2009; Bergfors et al. 2010; Femenía et al. 2011).

Common proper motion

The relationship between period and semi-major axis of an orbiting companion is described with Kepler's third law $P^2 \propto a^3$, where P is the orbital period and a is the semi-major axis. The orbital period of wide binary systems ($\gtrsim$ 100 AU) is very long – a binary with mean separation of $\sim$ 100 au would have period of $\sim$ 1000 years. Since both companions of a wide binary system have PM, and their PM is much larger than the change of their relative position (their orbital motion). Thus they appear to have common proper motion (CPM). Statistically two single stars with separation less than a few arcmins and CPM by random chance is very unlikely. CPM can thus be used to identify wide UCD binary systems (e.g. Pinfield et al. 2006; Pinfield et al. 2012; Zhang et al. 2010; Faherty et al. 2010; Burningham et al. 2010a; Day-Jones et al. 2011a; Luhman, Burgasser & Bochanski 2011; Allen et al. 2012; Gomes et al. 2013).

Other methods used to find UCD or exoplanet companions include: measurement of the radial velocity variation of the primary star caused by the gravity of companions; as-

trometric irregularities in the tangential motion of the primary star; NIR excess radiation of white dwarfs caused by UCD companions; eclipses of binaries; UCD spectral synthesis.

1.4.3 Large scale surveys

The discovery of ultracool dwarf populations largely benefits from modern large scale surveys. The magnitude limits of important large scale surveys are listed in Table 1.1. Combining data from these surveys provides a powerful tool for the identification of UCDs.

Sloan Digital Sky Survey

The Sloan Digital Sky Survey (SDSS) uses a dedicated 2.5 m telescope located at Apache Point Observatory (APO) in New Mexico. It is equipped with a large format mosaic CCD camera to image the sky in five optical bands (u, g, r, i, z), and two digital spectrographs to obtain the spectra of galaxies, quasars and late-type stars selected from the imaging data (York et al. 2000; Stoughton et al. 2002). The eighth data release (DR8) of SDSS includes 14555 deg^2 of imaging data, and 9274 deg^2 of sky coverage for which spectroscopy has been obtained. There are over 1.84 million spectra in total, including 0.6 million stars, 0.13 million quasars and 0.95 galaxies. Figure 1.22 shows the SDSS sky coverage of of DR8 in imaging and spectroscopy (Aihara et al. 2011). The SDSS has largely contributed to UCD discoveries (e.g. Strauss et al. 1999; Fan et al. 2000; Tsvetanov et al. 2000; Leggett et al. 2000; Schneider et al. 2002; Hawley et al. 2002; Chiu et al. 2006; Metchev et al. 2008; Scholz et al. 2009; Zhang et al. 2009; Zhang et al. 2010; Schmidt et al. 2010b).

Two Micron All Sky Survey

The two Micron All Sky Survey (2MASS) is an all-sky survey, combining observations from two 1.3-m telescopes (at Mt. Hamilton, Arizona, and Cerro Tololo, Chile) to cover both northern and southern hemispheres (Cutri et al. 2003; Skrutskie et al. 2006). 2MASS used three HgCdTd 256-square arrays to obtain data simultaneously in the J, H and K_S passbands. First light for the survey was in June 1997 in the North and March 1998 in the South. Observations were completed in 2001, and the final catalogue was released in January 2003. 2MASS have had an enormous impact on our understanding of low-mass stars and brown dwarfs (e.g. Kirkpatrick et al. 1999b; Kirkpatrick et al. 2000;

Table 1.1: Magnitude limits of large scale surveys

SDSS filter	u	g	r	i	z
Effective wavelength (μm)	0.3551	0.4686	0.6166	0.7480	0.8932
Magnitude[c] (AB)	22.0	22.2	22.2	21.3	20.5
Sky coverage (deg^2)	[a]14555				
2MASS filter			J	H	K_s
Effective wavelength (μm)			1.25	1.65	2.16
Magnitude[d] (Vega)			15.8	15.1	14.3
Sky coverage (deg^2)	[a]41252				
UKIDSS filter	Z	Y	J	H	K
Effective wavelength (μm)	8.83	1.0305	1.2483	1.6313	2.2010
ULAS magnitude (Vega)	—	20.16	19.56	18.81	18.19
Sky coverage (deg^2)	[b]4000				
VISTA filter	Z	Y	J	H	K_s
Effective wavelength (μm)	0.878	1.021	1.254	1.646	2.149
VHS magnitude (Vega)	—	21.2	21.2	20.6	20.0
Sky coverage (deg^2)	[b]20000				
VIKING magnitude (Vega)	23.1	22.3	22.1	21.5	21.2
Sky coverage (deg^2)	[b]1000				
WISE filter		W1	W2	W3	W4
Effective wavelength (μm)		3.4	4.6	12	22
Magnitude (Vega)		16.5	15.5	11.2	7.9
Sky coverage (deg^2)	[a]41253				

[a] Survey is completed.

[b] Planed survey area to complete.

[c] 95% detection repeatability for point sources

[d] 10 σ point-source detection.

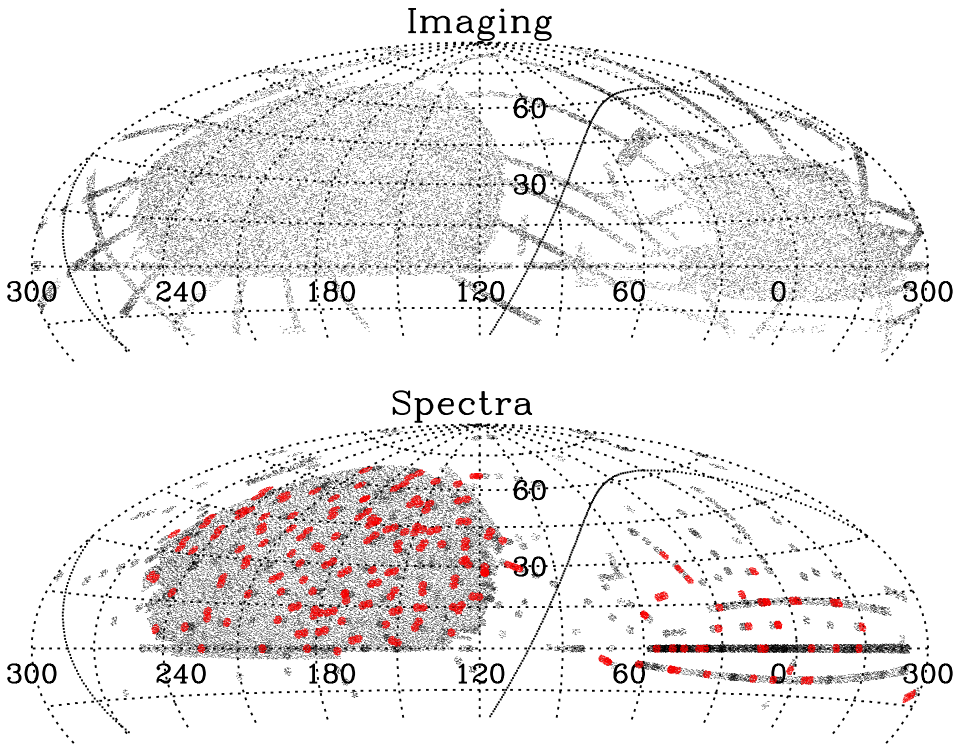

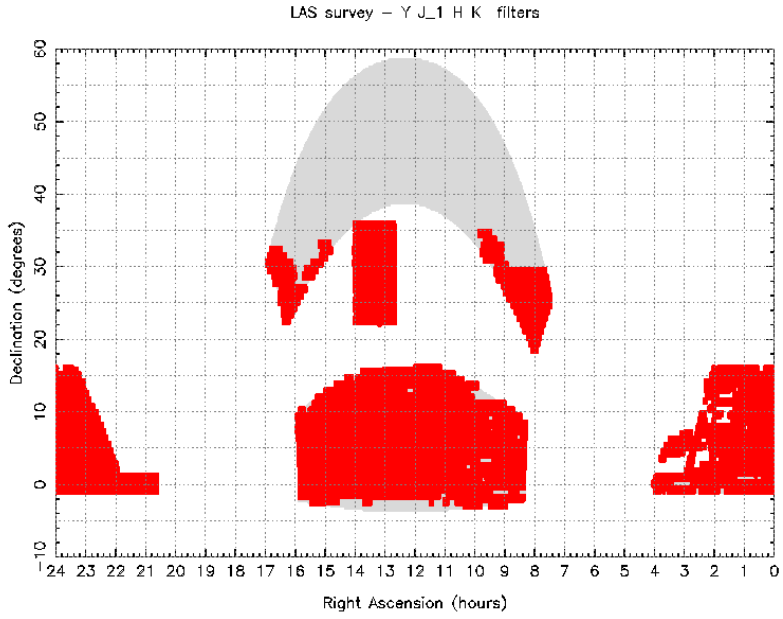

Figure 1.22: Top two panels: The sky coverage of DR8 in imaging (upper) and spectroscopy (lower). The Galactic plane is the solid curve that snakes through the figure. The red regions in the lower panel show the coverage of the SEGUE-2 plates. Figures are from Aihara et al. (2011). Bottom panel: The sky coverage of DR9 of UKIDSS Large Area Survey in four filters (3176.7 deg^2). The gray area is the planed survey area. The figures are from Aihara et al. (2011) and WSA: http://surveys.roe.ac.uk/wsa/.

Kirkpatrick et al. 2010; Kirkpatrick et al. 2006; Burgasser et al. 2000a; Burgasser et al. 2000b; Burgasser et al. 2002; Burgasser et al. 2003c; Burgasser et al. 2003a; Burgasser, McElwain & Kirkpatrick 2003; Burgasser et al. 2004; Burgasser, Cruz & Kirkpatrick 2007; Gizis, Kirkpatrick & Wilson 2001; Cruz et al. 2003; Cruz et al. 2007; Tinney et al. 2005; Ellis et al. 2005; Reid et al. 2008; Looper et al. 2008; Zhang et al. 2009; Cushing et al. 2009).

UKIRT Infrared Deep Sky Survey

The UKIRT Infrared Deep Sky Survey (UKIDSS, Lawrence et al. 2007) use the Wide Field Camera on the United Kingdom Infrared Telescope (UKIRT) on Mauna Kea, Hawai'i, to survey ∼7000 square degrees of sky at combination of Z, Y, J, H and K bands. It is made up of five surveys: the Large Area Survey (LAS; Ukidss 2012), the Galactic Plan Survey (GPS; Lucas et al. 2008), the Galactic Clusters Survey (GCS), the Deep Extragalactic Survey (DES) and the Ultra Deep Survey (UDS). The LAS is contributing significantly to the study of substellar objects, and has discovered over 100 T dwarfs (e.g. Kendall et al. 2007; Lodieu et al. 2007b; Lawrence et al. 2007; Warren et al. 2007; Chiu et al. 2008; Pinfield et al. 2008; Deacon et al. 2009; Scholz 2010b; Scholz et al. 2012; Burningham et al. 2008; Burningham et al. 2009; Burningham et al. 2010a; Burningham et al. 2010b; Goldman et al. 2010; Murray et al. 2011. LAS is observing 4000 deg^2 of the sky. The 9th data release of the LAS has covered over 3000 deg^2 in Y, J, H and K bands (see, bottom panel of Figure 1.22). The LAS is 3–4 magnitudes deeper than 2MASS, thus have a much larger survey volume. Since BDs emit most of their light in NIR wavelength, thus the LAS also have a larger survey volume for BDs, particular for T dwarfs than SDSS. Other UKIDSS sub-surveys also have contribution of brown dwarfs discovery e.g. GPS (Lucas et al. 2010; Burningham et al. 2011), GCS (Lodieu et al. 2007a; Lodieu et al. 2009a; Lodieu, Dobbie & Hambly 2011; Lodieu, Deacon & Hambly 2012; Lodieu et al. 2012b; Zhang et al. 2010) and DES (Lodieu et al. 2009b).

VISTA Public Surveys

The Visible and Infrared Survey Telescope for Astronomy (VISTA) is a UK built 4m survey telescope on Cerro Paranal, Chile. During its first five years of operation VISTA is mainly dedicated to performing six public surveys, which began taking data in late 2009 (Arnaboldi & Retzlaff 2011; Arnaboldi et al. 2012). The Cambridge Astronomy Surveys

Unit reduce data from VISTA and the Wide-field Astronomy Unit in Edinburgh maintain the VISTA Science Archive (Cross et al. 2012). These six publics surveys including the Vista Kilo-Degree Infrared Galaxy Survey (VIKING), the Vista Hemisphere Survey (VHS), the VISTA Variables in the Via Lactea (VVV; Saito et al. 2010; Saito et al. 2012), the VISTA Magellanic Survey (VMC; Cioni et al. 2011), the Vista Deep Extragalactic Observations survey (VIDEO; Jarvis et al. 2012) and the UltraVISTA survey.

Most of the UCD discoveries will come from two surveys, VIKING and VHS (e.g. Lodieu et al. 2012a) because they have largest survey volume and optical counterparts. The VHS is the largest survey and will image the rest of the southern hemisphere in the Y, J, H and K filters. VIKING will cover three times the volume of the UKIDSS Large Area Survey, providing data in the Z, Y, J, H and K_s filters. The Dark Energy Survey (DES; Banerji et al. 2008), the VST ATLAS and Kilo-Degree Survey (KIDS) surveys (Arnaboldi et al. 2007) will provide major optical counterparts for the VHS and VIKING.

Wide-field Infrared Survey Explorer

The Wide-field Infrared Survey Explorer (WISE; Wright et al. 2010; Cutri & et al. 2012) is an earth-orbiting NASA mission to survey the entire sky at wavelengths of 3.4, 4.6, 12 and 22 μm (W1, W2, W3 and W4 band respectively). Detection limit of each band is listed in Table 1.1. Two main science goals for WISE are red galaxies and cool BDs. The two shortest wavelength bands of WISE were specifically designed for optimum cool BD detection. Cool BDs emit most of it's flux at W2 band (see Figure 1.14., right) thus have very red W1 – W2 colour which can be used to separated them from red dwarfs and galaxies (e.g. Figure 12 of Wright et al. 2010). With good match to 2MASS, WISE is very useful to identify L dwarfs. But is particularly sensitive to very late-type T dwarfs, and indeed has recently discovered over 100 BDs include the first Y dwarfs (Mainzer et al. 2011a; Burgasser et al. 2011; Loutrel et al. 2011; Gelino et al. 2011; Scholz et al. 2011; Kirkpatrick et al. 2011; Kirkpatrick et al. 2012; Cushing et al. 2011; Liu et al. 2011a; Griffith et al. 2012; Pinfield et al. 2012; Tinney et al. 2012; Mace et al. 2013). The added adaptation of NEO-WISE facilitates is used to search for solar systems objects (Mainzer et al. 2011b).

Other surveys

The deep near-infrared southern sky survey (DENIS; Epchtein 1997) scan the sky in three bands down to $I = 18.0, J = 16.0, K_s = 13.5$ with an ESO 1-metre telescope. The DENIS has contributed to the early BD discovery (Delfosse et al. 1997; Tinney, Delfosse & Forveille 1997; Tinney et al. 1998; Kendall et al. 2004; Martín et al. 2010). The Canada-France Brown Dwarfs Survey is conducted with the MegaCam on the Canada-France-Hawaii Telescope (Delorme et al. 2008; Delorme et al. 2010; Delorme et al. 2012). The Panoramic Survey Telescope and Rapid Response System (Pan-STARRS; Kaiser et al. 2010; Tonry et al. 2012; Schlafly et al. 2012) scan the sky with an 1.4 billion pixel cameras on four 1.8m telescopes in five bands (g, r, i, z, y). The first telescope PS1 started to produced data since 2012 and has been used to identify BDs (Deacon et al. 2011; Deacon et al. 2012a; Deacon et al. 2012b; Liu et al. 2011a).

1.5 Motivation and thesis structure

Low-mass stars and BDs is a rapidly increasing and very active field of astronomy. The existence of BDs was predicted in early 1960s (Kumar 1963a; Hayashi & Nakano 1963). The first BDs were discovered three decades later (Rebolo, Zapatero Osorio & Martín 1995; Nakajima et al. 1995). Atmospheric and evolutionary models of low-mass stars and BDs are established in late 1990s (Baraffe et al. 1995; Tsuji et al. 1996; Burrows et al. 1997; Allard et al. 1997). More and more BDs were discovered thanks to modern optical and NIR surveys (see Section 1.4.3) from late 1990s (e.g. Delfosse et al. 1997; Kirkpatrick et al. 1999b; Burgasser et al. 2002; Chiu et al. 2006; Burningham et al. 2010b; Kirkpatrick et al. 2011). Theoretical models are being challenged by new discoveries e.g. low temperature BDs (Cushing et al. 2011), low-metallicity BDs (Burgasser et al. 2008b), L/T transition BDs (Burgasser 2007; Luhman 2013) and binaries (Burningham et al. 2010a).

The aim of this project is to discover and characterize UCDs in the Galactic disk and the halo, and explore our knowledge of ultracool dwarf science for metal-poor objects by discovering a sample of UCD benchmarks (Section 1.2.4) with solar and subsolar metallicity. UCDs and UCSDs discovered here will aid the calibration of UCD and UCSD properties, allowing the models to be refined, enabling them to reproduce observable properties with greater accuracy than is currently possible.

The thesis is split into seven chapters, outlining the main project components I have been working on over the course of this Ph.D, and are organized in the following structure:

Chapter 1: Presents the important background science to place the thesis work in context, and will be referred back to in subsequent discussion.

Chapter 2: This chapter describes techniques used to select UCDs in the SDSS, 2MASS and UKIDSS. I derive updated colour-spectral type relations for L and T dwarfs with SDSS and 2MASS magnitudes. I present 59 new nearby late-type M and L dwarfs and 129 L dwarfs candidates selected from the imaging catalogue of the 7th Data Release of SDSS. The main results of this work are published in the *"Astronomy & Astrophysics"* (Zhang et al. 2009).

Chapter 3: This chapter describes current research on L subdwarfs and their properties. I also present my latest results of a search for L subdwarfs based on the SDSS, UKIDSS and ground based large telescopes. I discovered three L subdwarfs with spectral types of sdL3, sdL7 and esdL6. I also re-examined spectral types and metal classes of known L subdwarfs and discuss the properties of halo BDs.

Chapter 4: In this chapter I present the discovery of 806 UCDs, including 34 new L dwarfs, from their SDSS *riz* photometric and spectroscopic data. I also present techniques used to search for UCDs in wide binary systems and describe my discovery of nine UCDs in widely separated binary systems, including the first L dwarf + giant binary system, η Cancri AB. The main results of this work are published in the *"Monthly Notices of the Royal Astronomical Society"* (Zhang et al. 2010).

Chapter 5: In this chapter I present the selection techniques for red subdwarfs and their binary systems. I present the discoveries from this project as well as high lighting several additional objects of interests. I find 30 wide and 15 partially resolved red subdwarf binary systems. I estimate the binary fraction of M subdwarfs. I fit relationships between spectral type and absolute magnitudes of r, i, z, J, H, K bands for M and L subdwarfs. I present a sample of 1800 M subdwarfs with constrained UVW space velocities. A paper on this work is accepted to publish in the *"Monthly Notices of the Royal Astronomical Society"* (Zhang et al. 2013).

Chapter 6: In this chapter I give a summary of this thesis, describe the main results and conclusions of this project.

Chapter 7: Finally I describe my research plans in the future.

Chapter 2

Ultra-cool dwarfs: new discoveries, proper motions, and improved spectral typing from SDSS and 2MASS photometric colors

2.1 Abstract

In this chapter I develop and implement techniques to identify UCDs in the large scale surveys SDSS, 2MASS and UKIDSS. These techniques are optimized to account for the observational characteristics of UCDs as reserved in Chapter 1. I initially identified candidates in the seventh data release of the SDSS with $i-z$ and $r-z$ colours. I also obtain proper motion data from SDSS, 2MASS, and UKIDSS and improve spectral typing from SDSS and 2MASS photometric colors. I selected UCD candidates from the SDSS DR7 with new photometric selection criteria, which are based on a parameterization study of known L and T dwarfs. The objects are then cross-identified with the 2MASS and the Fourth Data Release of the UKIDSS. I derive proper motion constraints by combining SDSS, 2MASS, and UKIDSS positional information. In this way I am able to assess, to some extent, the credence of my sample using a multi epoch approach, which complements spectroscopic confirmation. Some of the proper motions are affected by short baselines, but, as a general tool, this method offers great potential to confirm faint L dwarfs as UKIDSS coverage increases. In addition I derive updated color-spectral type relations

for L and T dwarfs with SDSS and 2MASS magnitudes. I present 59 new nearby M and L dwarfs selected from the imaging catalog of the SDSS DR7, including proper motions and spectral types calculated from the updated color-spectral type relations, and obtain proper motions from SDSS, 2MASS, and UKIDSS for all of my objects. I also present 127 L dwarfs candidates, some of them recently been confirmed as L dwarfs by Kirkpatrick et al. (2011).

2.2 Publication, Zhang et al. 2009, A&A, 497, 619-633

I started this work for my MSc at the Chinese Academy of Sciences and finished it off during my PhD. This work has been published in the journal of the *"Astronomy & Astrophysics"* (Zhang et al. 2009, bond at the end of the thesis).

Chapter 3

Discovery and characterization of L subdwarfs of the Galactic halo

L subdwarfs are a mixture of lowest mass stars and brown dwarfs with subsolar abundance and effective temperatures less than $\sim$ 2500 K. L subdwarfs are the low mass end of the stellar Population II (Figure 1.2). They formed at the beginning of the Galaxy, as fully convective objects (Reiners & Basri 2009) they remain stable as homogeneous, retaining the original chemistry of the early Galaxy. They are poorly studied due to the lack of known L subdwarfs.

3.1 Observation of L subdwarfs

There are only seven L subdwarfs discovered and published in the literature (Burgasser et al. 2003a; Burgasser 2004b; Cushing et al. 2009; Sivarani et al. 2009; Lodieu et al. 2010; Lodieu et al. 2012c). Only 2MASS J05325346+8246465 (2MASS J0532) has estimated mass (according to theoretical models of Burrows et al. 2001 and Baraffe et al. 1997) just blow the sustained hydrogen burning limit, and is therefore a possible substellar subdwarf or halo brown dwarf. Four metal-poor L dwarfs have also been reported (Schmidt et al. 2010a; Bowler, Liu & Dupuy 2010; Burningham et al. 2010a; Kirkpatrick et al. 2010), have metallicity between $-0.4 \lesssim$ [M/H] $\lesssim -0.3$, thus should not be classified as L subdwarfs. Spectral types of L subdwarfs have been assigned by comparing their optical spectra with that of L dwarfs (See Figure 1.9). L subdwarfs are kinematically associated with the Galactic halo and thick disk, thus have higher space velocities, high proper motions,

tangential velocities and radial velocities than disk dwarfs. L subdwarfs are expected to have bluer optical and near-infrared colours (e.g. $i-z, i-J, z-J, J-K$) than L dwarfs with same $T_{\rm eff}$ due to enhanced collision-induced H_2 absorption (CIA) which suppresses flux at K and H bands.

3.2 Searching for L subdwarfs in UKIDSS and SDSS

I combine the capability of the SDSS in optical, with the UKIDSS and VISTA NIR surveys. I use combined optical-infrared colours to select L subdwarf candidates, measure proper motions via epochs from different data sets, then estimate distances base on relationships of colours and absolute magnitudes from ultracool subdwarfs with parallax distance measurements. Finally I use reduced proper motions and tangential velocities to remove contamination of disk dwarfs. Final confirmation of our candidates is made via spectroscopy.

3.2.1 Selection of L subdwarf candidates

I conduct the search for L subdwarf candidates by combining the SDSS and UKIDSS LAS (ULAS) databases. I use both photometric and proper motion methods to select L subdwarf candidates from the 9th data release of ULAS and the 8th data release of SDSS which have an overlap of about 3000 square degrees. I required five colour cuts, $Y-J>0.6$ AND $J-K<Y-J$ AND $3.0<i-J<6.0$ AND $J-K<0.2*(i-J)$ AND $1.4<z-J<3.2$ and one magnitude cut, $12<J<18$ in ULAS and SDSS. These criteria are based on location of six known L subdwarfs and metal-poor L dwarfs (observed in ULAS) in the $i-j$, $J-K$ diagram and consideration of locations of L dwarfs, T dwarfs and normal stars.

Figure 3.1 shows the $i-J$ vs. $J-K$ colours of known and new L subdwarfs. Main sequence stars, late-type M dwarfs (West et al. 2008), L and T dwarfs (DwarfArchives.org) are also plotted for comparison. Eight late-type M subdwarfs from Lépine & Scholz (2008) are plotted to indicate the trend of low metallicity objects (M subtype is labelled). 2MASS photometry of L subdwarfs (cyan filled circles) are converted to MKO system based on colour difference between MKO and 2MASS of L dwarfs calculated by Hewett et al. (2006). I estimated $i-J$ colours for three objects (with magenta labels) which were not in SDSS sky coverage, according to L subdwarfs with similar spectral types. My colour selection

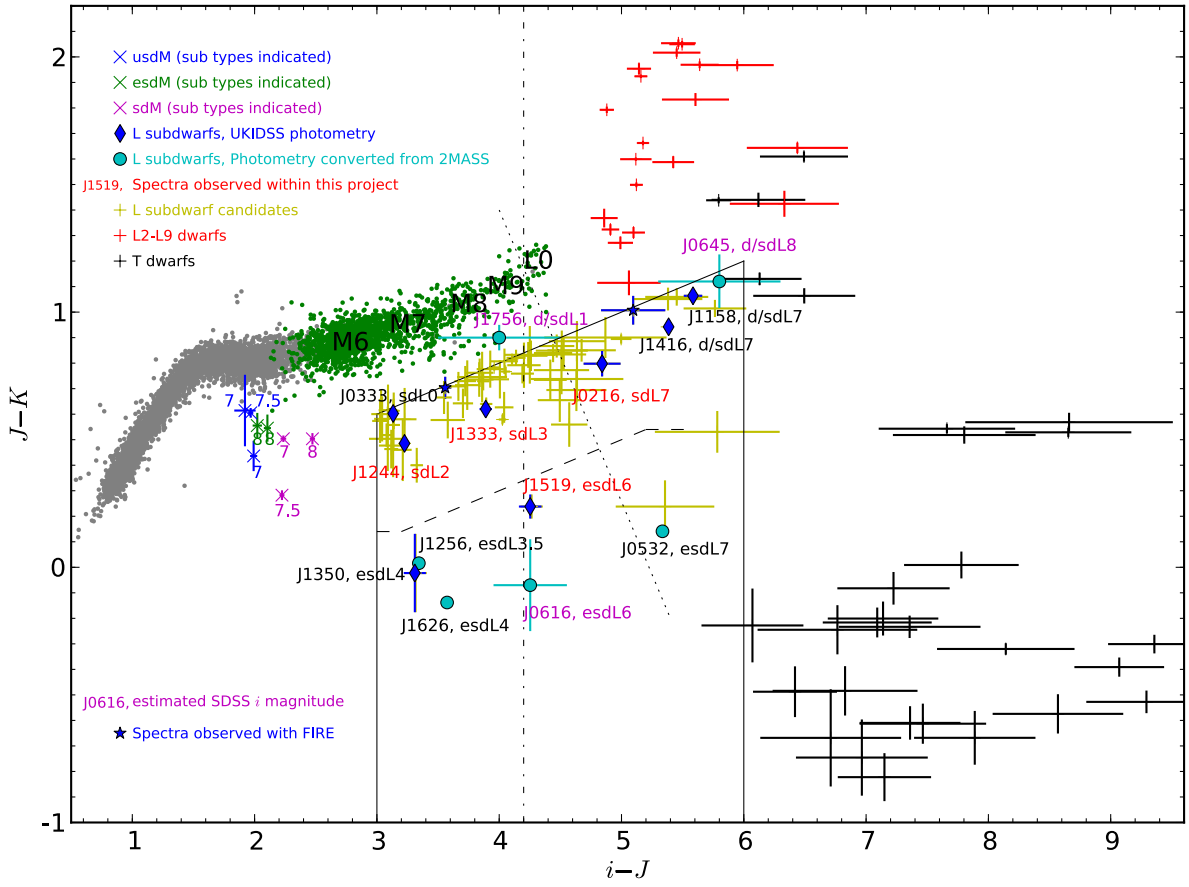

Figure 3.1: The $i-J$ vs. $J-K$ colours of L subdwarfs. Grey dots are 5000 point sources selected from 10 square deg area of UKIDSS with $14 < J < 16$. Green dots are 1820 spectroscopically confirmed late-type M dwarfs (spectral type indicated) from West et al. (2008). The solid lines region indicates my $i-J$ and $J-K$ colour cuts. The dashed line shows the likely boundary of L subdwarf and extreme L subdwarf (Section 3.3.1). A dash-dot line indicates the likely substellar subdwarf gap predicted by theoretical models (Section 3.3.4). A dotted line indicate the minimum substellar subdwarf boundary based on field BD (L0 dwarfs) and the 0.08 $M_{\odot}$ esdL7 halo BD 2MASS J0532 (Section 3.3.4). I converted 2MASS magnitudes to MKO magnitudes for L subdwarfs not covered in UKIDSS (cyan filled circles). See Table 3.1 and 3.2 for photometric and astrometric parameters of L subdwarfs in this plot.

criteria is designed to select mid to late-type L subdwarfs, avoiding contamination from stars, L dwarfs and T dwarfs. Some contamination of T dwarfs at the red $i-J$ extreme, L dwarfs at the red $J-K$ extreme, and stars with scattered colours of red $J-K$ colour is expected. Table 3.1 and 3.2 shows the photometric and astrometric properties of these known L subdwarfs and metal poor L dwarfs.

L subdwarfs show in red in the SDSS *gri* colour images. I visually inspected all candidates in SDSS images with Navigate to remove mis-matches and objects which are in blue, yellow and orange. For objects which survived all colour cuts, I measured their proper motions based on ULAS and SDSS epochs (following Zhang et al. 2009). Figure 3.2 shows reduced proper motions of L subdwarf candidates. I selected 66 candidates, three are known to be L subdwarfs (sdL0, sdL0.5, sdL5), and two are known metal poor L dwarfs. I have followed up and confirmed four L subdwarfs including an independently identification of a known L subdwarf announced recently (Lodieu et al. 2012c). Thus I have 58 targets left to follow up. I divided our targets into four priority groups based on their $i-J$ and $J-K$ colours and proper motions. Nine targets have priority 1 (high), 13 priority 2, 22 priority 3 and 14 priority 4. Table 3.3 shows the list of my L subdwarf candidates.

To confirm they are halo objects I estimated their tangential velocities. First I assumed that they are normal disc dwarfs and estimated their distance according to the M_i versus $i-J$ relationship of M and L dwarfs from Hawley et al. (2002). With these distances and their proper motions, the estimated tangential velocities are extremely high (3-4 times that of cool subdwarfs) and the logical explanation is that most of them are L subdwarfs and their distances are over estimated since they were treated as brighter M6-L0 dwarfs when I use the relationship of Hawley et al. (2002). Because mid L subdwarfs have similar $i-J$ colour with M6-L0 dwarfs (e.g. Figure 3.1) but much fainter (see Zhang et al. 2013). Thus the estimated distances were much larger. When I assume they are L subdwarfs I get reasonable halo tangential velocities distribution. I estimated their spectral type based on their $i-J$ colours according to five known L subdwarfs. Then estimate their distances based on M_{JHK} and spectral types in Cushing et al. (2009). The accuracy of the distances and kinematics, and the spectral character of the objects themselves needs to be substantially improved. In order to properly determine halo membership I need spectroscopy - (i) to confirm that the objects have the spectral characteristics of known UCSDs, and (ii) to allow us to determine more accurate spectroscopic distances to give better tangential velocities.

There are already eight confirmed L subdwarfs and blue L dwarfs within my sample (Blue diamonds in Figure 3.1). Five of them are known from the literature (2MASS J11582077+0435014, SDSS J141624.08+134826.7, ULAS J135058.85+081506.8, ULAS J033351.10+001405.8, ULAS J124425.75+102439.3). Three are new from this project. One of my targets was confirmed as L subdwarf with SDSS optical spectrum (SDSS J133348.24+273508.8; see Section 3.2.2.1), one was confirmed with an IMACS optical spectrum (ULAS J124425.75+102439.3; see Section 3.2.2.2). Two were confirmed with X-shooter (ULAS J021642.97+004005.6, ULAS J151913.03−000030.0; see Section 3.2.2.3 and 3.2.2.4). Another two targets were observed with FIRE on Magellan Telescope on 8 May 2012. Fifteen and twenty six hours time of the OSIRIS on the Gran Telescopio CANARIAS (GTC) were awarded to this project in 2012B and 2013A to follow up more candidates.

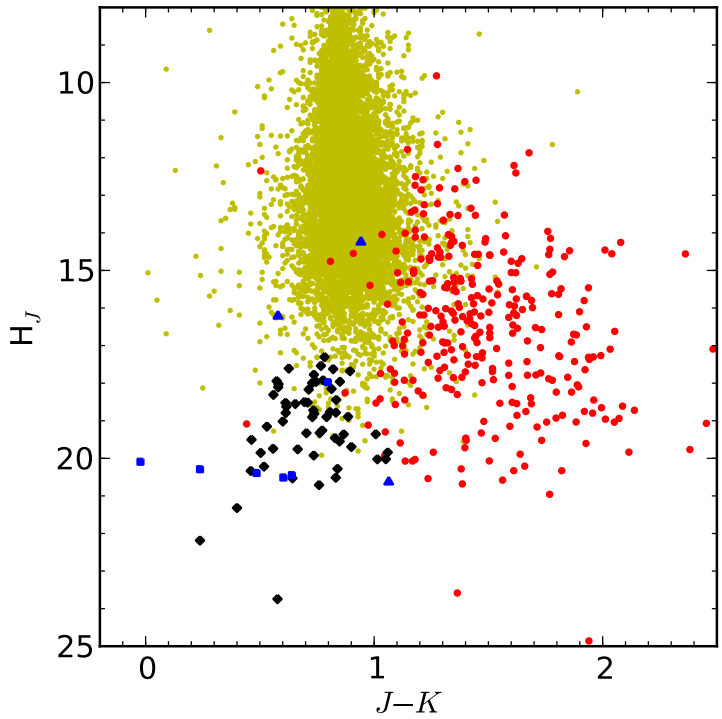

Figure 3.2: The reduced proper motions of L subdwarf candidates. Yellow dots are 9024 M dwarfs within $\sim$ 300 pc (West et al. 2008). Red dots are 303 L dwarfs from DwarfArchives.org. Blue triangles are three blue L dwarfs. Blue squares are confirmed L subdwarfs. Black diamonds are candidates been following up.

Table 3.1: Photometry of L subdwarfs and mild subdwarfs

Name	SpT[a]	SpT[b]	SDSS i	SDSS z	J	H	K	Ref.
2MASS J05325346+8246465	sdL7	esdL7	20.37±0.05	17.58±0.02	[c]15.18±0.06	14.90±0.09	14.92±0.15	1
2MASS J16262034+3925190	sdL4	esdL4	17.90±0.01	16.16±0.01	[c]14.44±0.03	14.53±0.05	14.47±0.07	2
SDSS J125637.13−022452.4	sdL3.5	esdL3.5	19.41±0.02	17.71±0.02	[c]16.10±0.10	15.79±0.15	15.44:	3
					[c]16.16±0.01	16.06±0.01	16.06±0.02	4
2MASS J06164006−6407194	sdL5	esdL6	—	—	[c]16.40±0.11	16.27±0.23	16.38:	5
ULAS J135058.85+081506.8	sdL5	esdL4	21.24±0.08	19.51±0.06	[d]17.93±0.04	18.07±0.10	17.95±0.15	6
ULAS J033351.10+001405.8	sdL0	—	19.24±0.02	17.87±0.02	16.11±0.01	15.77±0.01	15.50±0.02	10
ULAS J124425.75+102439.3	sdL0.5	sdL2	19.48±0.02	18.01±0.02	16.26±0.01	16.00±0.01	15.77±0.02	10
ULAS J021642.97+004005.6	—	sdL7	22.14±0.15	20.03±0.10	[d]17.30±0.03	16.96±0.04	16.51±0.04	7
ULAS J151913.03−000030.0	—	esdL6	21.46±0.09	19.33±0.06	[d]17.21±0.02	17.07±0.03	16.97±0.04	7
SDSS J133348.24+273508.8	—	sdL3	20.51±0.05	18.75±0.04	[d]17.47±0.02	16.62±0.01	16.00±0.02	7
SDSS J141624.08+134826.7	blue L7	d/sdL7	18.38±0.01	15.91±0.01	[c]13.15±0.03	12.46±0.03	12.11±0.02	8
					[d]12.99±0.01	12.47±0.01	12.05±0.01	8
2MASS J06453153−6646120	sdL8	—	—	—	[c]15.60±0.07	14.70±0.07	14.37±0.08	9
2MASS J11582077+0435014	sdL7	d/sdL7	20.37±0.07	17.95±0.03	[c]15.61±0.06	14.68±0.06	14.44±0.06	9
					[d]15.43±0.01	14.88±0.01	14.37±0.01	7
2MASS J17561080+2815238	sdL1	d/sdL1	—	—	[c]14.71±0.03	14.13±0.04	13.81±0.04	9

Reference: (1) Burgasser et al. (2003a); (2) Burgasser (2004b); (3) Sivarani et al. (2009); (4) Schilbach, Röser & Scholz (2009); (5) Cushing et al. (2009); (6) Lodieu et al. (2010); (7) This thesis; (8) Bowler, Liu & Dupuy (2010); Schmidt et al. (2010a); Burningham et al. (2010a); (9) Kirkpatrick et al. (2010); (10) Lodieu et al. (2012c).

[a] Spectral types from literature. [b] Spectral types adopted in this thesis. [c] 2MASS filters. [d] UKIDSS filters.

Table 3.2: Proper motions and parallaxes of L subdwarfs and mild subdwarfs

Name	SpT	$J-K^a$	$\mu_{\rm RA}$(mas/yr)	$\mu_{\rm Dec}$(mas/yr)	π(abs)	Dis(pc)	Ref.
2MASS J05325346+8246465	esdL7	0.26	2041.90±1.40	−1648.19±1.13	37.50±1.70	26.67±1.21	1
2MASS J05325346+8246465	esdL7	0.24	2039.46±1.52	−1661.79±1.64	42.28±1.76	23.65±0.99	2
2MASS J16262034+3925190	esdL4	0.03; 0.04	−1374.14±0.96	238.01±0.87	29.85±1.08	33.50±1.21	2
SDSS J125637.13−022452.4	esdL3.5	0.10	−512.09±1.90	−297.71±1.79	11.10±2.88	90.09±25.06	2
2MASS J06164006−6407194	esdL6	0.02	1304.00±3.90	−31.90±3.70	19.90±6.50	50.25±18.37	3
ULAS J135058.85+081506.8	esdL4	(-0.02)	−235.96±5.87	−225.18±7.45	—	153.80±20.39	4
ULAS J033351.10+001405.8	sdL0	(0.60)	770.41±4.27	−60.21±8.29	—	[b]92.13±12.40	4
ULAS J124425.75+102439.3	sdL2	(0.49)	−432.08±8.90	−529.93±9.81	—	[b]79.43±10.65	4
ULAS J021642.97+004005.6	sdL7	(0.80)	−91.66±123.68	100.77±118.86	—	[b]65.48±9.29	4
ULAS J151913.03−000030.0	esdL6	(0.24)	−21.65±9.61	−421.24±9.61	—	[b]79.03±10.48	4
SDSS J133348.24+273508.8	sdL3	(0.62)	102.65±6.06	−604.48±6.05	—	[b]80.18±10.93	4
SDSS J141624.08+134826.7	d/sdL7	1.03; (0.94)	95.10±3.00	161.30±2.80	109.90±1.80	9.10±1.53	5
2MASS J06453153−6646120	"sdL8"	1.23	−877.94±44.74	1301.58±66.32	—	16	6
2MASS J11582077+0435014	d/sdL7	1.17; (1.06)	585.19±13.01	−911.26±9.67	—	16	4,6
2MASS J17561080+2815238	d/sdL1	0.90	−754.31±111.43	−453.24±66.96	—	35	6

Reference: (1) Burgasser et al. (2008b); (2) Schilbach, Röser & Scholz (2009); (3) Faherty et al. (2012); (4) This thesis; (5) Dupuy & Liu (2012); (6) Kirkpatrick et al. (2010).

[a] Values in brackets are in UKIDSS filters, the rest are in 2MASS filters.

[b] Distances are estimated based on spectral types and absolute magnitude relationships from scitezhang13.

3.2.2 Confirmed new L subdwarfs

3.2.2.1 SDSS J133348.24+273508.8 (sdL3)

The SDSS observes the sky in five optical bands (u, g, r, i, z). Since L subdwarfs are faint and red, they are usually beyond the detection limit in the u, g, r bands. Most of the known L subdwarfs could only be detected in the i and z bands. But i and z bands are not enough to distinguish L subdwarfs from M dwarfs, because they have similar $i - z$ colour. While SDSS is also a spectroscopic survey, and can obtain 600 spectra using multi fibre technology. L subdwarfs can be selected into SDSS's red spectroscopic target list. One sdL3.5 subdwarf SDSS J125637.13−022452.4 (SDSS J1256, Sivarani et al. 2009) and one metal-poor L7 dwarf SDSS J141624.08+134826.7 (SDSS J1416, Schmidt et al. 2010a; Bowler, Liu & Dupuy 2010) have been discovered using SDSS spectroscopy.

One of our high proper motion candidate, SDSS J133348.24+273508.8 (J1333) was observed by the SDSS spectroscopy survey. Figure 3.3 shows its SDSS red optical spectrum. Flat optical flux before 7700 Å indicates that it is not an early-late type M dwarf. VO at 7900Å is barely present, and a slight depression in the continuum between 7800 and 8200Å indicates that it is neither a late-type M or early-type L dwarf. The VO index is at its strongest at L0 (7800-8000Å portion of spectrum is flat), and weakens from L1 to L3 and from M9 to M6, and vanished in L4 and M5 (Figure 1.6 and 1.8). Some characteristics of the L3 type are seen in the spectrum of SDSS J1333, but the TiO and CaH indices of SDSS J1333 do not fit with an normal L3 dwarf spectrum. Its z band spectrum is suppressed compare with an normal L3 dwarf. SDSS J1333 compares very well with the esdL3.5 SDSS J1256 (Section 3.3.3.3). However it has bluer $J - K$ colour and redder $i - J$ colour than the SDSS J1256 suggesting it has higher metallicity. Thus I assigned its spectral type to be sdL3±1.

3.2.2.2 ULAS J124425.75+102439.3 (sdL2)

The optical spectrum of ULAS J124425.75+102439.3 (ULAS J1244) was obtained with IMACS Short-Camera on the Baade of the Magellan Telescopes on 5 May 2010. The spectral coverage range was 6550-10000 Å, with a dispersion of 1.98 Å. Three integrations of 1800 seconds were took individual for this spectrum.

The spectra were extracted using the standard reduction procedures in the IRAF[1]

[1]IRAF is distributed by the National Optical Observatory, which is operated by the Association of

Table 3.3: L subdwarf candidates

Name	SDSS i	UKIDSS J	UKIDSS K
ULAS J001931.33+063111.0	21.79±0.13	17.53±0.04	16.71±0.05
ULAS J010045.94+101336.7	20.93±1.15	17.78±0.03	17.17±0.08
ULAS J011711.98−005213.4	20.67±0.04	17.53±0.03	16.92±0.07
ULAS J020628.22+020255.6	20.79±0.04	17.65±0.03	17.10±0.10
ULAS J021258.08+064115.9	21.13±0.08	17.43±0.03	16.78±0.05
ULAS J021635.85+012118.1	21.20±0.07	17.97±0.07	17.39±0.10
ULAS J021642.96+004005.7	22.14±0.15	17.30±0.03	16.51±0.04
ULAS J024035.36+060629.3	21.07±0.15	17.99±0.04	17.48±0.12
ULAS J033351.10+001405.8	19.24±0.02	16.11±0.01	15.50±0.02
ULAS J075335.23+200622.4	19.83±0.04	15.87±0.01	15.09±0.01
ULAS J081135.60+284157.5	22.80±0.28	17.42±0.03	16.37±0.03
ULAS J082206.61+044101.8	20.35±0.04	16.29±0.01	15.53±0.02
ULAS J084633.52−001117.2	22.34±0.17	17.84±0.04	17.18±0.07
ULAS J090645.63+301627.5	21.52±0.09	17.78±0.03	17.07±0.09
ULAS J090729.57+003713.1	21.33±0.14	17.75±0.03	17.17±0.07
ULAS J093846.84+310520.9	21.72±0.11	17.88±0.03	17.15±0.06
ULAS J094023.80+313342.1	21.60±0.09	17.41±0.02	16.65±0.03
ULAS J095921.11+025133.9	23.51±0.51	17.73±0.04	17.20±0.07
ULAS J101915.85+011522.7	21.38±0.11	17.34±0.03	16.53±0.04
ULAS J102432.59+123307.6	21.37±0.07	17.33±0.03	16.70±0.05
ULAS J103519.54−013859.7	21.78±0.19	17.92±0.06	17.18±0.08
ULAS J111346.98+084501.7	21.92±0.28	17.25±0.02	16.40±0.04
ULAS J111429.54+072809.5	20.70±0.05	17.59±0.03	17.12±0.07
ULAS J111959.85+012832.1	22.30±0.24	17.67±0.05	16.98±0.06
ULAS J112438.49+154258.8	21.10±0.08	16.96±0.02	16.14±0.02
ULAS J115109.05+103139.2	22.57±0.23	17.94±0.03	17.05±0.07
ULAS J115347.97+021425.3	21.98±0.13	17.78±0.05	16.99±0.07
ULAS J115403.44+082525.1	21.34±0.08	17.61±0.02	16.88±0.05
ULAS J115821.09+043453.9	21.02±0.08	15.43±0.00	14.37±0.01
ULAS J120434.02+062427.0	21.66±0.07	17.66±0.03	16.92±0.07
ULAS J120730.29−001512.2	22.16±0.20	17.91±0.06	17.07±0.10
ULAS J120914.90+110731.7	22.57±0.38	17.93±0.04	17.20±0.08
ULAS J123142.99+015045.4	21.38±0.11	17.54±0.03	16.78±0.05

Table 3.3: continued.

Name	SDSS i	UKIDSS J	UKIDSS K
ULAS J124425.75+102439.3	19.48±0.02	16.26±0.01	15.77±0.02
ULAS J124913.27+042517.8	22.39±0.21	17.87±0.04	17.02±0.07
ULAS J124947.04+095019.8	20.39±0.04	16.83±0.02	16.12±0.04
ULAS J125217.26+282817.4	22.16±0.18	17.63±0.04	16.80±0.05
ULAS J133348.27+273505.5	20.51±0.05	16.62±0.01	15.98±0.02
ULAS J133504.58+292137.4	21.74±0.11	17.82±0.03	17.04±0.06
ULAS J133836.97−022910.7	22.47±0.26	17.37±0.03	16.37±0.05
ULAS J134206.86+053724.9	21.90±0.14	17.43±0.03	16.56±0.04
ULAS J134423.98+280603.8	22.64±0.26	17.19±0.02	16.13±0.03
ULAS J134505.85+342441.8	20.64±0.04	16.77±0.02	16.04±0.03
ULAS J134749.79+333601.7	19.87±0.03	15.85±0.01	15.27±0.02
ULAS J135058.85+081506.8	21.25±0.08	17.93±0.04	17.95±0.15
ULAS J135216.31+312327.0	20.00±0.04	16.93±0.02	16.41±0.04
ULAS J135359.58+011856.7	21.59±0.10	17.36±0.03	16.52±0.04
ULAS J140831.72+012139.5	22.49±0.22	17.98±0.06	17.21±0.07
ULAS J141203.85+121609.9	21.32±0.08	16.33±0.01	15.43±0.02
ULAS J141624.12+134827.4	18.37±0.02	12.99±0.00	12.05±0.00
ULAS J141832.35+025323.0	20.10±0.04	16.00±0.01	15.19±0.01
ULAS J143154.18−004114.3	20.86±0.06	17.19±0.03	16.48±0.05
ULAS J145234.65+043738.4	20.83±0.05	17.28±0.03	16.62±0.06
ULAS J151913.03−000030.0	21.47±0.09	17.21±0.02	16.97±0.04
ULAS J153357.84+065115.1	20.80±0.05	17.77±0.04	17.20±0.07
ULAS J154638.34−011213.0	22.08±0.14	17.51±0.04	16.95±0.08
ULAS J223302.03+062030.8	21.11±0.05	17.90±0.05	17.44±0.11
ULAS J223440.80+001002.6	22.05±0.13	17.63±0.04	16.90±0.07
ULAS J225655.64+105415.1	22.84±0.50	17.98±0.04	17.08±0.07
ULAS J225902.14+115602.1	21.49±0.16	17.05±0.02	16.21±0.03
ULAS J230354.95+104922.0	23.09±0.40	17.74±0.04	17.50±0.09
ULAS J230614.69+100914.7	20.98±0.06	17.95±0.05	17.35±0.08
ULAS J231924.35+052524.5	20.66±0.05	17.33±0.02	16.93±0.06
ULAS J233227.03+123452.0	22.66±0.26	16.90±0.02	15.88±0.03
ULAS J234241.67+001756.6	20.97±0.05	17.88±0.06	17.27±0.08
ULAS J235050.07+094952.3	20.88±0.05	17.84±0.04	17.26±0.08

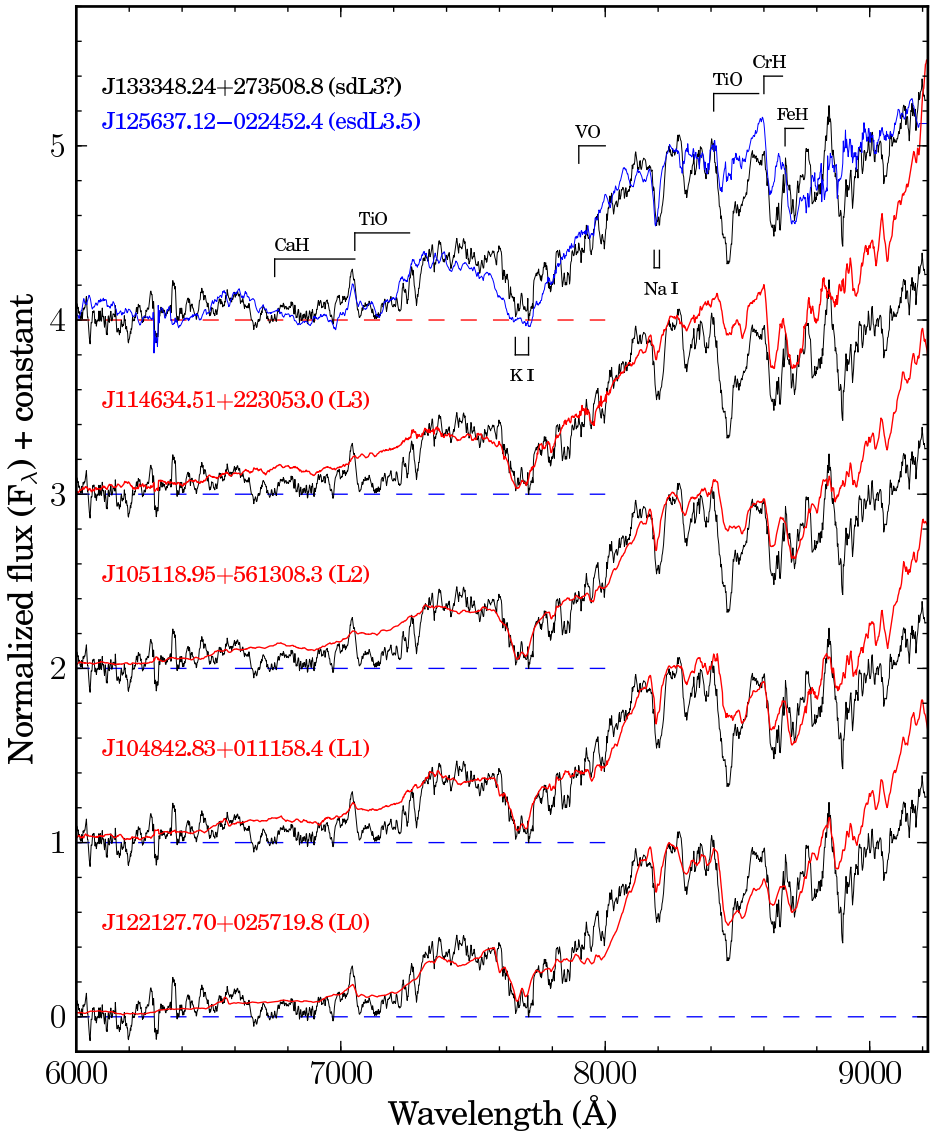

Figure 3.3: The SDSS optical spectrum of SDSS J133348.24+273508.8 (black). Spectra of the sdL3.5 dwarfs SDSS J1256 (blue) and L0-L3 dwarfs (red) are plotted for comparison. Spectra are normalized at 8250Å.

twodspec and echelle package (bias subtraction, flat-field division, extraction of the spectra, telluric correction and wavelength and flux calibration). I obtained the wavelength calibration by taking spectra of a Th-Ar lamp. The average signal-to-noise of the data, measured as the square root of the signal (at $\approx$ 8100 Å) is $\approx$200.

Figure 3.4 shows the spectrum of ULAS J1244. It is different from that of L0-L3 dwarfs, showing stronger CaH and TiO bands, no VO band and a flat z band spectrum. Its spectrum compares closely to that of the SDSS J1256 (esdL3.5) and SDSS J1333 (sdL3), but looks slightly earlier. Thus I assigned its spectral type to be sdL2$\pm$1. Its bluer $J-K$ colour than the esdL3.5 supports the metal class of "sd". ULAS J1244 has been discovered independently by Lodieu et al. (2012c). The author classified it as an sdL0.5 by compare its optical spectrum with an sdM9.5 SSSPM1013-1356 (Scholz et al. 2004). There is a disagreement of spectral types classification of early-type L subdwarfs with these two approaches either by comparing with spectra of late-type M subdwarfs or mid L subdwarfs. This indicate that current spectral classification method for L subdwarfs need to be improved. Lodieu et al. (2012c) also confirmed another L subdwarf (ULAS J033351.10+001405.8) which is one of my early-type L subdwarf candidate.

3.2.2.3 ULAS J021642.97+004005.6 (sdL7)

ULAS J021642.97+004005.6 (ULAS J0216) was observed with X-shooter (Vernet et al. 2011) on the *Very Large Telescope* on 28 January 2012. I used the echelle slit mode, which covers the wavelength range 300–2500 nm. This is split into three separate arms, the UVB (300-550 nm), VIS (550-1000 nm) and NIR (1000-2500 nm). Using slit widths of 1.0 arcsec for the UVB arm and 0.9 arcsec for the VIS and NIR arms I took two integrations of 400 seconds in VIS, two 330 seconds in UVB and two 490 seconds in NIR for this spectrum. Telluric standard stars were taken before and after the target, which were paired together so they were in roughly the same airmass. Sky flats and arc frames were also taken at the beginning of the night.

The data were reduced using the ESO X-shooter pipeline (version 1.3.7). The pipeline removes non-linear pixels, subtract the bias (in the UVB and VIS arm) or dark frames (in the NIR arm only) and divide the raw frames by flat fields. Images are pair-wise subtracted to remove sky background. The pipeline then extracts and merges the different orders in each arm, rectifying them using a multi pinhole arc lamps (taken during the

Universities for Research in Astronomy, Inc., under contract with the National Science Foundation.

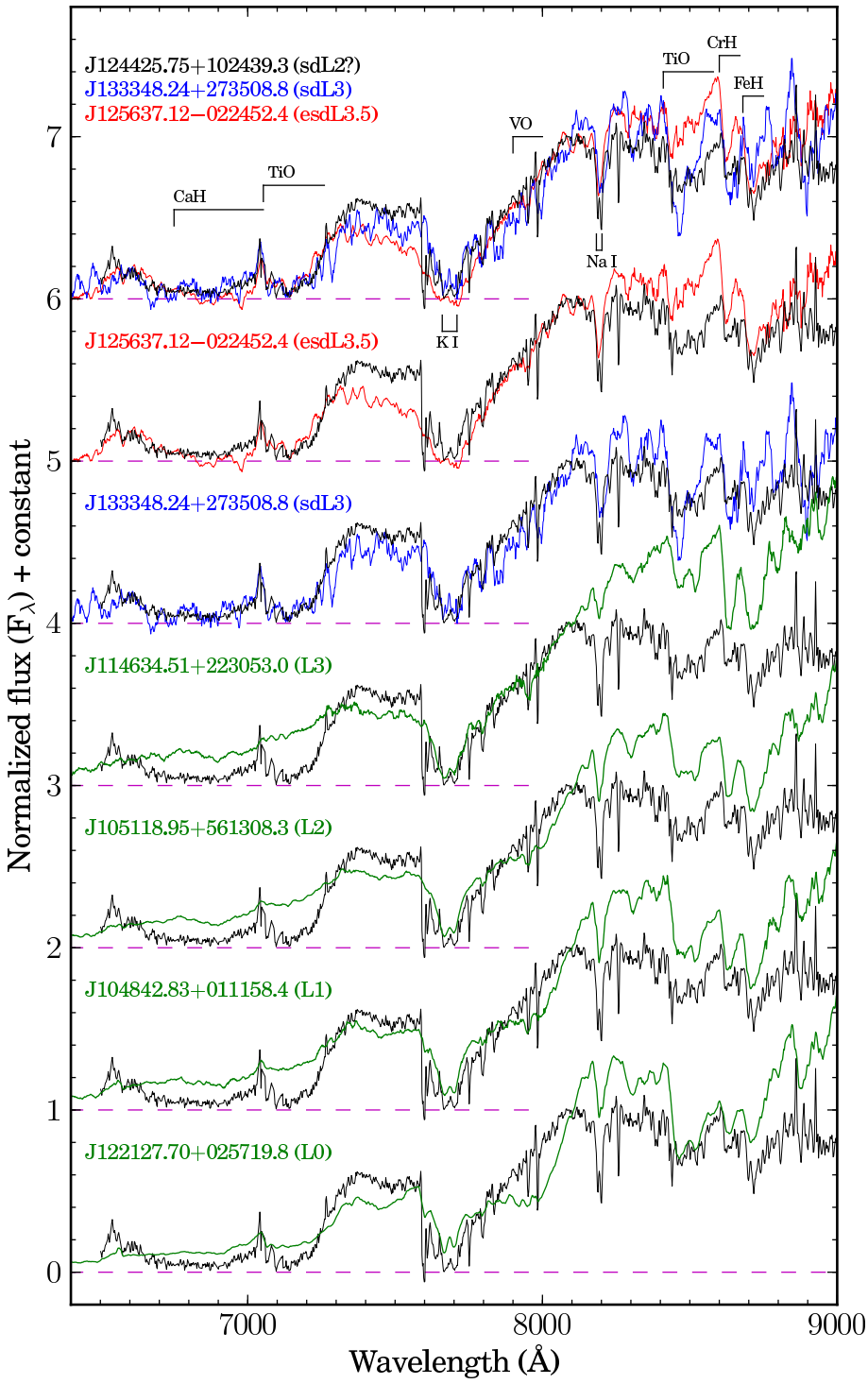

Figure 3.4: IMACS optical spectrum of SDSS J124425.75+102439.3 (black). Spectra of the sdL3.5 SDSS J1256 (red), sdL3 SDSS J1333 (blue) and L0-L3 dwarfs (green) are plotted for comparison. All spectra are normalized at 8100Å.

day-time calibration) and correcting for the flexure of the instrument using single pinhole arc lamps (taken at night, one for each object observed). Telluric stars are reduced in the same way, except that sky subtraction is done by fitting the background (as tellurics are not observed in nodding mode). The spectra were telluric corrected and flux calibrated using IDL routines, following a standard procedure: first the telluric spectrum is cleared of HI absorption lines (by interpolating over them) and scaled to match the measured magnitudes; then is divided by a black body curve for the appropriate temperature, to obtain the instrument+atmosphere response curve; finally the target spectra is multiplied by the response curve obtained to flux calibrate it. The three arms (UVB, VIS and NIR) were then merged by matching the flux level in the overlapping regions between them. The flux calibration was checked by determining the targets synthetic MKO YJHK magnitudes, that were compared to those obtained in the ULAS. Finally, each spectrum was visually inspected to check for possible problems during the extraction or merging stage. The spectra were then binned (in the direction) by 40 times to produce an average SNR= 30 for resolution R= 880 and 510 in the VIS and NIR arms, respectively.

I assigned its spectral type as sdL7 by comparing its spectra with an sdL7 subdwarf, 2MASS J0532 (Burgasser et al. 2003a), an sdL4 subdwarf, 2MASS J16262034+3925190 (2MASS J1626; Burgasser 2004b) and an L7 dwarf, 2MASS J09153413+0422045 (J0915; Burgasser 2007). Figure 3.5 (top) shows optical and NIR spectra of ULAS J0216, 2MASS J0532, 2MASS J1626 and 2MASS J0915. Optical and NIR spectra of 2MASS J0532 are obtained with LRIS and NIRSPEC on Keck I and II. I joined these two spectra based on SED measured with SDSS and 2MASS photometry. It looks different from the spectrum plotted in Burgasser et al. (2003a). This is because I re-scaled the optical spectrum of 2MASS J0532 by a factor of 1.54 to match with the SED. ULAS J0216 compares well with 2MASS J0532 at $0.85 - 1.55$ μm. Slightly higher flux at H and K bands indicates weaker CIA H_2 and thus higher metallicity than 2MASS J0532 which was suggested to be classified as esdL7 by Kirkpatrick et al. (2010). ULAS J0216 appears to have more flux than 2MASS J0532 at $0.80 - 0.85$ μm, but I note that there is low SNR in optical bands. ULAS J0216 also comparing well with a L7 dwarf standard at $0.85 - 1.08$ μm. Thus I assigned a spectral type of sdL7 to ULAS J0216. I will discuss the metal classes of L subdwarfs in Section 3.3.3.

3.2.2.4 ULAS J151913.03−000030.0 (esdL6)

ULAS J151913.03−000030.0 (ULAS J1519) was observed with X-shooter on the *Very Large Telescope* on 28 January 2012. The spectrum was observed and reduced in the same way as ULAS J0216 (Section 3.2.2.3). I assigned its spectral type as esdL6 by comparing the spectrum with known L subdwarfs (2MASS J0532, sdL7, Burgasser et al. 2003a; 2MASS J1626, sdL4, Burgasser 2004b; 2MASS J06164006−6407194, sdL5, Cushing et al. 2009). I re-examined the spectral type and metal classes of these known L subdwarfs (see, Section 3.3.1). Spectrum of ULAS J1519 compares well with that of 2MASS J0532 from 1.25μm to the H and K bands indicates that they are of the same metal class. More flux short of 1.2 μm indicates that ULAS J1519 may have a slightly earlier spectral type than 2MASS J0532. Significantly deeper H_2O absorption bands around 1.15 and 1.40 μm indicate it is later than 2MASS J1626. ULAS J1519 has more similar features to 2MASS J0532 than 2MASS J1626, particularly the H_2O absorption bands around 1.15 and 1.40 μm. Thus I assigned its spectral type as esdL6. Its $i-J$ and $J-K$ colours also indicate that it has the same metal class as 2MASS J0532 and 2MASS J1626 and a spectral type intermediate between them. It is interesting to notice that the Y band spectrum has the brightest flux peak for an esdL6 subdwarf. The J band flux peak only take over at esdL7. While for dwarfs the flux peak moves from Y to J around M7-L0 which is around stellar/substellar boundary (Figure 1.6).

3.3 Characterization of L subdwarfs

Spectral type classification for L subdwarfs has not been properly established due to the lack of known L subdwarfs and our incomplete understanding of metal-poor ultracool atmospheres. L subdwarfs are current classified by comparing their red optical spectra with those of L dwarfs. This is a temporary method in use before enough L subdwarfs been identified to build up subdwarf spectral type and metal sequences. L subdwarfs have similar optical spectra with L dwarfs at 0.6-1.0 μm (see Figure 3.5). Thus it is difficult to assign metal classes for L subdwarfs only based on red optical spectra. It is also difficult to classify L subdwarfs only with NIR spectra, because both temperature and metallicity will affect the shape of NIR spectra in related ways. Both optical and NIR spectra need to be considered for L subdwarf classification. Thus spectral types assigned to known L subdwarfs have larger uncertainties and are not reliable.

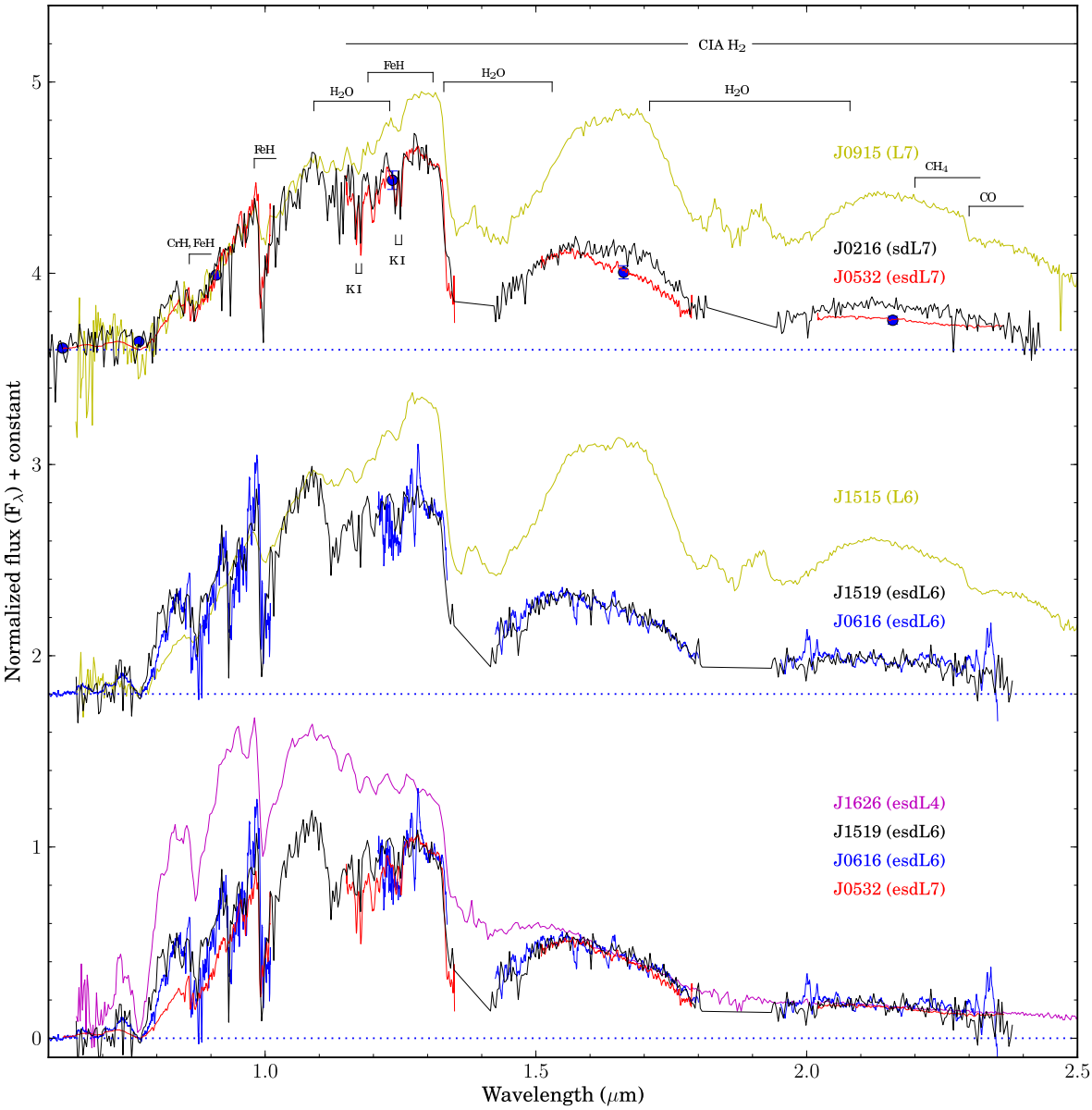

Figure 3.5: Optical and NIR spectra of ULAS J0216 and ULAS J1519. Spectra of known L subdwarfs and dwarfs are also plotted for comparison. Blue crosses show the SED of 2MASS J0532. Spectra in top and middle panels are normalized at 1.08 μm. Spectra in bottom panel are normalized at 1.6 μm.

3.3.1 Metal classes of L subdwarfs

L subdwarfs exhibit the characteristic spectral signature of strong metal hydrides (CaH, MgH, AlH, CrH and FeH), weak or absent metal oxides (TiO, VO and CO), and enhanced CIA H_2. By comparing optical and NIR spectra of L7 type dwarfs with different metallicities, I find a smooth suppressing of J, H and K band spectra moving across objects classified as, extreme red L7.5, red L7, normal L7, blue L7, d/sdL7, sdL7 and esdL7 due to the CIA H_2. Figure 3.6 shows optical and NIR spectra of L7 dwarfs with different strength of CIA H_2, an indicator of differing metallicity. Most of these spectra are taken from the SpeX Prism Library [2]. All the spectra are normalized at 1.08 μm. A variation at J, H and K bands is clearly. The L7 NIR standard 2MASSI J0103320+193536 (Cruz et al. 2004, L6 in optical) is the reddest L7, thus is not suitable as a standard. The L7 optical standard DENIS-P J0205-1159 (with NIR spectral type of L5.5) is the bluest L7 (Burgasser et al. 2010). 2MASS J09153413+0422045 is used as an L7 standard by Burgasser (2007) and turns out to be the most normal L7 dwarf (see, Figure 1.8). These three spectra are selected for comparison with known and new metal-poor L7 dwarfs. The bottom panel of Figure 3.6 shows optical spectra of L7 dwarfs and subdwarfs. SDSS J1416 is a blue L dwarf with disk kinematics classified as d/sdL7 (Section 3.3.3.6). J0047 is an extreme red L dwarfs recently identified by Gizis et al. (2012). Weather its unusually red NIR spectrum due to high metallicity or different atmosphere is not clear. It may younger than 1 Gyr but should not be a very young, because its H band spectrum does not shows an obvious triangle shape which is an indicator for low gravity of young L dwarfs (e.g. Faherty et al. 2013).

The most notable features of an L7 subdwarf spectra that differ from an L7 dwarf spectra are the much stronger FeH lines and absence of the CO band around 2.3 μm. The 2.3 μm CO band appears in spectra of M7 to T1 dwarfs, and disappear after T2 due to the strengthening of CH_4 absorption (Figure 1.8 and 1.13). The absence of 2.3 μm CO band in the spectra of known L subdwarfs suggests that it is an indicator of a low metallicity population.

The $i-J$ colour is a good indicator of $T_{\rm eff}$ and spectral type, while the $J-K$ colour is a good indicator of CIA H_2 and thus also metallicity. H and K band suppression in spectra of low metallicity ultracool subdwarfs is predicted by atmospheric models (Witte, Helling & Hauschildt 2009; see Figure 1.11 and 1.18). Known L subdwarfs are well separated into

[2]The SpeX Prism Spectral Libraries, maintained by Adam Burgasser at http://pono.ucsd.edu/ adam/browndwarfs/spexprism

two groups with a dash line in Figure 3.1. The lower group of L subdwarfs should have lower metallicity than the higher group because they have bluer $J-K$ colour. L subdwarfs above and below the dash line are sdLs and esdLs. In addition, the $J-K$ colours of L subdwarfs with same metallicity also get redder as $T_{\rm eff}$ decreases from mid to late-type L types. The DRIFT-PHOENIX model grids have predicted the change of $J-K$ colours with $T_{\rm eff}$ for early-type L subdwarfs. The bottom panel of Figure 1.18 shows that $J-K$ colours of UCSDs with different metallicity reach their bluest point at $T_{\rm eff} \approx 2000-2100$ K corresponding to L2±1 type, then get redder for cooler ($T_{\rm eff} \approx 2100-2200$ K) and later types (L3±1 types). However, the model did not predict the change of $i-J$ colour well as $T_{\rm eff}$ decreases because i band magnitudes are highly sensitive to the strong molecular opacity present at these wavelengths.

We know that BDs are evolving all the life time, they keep cooling down and changing their spectral types. For instance, a 30 $M_{\rm Jup}$ BD could be a 3000 K late-type type M dwarf when its was very young, then keep cooling down and become an L dwarf, then become a T dwarf at 1 Gyr old and become a Y dwarf at 10 Gyr old cooler than 500 K. Of course it is not possible to observed this change directly through one BD. But we could find BDs with very different masses and ages but have similar $T_{\rm eff}$ or spectral types, if they are either massive and old or less massive and young. BDs listed in Figure 3.6 is such an example. They have different metallicities and ages, but they all have similar $T_{\rm eff} \sim 1500 \pm 200$ K, thus they have very different masses. Metal-poor or older ones are massive BDs, while metal-rich or younger ones are low-mass BDs. Their mass ranges from 20 $M_{\rm Jup}$ for the reddest and youngest one to 80 $M_{\rm Jup}$ for the bluest and oldest one. Looking at Figure 3.6 we could feel that BDs are always evolving and cooling down.

3.3.2 Space velocities

Dwarf stars are orbiting the Galactic centre in the Galactic disk in a similar direction, while cool subdwarfs are orbiting in the Galactic spheroid randomly. Thus nearby disk stars have lower UVW space velocities observing from the solar system. The U positive in the direction of the Galactic anti center, V positive in the direction of galactic rotation, and W positive in the direction of the North Galactic Pole (Johnson & Soderblom 1987). Thus the UVW space velocity could indicates memberships of Galactic populations.

I measure UVW space velocities of L subdwarfs based on their distances, radial velocities and proper motions. I estimate and measure these parameters by myself for

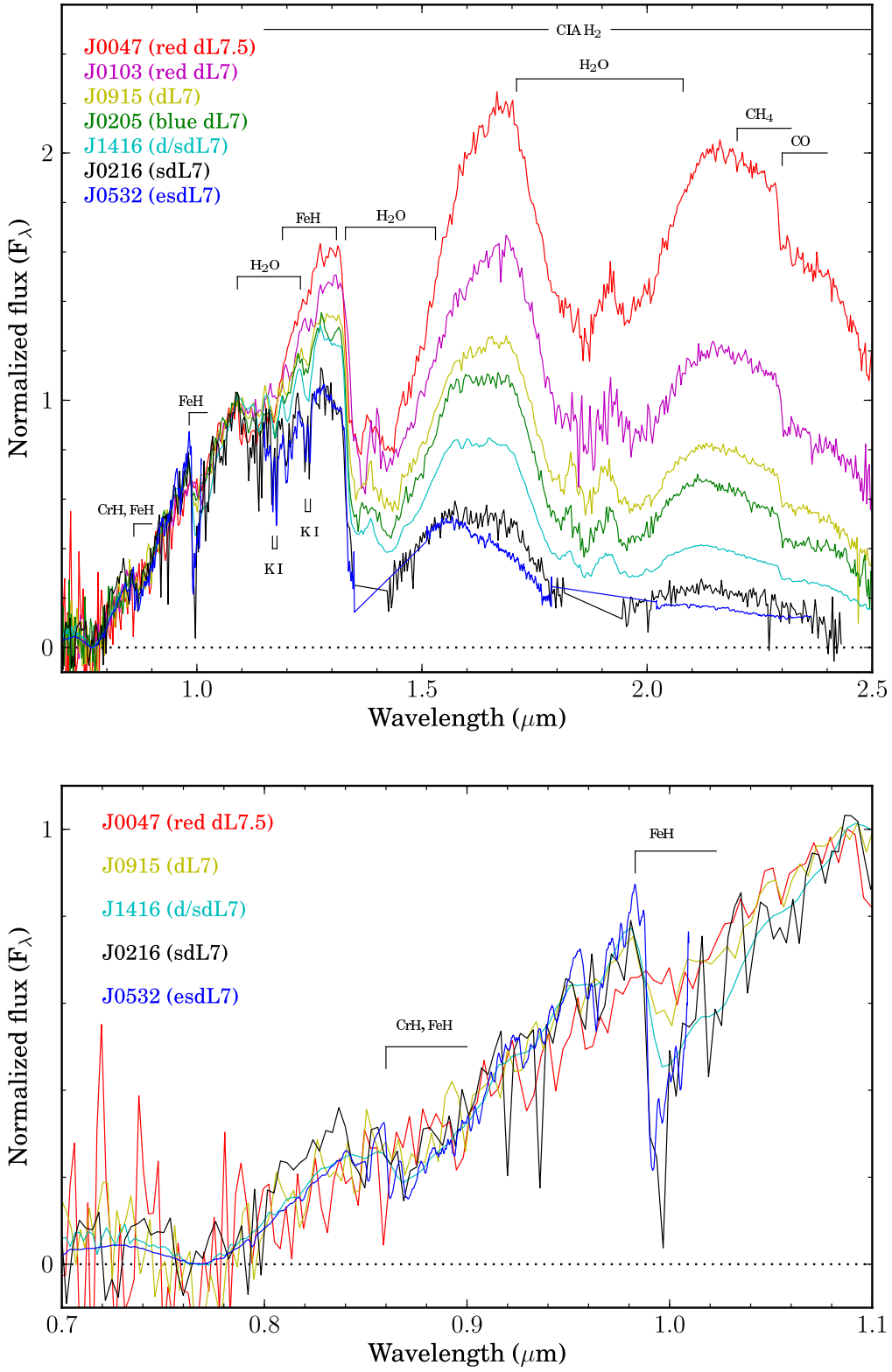

Figure 3.6: Metallicity sequences of optical and NIR spectra of L7 dwarfs and subdwarfs. The absence 2.3 μm CO band which presents in spectra of M7 – T1 dwarfs might be a indicator of halo L subdwarfs. Spectra are normalized at 1.08 μm.

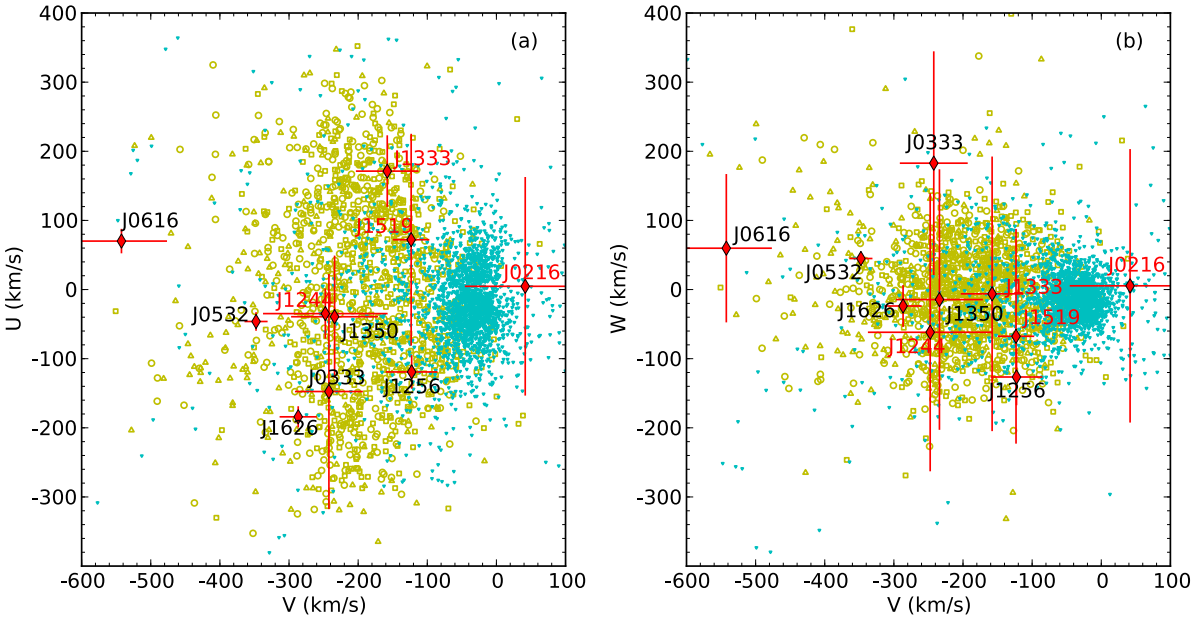

Figure 3.7: *UVW* space velocities of L subdwarfs. M dwarfs (cyan dots), sdM (yellow squares), esdM (yellow circles) and usdM (yellow triangles) are also plotted for comparison (data are from Zhang et al. 2013). M dwarfs and subdwarfs are all have proper motion larger than 100mas/yr.

new and known objects which are not in the literature. Distances of ULAS J0216, ULAS J0333, ULAS J1244, SDSS J1333 and ULAS J1519 are estimated based on relationships between spectral types and absolute magnitudes from Zhang et al. (2013) which are based on parallax measurements of esdL3.5-esdL7 type subdwarfs, and are also sensitive to spectral types and metallicity. Distances of less metal-poor L subdwarfs (ULAS J1244, SDSS J1333, ULAS J0216) may be over estimated because their absolute magnitudes cold be over estimated, more metal-poor L dwarfs are brighter in J band. No early-type L subdwarf parallax measurement is used in the fit of the relationships. Early-type L subdwarfs also have larger error of their spectral types (e.g. ULAS J0333, 2MASS J17561080+2815238), because there is no early-type sdL standard. Thus early-type L subdwarfs would have large errors of their distances. I assumed a radial velocity of 0.0±200.0 km/s for ULAS J0216, ULAS J0333, ULAS J1244, SDSS J1333, ULAS J1519 which do not have radial velocity measurements. Figure 3.7 shows space velocities of L subdwarfs.

3.3.3 Classification of known L subdwarfs

I re-examine the spectral types of five know L subdwarfs and four metal-poor L dwarfs based on their optical and NIR spectra, and $i-J$ and $J-K$ colours. I present a practically useful approach to assigning preliminary spectral types, and discuss my results in the context of prevision work.

3.3.3.1 2MASS J05325346+8246465 (esdL7)

2MASS J0532 was the first L subdwarf discovered (Burgasser et al. 2003a). It was initially selected as a T dwarf candidate because it has blue $J-K$ colour and red optical/NIR colours. Burgasser, Cruz & Kirkpatrick (2007) assigned its spectral type as sdL7 by comparing its optical spectrum with L dwarf spectra, and proposed that it is the first brown dwarf of the Galactic halo. Kirkpatrick et al. (2010) compared its optical and NIR spectra with two metal-poor L dwarfs and suggested that it looks more like an esdL7 dwarf. The optical and NIR spectra were obtained using NIRSPEC and LRIS on the Keck II and I Telescopes separately, and joined together by over-plot with spectrum of an L7 dwarf DENIS 0205-1159AB. I re-calibrated the optical and NIR spectral ratio with SDSS and 2MASS photometry. Blue pluses in Figure 3.5 are SDSS and 2MASS SEDs of 2MASS J0532. I normalized the optical spectrum of 2MASS J0532 (Burgasser et al.

2003a) by a factor of 1.54 to match with its photometric SED and NIR spectrum. Spectra of L subdwarfs at wavelengths beyond 1.08μm are largely suppressed (e.g. top panel of Figure 3.5).

The top panel of Figure 3.6 shows the optical and NIR spectra of L7 dwarfs. It clearly shows that there is diversity in spectral morphology after 1.2μm which suggests a variation of metallicity from red to blue L7 dwarfs. Figure 3.6 bottom panel shows spectra with spectral types of red L7, normal L7, blue L7, d/sdL7, sdL7 and esdL7. The NIR region of these spectra are being incrementally suppressed as one moves along the sequence.

3.3.3.2 2MASS J16262034+3925190 (esdL4)

2MASS J1626 is the second L subdwarf discovered by Burgasser (2004b). It was also a T dwarf candidate due to its blue $J-K$ colour but was rejected because its optical magnitudes are to bright to be a T dwarf. It was re-examined as a late-type subdwarf target after the discovery of the L7 subdwarf 2MASS J0532. It is classified as an sdL4 subdwarf by Burgasser, Cruz & Kirkpatrick (2007). 2MASS J1626 has bluer $J-K$ colour than 2MASS 0532 which suggests it should be an esdL4 rather than an sdL4 subdwarf. The spectrum of 2MASS J1626 is shown in Figure 3.14. 2MASS J1626 has a higher temperature than 2MASS J0532 and ULAS J1519, and the large K band flux suppression suggests it has similar metallicity to 2MASS J0532 and ULAS J1519. DRIFT model spectral fits suggest 2MASS J1626 has a metallicity of [M/H] ~ -1.5 (Figure 3.8). The model fit by Burgasser, Cruz & Kirkpatrick (2007) suggests that 2MASS J1626 has metallicity of $-1.8 <$ [M/H] < -1.3. Thus a spectral type of esdL4 should more suitable for 2MASS J1626.

Spectral ratio of CaH2+CaH3 and TiO5 absorption bands are indicators of metallicity for M subdwarfs (e.g. Gizis 1997; Lépine, Rich & Shara 2007). Fig. 6 in Burgasser, Cruz & Kirkpatrick (2007) shows that 2MASS J1626 falls into the extension area of sdMs in a CaH2+CaH3 versus TiO5 plot. This suggests that optical indices of CaH2, CaH3 and TiO5 are not suitable for the classification of L subdwarfs.

3.3.3.3 SDSS J125637.13−022452.4 (esdL3.5)

SDSS J1256 was discovered in the SDSS spectroscopic survey by Sivarani et al. (2009). Burgasser et al. (2009) observed higher resolution and SNR optical and NIR spectra and

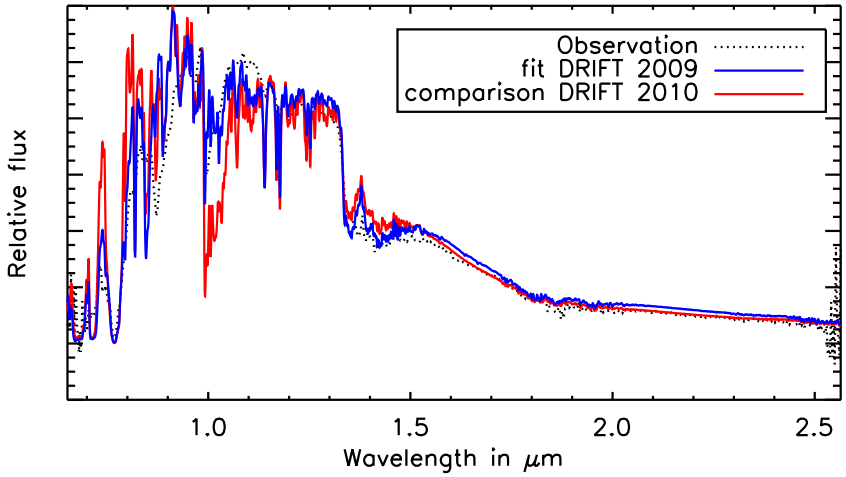

Figure 3.8: Spectrum of 2MASS J1626 (black, dotted) and fits with the DRIFT 2009 models (blue, solid; Witte, Helling & Hauschildt 2009) and DRIFT 2010 models (red, solid; Witte et al. 2011). Both models have $T_{\rm eff}$ = 2100K, log(g)=5.0 and a metallicity [Fe/H]= −1.5. The figure is from West et al. (2011).

assigned its spectral type as an sdL3.5. Model fits showed that SDSS J1256 has metallicity $-1.5 \leq$ [M/H] < -1.0, and likely closer to −1.5. It has bluer $J-K$ and $i-J$ colours than 2MASS J0532 and ULAS J1519 and a similar to 2MASS J1626. It also has a similar spectrum as 2MASS J1626. It seams likely that it has slightly higher metallicity than 2MASS J1626, though is still classified as esdL.

3.3.3.4 2MASS J06164006−6407194 (esdL6)

2MASS J06164006−6407194 (2MASS J0616) is an out halo object with very blue $J-K$ colour. It was classified as sdL5 by Cushing et al. (2009). But I found it has a very similar spectral profile to ULAS J1519 and should be classified as an esdL6. Figure 3.14 shows spectra of ULAS J1519 and another three L type extreme subdwarfs. The spectral type versus absolute magnitude relationships of late-type M to L dwarfs and subdwarfs support a spectral type of esdL6 for 2MASS J0616 (Figure 1.17). L subdwarfs have brighter magnitudes in J band than L dwarfs and similar magnitudes in H and K bands. It is clear that a spectral type of sdL5 could not make 2MASS J0616 fit consistently with other L subdwarfs, however, a type of esdL6 could. Thus 2MASS J0616 should be classified as an esdL6 rather than sdL5.

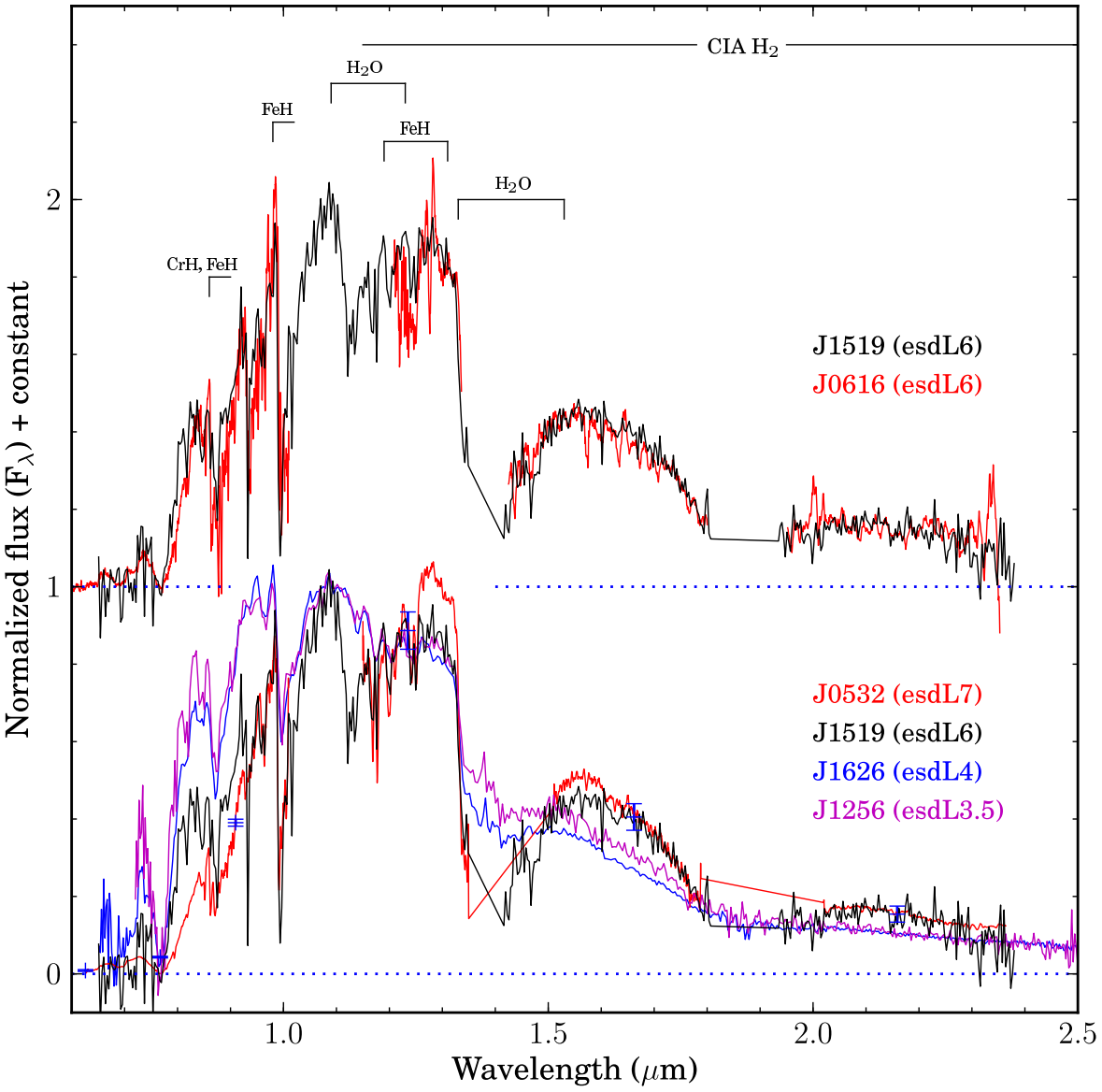

Figure 3.9: Optical and NIR spectra of five L type extreme subdwarfs. Spectra are normalized at 1.08 μm.

3.3.3.5 ULAS J135058.85+081506.8 (esdL4)

ULAS J135058.85+081506.8 (ULAS J1350) is the first L subdwarf discovered in UKIDSS by Lodieu et al. (2010). It was classified as an sdL5 based on its optical spectrum with low SNR. Figure 3.10 shows spectrum and SED of ULAS J1350. Its optical spectrum at 700-900nm which normally used for L subdwarf spectral typing (e.g. Figure 1.9) is more like that of 2MASS J1626 than 2MASS J0616. Slightly more flux at 900-1000nm (also bluer $J-K$ colour) might due to slightly higher metallicity than 2MASS J1626. Indeed, it it also a noisy spectrum.

It has similar shape of SEDs (i, z, J, H, K) to 2MASS J1626. ULAS J1350 also has very similar $i-J$ & $J-K$ to 2MASS J1626 and SDSS J1256 (Figure 3.1). Thus I suggest to classify ULAS J1350 as an esdL4 subdwarf.

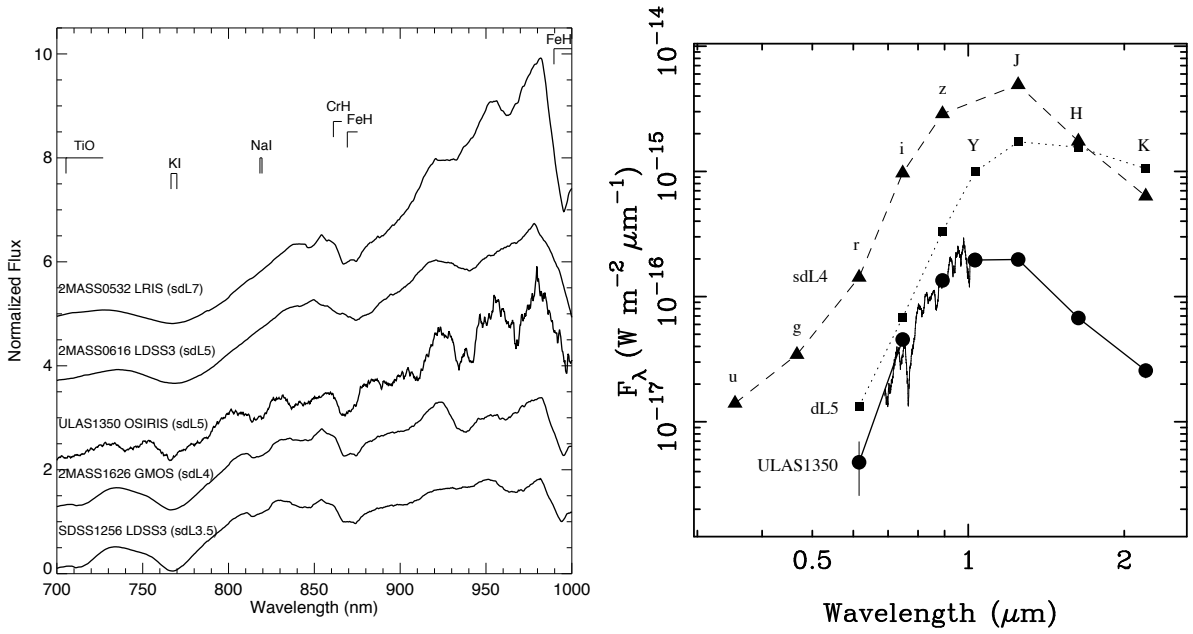

Figure 3.10: Right panel: Spectra of ULAS J1350 and four known L subdwarfs. Note I have re-examined spectral types and metal classes of other known L subdwarfs. Left panel: SDSS/UKIDSS SED of ULAS J1350 and 2MASS J1626. ULAS J1350 has a very similar spectrum at 700–900 nm to 2MASS J1626. They also have similar red optical and NIR SEDs. The figures are from Lodieu et al. (2010).

3.3.3.6 Four metal-poor L dwarfs

Considering L and T dwarfs together, it is known that low metallicity classes have suppressed K band flux (e.g. Kirkpatrick et al. 2010; Murray et al. 2011). The existence of metal poor binary systems containing UCDs allows us to boot-strap metallicity assessments through comparison of cool companions. ULAS J1416 is a metal-poor T7.5 dwarf discovered by Burningham et al. (2010a). It is a companion to the metal-poor L dwarf SDSS J1416. Burningham et al. (2010a) estimated the metallicity of ULAS J1416 (SDSS J1416B) of [M/H]=−0.30, and classified SDSS J1416 (SDSS J1416A) as d/sdL7. Burgasser et al. (2010) also estimated the metallicity of SDSS J1416B to be [M/H] ≤ -0.3. Figure 3.11 shows the spectra of SDSS J1416B and another metal-poor T8 dwarf BD+01 2920B discovered by Pinfield et al. (2012). A spectrum of a normal T8 dwarf 2MASS J04151954–093506.6 is over plotted with spectra of ULAS J1416 and BD+1 2920B for comparison. BD+01 2920B is a companion to a nearby metal-poor G1V star with well constrained properties including metallicity [M/H] = −0.38± 0.06 dex. The similar K band flux suppression levels of SDSS J1416B and BD+01 2920B suggests they have similar metallicity (bottom panel of Figure 3.11). Thus the metallicity of SDSS J1416AB is around $-0.4 \leq$ [M/H] ≤ -0.3. Kinematics of SDSS J1416A indicated a thin disc membership (Schmidt et al. 2010a; Bowler, Liu & Dupuy 2010). By extension then, the classification of d/sdL7 for SDSS J1416A by Burningham et al. (2010a) seams reasonable. The NIR spectrum of SDSS J1416 fits in the spectral sequences between blue L7 and sdL7 very well in Figure 3.6.

Figure 3.12 shows that 2MASS J11582077+0435014 (2MASS J1158) has a very similar spectrum as SDSS J1416 which suggests 2MASS J1158 is more likely to be an mildly L7 subdwarf than an L7 subdwarf. It also has redder $J - K$ colour than the sdL7 ULAS J0216 and esdL7 2MASS J0532 (Figure 3.1). The space velocity of 2MASS J1158 was measured by Kirkpatrick et al. (2010), and indicated a thick-disk membership (e.g. Figure 11 of Burgasser, Cruz & Kirkpatrick 2007). Figure 3.13 shows spectra of 2MASS J1158, 2MASS J06453153−6646120 (2MASS J0645) and 2MASS J17561080+2815238. 2MASS J0645 and 2MASS J17561080+2815238 also do not have enough suppressed H and K band flux to be L subdwarfs. The CO band at 2.3 μm is presented in the spectra of these three objects. 2MASS J0645 has FeH in H band, and the presence of the CO band is not very clear which will support the sdL8 inference, but its relative red $J - K$ colour suggests that it may not be an L subdwarf. Further optical and K band spectra with better SNR are needed to confirm if 2MASS J0645 is an sdL8 or d/sdL8. For now I

suggest to classify these three metal-poor objects discovered by Kirkpatrick et al. (2010) as mildly L subdwarfs.

3.3.4 Halo brown dwarfs

The most massive BDs have spectral types of late-type M and are usually found in young open clusters ($\sim$ 100 Myr age). BDs of the Galactic disk are usually a few Gyr old (Figure 1.19) start with spectral types of L0. After about 10 Gyr of cooling, BDs would have temperature lower than 1600 K, corresponding to spectral types of late-type L, T and Y (Figure 1.3). Thus spectral types of old BDs in the halo should start with late-type L.

The esdL7, 2MASS J0532 is the first L subdwarf discovered and is the only one with theory predicated mass ($\sim$ 0.08 $M_{\odot}$) just below the hydrogen burning minimum mass (Section 1.1.1). Figure 3.14 (Bottom) shows spectra of M7 to L2 dwarfs which cover the star-BD transition region. H_2O absorption bands are strengthening from M7 to L2. Figure 3.14 (Top) shows spectra of four L subdwarfs. The depth of the H_2O absorption band around 1.4 μm in the spectrum of 2MASS J1626 is similar to that seen in late-type M dwarfs, a few Gyr old lowest mass stars with solar abundance. While the H_2O absorption depth (around 1.4 μm) of the spectrum of ULAS J1519 is similar to that of early-type L dwarfs, a few Gyr old massive BDs with solar abundance. The 1.15 μm H_2O band in ULAS J1519 is also much stronger than that in 2MASS J1626. With only two subtype difference, spectra of 2MASS J1626 and ULAS J1519 are showing significantly different features. Could the strengthen of 1.4 μm H_2O absorption band in ULAS J1519 be an indicator of a substellar subdwarf? If this is true 2MASS J0532, J0616, ULAS J1519 and ULAS J0216 would be the first four BDs discovered in the Galactic halo. Optical-NIR colours (e.g. $i - J$) are good indicator of spectral thus also $T_{\rm eff}$ for UCDs (Figure 1.21). A vertical dash-dot line ($i - J = 4.2$) in Figure 3.1 could then provide an indicative separation for lowest mass stars and BDs in the halo. The stellar-substellar gap between dwarfs and subdwarfs is likely to be around $i - J = 4.2$ corresponding to spectral type between esdL4 and esdL6 for extreme subdwarfs. A dot line indicates a minimum stellar-substellar boundary based on the facts that spectral types of disk field BD start with L0 and the known esdL7 halo BD 2MASS J0532. Further analysis based on the latest model grids and new astrometric observations are need to confirmed this hypothesis.

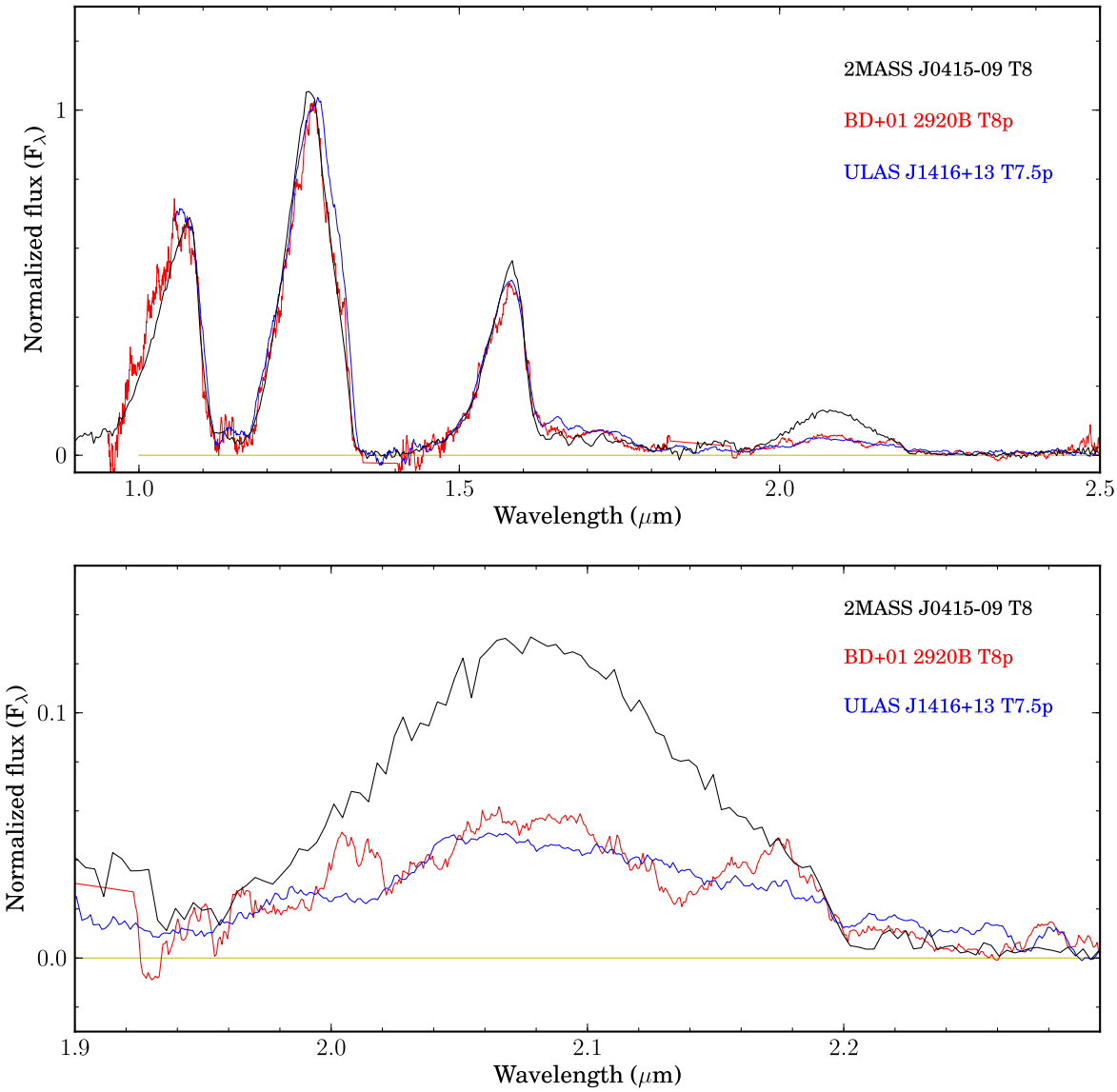

Figure 3.11: Spectra of two metal-poor T dwarfs in binary systems. The spectra are normalized to one at 1.28 μm. The IRCS JHK spectrum for ULAS J1416+13 is taken from Burningham et al. (2010a). GNIRS spectra for WISEP J1423+0116 (BD+01 2920B) is taken from Pinfield et al. (2012). The T8 spectral type template 2MASS J04151954–0935066 is taken from Burgasser et al. (2006a). A zoomed in plot of the K-band spectra is shown in the lower panel.

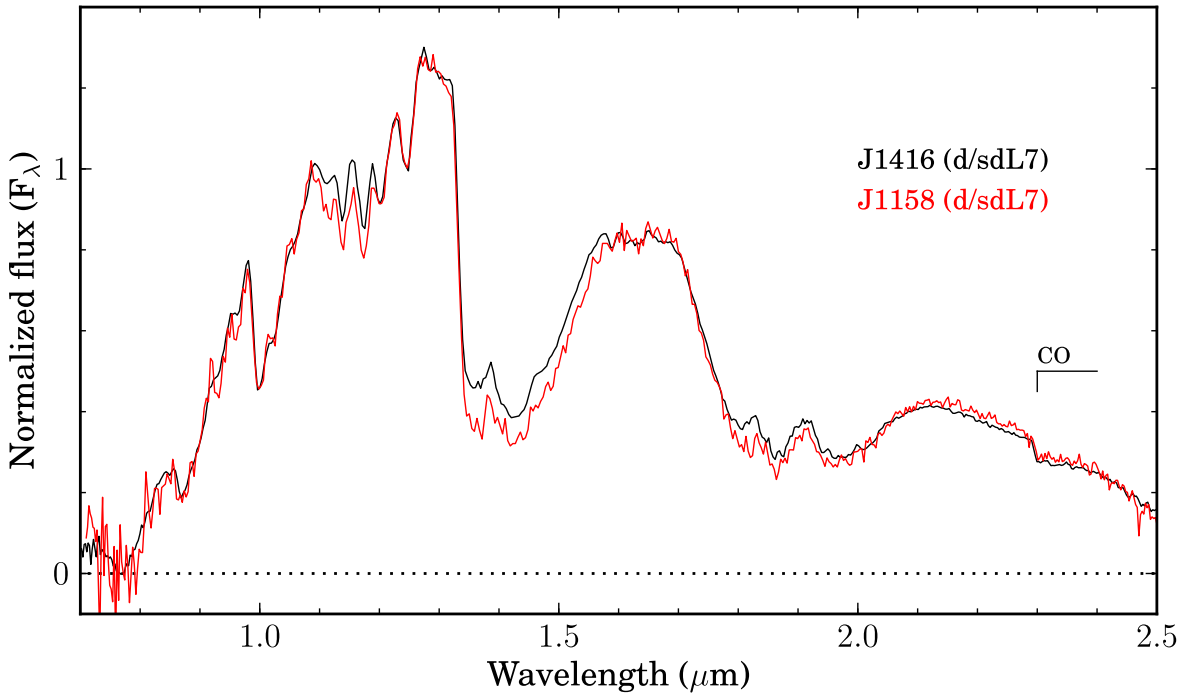

Figure 3.12: SpeX spectra of SDSS J1416 and 2MASS J1158. Very similar spectra indicate that they have the same spectral type. Spectra are normalized at 1.08 μm.

3.3.5 Purple dwarfs

In this section I will discuss the issue of what we call very cool dwarfs with subsolar abundance. I will discuss context, and practical factors that influence the choice, and present my own ideas.

Metal-deficient ultracool dwarfs of the Galactic halo are different from their counterparts in the Galactic disk, both observationally and physically. Halo ultracool dwarfs have much bluer NIR colours, and different kinematics compare to disk ultracool dwarfs. They formed at the beginning of the Galaxy and lived for long thus have different formation history.

Cool dwarfs with subsolar abundance were called subdwarfs by Kuiper (1939) because they lie below the main sequence in the Hertzsprung-Russell diagram. Now we known that cool subdwarfs lying below main sequence in the HRD is because they are bluer than equivalent-mass main sequence dwarfs. Main sequence dwarf stars appear more luminous than same colour cool subdwarfs is because they are more massive, and not comparable. Thus cool subdwarfs are not sub-luminous dwarfs but bluish dwarfs.

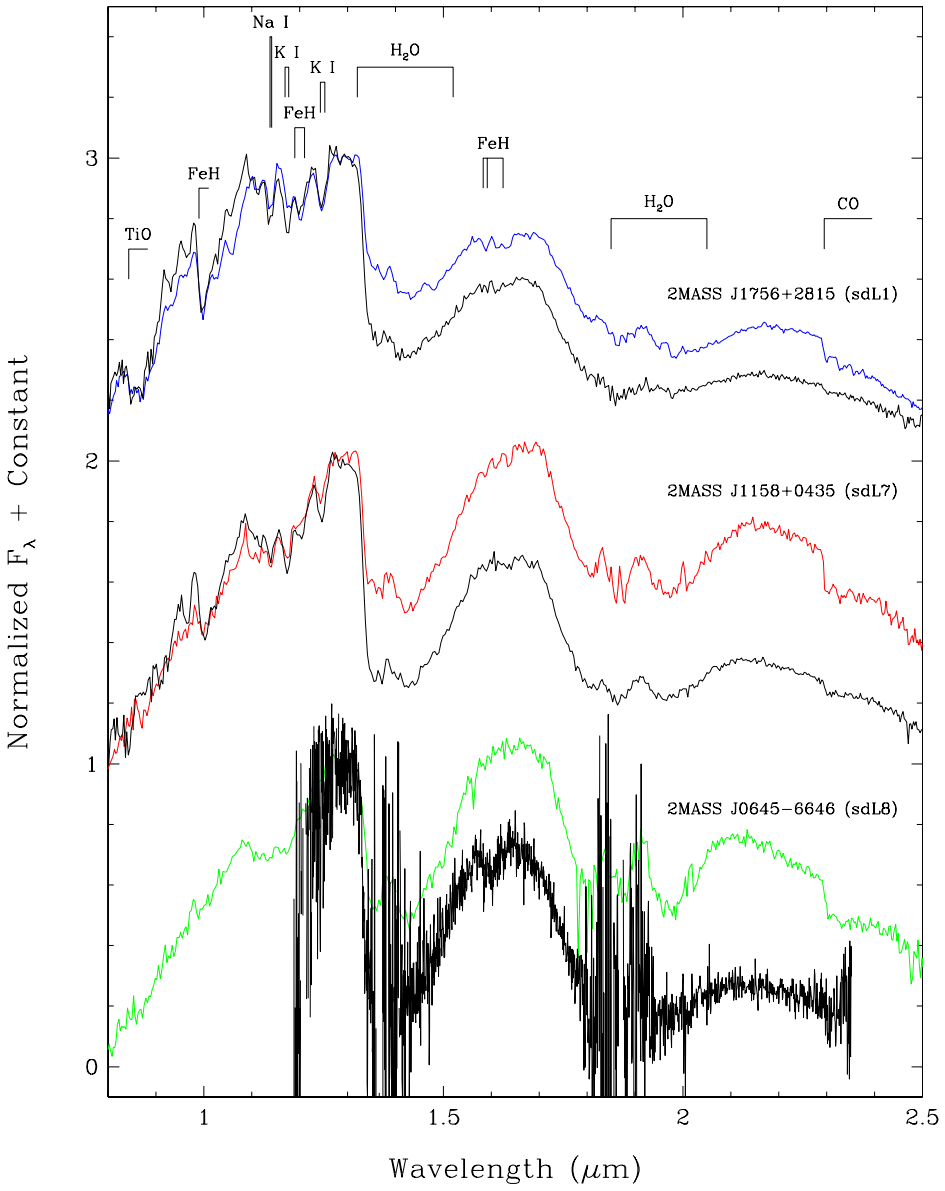

Figure 3.13: NIR spectra of three mildly L subdwarfs (black lines) discovered by Kirkpatrick et al. (2010). Over plotted for comparison are near-infrared standards: the L1 dwarf 2MASS J2130−0845 (blue), the L7 dwarf 2MASS J0103+1935 (red), and the L8 dwarf 2MASS J1632+1904 (green). Spectra are normalized to one at 1.28 μm and integer offsets added when needed to separate the spectra vertically. The figure is from Kirkpatrick et al. (2010).

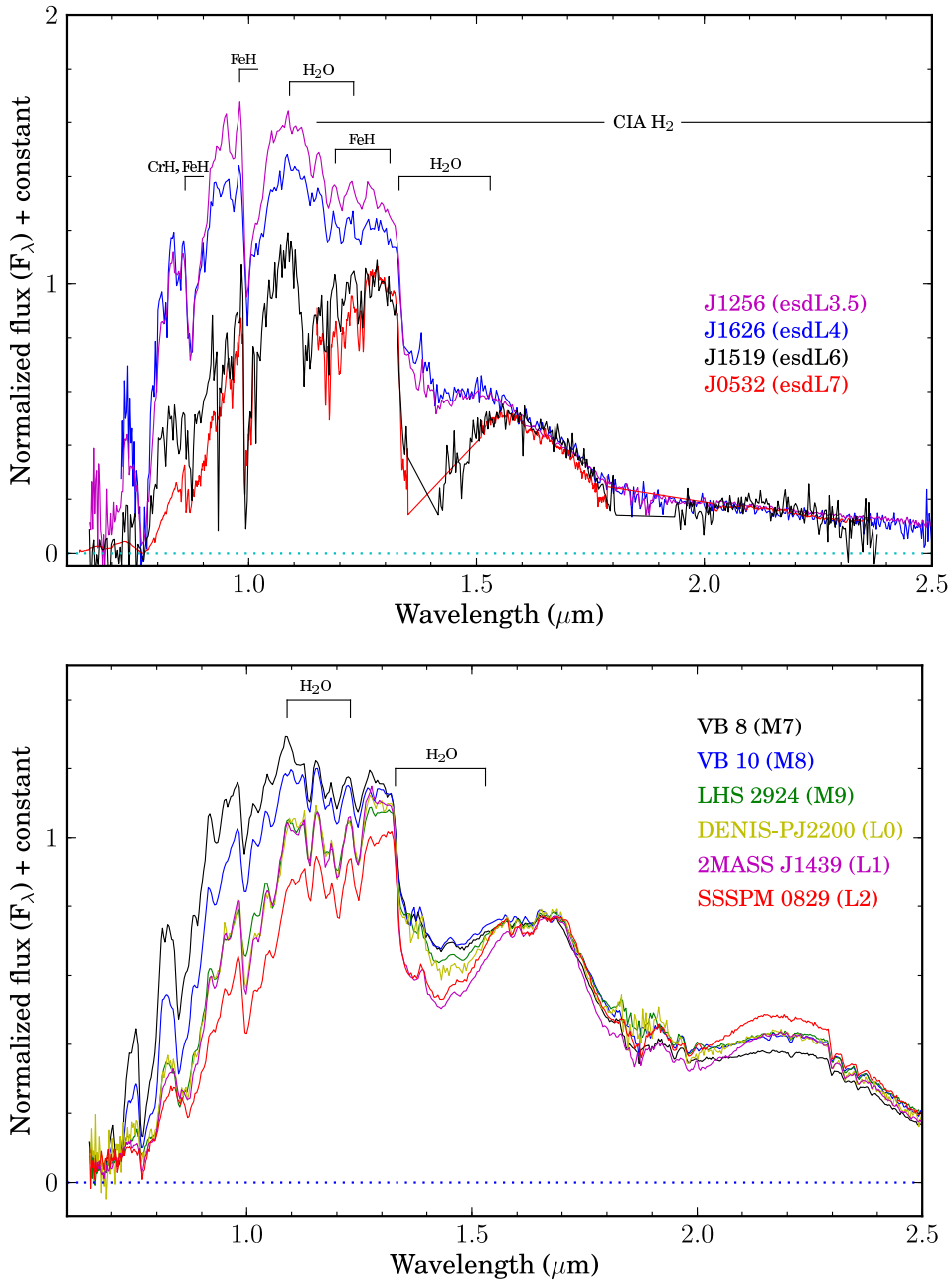

Figure 3.14: Top: Optical and NIR spectra of four L type extreme subdwarfs. Deep 1.4 μm H_2O absorption in ULAS 1519 and 2MASS J0532 which are different from 2MASS J1626 indicates that they might be halo brown dwarfs or substellar subdwarfs. Bottom: Spectra of M7 - L2 dwarfs. Spectra are normalized at 1.6 μm.

Absolute magnitude - spectral type relationships of M and L subdwarfs in r, i, z and J bands show that subsolar abundance cool dwarfs are "sub" dwarf only at $\leq$M5 type, and become "super" dwarfs from M6 to L type (Zhang et al. 2013) and appear above the dwarf sequence. Thus it is not suitable to use prefix "sub" to address the metal-poor ultracool dwarfs which are actually brighter than or "above" the dwarf sequence.

Tarter (1975) first used "brown dwarfs" to distinguish substellar dwarfs from dwarf stars in her thesis before they were actually discovered. A colour prefix could also be a good option to distinguish lowest-mass stars and BDs with subsolar and solar abundances. "purple dwarf" is one option, because metal-deficient very low mass stars and BDs are very cool and red but bluer than their solar metallicity counterpart. Jao et al. (2008) suggest not to use "sd" (e.g. sdK, sdM) to distinguish low metallicity cool subdwarfs from other populations because it is also used for a different population hot subdwarfs (sdO, sdB). We can use "pd" as a short prefix to the spectral types. For instance, ULAS J0216 is a pdL7 type purple dwarf. We still can use "e" of extreme, "u" of ultra as indicators of metal classes. For instance, 2MASS J0532 is an epdL7 type purple dwarf.

3.4 Summary

In this Chapter I discussed properties of L subdwarfs, and described methods I have developed to search for L subdwarfs in large scale surveys (SDSS, UKIDSS). I reported and discussed my results in the context of the literature and theoretical expectations. Four of my candidates have been followed up and confirmed as L subdwarfs with ground based telescopes (VLT, Magellan). Three of them are new discoveries, bringing the known number of L subdwarfs from seven to ten. I re-examined the spectral types and metallicity estimates of new and known L subdwarfs. I presented a metallicity standard sequence for L7 dwarfs ranging from red dL7 to normal dL7 to sdL7. I proposed to use the absence of the CO absorption band at 2.3-2.4 μm to distinguish L subdwarfs from L dwarfs. I discussed the possibility that a substellar subdwarf gap can be found in the $i-J$ vs $J-K$ colour-colour plot. I discussed spectral signatures of halo BD and listed four L subdwarfs as candidates. Two of them are discovered in this thesis project. More L subdwarfs are expected to be discovered from my ongoing projects based on SDSS, UKIDSS and VISTA surveys and ground based telescopes (Section 7.2.1).

Chapter 4

Discovery of the first wide L dwarf giant binary system and eight other ultracool dwarfs in wide binaries

4.1 Abstract

In this chapter I expand on my search for ultracool dwarfs (Chapter 2), and report on my work to identify such objects as companions in binary or multiple systems, where the physics of their atmospheres and structure can be more robustly tested. I have identified 806 ultra-cool dwarfs from their SDSS *riz* photometry (of which 34 are newly discovered L dwarfs) and obtain proper motions through cross matching with UKIDSS and 2MASS. Proper motion and distance constraints show that nine of my ultra-cool dwarfs are members of widely separated binary systems; SDSS J0101 (K5V+M9.5V), SDSS J0207 (M1.5V+L3V), SDSS J0832 (K3III+L3.5V), SDSS J0858 (M4V+L0V), SDSS J0953 (M4V+M9.5V), SDSS J0956 (M2V+M9V), SDSS J1304 (M4.5V+L0V), SDSS J1631 (M5.5V+M8V), SDSS J1638 (M4V+L0V). One of these (SDSS 0J832) is shown to be a companion to the bright K3 giant η Cancri. Such primaries can provide age and metallicity constraints for any companion objects, yielding excellent benchmark objects. η Cancri AB is the first wide ultra-cool dwarf + giant binary system identified. I present new observations and analysis that constrain the metallicity of η Cancri A to be near solar, and use recent evolutionary models to constrain the age of the giant to be 2.2−6.1 Gyr. If η Cancri B is a single object, I estimate its physical attributes to be; mass =

63−82 M_{Jup}, $T_{\rm eff}$ = 1800±150 K, log g = 5.3−5.5, [M/H] = 0.0±0.1. Its colours are non typical when compared to other ultra-cool dwarfs, and I also assess the possibility that η Cancri B is itself an unresolved binary, showing that the combined light of an L4 + T4 system could provide a reasonable explanation for its colours.

4.2 Publication, Zhang et al. 2010, MNRAS, 404, 1817-1834

This chapter has been published as an peer reviewed paper in the journal *"Monthly Notices of the Royal Astronomical Society"* (Zhang et al. 2010, bond at the end of the thesis).

Chapter 5

A spectroscopic and proper motion search of SDSS. Red subdwarfs in binary systems

5.1 Abstract

In this chapter I build on my search methods for ultracool halo dwarfs (Chapter 3), and also on the idea of finding benchmark objects in binary systems. I report on my search for ultracool subdwarfs as members of binary systems. M subdwarfs in binary systems are the key for both model calibration and spectral classification/characterization. I have identified M subdwarfs in binary systems from a search of high proper motion objects in SDSS that have spectroscopy. I present my discoveries from the main paper as well as high lighting several additional objects of interests. I find 30 cool subdwarf wide binary systems, two of which have spectral type esdM5.5, six of which are companions to white dwarfs, and three of which are carbon subdwarfs. A carbon dwarf is a carbon enhanced cool dwarf and have C_2 swan bands in its optical spectrum. A carbon subdwarf is a carbon enhanced cool subdwarf, and has spectral features of both carbon dwarfs and cool subdwarfs. I also present 15 cool subdwarfs that are partially resolved close binary systems. I estimate the binary fraction of M subdwarfs. A spectroscopic esdK7+WD binary is also reported. Thirty new M subdwarfs have spectral type of M6 or later in our sample and are thus ultracool. I fit the relationships between spectral type and optical and NIR absolute magnitude for M and L subdwarfs. I measure the UVW space velocities

of my M subdwarf sample.

5.2 Publication, Zhang et al. 2013, MNRAS, e-print, astro-ph/1306.3060

This chapter forms a paper has been accepted to publish on the journal *"Monthly Notices of the Royal Astronomical Society"* (Zhang et al. 2013, bond at the end of the thesis).

Chapter 6

Conclusions

In this Chapter I will summarize scientific results and scientific impacts of this thesis project described in Chapter 2–5.

6.1 Discovery of ultracool dwarfs with large scale surveys

I used photometric and astrometric data from the large scale surveys, SDSS, UKIDSS and 2MASS (Chapter 1.4.3). I identified around 1000 ultracool dwarfs, mostly late M and L dwarfs, including 82 spectroscopy confirmed L dwarfs and 129 L dwarf candidates (Chapter 2 & 4). Twelve of these objects are at the L/T transition region. This work largely increased the known number of ultracool dwarfs in the solar neighbourhood. I measured proper motions of these objects based on epochs of different surveys. Proper motions are used to identify wide binary companions of these ultracool dwarfs. Eighteen new UCD wide binary systems are identify in this UCD sample. I also updated colour-spectral type relations for L and T dwarfs. This relationship is used to estimate the spectral types of ultracool dwarf candidates which only have photometric data available. With this relationship I estimated the spectral types of 129 L dwarf candidates, and some of them are confirmed as L dwarfs recently (e.g. Kirkpatrick et al. 2011; Day-Jones et al. 2013).

One L dwarf SDSS J141624.08+134826.7 (SDSS J1416) is missed by my search (Zhang et al. 2009) because it is too bright to survive my criteria. SDSS J1416 is found

to be a blue L7 dwarf with metallicity around $-0.4 < [M/H] < -0.3$ later (Bowler, Liu & Dupuy 2010; Schmidt et al. 2010a; Cushing, Saumon & Marley 2010). Even more interestingly, SDSS J1416 is found to be a wide binary system with a very blue T7.5 dwarf companion (Burningham et al. 2010a; Scholz 2010a; Burgasser, Looper & Rayner 2010). A binary brown dwarf at 2 parsec from the sun is discovered recently by Luhman (2013). The L7.5 + T0.5 binary now referred as "Luhman 16" is an extreme interesting flux reversal binary at the L dwarf/T dwarf transition (Mamajek 2013; Kniazev et al. 2013; Burgasser, Sheppard & Luhman 2013; Gillon et al. 2013). These two cases show that there are still some particular brown dwarfs to be discovered in the solar neighbourhood which could reveal new features of brown dwarfs.

6.2 Populations of chemically peculiar low-mass stars

Chemically peculiar populations contain more information of the Galaxy. We can study the formation, structure and evolution of of the Galaxy by measure binary fraction, kinematics and metallicity distribution of low mass subdwarfs.

I selected about 1800 red subdwarfs with proper motion greater than 100 mas/yr from the SDSS. Forty two of these objects are late M subdwarfs with spectral type ≥M6. Thirty of them are new ones, including nine M6.5–M7.5 subdwarfs. Late type M subdwarfs are significantly less numerous than early type M subdwarfs because they are fainter and have lower space density than early M types according to the mass function (Figure 1.20). There are only around seventy ≥M7 subdwarfs that have been found before my work. I fitted the absolute magnitude – spectral type relationship of subdwarfs covering M and L types for the first time. I found subdwarfs behave different compare with M and L dwarfs. Metal-poor cool dwarfs are "sub" dwarf only for spectral types of ≤M5, and become "super" dwarfs for >M5 and into the L dwarf region for r, i, z and J band magnitudes.

I estimated distances of M subdwarfs in my sample using the absolute magnitude – spectral type relationships, and derived U, V, W space velocities. I found a fraction of M dwarfs have halo like kinematics. There are also some M subdwarfs have disk kinematics in the original sample. Study by Spagna et al. (2010) based on FGK stars shows that the metallicity of thick disk population is down to [m/H] ∼ –1.2. Halo and disk populations have overlaps of metallicity and kinematics. Thus a star has either metallicity down to [m/H] ∼ –1.2 or halo-like kinematics does not always mean it is belong to the Population

II. It is not clear weather these red subdwarfs with disk-like kinematics are formed in metal-poor regions of the Galactic disk or in the halo but had interaction with disk population. We also do not known why some red dwarfs have halo-like kinematics. More precise observations are need to address these issues. We might be able to answer these questions with the Gaia space telescope in future.

Five M subdwarfs are found to have much higher gravity than normal subdwarfs. They normally have very low metallicity [M/H] $\sim$ –2.0. These objects provide a good testbed for gravity effects on the spectra of red cool stars. These high gravity features are only found in M ultra subdwarfs which may reveal the role that metallicity plays in the formation and evolution history of low mass stars.

I identified fourteen carbon rich red subdwarfs which represents a new population, "carbon subdwarfs". They are presumably very old versions of the galactic population of carbon stars. It is still not clear that where the carbon abundance of carbon dwarfs and subdwarfs comes from. Hundreds of carbon subdwarfs could be identified with current spectroscopic surveys (e.g. SDSS, LAMOST).

6.3 Purple dwarfs: lowest-mass stars and brown dwarfs of the Galactic halo

I identified three new L subdwarfs from SDSS and UKIDSS (Chapter 3). One of these L subdwarfs is confirmed as an L3 subdwarf with an SDSS spectrum. One is confirmed as an L7 subdwarf, one as an L6 extreme subdwarf with the X-Shooter on the Very Large Telescope. This project increased the number of known L subdwarfs from seven to ten. I also independently confirmed a known L subdwarf which was discovered by Lodieu et al. (2012c). I obtained its optical spectrum with the Magellan Telescope in 2010. I presented a metal sequence of L7 dwarfs and subdwarfs and proposed to use 2.3 μm CO line as an indicator of L subdwarfs. L subdwarf classification system has not been established due to the lack of known L subdwarfs. Current classification of known L subdwarfs have large uncertainties. Thus I re-examined corrected the spectral types and metal classes of all known L subdwarfs. I found four of these ten L subdwarfs are possible halo brown dwarfs or substellar subdwarfs, two them are discovered by myself. I discussed the spectral features of halo BDs. I proposed a new name "purple dwarf" for the lowest-mass stars and brown dwarfs with subsolar abundance. This work shows what halo brown dwarfs look

like. Dr Mark Marley, a modeller said this work triggers him to develop the atmospheric models (Marley et al. 2002) of low-metallicity.

I am not be able to measure the ultracool halo luminosity and mass function in this thesis because my L subdwarf sample is still too small. However, my work has shows the potential to discover more L subdwarfs with ongoing sky surveys. I am following up more candidates with the large ground based telescopes. I expect to measure the ultracool mass function of the Galactic halo in one or two years (Section 7.2.1).

6.4 Discovery of ultracool dwarf benchmarks

I discovered nineteen widely separated binary systems in Zhang et al. (2010) and Zhang et al. (2013) . One of these systems, η Cancri AB is the first giant + BD binary identified. Such primaries can provide age and metallicity constraints for any companion objects, yielding excellent benchmark objects. I present new observations and analysis that constrain the metallicity of η Cancri A to be near solar, and use recent evolutionary models to constrain the age of the giant to be 2.2−6.1 Gyr. If η Cancri B is a single object, I estimate its physical attributes to be; mass = 63−82 M_{Jup}, $T_{\rm eff}$ = 1800±150 K, log g = 5.3−5.5, [M/H] = 0.0±0.1. Colours of η Cancri B are non typical when compared to other ultracool dwarfs, and I also assess the possibility that η Cancri B is itself an unresolved binary, showing that the combined light of an L4 + T4 system could provide a reasonable explanation for its colours.

I have observed the optical and NIR spectra of η Cancri B with the Gemini North Telescope. I will analysis of these new spectra to unveil the binary status of η Cancri B in the near future (Section 7.1). If confirmed as an unresolved binary, η Cancri B would be an ideal brown dwarf benchmark with constrained distance, age, metallicity and mass, and could be used to calibrate ultracool atmospheric and evolutionary models. If it is shown to be a single object then its unusual colours may be revealing interesting sensitivity to its physical properties.

6.5 Red subdwarf binaries and binary fraction

Ultracool atmosphere models in low-metallicity regions have not been well calibrated due to the lack of metal-poor ultracool benchmarks. M subdwarf binary fraction is not

well measured due to the size and completeness of previous samples (e.g. Riaz, Gizis & Samaddar 2008; Jao et al. 2009; Lodieu, Zapatero Osorio & Martín 2009). Gravity is not considered in current M subdwarf classification method (e.g. Lépine, Rich & Shara 2007; Jao et al. 2008). I search for binaries in my red subdwarf sample from SDSS, and find 45 red subdwarf binary systems.

Thirty red subdwarfs in wide binary systems are identified by common proper motions and visual inspection. G 224-58AB is one of my widest binary systems which contains an esdK2 and an esdM5.5 type subdwarf. Such binary systems are rare and valuable for model calibration. SDSS J210105.37–065633.0AB is a closer binary system contain an esdK1.5 and an esdK5.5 type subdwarf. I have obtained the optical spectra of both companions with GMOS on the Gemini North Telescope recently. I will use this binary to calibrate ultracool metal-poor atmospheres, test classification methods and gravity effects of M subdwarfs (Section 7.2.3). Six of my red subdwarfs are companions to white dwarfs. With age constraints from white dwarf companions of these systems I would be able to study the chemistry evolution as a function of time. Three carbon subdwarfs are found to be in binary systems with subdwarf companions. With the help of these binary systems I identified a new population of carbon subdwarfs. These binaries will help us to measure carbon and metallicity abundance accurately. I also found fifteen partially resolved red subdwarf binary systems.

My binary search is not complete. Fainter companions are missed due to the depth of surveys and incompleteness of proper motion catalogue. These binaries could allow us to put a low limit of binary fraction of red subdwarfs. I find the binary fraction of red subdwarfs at $\gtrsim$100 au is larger than $\sim$ 5%. I also find that the binary fraction of red subdwarfs reduces with the decreasing masses and metallicities of subdwarfs.

Deep imaging survey would be very useful to find cooler companions of red subdwarfs. I have selected a few hundreds of colour selected candidates of red subdwarf binary from SDSS. I plan to measure their PMs to confirmed their binary status. I have obtained second epoch images of candidates not in UKIDSS coverage with the ISPI on the Blanco telescope (Section 7.2.2). More complete and deeper PM catalogues (e.g. Gaia) and deep imaging surveys are needed to find wide and cooler companions of my red subdwarfs. High spatial resolution imaging is needed to search for close binaries ($<$ 100 au). These new searches would not only allow us to put tighter constraint on binary fraction but also find ultracool subdwarfs benchmarks which can be used to test low-metallicity ultracool atmosphere models.

6.6 Summary

This project discovered a large number of lowest mass stars and BDs with various physical properties. The discovery of new UCDs would aid the statistical study of BDs. L/T transition BDs and UCSDs found here are particular useful because the physics of L/T transition and metal-poor regions are poorly understood. Extreme wide binary systems found in the thesis is a challenge of formation theories of low-mass star and BDs. I found that the binary fraction of red subdwarfs reduces with the decreasing masses and metallicities of subdwarfs. New discovery of new halo BDs opening new views of ultracool objects of the Galactic halo. I also discovered new populations of carbon rich subdwarfs and high gravity subdwarfs which might related to new physical processes of star formation and evolution. M subdwarfs confirmed in this thesis could be targeted for the search of first planets. Chapter 7 describe works I plan to do in future following the thesis project.

Chapter 7

Future work

In this Chapter I will describe how I plan to follow on from the research (described in Chapters 3, 4 and 5) in the near future.

7.1 Calibrating ultracool models with η Cancri B

This work is following results from Chapter 4. η Cancri B is an L3.5 dwarf companion to the K3 III giant η Cancri A, which has good measurement of distance, constraints of age (2.2-6.1 Gyr) and metallicity ([M/H] = 0.0±0.1 dex. It has mass of 63-82 $M_{\rm Jup}$, just below the hydrogen burning minimum mass. However, its NIR colours are unusual when compared to other UCDs. The $Y-J, J-H$ and $J-K$ colours stand out amongst its full compliment of colour criteria as significantly bluer than expected for its spectral type. In fact, these unusual colour are consistent with η Cancri B itself being an unresolved binary containing an L and a T dwarf, where it is the emission of the T dwarf that has resulted in the observed bluer near infrared colours. Indeed, I have used empirical absolute magnitude – spectral type relations (e.g. Liu et al. 2006) to demonstrate that the combined light of an L4 + T4 unresolved binary could provide a good explanation for all the observed colours (Zhang et al. 2010)).

I have obtained optical and NIR spectrum of *eta* Cancri B with GMOS and GNIRS on the Gemini North Telescope. This data will allow us to achieve the following. (i) By fitting a series of composite template spectra to the observed spectrum of η Cancri B, I will comprehensively establish if an unresolved binary provides a good explanation for the full optical-NIR spectrum of this object. In this case I will determine the optimal combination

of L/T dwarfs that make up the unresolved system (e.g. Burgasser et al. 2010). Optical and NIR coverage will facilitate a particularly rigorous test of the binary scenario, and allow an accurate determination of the spectral types of the L/T constituents. (ii) I will use the $izZYJHK$ photometry to calibrate the full optical NIR SED for η Cancri B and thus accurately measure the bolometric flux for the source (e.g. Burningham et al. 2009). Combined with the system's known distance (from the parallax of the primary) this will lead to a well determined luminosity and thus $T_{\rm eff}$ for this benchmark object or objects (via recourse only to well constrained theoretical radii for such system ages). I will then be able to infer more reliable mass(es) and log$g$(s) by comparison with evolutionary model predicted luminosities. (iii) Spectral type constraints will establish an independent spectroscopic distance for η Cancri B, and I would expect this to further decrease the (already very small) probability of the system being a change alignment.

I will thus establish the multiplicity of this benchmark object, and greatly improve the accuracy with which we know the properties of the ultracool component(s). If confirmed as an unresolved binary, then η Cancri B would become a very compelling target for high spatial resolution adaptive optics observations that may be able to resolve the components and measure the orbit. This could yield dynamical mass determinations (and log$g$ determinations) via absolute astrometric monitoring (e.g. King et al. 2010).

Irrespective of the multiplicity of η Cancri B, it will provide a valuable test for dusty model atmospheres, and if a resolvable multiple, could eventually provide a wealth of benchmark information to test our understanding of ultracool dusty atmospheres.

7.2 Studies of the galactic Halo via Its NEarby low-mass Dwarfs (SHINED)

The SHINED project is trying to understand the formation and structure of the galactic halo by measuring the mass function, binary fraction and kinematics of nearby red and ultracool subdwarfs. Chapters 3 and 5 are also part of this project.

7.2.1 Measuring the halo ultracool mass function

The project is a continuation of Chapter 3. L subdwarf candidates selected from SDSS+ULAS (see Section 3.2) have been followed up spectroscopically. Eight L subdwarfs have been

found in my candidate list. Around 40 L subdwarfs are expected to be identified in the SDSS+ULAS DR9 sample. With this sample we will be able to a new define the L subdwarf classification system. In turn this new population will provide a measure of the halo luminosity function in the ultracool region. I will use standard techniques to measure the luminosities for my sample. With my sample of L subdwarfs, I plan to constrain the halo ultracool LF at a level of ±16% (considering Possion statistics).

Forty one hours of the 10.4 m Gran Telescopio Canarias time has been awarded to this project in 2012B and 2013A. I will update my search for L subdwarfs with the new ULAS data releases. I also plan to expand the search for L subdwarfs in the VHS and VIKING VISTA surveys and will conduct an ongoing systematic search as the coverage is released.

7.2.2 Searching for ultracool subdwarf binaries

This project is a continuation and expansion of Chapter 5. Cool subdwarfs in binary systems are the key for model calibration and spectral classification/characterization. Discovery of a sample of subdwarf binary systems is therefore critical. I have started a project to identify ultracool subdwarf binaries. I identify UCSD binaries with three methods: common proper motions, high resolution imaging and spectra fitting.

The first method is to look for common proper motion pairs of UCSDs. Common proper motion has widely used to identify wide ultracool dwarf binaries (e.g. Pinfield et al. 2012; Day-Jones et al. 2011a; Burningham et al. 2010a; Faherty et al. 2010; Zhang et al. 2010). I have discovered 30 red cool subdwarf (late type K to late type M) binary systems using the common proper motion method (Chapter 5). I would apply the method on the search for UCSD binary systems. The LAMOST could provide much more M subdwarfs than SDSS, and I have immediate access to the LAMOST data via my collaborators in China. Will also cross match UCSD candidates from SDSS/UKIDSS/VISTA/WISE searches with SDSS and LAMOST M subdwarfs. Good binary candidates will be followed up with second epoch imaging to measure proper motions. Confirmed common proper motion binaries will be follow up with spectroscopy.

The second method to look for faint or close companions of known M and L subdwarfs by deep or high resolution imaging. The first L, T and Y dwarfs are all discovered as companions to brighter stars/white dwarfs (GD 165B, Becklin & Zuckerman 1988; Gliese 229B, Nakajima et al. 1995; CFBDSIR J1458+1013B, Liu et al. 2011b; WD 0806-

661B,Luhman, Burgasser & Bochanski 2011; Luhman et al. 2012). I have selected more than 5000 spectroscopic confirmed M subdwarfs from SDSS. Some of them are resolved as close binaries in SDSS (0.4"/pixel) and UKIDSS images (0.2"/pixel). I am planning to start a project to search for companions of these SDSS M subdwarfs with space and grand based telescopes (e.g. ACS/WFC on the HST and the GSAOI on Gemini South).

The third method to identify close binaries is by fitting the observed spectra with combined template spectra (e.g. Burgasser et al. 2010). I was part of a collaboration that was awarded 26 nights of VLT X-shooter time to study the Galactic brown dwarf birthrate. I selected all the targets for this project. I have obtained over 200 spectra in the 26 nights (Day-Jones et al. 2013). A systematic search for close unresolved brown dwarf binaries has been conduced by the team. I will adopt this method to searches for L and T subdwarf binaries in my sample.

I selected subdwarf targets from the SDSS spectroscopic database according to the $g-r$ and $r-i$ colours of M subdwarfs. I downloaded all the spectra of objects in SDSS DR7 with the colours of M subdwarfs and measured their spectral type with a late K and M subdwarf classification code (Lépine, Rich & Shara 2007). About 5639 M subdwarfs are identified in the sample. Then I selected a subdwarf binary candidate sample based on proper motions and colours, and cross matched to identify candidate associations. Thirty wide cool subdwarf binaries are already identified (Zhang et al. 2013), of which with ultracool components will be used to calibrate metal-poor ultracool atmospheres, of which with two different subtype M subdwarf components will be used to calibrate M subdwarf classification methods.

I also selected around 300 binary candidate based on colours only. I will measure their proper motions base on their SDSS and ULAS epochs with IRAF. I obtained second epoch images with ISPI on the Blanco Telescope for over 100 binary candidates with a short baseline between the SDSS and UKIDSS images ($<$ 3yr) or not covered in UKIDSS. A sample of M subdwarf binaries are expected to be identified from this work. Confirmed M subdwarf binary systems will be followed up with spectroscopic observations for further study of the binary fraction, ultracool metal-poor model atmospheres (e.g. Drift-PHOENIX, Witte, Helling & Hauschildt 2009) calibration, and M subdwarf spectral classification methods.

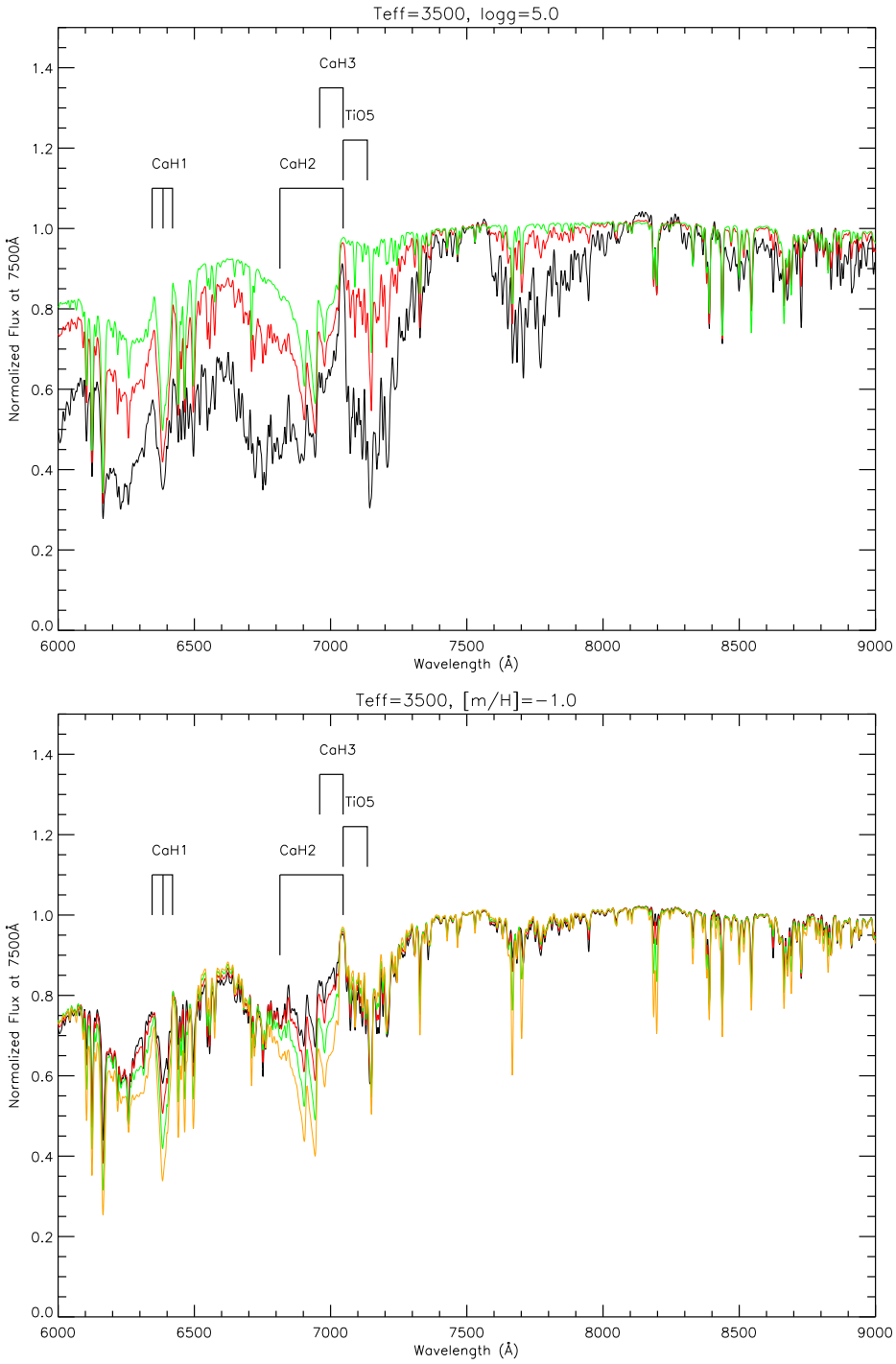

Figure 7.1: Top plot shows Gaia model spectra at fixed log $g = 5.0$ and $T = 3500$K. Black, red and green lines represent various metallicities of [m/H] = 0.0, −1.0 and −2.0, respectively. The bottom plot shows Gaia-Phoenix model spectra at fixed metallicity ([m/H]= −1.0) and effective temperature (3500K). Black, red, green and yellow lines represent *log* $g = 4.0$, 4.5, 5.0 and 5.5, respectively. The figures are from Jao et al. (2008).

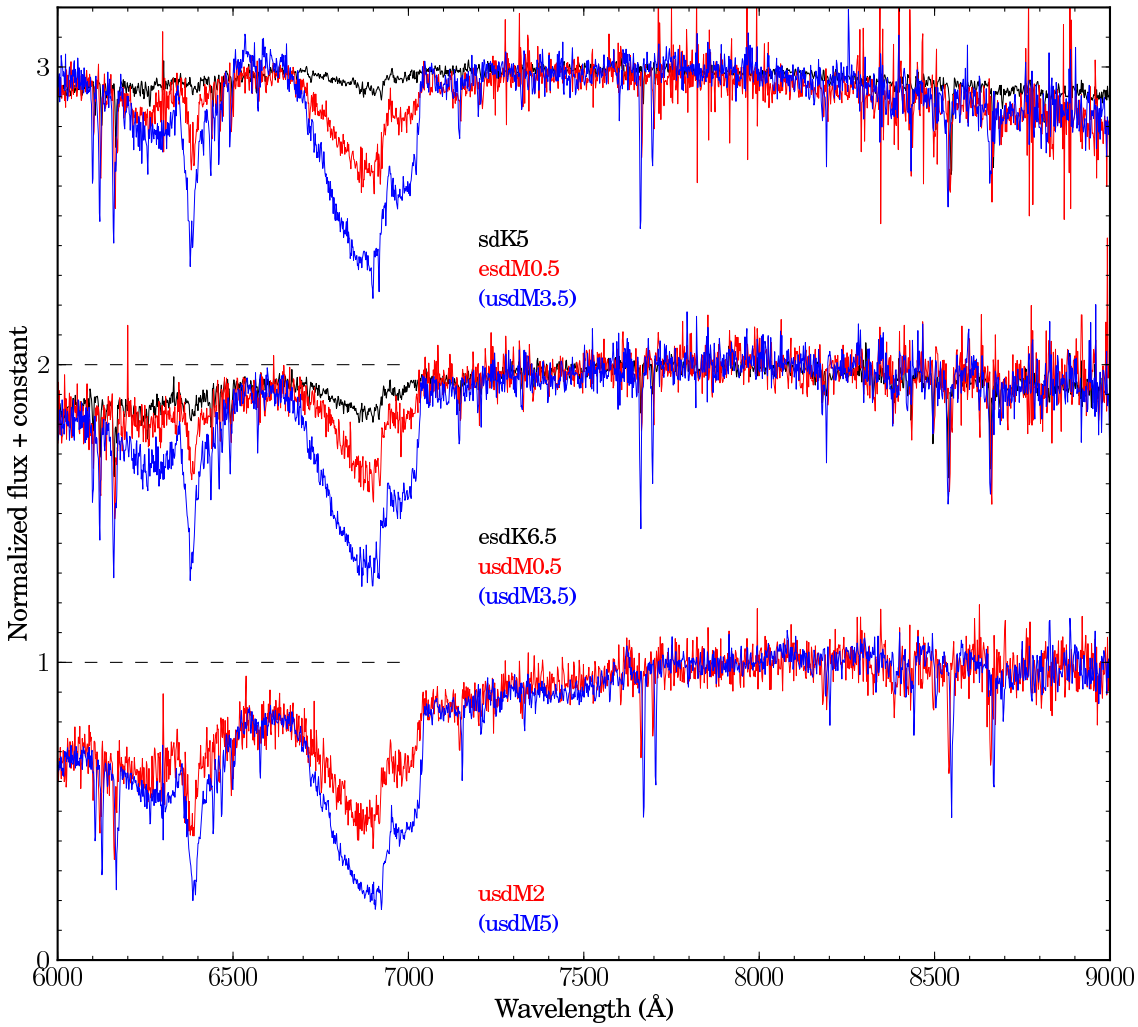

Figure 7.2: SDSS spectra of cool subdwarfs with different gravities. Each set of spectra have the same overall profile ($T_{\rm eff}$) and depth of TiO index ([M/H]) but different depth of CaH indices (gravity). Spectral types given above are based on Lépine, Rich & Shara (2007). Small wavelength shifts in the lines are due to different radial velocity. All spectra are normalized at λ8000Å.

7.2.3 Measuring gravity affects on M subdwarf spectra

Cool subdwarfs classification and characterization is a rapidly evolving field. There is a debate about cool subdwarf classification. M subdwarfs are classified into three metal classes: subdwarf (sdM), extreme subdwarf (esdM) and ultra subdwarf (usdM) based on the ratio of TiO to CaH (Lépine, Rich & Shara 2007). The CaH and TiO indices are easy to measure and sensitive to temperature and metallicity. But Jao et al. (2008) found that the CaH and TiO indices are affected in complicated ways by combinations of temperatures, metallicities and gravities of M subdwarfs.

Model spectra shows that the TiO5 line is less sensitive to gravity but more sensitive to metallicity than the CaH indices. The overall profile of subdwarf spectra are mainly affected by temperature, and also by metallicity (see Figure 1.7). When temperature decreases both CaH and TiO5 absorption bands get deeper. When metallicity decreases both CaH and TiO5 bands get shallower, but TiO5 is affected more dramatically (top of Figure 7.1). When gravity increases CaH get deeper and TiO5 remains the same. TiO5 will lose its oxygen when there is not much or when more H_2O is formed under high gravity. I did found some M subdwarfs show variation of gravity from their spectra. Figure 7.2 shows SDSS spectra of three high gravity M subdwarfs. Spectra of three normal M subdwarfs are over plotted for comparison. Similar overall profile indicates that each set of spectra have similar temperature; similar TiO5 absorption depth indicates similar metallicity for each set of spectra; but different absorption depth show different gravity. The effect of higher gravity on CaH indices will be treated as effect of lower temperature and metallicity in the spectral typing method based on the ratio of TiO to CaH. In this case we would not be able to measure the correct metallicity and subtype for subdwarfs with unusual gravity. Each set of spectra with same overall profile and TiO index will classify into different spectral types and metallicity class according Lépine, Rich & Shara (2007).

An ideal test of the affects of gravity on the spectra of M subdwarfs is a binary system with two M subdwarfs which have the same age and metallicity. With the same affect on spectra from metallicity, we would be able to measure the difference in the gravity affect on broad band indices of CaH2, CaH3 and TiO5. M subdwarf binaries used for this project were discovered in Zhang et al. (2013) and new discoveries from Section 7.2.2.

7.3 First planets and first stars

I describe two projects I plan to do in the longer future. They are the discovery of the first planets around low mass stars of the Population II and the discovery of low mass stars of Population III.

7.3.1 Advanced Planets Of Local LOw-metallicity stars (APOLLO)

Johnson & Li (2012) estimated a lower limit for the critical abundance for planet formation of $[\mathrm{M/H}]_{cri} \simeq -1.5 + \log(r/1\ \mathrm{au})$, where r is the distance of a planet from its parent star. Thus planets could form around stars with metallicity of $[\mathrm{M/H}] = -1.5 \pm 1.0$. Giant planets have been found around metal-poor stars of globular clusters and the outer Galactic halo (Ford et al. 2000; Sigurdsson et al. 2003; Setiawan et al. 2010). Giant planet frequency is a strong function of metallicity, even in the low-metallicity tail, the frequencies are most likely higher than previously thought (Mortier et al. 2012).

Earth-sized planets of other stars are more common than we though. Analysis of data from the Kepler mission (Koch et al. 2010) shows that 16.5% ±3.6% of main-sequence FGK stars have at least one planet between 0.8 and 1.25 $R_\oplus$ (Fressin et al. 2013). Earth-mass planets in the habitable zone (e.g. Kasting, Whitmire & Reynolds 1993; Selsis et al. 2007; Kopparapu et al. 2013) of their parent stars have been discovered (e.g. Borucki et al. 2012; Borucki et al. 2013; Tuomi et al. 2013a; Tuomi et al. 2013b; Barclay et al. 2013).

Cool subdwarfs of the solar neighbourhood have potential to be harbouring complex life according to a model of the Galactic habitable zone (Lineweaver, Fenner & Gibson 2004). Habitable planets around cool subdwarfs would have been exited for over $\sim$ 10 Gyr, have much longer time to evolve compare to the Earth, thus have larger chance to harbour life even advanced civilization. The APOLLO project is targeting red subdwarfs within 100$\sim$200 parsec of the Sun search for first planets of the Galaxy, aims to measure the frequency of planets around red subdwarfs of the local area of the Sun. Targets selection will be carried out with spectroscopy and proper motion surveys (e.g. SDSS, LAMOST, Pan-STARRS, VISTA, LSST, Euclid). Targets will be followed up by redial velocity, transit and directory imaging surveys.

7.3.2 FIrst Stars Hunting IN the Galaxy (FISHING)

Numerical simulations show that metal-free stars with mass down to $\sim 0.1\ M_{\odot}$ could form due to gravitational instability recurs periodically (Clark et al. 2011; Greif et al. 2011; Basu, Vorobyov & DeSouza 2012). First stars with mass less than $\sim 0.8\ M_{\odot}$ could still exist in the Galaxy. Extreme metal-poor stars have been discovered (Christlieb et al. 2002; Cayrel et al. 2004; Frebel et al. 2005; Bonifacio et al. 2009; Caffau et al. 2011). The FISHING project aims to find low mass primordial stars in the Galaxy with the future large scale surveys (e.g. Gaia, LSST, Euclid).

References

Ackerman A. S., Marley M. S., 2001, ApJ, 556, 872
Aihara H. et al., 2011, ApJS, 193, 29
Alcock C. et al., 2000, ApJ, 542, 281
Allard F., Hauschildt P. H., 1995, ApJ, 445, 433
Allard F., Hauschildt P. H., Alexander D. R., Starrfield S., 1997, ARA&A, 35, 137
Allard F., Hauschildt P. H., Alexander D. R., Tamanai A., Schweitzer A., 2001, ApJ, 556, 357
Allard F., Allard N. F., Homeier D., Kielkopf J., McCaughrean M. J., Spiegelman F., 2007, A&A, 474, L21
Allard F., Homeier D., Freytag B., 2011, in Johns-Krull C., Browning M. K., West A. A., eds, Astronomical Society of the Pacific Conference Series. p. 91
Allen P. R., Koerner D. W., Reid I. N., Trilling D. E., 2005, ApJ, 625, 385
Allen P. R., Burgasser A. J., Faherty J. K., Kirkpatrick J. D., 2012, AJ, 144, 62
Alves de Oliveira C., Moraux E., Bouvier J., Bouy H., 2012, A&A, 539, A151
Alves de Oliveira C., Moraux E., Bouvier J., Duchêne G., Bouy H., Maschberger T., Hudelot P., 2013, A&A, 549, A123
Arnaboldi M., Retzlaff J., 2011, The Messenger, 146, 45
Arnaboldi M., Neeser M. J., Parker L. C., Rosati P., Lombardi M., Dietrich J. P., Hummel W., 2007, The Messenger, 127, 28
Arnaboldi M. et al., 2012, The Messenger, 149, 7
Attwood R. E., Goodwin S. P., Stamatellos D., Whitworth A. P., 2009, A&A, 495, 201
Baade W., 1944, ApJ, 100, 137
Bahcall J. N., Casertano S., 1986, ApJ, 308, 347
Banerji M., Abdalla F. B., Lahav O., Lin H., 2008, MNRAS, 386, 1219
Baraffe I., Chabrier G., 1996, ApJL, 461, L51
Baraffe I., Chabrier G., Allard F., Hauschildt P. H., 1995, ApJL, 446, L35
Baraffe I., Chabrier G., Allard F., Hauschildt P. H., 1997, A&A, 327, 1054
Baraffe I., Chabrier G., Allard F., Hauschildt P. H., 2002, A&A, 382, 563
Baraffe I., Chabrier G., Barman T. S., Allard F., Hauschildt P. H., 2003, A&A, 402, 701
Barclay T. et al., 2013, ApJ, 768, 101

Bastian N., Covey K. R., Meyer M. R., 2010, ARA&A, 48, 339
Basu S., Vorobyov E. I., 2012, ApJ, 750, 30
Basu S., Vorobyov E. I., DeSouza A. L., 2012, in Umemura M., Omukai K., eds, American Institute of Physics Conference Series. p. 63
Bate M. R., Bonnell I. A., Bromm V., 2003, MNRAS, 339, 577
Bate M. R., 2012, MNRAS, 419, 3115
Becklin E. E., Zuckerman B., 1988, Nature, 336, 656
Béjar V. J. S. et al., 2001, ApJ, 556, 830
Bergfors C. et al., 2010, A&A, 520, A54
Bessell M. S., 1982, PASAu, 4, 417
Bessell M. S., 1991, AJ, 101, 662
Bochanski J. J., West A. A., Hawley S. L., Covey K. R., 2007, AJ, 133, 531
Bonifacio P. et al., 2009, A&A, 501, 519
Borucki W. J. et al., 2012, ApJ, 745, 120
Borucki W. J. et al., 2013, Science, 340, 587
Boudreault S., Lodieu N., Deacon N. R., Hambly N. C., 2012, MNRAS, 426, 3419
Bouvier J. et al., 2008, A&A, 481, 661
Bowler B. P., Liu M. C., Cushing M. C., 2009, ApJ, 706, 1114
Bowler B. P., Liu M. C., Dupuy T. J., 2010, ApJ, 710, 45
Burgasser A. J., Kirkpatrick J. D., 2006, ApJ, 645, 1485
Burgasser A. J., Bardalez-Gagliuffi D. C., Gizis J. E., 2011, AJ, 141, 70
Burgasser A. J., Cruz K. L., Kirkpatrick J. D., 2007, ApJ, 657, 494
Burgasser A. J. et al., 2000, ApJL, 531, L57
Burgasser A. J. et al., 2000, AJ, 120, 1100
Burgasser A. J. et al., 2002, ApJ, 564, 421
Burgasser A. J. et al., 2003, ApJ, 592, 1186
Burgasser A. J., Kirkpatrick J. D., Liebert J., Burrows A., 2003, ApJ, 594, 510
Burgasser A. J., Kirkpatrick J. D., McElwain M. W., Cutri R. M., Burgasser A. J., Skrutskie M. F., 2003, AJ, 125, 850
Burgasser A. J., Kirkpatrick J. D., Reid I. N., Brown M. E., Miskey C. L., Gizis J. E., 2003, ApJ, 586, 512
Burgasser A. J., McElwain M. W., Kirkpatrick J. D., Cruz K. L., Tinney C. G., Reid I. N., 2004, AJ, 127, 2856
Burgasser A. J., Geballe T. R., Leggett S. K., Kirkpatrick J. D., Golimowski D. A., 2006, ApJ, 637, 1067
Burgasser A. J., Kirkpatrick J. D., Cruz K. L., Reid I. N., Leggett S. K., Liebert J., Burrows A., Brown M. E., 2006, ApJS, 166, 585
Burgasser A. J., Liu M. C., Ireland M. J., Cruz K. L., Dupuy T. J., 2008, ApJ, 681, 579
Burgasser A. J., Vrba F. J., Lépine S., Munn J. A., Luginbuhl C. B., Henden A. A., Guetter H. H., Canzian B. C., 2008, ApJ, 672, 1159
Burgasser A. J., Witte S., Helling C., Sanderson R. E., Bochanski J. J., Hauschildt P. H., 2009, ApJ, 697, 148
Burgasser A. J., Cruz K. L., Cushing M., Gelino C. R., Looper D. L., Faherty J. K., Kirkpatrick J. D., Reid I. N., 2010, ApJ, 710, 1142
Burgasser A. J. et al., 2011, ApJ, 735, 116

Burgasser A. J., Looper D., Rayner J. T., 2010, AJ, 139, 2448
Burgasser A. J., McElwain M. W., Kirkpatrick J. D., 2003, AJ, 126, 2487
Burgasser A. J., Sheppard S. S., Luhman K. L., 2013, ArXiv e-prints
Burgasser A. J., 2004, ApJS, 155, 191
Burgasser A. J., 2004, ApJL, 614, L73
Burgasser A. J., 2007, ApJ, 659, 655
Burningham B. et al., 2008, MNRAS, 391, 320
Burningham B. et al., 2009, MNRAS, 395, 1237
Burningham B. et al., 2010, MNRAS, 404, 1952
Burningham B. et al., 2010, MNRAS, 406, 1885
Burningham B. et al., 2011, MNRAS, 414, L90
Burrows A., Sharp C. M., 1999, ApJ, 512, 843
Burrows A. et al., 1997, ApJ, 491, 856
Burrows A., Hubbard W. B., Lunine J. I., Liebert J., 2001, Reviews of Modern Physics, 73, 719
Burrows A., Heng K., Nampaisarn T., 2011, ApJ, 736, 47
Burrows A., Sudarsky D., Hubeny I., 2006, ApJ, 640, 1063
Burrows A., Sudarsky D., Lunine J. I., 2003, ApJ, 596, 587
Caballero J. A. et al., 2007, A&A, 470, 903
Caffau E. et al., 2011, Nature, 477, 67
Cardoso C. V. et al., 2009, in Stempels E., ed, American Institute of Physics Conference Series. p. 509
Casertano S., Ratnatunga K. U., Bahcall J. N., 1990, ApJ, 357, 435
Cayrel R. et al., 2004, A&A, 416, 1117
Chabrier G., Baraffe I., Allard F., Hauschildt P., 2000, ApJ, 542, 464
Chabrier G., Baraffe I., Allard F., Hauschildt P. H., 2005, ArXiv Astrophysics e-prints
Chabrier G., 2003, PASP, 115, 763
Chamberlain J. W., Aller L. H., 1951, ApJ, 114, 52
Chauvin G., Lagrange A.-M., Dumas C., Zuckerman B., Mouillet D., Song I., Beuzit J.-L., Lowrance P., 2004, A&A, 425, L29
Chauvin G. et al., 2012, A&A, 548, A33
Chiu K., Fan X., Leggett S. K., Golimowski D. A., Zheng W., Geballe T. R., Schneider D. P., Brinkmann J., 2006, AJ, 131, 2722
Chiu K. et al., 2008, MNRAS, 385, L53
Christlieb N. et al., 2002, Nature, 419, 904
Cioni M.-R. et al., 2011, The Messenger, 144, 25
Clark P. C., Glover S. C. O., Smith R. J., Greif T. H., Klessen R. S., Bromm V., 2011, Science, 331, 1040
Clarke J. R. A. et al., 2010, MNRAS, 402, 575
Corbelli E., Palla F., Zinnecker H., eds, The Initial Mass Function 50 years later, 2005
Costa E., Méndez R. A., Jao W.-C., Henry T. J., Subasavage J. P., Brown M. A., Ianna P. A., Bartlett J., 2005, AJ, 130, 337
Costa E., Méndez R. A., Jao W.-C., Henry T. J., Subasavage J. P., Ianna P. A., 2006, AJ, 132, 1234
Cross N. J. G. et al., 2012, A&A, 548, A119

Cruz K. L., Reid I. N., Liebert J., Kirkpatrick J. D., Lowrance P. J., 2003, AJ, 126, 2421
Cruz K. L., Burgasser A. J., Reid I. N., Liebert J., 2004, ApJL, 604, L61
Cruz K. L. et al., 2007, AJ, 133, 439
Currie T., Bailey V., Fabrycky D., Murray-Clay R., Rodigas T., Hinz P., 2010, ApJL, 721, L177
Cushing M. C., Looper D., Burgasser A. J., Kirkpatrick J. D., Faherty J., Cruz K. L., Sweet A., Sanderson R. E., 2009, ApJ, 696, 986
Cushing M. C. et al., 2011, ApJ, 743, 50
Cushing M. C., Rayner J. T., Vacca W. D., 2005, ApJ, 623, 1115
Cushing M. C., Saumon D., Marley M. S., 2010, AJ, 140, 1428
Cutri R. M., et al., 2012, VizieR Online Data Catalog, 2311, 0
Cutri R. M. et al., 2003, 2MASS All Sky Catalog of point sources.
Dahn C. C., Liebert J., Harris H. C., Guetter H. H., 1995, in Tinney C. G., ed, The Bottom of the Main Sequence - and Beyond. p. 239
Day-Jones A. C. et al., 2011, MNRAS, 410, 705
Day-Jones A. C. et al., 2011, Research, Science and Technology of Brown Dwarfs and Exoplanets: Proceedings of an International Conference held in Shangai on Occasion of a Total Eclipse of the Sun, Shangai, China, Edited by E.L. Martin; J. Ge; W. Lin; EPJ Web of Conferences, Volume 16, id.06012, 16, 6012
Day-Jones A. C. et al., 2013, MNRAS, 430, 1171
de Marchi G., Paresce F., 1995, A&A, 304, 202
Deacon N. R., Hambly N. C., 2006, MNRAS, 371, 1722
Deacon N. R., Hambly N. C., King R. R., McCaughrean M. J., 2009, MNRAS, 394, 857
Deacon N. R. et al., 2011, AJ, 142, 77
Deacon N. R. et al., 2012, ApJ, 757, 100
Deacon N. R. et al., 2012, ApJ, 755, 94
Dehn M., Helling C., Woitke P., Hauschildt P., 2007, in T. Kuroda, H. Sugama, R. Kanno, & M. Okamoto, ed, IAU Symposium. p. 227
Delfosse X. et al., 1997, A&A, 327, L25
Delorme P. et al., 2008, A&A, 484, 469
Delorme P. et al., 2010, A&A, 518, A39
Delorme P. et al., 2012, A&A, 548, A26
Digby A. P., Hambly N. C., Cooke J. A., Reid I. N., Cannon R. D., 2003, MNRAS, 344, 583
Dupuy T. J., Liu M. C., 2012, ApJS, 201, 19
Dupuy T. J., Liu M. C., Ireland M. J., 2009, ApJ, 692, 729
Ellis S. C., Tinney C. G., Burgasser A. J., Kirkpatrick J. D., McElwain M. W., 2005, AJ, 130, 2347
Epchtein N., 1997, in Garzon F., Epchtein N., Omont A., Burton B., Persi P., eds, The Impact of Large Scale Near-IR Sky Surveys. p. 15
Faherty J. K., Burgasser A. J., West A. A., Bochanski J. J., Cruz K. L., Shara M. M., Walter F. M., 2010, AJ, 139, 176
Faherty J. K. et al., 2012, ApJ, 752, 56
Faherty J. K., Rice E. L., Cruz K. L., Mamajek E. E., Núñez A., 2013, AJ, 145, 2
Fan X. et al., 2000, AJ, 119, 928

Femenía B. et al., 2011, MNRAS, 413, 1524
Ford E. B., Joshi K. J., Rasio F. A., Zbarsky B., 2000, ApJ, 528, 336
Frebel A. et al., 2005, Nature, 434, 871
Freedman R. S., Marley M. S., Lodders K., 2008, ApJS, 174, 504
Fressin F. et al., 2013, ApJ, 766, 81
Gelino C. R. et al., 2011, AJ, 142, 57
Gillon M., Triaud A. H. M. J., Jehin E., Delrez L., Opitom C., Magain P., Lendl M., Queloz D., 2013, ArXiv e-prints
Gizis J. E., Harvin J., 2006, AJ, 132, 2372
Gizis J. E., Jao W.-C., Subasavage J. P., Henry T. J., 2007, ApJL, 669, L45
Gizis J. E. et al., 2012, AJ, 144, 94
Gizis J. E., Kirkpatrick J. D., Wilson J. C., 2001, AJ, 121, 2185
Gizis J. E., 1997, AJ, 113, 806
Goldman B., Marsat S., Henning T., Clemens C., Greiner J., 2010, MNRAS, 405, 1140
Gomes J. I. et al., 2013, MNRAS
Gould A., Flynn C., Bahcall J. N., 1998, ApJ, 503, 798
Gould A., 2003, ApJ, 583, 765
Greif T. H., Springel V., White S. D. M., Glover S. C. O., Clark P. C., Smith R. J., Klessen R. S., Bromm V., 2011, ApJ, 737, 75
Griffith R. L. et al., 2012, AJ, 144, 148
Hambly N. C., Hodgkin S. T., Cossburn M. R., Jameson R. F., 1999, MNRAS, 303, 835
Hauschildt P. H., Allard F., Baron E., 1999, ApJ, 512, 377
Hauschildt P. H., Allard F., Baron E., Aufdenberg J., Schweitzer A., 2003, in U. Munari, ed, GAIA Spectroscopy: Science and Technology. p. 179
Hawley S. L. et al., 2002, AJ, 123, 3409
Hayashi C., Nakano T., 1963, Progress of Theoretical Physics, 30, 460
Helling C. et al., 2008, MNRAS, 391, 1854
Helling C., Dehn M., Woitke P., Hauschildt P. H., 2008, ApJL, 675, L105
Helling C., Woitke P., Thi W.-F., 2008, A&A, 485, 547
Hennebelle P., Chabrier G., 2008, ApJ, 684, 395
Herschel W., 1803, Royal Society of London Philosophical Transactions Series I, 93, 339
Hertzsprung E., 1911, Publikationen des Astrophysikalischen Observatoriums zu Potsdam, 63
Hewett P. C., Warren S. J., Leggett S. K., Hodgkin S. T., 2006, MNRAS, 367, 454
Hogan E., Jameson R. F., Casewell S. L., Osbourne S. L., Hambly N. C., 2008, MNRAS, 388, 495
Jao W.-C., Henry T. J., Beaulieu T. D., Subasavage J. P., 2008, AJ, 136, 840
Jao W.-C., Mason B. D., Hartkopf W. I., Henry T. J., Ramos S. N., 2009, AJ, 137, 3800
Jarvis M. J. et al., 2012, MNRAS, , 119
Jayawardhana R., Ivanov V. D., 2006, Science, 313, 1279
Johnas C. M. S., Helling C., Dehn M., Woitke P., Hauschildt P. H., 2008, MNRAS, 385, L120
Johnson J. L., Li H., 2012, ApJ, 751, 81
Johnson D. R. H., Soderblom D. R., 1987, AJ, 93, 864
Jones H. R. A., Tsuji T., 1997, ApJL, 480, L39

Jones H. R. A., Longmore A. J., Jameson R. F., Mountain C. M., 1994, MNRAS, 267, 413
Kaiser N. et al., 2010, in Society of Photo-Optical Instrumentation Engineers (SPIE) Conference Series
Kalas P. et al., 2008, Science, 322, 1345
Kasting J. F., Whitmire D. P., Reynolds R. T., 1993, Icarus, 101, 108
Kendall T. R., Delfosse X., Martín E. L., Forveille T., 2004, A&A, 416, L17
Kendall T. R. et al., 2007, A&A, 466, 1059
King R. R., McCaughrean M. J., Homeier D., Allard F., Scholz R.-D., Lodieu N., 2009, in Stempels E., ed, American Institute of Physics Conference Series. p. 537
King R. R., McCaughrean M. J., Homeier D., Allard F., Scholz R.-D., Lodieu N., 2010, A&A, 510, A99
Kirkpatrick J. D., McCarthy Jr. D. W., 1994, AJ, 107, 333
Kirkpatrick J. D., Kelly D. M., Rieke G. H., Liebert J., Allard F., Wehrse R., 1993, ApJ, 402, 643
Kirkpatrick J. D., Allard F., Bida T., Zuckerman B., Becklin E. E., Chabrier G., Baraffe I., 1999, ApJ, 519, 834
Kirkpatrick J. D. et al., 1999, ApJ, 519, 802
Kirkpatrick J. D. et al., 2000, AJ, 120, 447
Kirkpatrick J. D., Barman T. S., Burgasser A. J., McGovern M. R., McLean I. S., Tinney C. G., Lowrance P. J., 2006, ApJ, 639, 1120
Kirkpatrick J. D. et al., 2010, ApJS, 190, 100
Kirkpatrick J. D. et al., 2011, ApJS, 197, 19
Kirkpatrick J. D. et al., 2012, ApJ, 753, 156
Kirkpatrick J. D., Henry T. J., Irwin M. J., 1997, AJ, 113, 1421
Kirkpatrick J. D., Henry T. J., Liebert J., 1993, ApJ, 406, 701
Kirkpatrick J. D., Henry T. J., McCarthy Jr. D. W., 1991, ApJS, 77, 417
Kirkpatrick J. D., 2005, ARA&A, 43, 195
Kniazev A. Y. et al., 2013, ApJ, 770, 124
Koch D. G. et al., 2010, ApJL, 713, L79
Kopparapu R. K. et al., 2013, ApJ, 765, 131
Kroupa P., 2002, Science, 295, 82
Kuiper G. P., 1939, ApJ, 89, 548
Kumar S. S., 1963, ApJ, 137, 1121
Kumar S. S., 1963, ApJ, 137, 1126
Labadie L. et al., 2011, A&A, 526, A144
Lachaume R., Dominik C., Lanz T., Habing H. J., 1999, A&A, 348, 897
Lawrence A. et al., 2007, MNRAS, 379, 1599
Leggett S. K. et al., 2000, ApJL, 536, L35
Lépine S., Scholz R.-D., 2008, ApJL, 681, L33
Lépine S., Shara M. M., 2005, AJ, 129, 1483
Lépine S., Rich R. M., Shara M. M., 2003, ApJL, 591, L49
Lépine S., Rich R. M., Shara M. M., 2007, ApJ, 669, 1235
Lépine S., Shara M. M., Rich R. M., 2003, AJ, 126, 921
Lépine S., Shara M. M., Rich R. M., 2003, ApJL, 585, L69

Lépine S., Shara M. M., Rich R. M., 2004, ApJL, 602, L125
Lépine S., 2005, AJ, 130, 1247
Lépine S., 2008, AJ, 135, 2177
Lineweaver C. H., Fenner Y., Gibson B. K., 2004, Science, 303, 59
Liu M. C., Leggett S. K., Golimowski D. A., Chiu K., Fan X., Geballe T. R., Schneider D. P., Brinkmann J., 2006, ApJ, 647, 1393
Liu M. C. et al., 2011, ApJL, 740, L32
Liu M. C. et al., 2011, ApJ, 740, 108
Lodieu N., Deacon N. R., Hambly N. C., 2012, MNRAS, 422, 1495
Lodieu N., Dobbie P. D., Hambly N. C., 2011, A&A, 527, A24
Lodieu N., Scholz R.-D., McCaughrean M. J., Ibata R., Irwin M., Zinnecker H., 2005, A&A, 440, 1061
Lodieu N., Hambly N. C., Jameson R. F., Hodgkin S. T., Carraro G., Kendall T. R., 2007, MNRAS, 374, 372
Lodieu N. et al., 2007, MNRAS, 379, 1423
Lodieu N., Burningham B., Hambly N. C., Pinfield D. J., 2009, MNRAS, 397, 258
Lodieu N., Dobbie P. D., Deacon N. R., Venemans B. P., Durant M., 2009, MNRAS, 395, 1631
Lodieu N., Zapatero Osorio M. R., Martín E. L., Solano E., Aberasturi M., 2010, ApJL, 708, L107
Lodieu N., de Wit W.-J., Carraro G., Moraux E., Bouvier J., Hambly N. C., 2011, A&A, 532, A103
Lodieu N. et al., 2012, A&A, 548, A53
Lodieu N., Deacon N. R., Hambly N. C., Boudreault S., 2012, MNRAS, 426, 3403
Lodieu N., Espinoza Contreras M., Zapatero Osorio M. R., Solano E., Aberasturi M., Martín E. L., 2012, A&A, 542, A105
Lodieu N., Hambly N. C., Jameson R. F., 2006, MNRAS, 373, 95
Lodieu N., Zapatero Osorio M. R., Martín E. L., 2009, A&A, 499, 729
Looper D. L., Gelino C. R., Burgasser A. J., Kirkpatrick J. D., 2008, ApJ, 685, 1183
López-Morales M., 2007, ApJ, 660, 732
Loutrel N. P., Luhman K. L., Lowrance P. J., Bochanski J. J., 2011, ApJ, 739, 81
Lucas P. W. et al., 2008, MNRAS, 391, 136
Lucas P. W. et al., 2010, MNRAS, 408, L56
Luhman K. L., Burgasser A. J., Bochanski J. J., 2011, ApJL, 730, L9
Luhman K. L., Burgasser A. J., Labbé I., Saumon D., Marley M. S., Bochanski J. J., Monson A. J., Persson S. E., 2012, ApJ, 744, 135
Luhman K. L., 2013, ApJL, 767, L1
Luyten W. J., 1979a, LHS catalogue. A catalogue of stars with proper motions exceeding 0”5 annually
Luyten W. J., 1979b, New Luyten catalogue of stars with proper motions larger than two tenths of an arcsecond; and first supplement; NLTT. (Minneapolis (1979)); Label 12 = short description; Label 13 = documentation by Warren; Label 14 = catalogue
Mace G. N. et al., 2013, ApJS, 205, 6
Mainzer A. et al., 2011, ApJ, 726, 30
Mainzer A. et al., 2011, ApJ, 736, 100

Majewski S. R., 1993, ARA&A, 31, 575
Mamajek E. E., 2013, ArXiv e-prints
Marley M. S., Seager S., Saumon D., Lodders K., Ackerman A. S., Freedman R. S., Fan X., 2002, ApJ, 568, 335
Marocco F. et al., 2010, A&A, 524, A38
Marois C., Macintosh B., Barman T., Zuckerman B., Song I., Patience J., Lafrenière D., Doyon R., 2008, Science, 322, 1348
Marois C., Zuckerman B., Konopacky Q. M., Macintosh B., Barman T., 2010, Nature, 468, 1080
Marshall J. L., 2008, AJ, 135, 1000
Martín E. L. et al., 2010, A&A, 517, A53
Martin E. L., Rebolo R., Zapatero-Osorio M. R., 1996, ApJ, 469, 706
McCaughrean M. J., Close L. M., Scholz R.-D., Lenzen R., Biller B., Brandner W., Hartung M., Lodieu N., 2004, A&A, 413, 1029
Metchev S. A., Kirkpatrick J. D., Berriman G. B., Looper D., 2008, ApJ, 676, 1281
Mohanty S., Jayawardhana R., Basri G., 2004, ApJ, 609, 885
Montalbán J., D'Antona F., Mazzitelli I., 2000, A&A, 360, 935
Moraux E., Bouvier J., Stauffer J. R., Cuillandre J.-C., 2003, A&A, 400, 891
Mortier A., Santos N. C., Sozzetti A., Mayor M., Latham D., Bonfils X., Udry S., 2012, A&A, 543, A45
Muench A. A. et al., 2003, AJ, 125, 2029
Munn J. A. et al., 2004, AJ, 127, 3034
Murray D. N. et al., 2011, MNRAS, 414, 575
Mužić K., Scholz A., Geers V., Jayawardhana R., Tamura M., 2012, ApJ, 744, 134
Nakajima T., Oppenheimer B. R., Kulkarni S. R., Golimowski D. A., Matthews K., Durrance S. T., 1995, Nature, 378, 463
Oppenheimer B. R., Kulkarni S. R., Matthews K., Nakajima T., 1995, Science, 270, 1478
Padoan P., Nordlund Å., 2004, ApJ, 617, 559
Peña Ramírez K., Béjar V. J. S., Zapatero Osorio M. R., Petr-Gotzens M. G., Martín E. L., 2012, ApJ, 754, 30
Perryman M. A. C., ESA, eds, The HIPPARCOS and TYCHO catalogues. Astrometric and photometric star catalogues derived from the ESA HIPPARCOS Space Astrometry Mission, 1997
Pinfield D. J., Jones H. R. A., Lucas P. W., Kendall T. R., Folkes S. L., Day-Jones A. C., Chappelle R. J., Steele I. A., 2006, MNRAS, 368, 1281
Pinfield D. J. et al., 2008, MNRAS, 390, 304
Pinfield D. J. et al., 2012, MNRAS, 422, 1922
Pokorny R. S., Jones H. R. A., Hambly N. C., Pinfield D. J., 2004, A&A, 421, 763
Pokorny R. S., Jones H. R. A., Hambly N. C., 2003, A&A, 397, 575
Rebolo R., Zapatero Osorio M. R., Martín E. L., 1995, Nature, 377, 129
Reid I. N., Cruz K. L., 2002, AJ, 123, 2806
Reid I. N., Cruz K. L., Kirkpatrick J. D., Allen P. R., Mungall F., Liebert J., Lowrance P., Sweet A., 2008, AJ, 136, 1290
Reid I. N., Hawley S. L., Gizis J. E., 1995, AJ, 110, 1838
Reiners A., Basri G., 2009, A&A, 496, 787

Reipurth B., Clarke C., 2001, AJ, 122, 432
Riaz B., Gizis J. E., Samaddar D., 2008, ApJ, 672, 1153
Rice E. L., Barman T., Mclean I. S., Prato L., Kirkpatrick J. D., 2010, ApJS, 186, 63
Richer H. B. et al., 2002, ApJL, 574, L151
Roman N. G., 1950, ApJ, 112, 554
Roman N. G., 1952, ApJ, 116, 122
Roman N. G., 1954, AJ, 59, 307
Ruiz M. T., Wischnjewsky M., Rojo P. M., Gonzalez L. E., 2001, ApJS, 133, 119
Ruiz M. T., Leggett S. K., Allard F., 1997, ApJL, 491, L107
Russell H. N., 1913, The Observatory, 36, 324
Saito R. et al., 2010, The Messenger, 141, 24
Saito R. K. et al., 2012, A&A, 537, A107
Salim S., Gould A., 2003, ApJ, 582, 1011
Salpeter E. E., 1955, ApJ, 121, 161
Sandage A. R., Eggen O. J., 1959, MNRAS, 119, 278
Saumon D., Marley M. S., 2008, ApJ, 689, 1327
Schilbach E., Röser S., Scholz R.-D., 2009, A&A, 493, L27
Schlafly E. F. et al., 2012, ApJ, 756, 158
Schmidt S. J., West A. A., Burgasser A. J., Bochanski J. J., Hawley S. L., 2010, AJ, 139, 1045
Schmidt S. J., West A. A., Hawley S. L., Pineda J. S., 2010, AJ, 139, 1808
Schneider D. P. et al., 2002, AJ, 123, 458
Scholz R.-D., McCaughrean M. J., Lodieu N., Kuhlbrodt B., 2003, A&A, 398, L29
Scholz R.-D., Lehmann I., Matute I., Zinnecker H., 2004, A&A, 425, 519
Scholz R.-D., Storm J., Knapp G. R., Zinnecker H., 2009, A&A, 494, 949
Scholz R.-D., Bihain G., Schnurr O., Storm J., 2011, A&A, 532, L5
Scholz R.-D., Bihain G., Schnurr O., Storm J., 2012, A&A, 541, A163
Scholz R.-D., Lodieu N., McCaughrean M. J., 2004, A&A, 428, L25
Scholz R.-D., Meusinger H., Jahreiß H., 2005, A&A, 442, 211
Scholz R.-D., 2010, A&A, 510, L8
Scholz R.-D., 2010, A&A, 515, A92
Schweitzer A., Scholz R.-D., Stauffer J., Irwin M., McCaughrean M. J., 1999, A&A, 350, L62
Selsis F., Kasting J. F., Levrard B., Paillet J., Ribas I., Delfosse X., 2007, A&A, 476, 1373
Setiawan J., Klement R. J., Henning T., Rix H.-W., Rochau B., Rodmann J., Schulze-Hartung T., 2010, Science, 330, 1642
Sigurdsson S., Richer H. B., Hansen B. M., Stairs I. H., Thorsett S. E., 2003, Science, 301, 193
Sivarani T., Lépine S., Kembhavi A. K., Gupchup J., 2009, ApJL, 694, L140
Skrutskie M. F. et al., 2006, AJ, 131, 1163
Slesnick C. L., Hillenbrand L. A., Carpenter J. M., 2008, ApJ, 688, 377
Song I., Schneider G., Zuckerman B., Farihi J., Becklin E. E., Bessell M. S., Lowrance P., Macintosh B. A., 2006, ApJ, 652, 724
Spagna A., Lattanzi M. G., Re Fiorentin P., Smart R. L., 2010, A&A, 510, L4

Stamatellos D., Whitworth A. P., 2009, MNRAS, 392, 413
Stamatellos D., Whitworth A. P., Ward-Thompson D., 2007, MNRAS, 379, 1390
Stassun K. G., Mathieu R. D., Valenti J. A., 2006, Nature, 440, 311
Stauffer J. R., Schultz G., Kirkpatrick J. D., 1998, ApJL, 499, L199
Stoughton C. et al., 2002, AJ, 123, 485
Strauss M. A. et al., 1999, ApJL, 522, L61
Tarter J. C., 1975, PhD thesis, California Univ., Berkeley.
Tinney C. G., Burgasser A. J., Kirkpatrick J. D., 2003, AJ, 126, 975
Tinney C. G., Delfosse X., Forveille T., 1997, ApJL, 490, L95
Tinney C. G., Delfosse X., Forveille T., Allard F., 1998, A&A, 338, 1066
Tinney C. G., Burgasser A. J., Kirkpatrick J. D., McElwain M. W., 2005, AJ, 130, 2326
Tinney C. G., Faherty J. K., Kirkpatrick J. D., Wright E. L., Gelino C. R., Cushing M. C., Griffith R. L., Salter G., 2012, ApJ, 759, 60
Tisserand P. et al., 2007, A&A, 469, 387
Tonry J. L. et al., 2012, ApJ, 750, 99
Tsuji T., Ohnaka K., Aoki W., Nakajima T., 1996, A&A, 308, L29
Tsvetanov Z. I. et al., 2000, ApJL, 531, L61
Tuomi M., Anglada-Escudé G., Gerlach E., Jones H. R. A., Reiners A., Rivera E. J., Vogt S. S., Butler R. P., 2013, A&A, 549, A48
Tuomi M. et al., 2013, A&A, 551, A79
Ukidss C., 2012, VizieR Online Data Catalog, 2310, 0
Vernet J. et al., 2011, A&A, 536, A105
Vrba F. J. et al., 2004, AJ, 127, 2948
Wang W., Boudreault S., Goldman B., Henning T., Caballero J. A., Bailer-Jones C. A. L., 2011, A&A, 531, A164
Warren S. J. et al., 2007, MNRAS, 381, 1400
West A. A., Hawley S. L., Bochanski J. J., Covey K. R., Reid I. N., Dhital S., Hilton E. J., Masuda M., 2008, AJ, 135, 785
West A. A., Bochanski J. J., Bowler B. P., Dotter A., Johnson J. A., Lépine S., Rojas-Ayala B., Schweitzer A., 2011, in Johns-Krull C., Browning M. K., West A. A., eds, 16th Cambridge Workshop on Cool Stars, Stellar Systems, and the Sun. p. 531
Whitworth A. P., Stamatellos D., 2006, A&A, 458, 817
Whitworth A. P., Zinnecker H., 2004, A&A, 427, 299
Whitworth A., Bate M. R., Nordlund Å., Reipurth B., Zinnecker H., 2007, Protostars and Planets V, , 459
Witte S., Helling C., Barman T., Heidrich N., Hauschildt P. H., 2011, A&A, 529, A44
Witte S., Helling C., Hauschildt P. H., 2009, A&A, 506, 1367
Wright E. L. et al., 2010, AJ, 140, 1868
Wyrzykowski Ł. et al., 2009, MNRAS, 397, 1228
York D. G. et al., 2000, AJ, 120, 1579
Zhang Z. H. et al., 2009, A&A, 497, 619
Zhang Z. H. et al., 2010, MNRAS, 404, 1817
Zhang Z. et al., 2011, in Johns-Krull C., Browning M. K., West A. A., eds, 16th Cambridge Workshop on Cool Stars, Stellar Systems, and the Sun. p. 1411
Zhang Z. H. et al., 2013, ArXiv, e-print, astro-ph/1306.3060

Appendix I

"Ultra-cool dwarfs: new discoveries, proper motions, and improved spectral typing from SDSS and 2MASS photometric colors",
Zhang et al. 2009, A&A, 497, 619-633

A&A 497, 619–633 (2009)
DOI: 10.1051/0004-6361/200810314

Astronomy & Astrophysics

Ultra-cool dwarfs: new discoveries, proper motions, and improved spectral typing from SDSS and 2MASS photometric colors⋆

Z. H. Zhang[1,3,2], R. S. Pokorny[1], H. R. A. Jones[2], D. J. Pinfield[2], P. S. Chen[1], Z. Han[1], D. Chen[1,2], M. C. Gálvez-Ortiz[2], and B. Burningham[2]

[1] National Astronomical Observatories/Yunnan Observatory, Chinese Academy of Sciences, Kunming 650011, PR China
e-mail: zenghuazhang@hotmail.com
[2] Centre for Astrophysics Research, Science and Technology Research Institute, University of Hertfordshire, College Lane, Hatfield AL10 9AB, UK
e-mail: h.r.a.jones@herts.ac.uk
[3] Graduate School of Chinese Academy of Sciences, Beijing 100049, PR China

Received 3 June 2008 / Accepted 14 January 2009

ABSTRACT

Aims. We try to identify ultra-cool dwarfs from the seventh Data Release of the Sloan Digital Sky Survey (SDSS DR7) with SDSS *i*-*z* and *r*-*z* colors. We also obtain proper motion data from SDSS, 2MASS, and UKIDSS and improve spectral typing from SDSS and 2MASS photometric colors.

Methods. We selected ultra-cool dwarf candidates from the SDSS DR7 with new photometric selection criteria, which are based on a parameterization study of known L and T dwarfs. The objects are then cross-identified with the Two Micron All Sky Survey and the Fourth Data Release of the UKIRT Infrared Deep Sky Survey (UKIDSS DR4). We derive proper motion constraints by combining SDSS, 2MASS, and UKIDSS positional information. In this way we are able to assess, to some extent, the credence of our sample using a multi epoch approach, which complements spectroscopic confirmation. Some of the proper motions are affected by short baselines, but, as a general tool, this method offers great potential to confirm faint L dwarfs as UKIDSS coverage increases. In addition we derive updated color-spectral type relations for L and T dwarfs with SDSS and 2MASS magnitudes.

Results. We present 59 new nearby M and L dwarfs selected from the imaging catalog of the SDSS DR7, including proper motions and spectral types calculated from the updated color-spectral type relations. and obtain proper motions from SDSS, 2MASS, and UKIDSS for all of our objects.

Key words. stars: low-mass, brown dwarfs – stars: late-type

1. Introduction

Brown dwarfs occupy the mass range between the lowest mass stars and the highest mass planets. The central temperature of a brown dwarf is not high enough to achieve stable hydrogen burning like a star, but all brown dwarfs will undergo short periods of primordial deuterium burning very early in their evolution. Since the first discovery of an L dwarf (GD165 B; Becklin & Zuckerman 1988) and a T dwarf (Gl229 B; Nakajima et al. 1995), the projects searching for brown dwarfs have involved a number of large scale surveys, for example, the Deep Near-Infrared Survey (DENIS; Epchtein et al. 1997), the Two Micron All Sky Survey (2MASS; Skrutskie et al. 2006) and the Sloan Digital Sky Survey (SDSS; York et al. 2000; Adelman-MaCarthy et al. 2008). 554 L dwarfs and 145 T dwarfs have been found in large scale sky surveys in the last decade (by January 2009, see, DwarfsArchives.org for a full list). 31 of L or T dwarfs have been found in DENIS (e.g. Delfosse et al. 1997), 185 in SDSS (e.g. Fan et al. 2000; Geballe et al. 2002; Hawley et al. 2002; Schneider et al. 2002; Knapp et al. 2004; Chiu et al. 2006), and 368 in 2MASS (e.g. Burgasser et al. 1999, 2002, 2004; Kirkpatrick et al. 1999, 2000; Gizis et al. 2000; Cruz et al. 2003, 2007; Kendall et al. 2003, 2007; Looper et al. 2007). More recently, the UKIRT Infrared Deep Sky Survey (UKIDSS; Lawrence et al. 2007) is beginning to be very effective in searching for T dwarfs (Kendall et al. 2007; Lodieu et al. 2007; Warren et al. 2007; Burningham et al. 2008; Pinfield et al. 2008).

In this paper we report the discovery of 59 late M and L dwarfs from the main photometric catalog of SDSS DR7.1. The photometric selection processes are presented in Sect. 2. The red optical spectra of the 36 new late M and L dwarfs from SDSS are presented in Sect. 3. Polynomial fitting for color-spectral type relationships are derived in Sect. 4. The UKIDSS matches for 23 ultra-cool dwarf candidates without SDSS spectra are presented in Sect. 5, and Sect. 6 presents some further discussion.

2. Photometric selection

The Sloan Digital Sky Survey uses a dedicated 2.5 m telescope located at Apache Point Observatory (APO) in New Mexico. It is equipped with a large format mosaic CCD camera to image the sky in five optical bands (*u*, *g*, *r*, *i*, *z*), and two digital spectrographs to obtain the spectra of galaxies, quasars and late type stars selected from the imaging data (York et al. 2000). The SDSS DR7 imaging data covers about 8420 deg^2 of the main survey area (legacy sky), with information on roughly 230 million distinct photometric objects. The SDSS magnitude limits

⋆ Table 7 is also available in electronic form at the CDS via anonymous ftp to cdsarc.u-strasbg.fr (130.79.128.5) or via http://cdsweb.u-strasbg.fr/cgi-bin/qcat?J/A+A/497/619

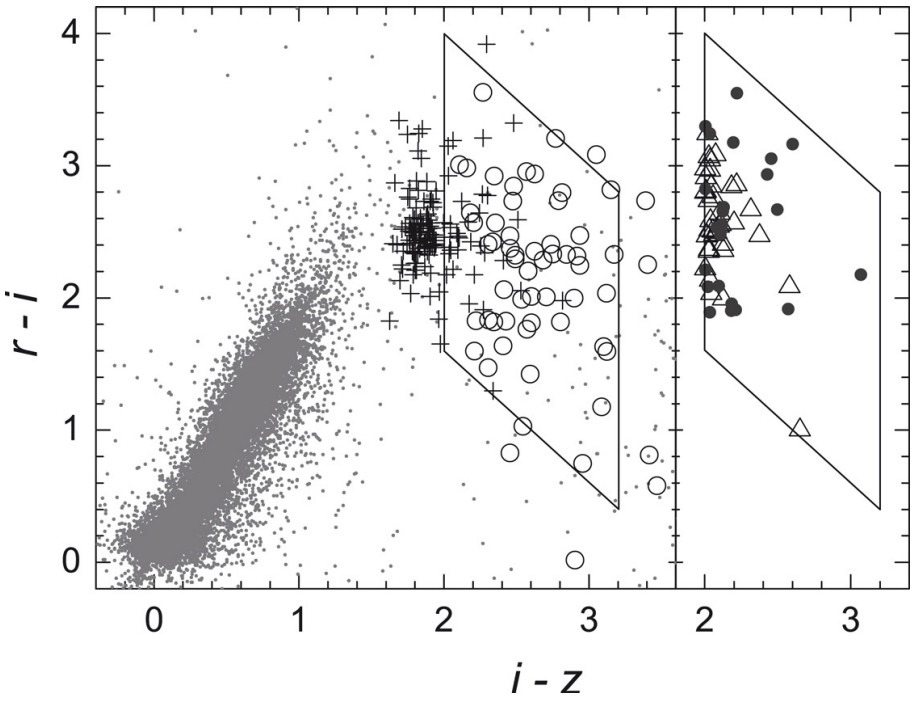

Fig. 1. $r-i$ vs. $i-z$ diagram for previously identified L dwarfs (*left hand panel*) and new M and L dwarfs (*right hand panel*). Previously identified L0-L4.5 and L5-L9.5 dwarfs are shown as *crosses* and *open circles* respectively. The 36 new M and L dwarfs with measured spectral types (from SDSS spectroscopy) are shown as *open triangles*, and the 23 new ultracool dwarf candidates (no SDSS spectra available) that we have cross-matched in UKIDSS DR4 are shown as *filled circles*. As a comparison, 24300 point sources with $15 < z < 20.5$ from 10 deg^2 of SDSS coverage are shown as *dots*. A parallelogram shows the boundary limits of our color selection.

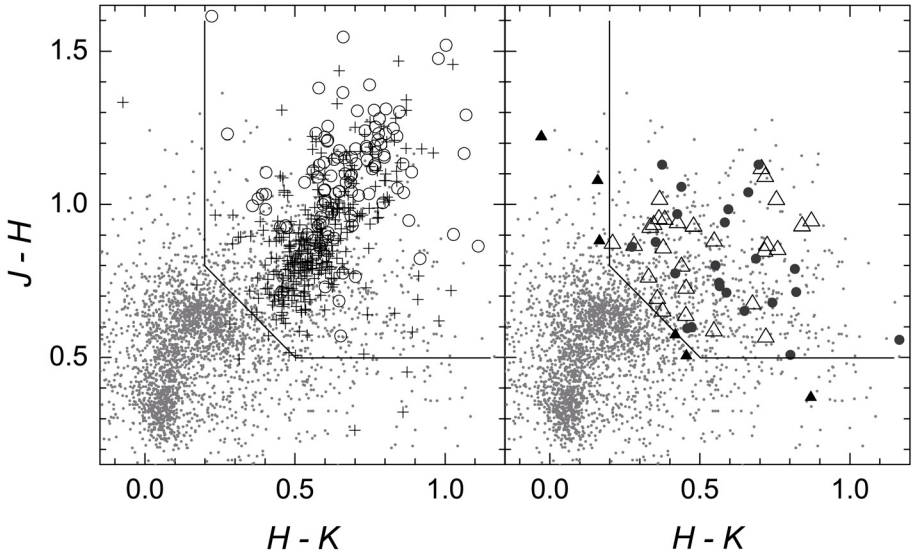

Fig. 2. $J-H$ vs. $H-K$ diagram for previously identified L dwarfs (*left hand panel*) and new M and L dwarfs (*right hand panel*). Symbols are as in Fig. 1 except that six of the new spectroscopically confirmed dwarfs (three M9, one L0 and two L1) are indicated with filled triangles, because they lie outside our 2MASS photometric selection criteria (solid lines). Note that the 2MASS criteria are only applied when selecting photometric candidates, and not when SDSS spectra are available. For comparison, the plot shows 2800 sources (dots) taken from 3.14 deg^2 of 2MASS sky.

(95% detection repeatability for point sources) for the u, g, r, i and z bands are 22.0, 22.2, 22.2, 21.3 and 20.5 respectively.

The $i-z$ color is particularly useful for L dwarf selection (as first pioneered by Fan et al. (2000), and expanded on by others e.g. via the i-band drop-out method; e.g. Chiu et al. 2006). For the cooler $T_{\rm eff}$ T dwarfs, almost all of the radiation is emitted beyond 10 000 Å, and as such these objects are optically much fainter than L dwarfs. SDSS is thus significantly less sensitive to T dwarfs than to L dwarfs, but has the sensitivity to identify L dwarfs out to distances well beyond 100 pc.

We have made a study of L dwarf color-color parameter-space using previously identified L and T dwarfs with photometric data available from either SDSS or 2MASS (from DwarfsArchives.org, as of September 25, 2007). Where two spectral types are available (optical and infrared) we used the mean average type. A total of 431 L and 84 T dwarfs have 2MASS photometric data (J, H, K), and 193 L and 46 T dwarfs have SDSS photometric data (u, g, r, i, z). We excluded L and T dwarfs known to be unresolved binary systems from our study. These optical and near-infrared parameter spaces are shown in the left-hand panels of Figs. 1 and 2, where crosses indicate early L dwarfs (L0-L4.5) and open circles indicate mid-late L dwarfs (L5-L9.5). Using these plots we have identified regions of color space that contain the vast majority of mid-late L dwarfs. We chose $i-z > 2$ to avoid too much contamination from red dwarfs, although this does leads to missing many early L dwarfs. Figure 1 shows the selection cuts in the $r-i$ versus $i-z$ diagram, in which a parallelogram shows the boundary limits. Two two sloping lines show the boundary limits $r-z = 3.6$ and $r-z = 6$, and the two vertical lines show $i-z = 2$ and $i-z = 3.2$. Taking into account also the photometric sensitivities of SDSS, we thus define a set of SDSS mid-late L dwarf photometric selection

criteria as follows:

$$19 < i < 23 \quad (1)$$
$$17 < z < 20 \quad (2)$$
$$3.6 < r - z < 6 \quad (3)$$
$$2 < i - z < 3.2 \quad (4)$$

Criterion (3) can also be written as

$$3.6 - (i - z) < r - i < 6 - (i - z) \quad (5)$$

in $r\,i\,z$ color-color space.

The left-hand panel of Fig. 2 shows the $J - H$ vs. $H - K$ diagram for known L dwarfs. As for Fig. 1 we define a set of color criteria to contain the majority of these L dwarfs. It is clear from Fig. 2 that the L dwarfs appear reasonably well separated from the M dwarfs in this 2-color space (see also Burgasser et al. 2002), and we would thus expect to improve our sample refinement significantly by combining our optical selection with additional near infrared photometry. Our chosen 2MASS color selection criteria are shown in the figure with solid lines, and are defined as:

$$J - H > 0.5 \quad (6)$$
$$H - K > 0.2 \quad (7)$$
$$J - K > 1. \quad (8)$$

More than 6000 candidates survived our color and magnitude optical selection from the main photometric catalog of SDSS DR7. Those candidates were matched with point sources in the 2MASS catalog (Skrutskie et al. 2006). We used a matching radius of 6″ to ensure that any ultra-cool dwarfs with high proper motion could be matched, despite possible motion over a period of up to ~8 years (between epochs). A total of 700 SDSS objects were cross-matched in 2MASS. Because the imaging depth of SDSS is deeper than that of 2MASS, many of the fainter SDSS candidates could not be found in 2MASS. Thus some of the candidates get wrongly matched with their nearest brighter neighbors in 2MASS. These are removed by checking their images in both the SDSS and 2MASS databases. On closer inspection, 2MASS mis-matches are usually very apparent, since the mis-matching objects generally have their own SDSS counterpart that immediately rules them out as high proper motion. As a more subtle check of the cross-matching, we assessed the spectral energy distribution of candidates (estimated from their SDSS and 2MASS photometry), and identified candidates that appeared to have unusual SEDs when compared to those of known ultra-cool dwarfs. It was assumed that these objects were also 2MASS mis-matches, and they were removed from our selection. Tens of wrongly matched objects were thus identified and removed from our selection. Implementation of our near infrared color selection criteria (for candidates that did not have SDSS spectroscopy) allowed us to remove more than 300 objects from our sample via the $J - H$ and $H - K$ color cuts listed in Eqs. (6)–(8).

3. Red optical spectra from the SDSS

The SDSS imaging data are used to select in a uniform way different classes of objects whose spectra will be taken with the SDSS 2.5 m telescope (York et al. 2000). The target selection algorithms for spectroscopic follow up are described by Stoughton et al. (2002). The DR7.1 main spectroscopic data base includes data for around 1.2 million objects, and covers 7470 deg^2. The wavelength coverage is from 3800 to 9200 Å with resolution $\lambda/(\Delta\lambda) = 1800$. The signal-to-noise ratio is better than 4 pixel^{-1} at $g = 20.2$ (Adelman-McCarthy et al. 2007). The spectra distributed by the SDSS have been sky subtracted and corrected for telluric absorption. The spectroscopic data are automatically reduced by the SDSS pipeline software.

Our final selection consisted of 275 objects of which 87 were cross- referenced with, and confirmed to be mostly L dwarfs. So 188 of these objects are new discoveries. Of these, 36 are confirmed through SDSS optical spectra. At first we only found 28 objects with SDSS spectra when we searched for the photometrically selected candidates in the SDSS spectroscopic catalog. Then we searched the spectra of SDSS color selected candidates with SDSS spectra which were removed with 2MASS criteria (6, 7, 8). We found six objects with SDSS spectra, three M9, one L0 and two L1 dwarfs. In Fig. 2, we can see that the 2MASS criteria (6, 7, 8) are set for L dwarfs and some late M early L dwarfs will be missed, including these six objects. Another two objects were found with SDSS spectra which are faint and therefore missed by the 2MASS survey. Table 1 lists the SDSS names, SDSS r, i, z, 2MASS J, H, K and SDSS spectral types for these 36 spectroscopically confirmed ultracool dwarfs. Note that we also performed a cross-match with UKIDSS DR4 (see Sect. 5) and that 23 objects without SDSS spectroscopy that were measured in UKIDSS are listed in Table 2. All remaining candidates (i.e. without SDSS spectroscopy or UKIDSS DR4 coverage) are given in Table 7.

In addition to the photometric and spectral type analysis we also derived proper motion constraints for our new sample, using the dual epoch coordinates from the SDSS and 2MASS databases and dividing any movement between the epochs by the observational epoch difference. Standard errors on these proper motions are calculated using the major axes of the position error ellipses from SDSS and 2MASS, and are dominated by the 2MASS positional uncertainties. Systematic astrometry errors between 2MASS-SDSS which have a shorter baseline, could lead to significant errors in calculating proper motions with coordinates and epoch differences, and can not be ignored. To correct the systematic offset of 2MASS-SDSS, we measured average proper motion of reference objects around every targets for which proper motion has been measured. Then we subtracted this average proper motion from the measured proper motion of each corresponding target. The number of reference objects ranged from around 100 to a few hundreds for different targets, with reference objects being selected to have low coordinate errors (mostly <0.1″, <0.2″ for the candidates with fewer reference objects). Reference objects are within 12′, 15′ or 20′ of our targets depends on availability. These proper motions are also given in Tables 1 and 3 and 7. Their quality and accuracy is assessed in Sect. 5 through comparison with additional epoch image data and measurement of motion relative to nearby sources surrounding each ultracool dwarf (see also Cols. 10 and 11 in Table 1).

For the 11 M9 and 25 L dwarfs with SDSS spectra. We assigned their spectral types by comparison with the SDSS spectral sequence of previously found M, L and T dwarfs as shown in Fig. 3, the dwarf classification scheme of Kirkpatrick et al. (1999), SDSS spectra of M and L dwarfs published by Hawley et al. (2002) and the low-mass dwarf template spectra from SDSS (Bochanski et al. 2007). One of the major points we have considered in the comparison is the shape of the normalized spectrum, such as the width of KI region around 7700 Å and the relative flux in the region from 8400 Å to

Table 1. SDSS and 2MASS photometry of objects with SDSS spectra.

SDSS Name	SDSS *r*	SDSS *i*	SDSS *z*	2MASS *J*	2MASS *H*	2MASS *K*	P. M.[a] ($''$yr^{-1})	P. M.[b] Angle	P. M.[c] ($''$yr^{-1})	P. M.[c] Angle	Spe. Type	S.T.by[d] Colors
SDSS J010718.70+132656.1[e]	23.24 ± 0.31	20.74 ± 0.06	18.68 ± 0.04	16.58 ± 0.15	16.21 ± 0.19	15.34 ...	0.51 ± 0.13	289 ± 15	0.43 ...	107 ...	M9	...
SDSS J012052.58+151827.3	23.54 ± 0.58	20.69 ± 0.08	18.65 ± 0.04	16.39 ± 0.13	15.44 ± 0.10	14.57 ± 0.12	0.48 ± 0.09	116 ± 11	0.13 ± 0.09	209 ± 32	M9	...
SDSS J075256.70+173433.8	23.91 ± 0.53	20.94 ± 0.06	18.93 ± 0.04	16.43 ± 0.12	15.80 ± 0.17	15.34 ...	0.13 ± 0.04	226 ± 16	0.06 ± 0.06	139 ± 136	L0	L1
SDSS J080322.77+123845.3	23.09 ± 0.22	20.73 ± 0.05	18.60 ± 0.03	16.31 ± 0.08	15.44 ± 0.08	15.23 ± 0.11	0.13 ± 0.03	223 ± 12	0.28 ± 0.23	199 ± 3	L2.5	L1
SDSS J084016.42+543002.1[e]	23.05 ± 0.31	20.83 ± 0.06	18.83 ± 0.05	16.39 ± 0.12	15.51 ± 0.13	15.35 ± 0.15	0.51 ± 0.81[f]	280 ...	1.66 ± 1.56[f]	298 ± 61	L1	L1.5
SDSS J084751.48+013811.0	23.96 ± 0.71	20.89 ± 0.08	18.86 ± 0.06	16.23 ± 0.13	15.12 ± 0.10	14.41 ± 0.09	0.66 ± 0.47[f]	263 ...	1.05 ± 1.39[f]	262 ± 39	L4	L3.5
SDSS J090023.68+253934.3	23.55 ± 0.40	21.47 ± 0.09	18.89 ± 0.04	16.43 ± 0.12	15.41 ± 0.12	14.66 ± 0.08	0.04 ± 0.03	154 ± 49	0.05 ± 0.05	165 ± 12	L6	L4.5
SDSS J090320.92+504050.6	23.46 ± 0.42	20.55 ± 0.05	18.54 ± 0.03	16.42 ± 0.12	15.49 ± 0.13	15.15 ± 0.14	0.17 ± 0.17	301 ± 73	0.24 ± 0.19	192 ± 113	M9	...
SDSS J090347.55+011446.0	23.47 ± 0.45	21.07 ± 0.08	18.94 ± 0.05	16.45 ± 0.14	15.60 ± 0.11	14.89 ± 0.13	0.67 ± 0.71[f]	205 ...	1.54 ± 1.43[f]	252 ± 71	L2	L2.5
SDSS J091714.76+314824.8	23.20 ± 0.24	20.85 ± 0.04	18.82 ± 0.03	16.30 ± 0.10	15.73 ± 0.14	15.01 ± 0.13	0.02 ± 0.04	145 ...	0.03 ± 0.02	196 ± 73	L2	L.5
SDSS J100016.92+321829.4	23.71 ± 0.54	21.04 ± 0.11	18.73 ± 0.05	16.62 ± 0.12	15.70 ± 0.11	15.36 ± 0.17	0.44 ± 0.05	243 ± 6	0.45 ± 0.40	245 ± 3	L3.5	L1.5
SDSS J100435.88+565757.4	23.63 ± 0.49	20.79 ± 0.07	18.61 ± 0.04	16.67 ± 0.11	15.81 ± 0.10	15.43 ± 0.17	0.19 ± 0.12	286 ± 38	...[g]	...	M9	...
SDSS J100817.07+052312.9[e]	23.79 ± 0.46	21.02 ± 0.06	18.97 ± 0.04	16.76 ± 0.16	16.19 ± 0.19	15.77 ± 0.28	0.07 ± 0.18	106 ...	0.30 ± 0.30	142 ± 5	M9	...
SDSS J102316.59+011549.6	23.20 ± 0.41	21.07 ± 0.09	19.03 ± 0.05	16.76 ± 0.16	15.91 ± 0.18	15.15 ± 0.17	0.28 ± 0.28	272 ...	1.50 ± 1.23	227 ± 98	M9	...
SDSS J102356.38+242430.3	22.59 ± 0.17	21.59 ± 0.12	18.94 ± 0.05	...	...	...	...	...	...	...	M9	...
SDSS J102947.68+483412.2	23.68 ± 0.49	20.89 ± 0.07	18.88 ± 0.05	16.76 ± 0.19	16.04 ± 0.21	15.59 ± 0.24	0.45 ± 0.18	237 ± 24	0.23 ± 0.16	112 ± 82	L0	L2
SDSS J103602.44+372448.5	22.75 ± 0.19	20.76 ± 0.06	18.63 ± 0.04	16.42 ± 0.12	15.54 ± 0.13	14.99 ± 0.11	0.10 ± 0.03	176 ± 17	0.12 ± 0.11	153 ± 48	L0	L1
SDSS J104407.47+015742.0	23.23 ± 0.32	20.87 ± 0.07	18.84 ± 0.05	16.59 ± 0.16	15.65 ± 0.13	15.22 ± 0.20	2.51 ± 1.22	113 ± 29	1.46 ± 1.08	168 ± 65	L1	L0.5
SDSS J104922.45+012559.2	23.85 ± 0.59	21.00 ± 0.09	18.78 ± 0.04	15.88 ± 0.07	14.95 ± 0.07	14.11 ± 0.06	0.07 ± 0.14	21 ...	0.13 ± 0.16	200 ± 23	L5	L5
SDSS J110009.62+495746.5	22.57 ± 0.19	20.08 ± 0.03	18.00 ± 0.02	15.28 ± 0.04	14.19 ± 0.04	13.47 ± 0.03	0.25 ± 0.03	241 ± 8	0.23 ± 0.20	230 ± 13	L4	L4
SDSS J112242.26+364928.6	23.29 ± 0.31	20.75 ± 0.05	18.65 ± 0.04	16.54 ± 0.11	15.61 ± 0.11	15.13 ± 0.11	0.07 ± 0.03	106 ± 27	0.04 ± 0.03	154 ± 84	M9	...
SDSS J114201.95+521917.0[e]	21.71 ± 0.08	19.13 ± 0.02	17.09 ± 0.01	15.08 ± 0.05	14.57 ± 0.07	14.12 ± 0.05	0.20 ± 0.05	219 ± 13	...[g]	...	M9	...
SDSS J115013.17+052012.3	23.75 ± 0.39	21.28 ± 0.07	18.91 ± 0.04	16.25 ± 0.14	15.46 ± 0.14	15.02 ± 0.17	0.72 ± 0.24	260 ± 20	...[g]	...	L5.5	L3
SDSS J132926.03+531733.9[e]	23.84 ± 0.50	20.87 ± 0.06	18.84 ± 0.04	16.82 ± 0.20	15.59 ± 0.17	15.62 ± 0.24	0.19 ± 0.12	177 ± 40	0.05 ± 0.05	152 ± 83	L1	L1
SDSS J133257.73+325813.1[e]	23.20 ± 0.25	20.73 ± 0.04	18.72 ± 0.03	16.57 ± 0.11	15.49 ± 0.11	15.33 ± 0.12	0.15 ± 0.04	224 ± 15	0.12 ± 0.12	218 ± 32	L0	L0.5
SDSS J134025.14+524505.0	23.71 ± 0.55	21.14 ± 0.08	18.94 ± 0.04	16.69 ± 0.15	15.67 ± 0.14	15.31 ± 0.12	0.21 ± 0.11	75 ± 33	0.15 ± 0.16	159 ± 81	M9	...
SDSS J141011.14+132900.8	24.11 ± 0.49	21.03 ± 0.07	18.96 ± 0.05	16.85 ± 0.14	15.89 ± 0.15	15.53 ± 0.19	0.18 ± 0.06	279 ± 21	0.17 ± 0.11	276 ± 5	L4	...
SDSS J143130.77+143653.4	22.25 ± 0.12	19.69 ± 0.02	17.58 ± 0.02	15.15 ± 0.04	14.50 ± 0.05	14.13 ± 0.06	0.45 ± 0.02	259 ± 3	0.45 ± 0.37	261 ± 3	L2	L1.5
SDSS J143832.63+572216.9	23.45 ± 0.40	20.81 ± 0.06	18.71 ± 0.04	15.96 ± 0.07	15.10 ± 0.08	14.37 ± 0.06	0.20 ± 0.05	86 ± 13	0.12 ± 0.14	75 ± 43	L5	L3.5
SDSS J151136.24+353511.4	23.45 ± 0.35	20.72 ± 0.05	18.69 ± 0.03	16.29 ± 0.10	15.62 ± 0.11	14.95 ± 0.12	0.06 ± 0.04	179 ± 48	0.16 ± 0.13	133 ± 70	L1	L1
SDSS J154502.87+061807.8	23.91 ± 0.42	20.87 ± 0.05	18.83 ± 0.04	16.37 ± 0.11	15.60 ± 0.12	15.28 ± 0.16	0.21 ± 0.08	282 ± 23	0.20 ± 0.14	263 ± 31	L4	L1
SDSS J154628.38+253634.3	22.66 ± 0.14	20.15 ± 0.03	18.12 ± 0.02	15.76 ± 0.07	15.07 ± 0.08	14.71 ± 0.08	0.51 ± 0.03	286 ± 4	0.34 ± 0.30	283 ± 13	L1	L0.5
SDSS J155215.38+065041.5	24.23 ± 0.53	20.99 ± 0.06	18.97 ± 0.04	16.78 ± 0.15	15.91 ± 0.14	15.63 ± 0.21	0.01 ± 0.09	264 ...	0.18 ± 0.18	294 ± 11	L0	L0.5
SDSS J161840.27+202045.6	23.40 ± 0.26	20.60 ± 0.04	18.59 ± 0.03	16.15 ± 0.09	15.20 ± 0.07	14.81 ± 0.09	0.15 ± 0.04	35 ± 14	0.04 ± 0.04	205 ± 97	M9	...
SDSS J172006.69+615537.7	23.35 ± 0.52	21.32 ± 0.13	19.27 ± 0.08	...	...	...	...	...	...	...	L3	...
SDSS J211846.77−001044.6	23.28 ± 0.30	20.80 ± 0.06	18.73 ± 0.04	16.20 ± 0.11	15.62 ± 0.16	15.07 ± 0.13	0.16 ± 0.19	18 ...	0.29 ± 0.27	223 ± 103	L1	L1

Note: SDSS magnitude limits (95% detection repeatability for point sources) for *r*, *i* and *z* bands are 22.2, 21.3 and 20.5 respectively; [a] 2MASS-SDSS data-base proper motions – found by dividing the difference between the 2MASS and SDSS coordinates (from the respective databases) by the observational epoch difference. Standard errors are calculated using the major axes of the position error ellipses from 2MASS and SDSS; [b] error ellipses of 2MASS and SDSS overlap for some objects, for which position angle errors are not meaningful; [c] 2MASS-SDSS relative proper motions – found by specifically measuring the relative movement of the ultracool dwarfs with respect to nearby reference objects in the 2MASS and SDSS images; [d] spectral types are based on the relationship between spectral type and SDSS and 2MASS colors (*i*-*z*, *i*-*J*, *i*-*H*, *i*-*K* are used largely and *r*-*i*, *z*-*J*, *z*-*H*, *z*-*K* with less weight); [e] objects with SDSS spectra which do not accord with the 2MASS color criteria (6, 7, 8); [f] objects only have a baseline of ∼3 months; [g] we do not measure their proper motions for they are very faint in 2MASS images or only have a few nearby reference objects.

Table 2. Photometric data of UKIDSS matched L dwarf candidates.

SDSS Name	SDSS *r*	SDSS *i*	SDSS *z*	2MASS *J*	2MASS *H*	2MASS *K*	UKIDSS *Y*	UKIDSS *J*	UKIDSS *H*	UKIDSS *K*	Sp. Type[a]
J004759.59+135332.0[b]	24.78 ± 0.88	22.11 ± 0.28	19.61 ± 0.10	16.81 ± 0.16	16.10 ± 0.17	15.51 ± 0.19	18.03 ± 0.03	17.22 ± 0.03	16.52 ± 0.03	16.00 ± 0.03	L3.5
J015141.04−005156.5[c]	22.23 ± 0.15	19.70 ± 0.03	17.61 ± 0.02	15.10 ± 0.05	14.27 ± 0.04	13.59 ± 0.05	16.24 ± 0.01	15.02 ± 0.00	14.29 ± 0.00	13.65 ± 0.00	L2
J022927.95−005328.5	24.19 ± 0.64	21.54 ± 0.11	19.41 ± 0.07	16.49 ± 0.10	15.75 ± 0.10	15.18 ± 0.14	...	16.62 ± 0.02	15.82 ± 0.02	15.15 ± 0.02	L3.5
J073241.77+264558.9	24.31 ± 0.46	22.40 ± 0.18	19.83 ± 0.08	17.37 ± 0.21	16.81 ± 0.25	15.64 ± 0.19	...	17.55 ± 0.02	...	...	L4.5
J074436.02+251330.5	24.28 ± 0.49	21.23 ± 0.07	18.77 ± 0.03	17.17 ± 0.25	16.04 ± 0.21	15.66 ± 0.22	...	16.68 ± 0.01	...	...	L1
J075754.16+221604.9	23.34 ± 0.36	21.45 ± 0.10	19.41 ± 0.06	16.61 ± 0.13	16.10 ± 0.22	15.30 ± 0.14	...	16.87 ± 0.01	...	...	L2.5
J081303.96+243355.9	23.41 ± 0.38	21.32 ± 0.08	19.30 ± 0.05	16.67 ± 0.12	15.63 ± 0.12	14.97 ± 0.09	...	16.57 ± 0.01	...	...	L3
J081409.45+260250.4	25.06 ± 0.67	21.88 ± 0.15	19.69 ± 0.10	17.18 ± 0.18	16.50 ± 0.21	15.76 ± 0.19	...	17.25 ± 0.02	...	...	L2
J083613.45+022106.2[c]	22.36 ± 0.16	19.12 ± 0.02	17.09 ± 0.01	14.76 ± 0.04	14.17 ± 0.04	13.71 ± 0.04	15.73 ± 0.01	14.72 ± 0.00	14.18 ± 0.00	13.68 ± 0.00	L0.5
J092745.81+010640.4	24.03 ± 0.68	21.34 ± 0.10	19.21 ± 0.06	16.97 ± 0.20	16.18 ± 0.21	15.37 ± 0.21	18.05 ± 0.03	17.11 ± 0.01	16.55 ± 0.02	15.99 ± 0.03	L1
J094624.37+344639.8	23.40 ± 0.30	20.92 ± 0.05	18.82 ± 0.03	16.44 ± 0.10	15.79 ± 0.13	15.14 ± 0.12	...	16.33 ± 0.01	...	...	L1
J095941.47+114146.0	23.51 ± 0.38	21.30 ± 0.08	19.29 ± 0.05	16.43 ± 0.14	15.66 ± 0.13	15.24 ± 0.19	...	...	...	15.27 ± 0.01	L3
J121238.73+000721.6	24.02 ± 0.66	20.85 ± 0.09	18.25 ± 0.03	15.81 ± 0.10	15.01 ± 0.09	14.46 ± 0.09	...	15.69 ± 0.01	...	...	L3.5
J133131.70+122531.4	24.62 ± 0.66	21.32 ± 0.10	19.32 ± 0.05	16.78 ± 0.16	15.72 ± 0.17	15.28 ± 0.15	17.83 ± 0.03	16.72 ± 0.01	16.03 ± 0.02	15.46 ± 0.01	L2.5
J134531.43+001551.2	24.14 ± 0.51	21.59 ± 0.11	19.47 ± 0.08	16.94 ± 0.21	15.98 ± 0.14	15.55 ± 0.23	18.19 ± 0.03	16.95 ± 0.02	16.19 ± 0.02	15.60 ± 0.02	L2.5
J150153.00−013507.1	22.71 ± 0.25	20.80 ± 0.07	18.62 ± 0.05	16.08 ± 0.09	14.95 ± 0.07	14.26 ± 0.09	...	...	15.02 ± 0.01	14.25 ± 0.01	L3.5
J154236.26−004545.9	24.71 ± 0.79	21.78 ± 0.15	19.35 ± 0.06	16.71 ± 0.13	15.98 ± 0.14	15.41 ± 0.20	18.07 ± 0.02	16.83 ± 0.02	16.21 ± 0.02	15.64 ± 0.02	L3.5
J154432.77+265551.2	23.22 ± 0.23	21.31 ± 0.07	19.10 ± 0.04	16.22 ± 0.10	15.24 ± 0.10	14.64 ± 0.10	...	16.23 ± 0.01	...	...	L4.5
J154740.16+053208.3	23.39 ± 0.30	20.57 ± 0.04	18.57 ± 0.03	16.18 ± 0.10	15.58 ± 0.11	15.11 ± 0.16	17.25 ± 0.01	16.18 ± 0.01	15.58 ± 0.01	15.02 ± 0.01	L0.5
J161711.68+322249.5	24.80 ± 0.88	21.25 ± 0.12	19.03 ± 0.06	16.56 ± 0.13	15.69 ± 0.15	15.42 ± 0.16	...	16.68 ± 0.01	...	...	L2
J232715.71+151730.4	23.26 ± 0.28	21.31 ± 0.09	19.13 ± 0.05	16.29 ± 0.11	15.35 ± 0.09	14.77 ± 0.13	17.54 ± 0.02	16.20 ± 0.01	15.36 ± 0.01	14.68 ± 0.01	L5
J234040.33−003337.2	23.54 ± 0.35	21.45 ± 0.10	19.35 ± 0.06	17.06 ± 0.16	16.34 ± 0.23	15.52 ± 0.20	17.94 ± 0.03	17.03 ± 0.02	16.46 ± 0.02	16.01 ± 0.04	L1
J234513.85+002441.6	24.80 ± 0.71	22.63 ± 0.29	19.56 ± 0.08	16.78 ± 0.16	15.90 ± 0.20	15.55 ± 0.19	17.67 ± 0.03	...	16.21 ± 0.02	15.59 ± 0.02	L8.5

Notes: UKIDSS magnitude limits for *Y*, *J*, *H* and *K* bands are 20.5, 20.0, 18.8 and 18.4 respectively. All magnitudes here are Vega based. We use 0.1″ as a typical position error for UKIDSS. Error ellipses of 2MASS and SDSS overlap for some objects for which proper motion angle errors are not listed; [a] spectral types are based on the relationship between spectral type and SDSS and 2MASS colors (*i-z*, *i-J*, *i-H*, *i-K* are used largely and *r-i*, *z-J*, *z-H*, *z-K* with less weight); [b] It is merged with a nearby faint galaxy in 2MASS image, so its 2MASS photometric data is not reliable. The spectral type is based on SDSS-UKIDSS colors (*i-J, i-H* and *i-K*) according to Eq. (9). [c] Data errors of *J, H, K* bands are less than 0.005.

Table 3. Seven objects with SDSS spectra matched in UKIDSS.

SDSS Name	UKIDSS *Y*	UKIDSS *J*	UKIDSS *H*	UKIDSS *K*	Proper motion[a] ($''$yr^{-1})	Proper motion Angle[b]
SDSS J012052.58+151827.3	17.11 ± 0.02	16.09 ± 0.01	15.50 ± 0.01	14.92 ± 0.01	0.04 ± 0.02	105 ± 36
SDSS J084751.48+013811.0	17.38 ± 0.02	16.09 ± 0.01	15.22 ± 0.01	14.45 ± 0.01	0.03 ± 0.02	242 ...
SDSS J090347.55+011446.0	17.58 ± 0.02	...	15.59 ± 0.01	14.96 ± 0.01	0.03 ± 0.02	259 ...
SDSS J091714.76+314824.8	...	16.36 ± 0.01	...	...	0.03 ± 0.03	345 ...
SDSS J100817.07+052312.9	...	...	16.36 ± 0.02	15.89 ± 0.03	0.21 ± 0.03	139 ± 10
SDSS J154502.87+061807.8	17.35 ± 0.02	16.21 ± 0.01	15.62 ± 0.01	15.07 ± 0.01	0.14 ± 0.04	251 ± 25
SDSS J155215.38+065041.5	...	...	15.93 ± 0.01	15.32 ± 0.01	0.02 ± 0.04	356 ...

[a] SDSS-UKIDSS data-base proper motions – found by dividing the difference between the SDSS and UKIDSS coordinates (from the respective databases) by the observational epoch difference. Standard errors are calculated using the major axes of the position error ellipses from SDSS and UKIDSS; [b] error ellipses of SDSS and UKIDSS overlap for some objects for which position angle errors are not meaningful.

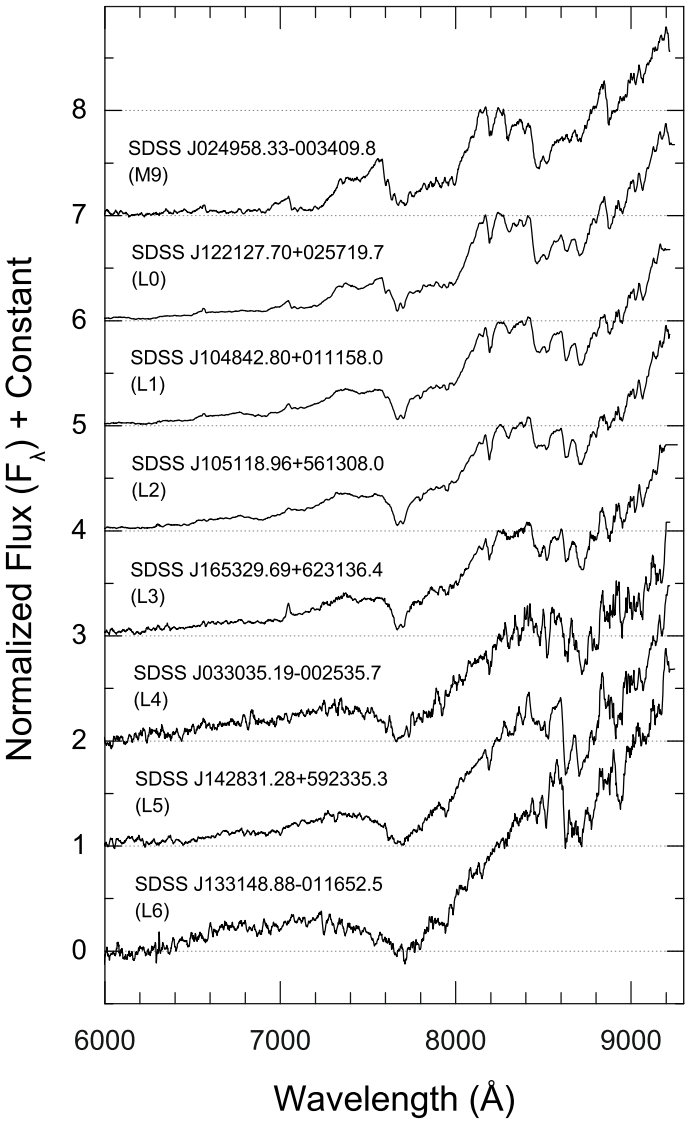

Fig. 3. SDSS spectra of 8 previously found M and L dwarfs, used for spectral typing. All spectra have been normalized to one at 8250 Å and vertically offset for clarity.

9000 Å. Another major point is the slope of the spectrum in the band from 8700 Å to 9200 Å. The last criterion is the depth of absorption lines which can be recognized in some spectra, such as NaI $\lambda\lambda$8183, 8195, CrH λ8661, FeH λ8692 and CsI $\lambda\lambda$8521, 8944. NaI $\lambda\lambda$8183, 8195 is a major feature of late M dwarfs. CrH λ8661 is equal in strength to FeH λ8692 for L4 dwarfs, and stronger for L5 dwarfs. CsI keeps strengthening from L1 to L8 type (Kirkpatrick et al. 1999). Finally, to double check the spectral type of each spectrum, we subtract the spectrum of a ultra-cool dwarf which has the same spectral type and has a good quality, and find a good agreement within our errors.

We note that our selected objects can not be giants because of the presence of the high gravity features such as KI, NaI and FeH, which are characteristic of dwarfs (e.g., Bessell 1991). Figure 3 shows 8 spectra of previously found M, L and T dwarfs as a comparison. SDSS J1428+5923 was recently confirmed and spectral-typed using its infrared spectrum as an L5 dwarf using the Two Micron Proper Motion (2MUPM) survey, under the name 2MASS J14283132+5923354 (Schmidt et al. 2007). SDSS J0249−0034, SDSS J1048+0111, SDSS J1653+6231 and SDSS J1331−0116 were classified by Hawley et al. (2002). SDSS J1221+0257 and SDSS J1051+5613 were discovered by Reid et al. (2008), and SDSS J0330−0025 was discovered by Fan et al. (2000).

Figures 4 and 5 shows the SDSS spectra of the 36 M and L dwarfs found in this work. The spectra shortward of 6000 Å are flat and noisy, and are not shown. The spectral types of our candidates extend from M9 to L6, and the spectral typing errors are estimated as about ±1 ∼ 2 sub-type. These SDSS spectra have been smoothed by 11 pixels and have been normalized to one at 8250 Å. There is a straight line in the spectrum of SDSS J1036+3724 which is an artifact. There is another artificial straight line in the spectrum of SDSS J1431+1436 across 8400 Å. The spectra of SDSS J0903+0114, SDSS J1329+5317, SDSS J1410+1329 and SDSS J1720+6155 are noisy which made it more difficult to assign their spectral types.

Using the relationship between absolute *J* and *z* band magnitudes and spectral types (Hawley et al. 2002), we estimated the approximate distance of the 36 new M and L dwarfs. Generally, early and mid L dwarfs in our sample are between 25 and 100 pc, and the M dwarfs beyond 100 pc.

4. Color-spectral type relationships

To estimate the spectral types of our ultra-cool dwarf candidates without spectra, we need to know the relationships between spectral types and colors. Hawley et al. (2002) gave the correlation between spectral type and average color for each subtype range from M0 to T6. The relationship is good for M dwarfs, but has large errors for L and T dwarfs. With a much larger number of L and T dwarfs now available, we made a study of the relationships between spectral types of L and T dwarfs and their colors from SDSS and 2MASS. To construct these relationships

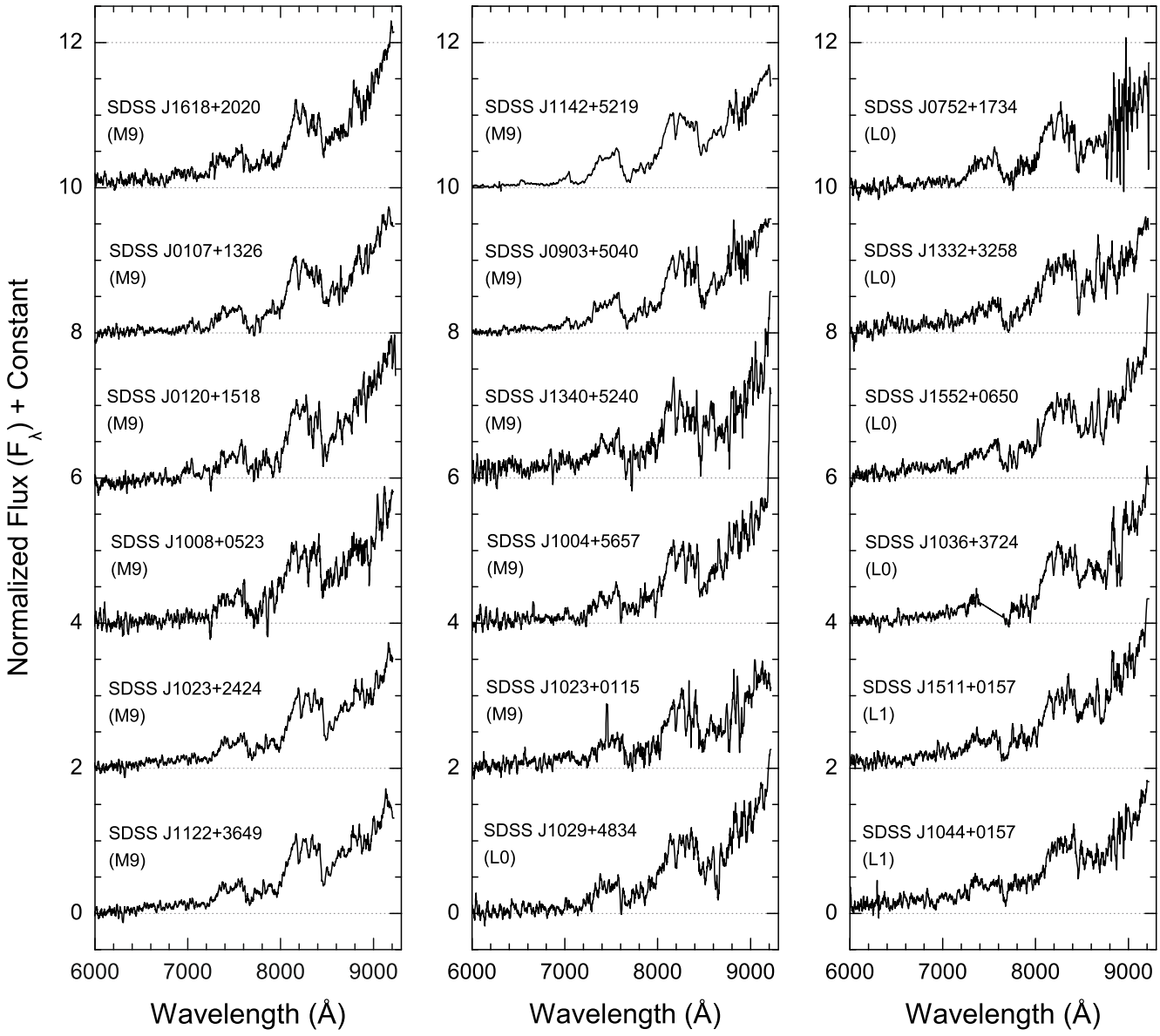

Fig. 4. The SDSS spectra of new M and L dwarfs. Spectral types are given in brackets. The spectra are normalized to one at 8250 Å and offset from one another for clarity. All the spectra are taken from the SDSS archive.

we used the same data set as that for the photometric selection criteria (see section 2). SDSS colors *r-i, i-z*, 2MASS colors *J-H*, *H-K* and optical-near infrared colors *i-J*, *i-H*, *i-K*, *z-J*, *z-H*, *z-K* are involved. We fit these relationships with a united polynomial equation,

$$\text{color} = a + b(\text{type}) + c(\text{type})^2 \quad (9)$$

where type is a number designed to incompass the full range of M, L and T spectral classes (type = 10 for L0, 15 for L5, 20 for T0, 25 for T5). Polynomial parameters *a*, *b* and *c* are different for different color ranges and our range of calculated values can be found in Table 4. As well as spectral type ranges, correlation coefficient *R* and sensitivity indices for the fitting equations are also available in Table 4, where the sensitivity index is defined as the rate of change of color with spectral type, and is thus an indication of the usefulness of a color as a spectral type estimator. Calculated values of the various colors are presented in Table 5 for spectral sub-types between L0 and T7.5. The *i-z*, *i-J*, *i-H* and *i-K* colors are the most sensitive to spectral type, and the first three of these are plotted as a function of spectral type in Fig. 6.

5. Cross matching the new sample with UKIDSS

To provide an additional epoch of deeper near infrared measurements that could improve candidate characterization (particularly for candidates without SDSS spectroscopy), we cross-matched our SDSS DR7 candidates with the Fourth Data Release of the UKIDSS Large Area Survey (Lawrence et al. 2007). UKIDSS magnitude limits for the *Y*, *J*, *H* and *K* bands are 20.5, 20.0, 18.8 and 18.4 respectively. We found that 23 of our candidates (without SDSS spectra) and 7 of our spectroscopically confirmed objects have UKIDSS DR4 counterparts. Table 2 lists the SDSS names, *r*, *i*, *z*, 2MASS *J*, *H*, *K*, UKIDSS *Y*, *J*, *H*, *K* and color-estimated spectral types (see Sect. 4) for the objects without spectroscopy, and Table 3 presents the additional UKIDSS information for 7 of the spectroscopic objects from Table 1.

Figure 7 shows the $Y - J$ versus $J - H$ diagram for the 15 candidates that had UKIDSS *Y* detections. In general these all had UKIDSS *YJH* magnitudes but in 2 cases we had to transform a 2MASS *J* into a UKIDSS *J* following the

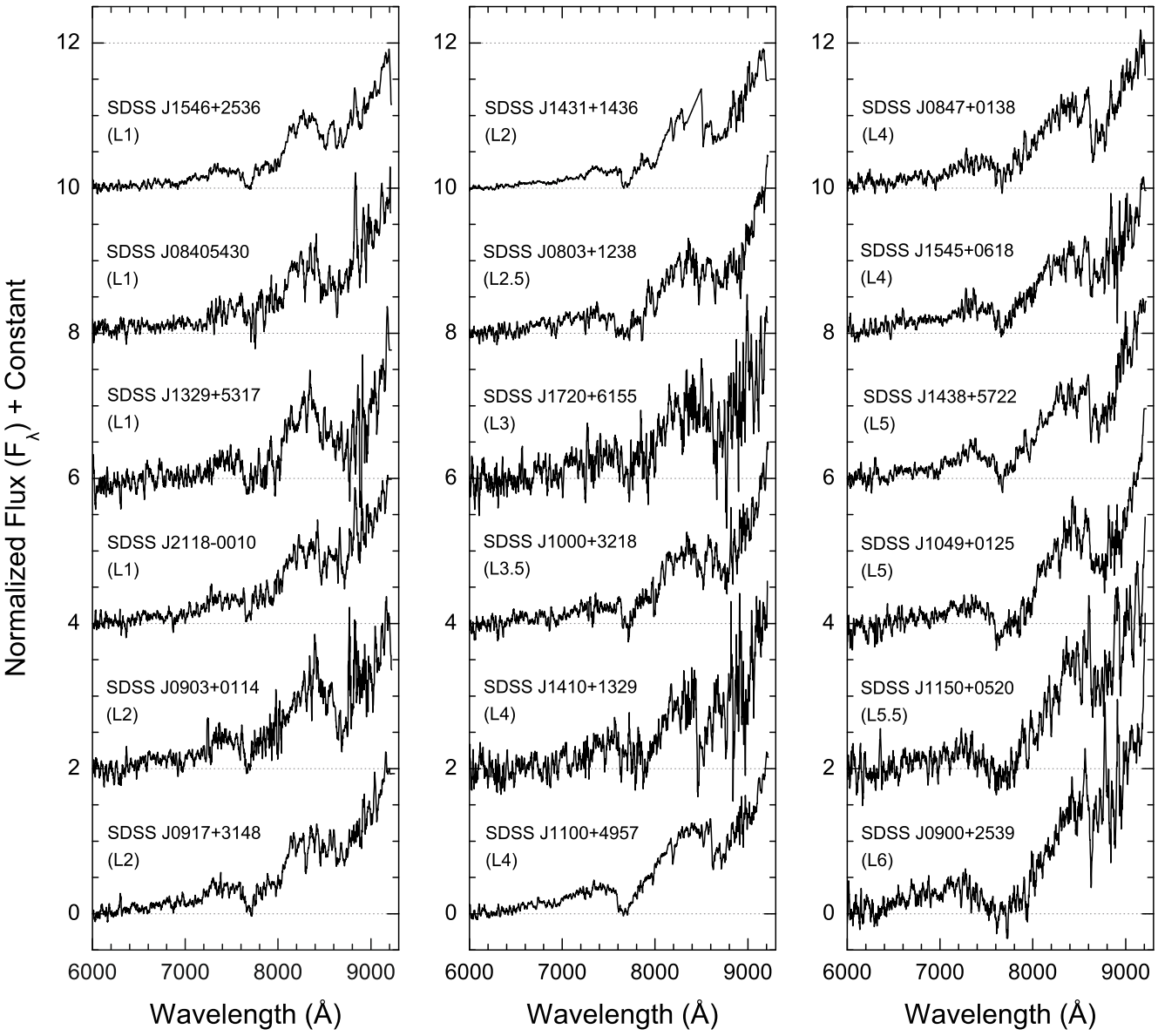

Fig. 5. The SDSS spectra of new M and L dwarfs. Same as Fig. 4.

Table 4. Parameters of fitting equations for color−type relationships.

Color	a	b	c	type Range	R	Sensitivity Index[a]
$r-i$	2.77242	0.01930	−0.00355	[10, 27.5]	0.62	0.073
$i-z$	0.89637	0.00812	0.00582	[13, 25]	0.89	0.225
$i-J$	4.46097	−0.12872	0.01099	[10, 25]	0.94	0.253
$i-H$	2.68743	0.22692	0	[10, 25]	0.92	0.227
$i-K$	2.04847	0.39856	−0.00567	[10, 25]	0.90	0.200
$z-J$	1.32530	0.10725	0	[10, 13.5]	0.59	0.107
$z-J$	0.61620	0.10826	0	[19, 26]	0.81	0.107
$z-H$	4.23705	−0.31004	0.02038	[10, 14]	0.70	0.158
$z-H$	4.60067	−0.03962	0	[17.5, 27.5]	0.53	0.040
$z-K$	3.93079	−0.21325	0.01860	[10, 14]	0.72	0.235
$z-K$	6.96601	−0.13083	0	[17.5, 27.5]	0.72	0.080
$H-K$	0.15050	0.03638	0	[10, 15]	0.40	0.040
$H-K$	2.19557	−0.08809	0	[17, 25]	0.66	0.088
$J-H$	0.06224	0.06903	0	[10,14]	0.49	0.088
$J-H$	5.58544	−0.21707	0	[20, 25]	0.90	0.100

Notes: the united polynomial fitting equation of color−spectral type relationships is: color = $a + b$(type) + c(type)^2, type = 10 for L0, 15 for L5, 20 for T0, 25 for T5; [a] Sensitivity indices are the rates of change of color ranges with spectral ranges covered by fitting lines.

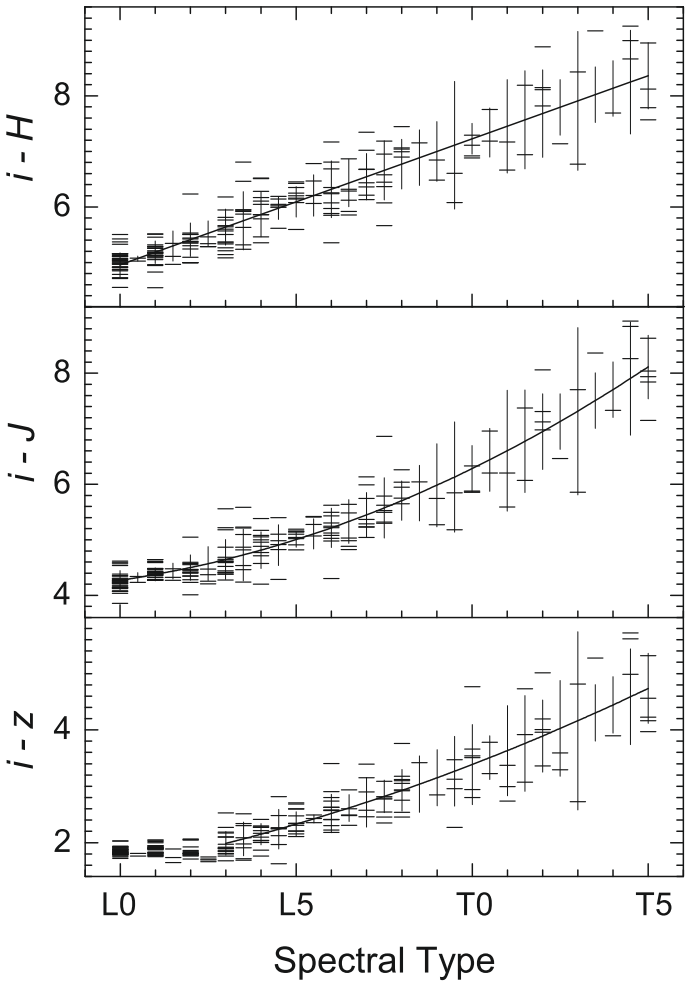

Fig. 6. Polynomial fitting for color-spectral type relationships are indicated with a solid line. The error bars of fitted colors indicate the standard deviation at each subtype. We used 0.5 as the error, if there is only one object available for a given subtype.

conversion of Hewett et al. (2006). This 2-color diagram can provide additional information on ultra-cool dwarf spectral types (e.g. Hewett et al. 2006). For example, the SDSS/2MASS colors of SDSS J2345−0024 suggest a spectral type between L7 and T2. However, Figure 7 suggests that SDSS J2345−0024 is more likely an early T dwarf than a late L dwarf.

To further assess the proper motions that we derive for all candidates using the coordinate and epoch information stored in the SDSS and 2MASS databases, we have measured additional proper motion constraints using several combinations of multi-epoch data (SDSS/UKIDSS, 2MASS/UKIDSS and 2MASS/SDSS combinations), as well as by measuring the motion of our ultracool dwarf candidates with respect to reference objects within 6′ in the SDSS z and UKIDSS *Y, J, H* and *K* images. For the relative proper motions, we used the Iraf routines GEOMAP and GEOXYTRAN to transform the pixel coordinates from the SDSS images into the pixel coordinate system of the UKIDSS images. Visual inspection of the image data revealed a small number of problematic sources. SDSS J0047+1353 is merged with a very nearby galaxy in the 2MASS image. In the main however, four separate proper motion measurements were made (combining $z/Y, z/J, z/H$ and z/K) where possible, and an average proper motion taken. UKIDSS centroiding accuracy was estimated from the standard deviation of these four measurements, and we also factored in a centroiding uncertainty associated with the SDSS z-band epoch, which we estimated to be 0.1″ (1/4 of an SDSS pixel) for these faint sources. The relative proper motions measured from 2MASS and SDSS images are given in Cols. 10 and 11 of Table 1 (for the spectroscopically confirmed objects). The relative proper motions measured from UKIDSS and SDSS images are given in Cols. 2 and 3 of Table 6. Database proper motions (i.e. calculated from cross-database coordinate/epoch information) for UKIDSS/SDSS, 2MASS/UKIDSS, and 2MASS/SDSS database combinations are given in Cols. 4–9 of Table 6, and for the UKIDSS/SDSS combination in Cols. 6, 7 of Table 3. A correction for systematic coordinate uncertainties between UKIDSS and 2MASS/SDSS was decreased as before (see Sect. 3). Figure 8 shows average proper motions of reference objects of objects in Table 6 which proper motions measured with 2MASS-SDSS-UKIDSS databases. The proper motion offsets of 2MASS-UKIDSS with the longest baseline have the smallest offsets (<0.008″ yr^{-1}) which indicated proper motion with a baseline of longer than 5 years (e.g. 2MASS-UKIDSS) will be a very good way for identified ultracool dwarfs.

- In most cases the 2MASS-SDSS proper motions calculated from the databases are in reasonable agreement with our derived relative proper motions to within the uncertainties. However, the uncertainties associated with the relative proper motions are often larger. This is because in general there is a reduced number of useful reference sources in the 2MASS images. This can sometimes be compounded if a sources is close to the edge of a 2MASS strip, since the number of reference sources can be reduced still further. We thus conclude that the database proper motions are to be preferred when combining 2MASS and SDSS survey data.
- In general, the UKIDSS/SDSS, 2MASS/UKIDSS and 2MASS/SDSS database proper motions agree well to within their uncertainties, except in a limited number of cases, where we find that on closer inspection the baseline between the database epochs is low and the 2MASS sources themselves are near the 2MASS detection limit. The 2MASS/SDSS database proper motions thus stand up reasonably well when compared to those measured from a combination of, on average, higher signal-to-noise imaging data.
- The UKIDSS-SDSS proper motions calculated from the databases are in very good agreement with our derived relative proper motions to within the uncertainties, and the estimated uncertainties from each method are comparable. This result is not surprising, but provides a useful verification for our database proper motion calculations.

We thus conclude that overall, our 2MASS-SDSS proper motions calculated from the databases offer a good balance of reasonably accurate measurements over a relatively large sky area.

6. Discussion

Although our photometric selection criteria have been shown to be optimized for mid-late L dwarfs (see Fig. 1), most of the sample that had SDSS spectra are actually late M and early L dwarfs. This partly results from a luminosity bias since later, less luminous L dwarfs are only detected by SDSS in a smaller volume. SDSS targeting priority for these objects was primarily determined through brightness, so our spectroscopic sample is reasonably close to a magnitude limited subset of our full photometric selection. However, in addition, later L dwarfs are redder,

Table 5. Different colors by different spectral types.

Sp.Type	*r-i*	*i-z*	*i-J*	*i-H*	*i-K*	*z-J*[a]	*z-H*[a]	*z-K*[a]	*J-H*[a]	*H-K*[a]
L0	2.61 ± 0.27	...	4.27 ± 0.17	4.96 ± 0.22	5.47 ± 0.26	2.40 ± 0.13	3.17 ± 0.17	3.66 ± 0.22	0.75 ± 0.11	0.51 ± 0.10
L0.5	2.58 ± 0.35	...	4.32 ± 0.09	5.07 ± 0.05	5.61 ± 0.10	2.45 ± 0.13	3.23 ± 0.09	3.74 ± 0.21	0.79 ± 0.09	0.53 ± 0.07
L1	2.56 ± 0.19	...	4.37 ± 0.12	5.18 ± 0.20	5.75 ± 0.21	2.51 ± 0.12	3.29 ± 0.22	3.84 ± 0.23	0.82 ± 0.14	0.55 ± 0.12
L1.5	2.52 ± 0.10	...	4.43 ± 0.14	5.30 ± 0.27	5.88 ± 0.13	2.56 ± 0.06	3.37 ± 0.13	3.94 ± 0.13	0.86 ± 0.14	0.57 ± 0.09
L2	2.49 ± 0.28	...	4.50 ± 0.23	5.41 ± 0.30	6.01 ± 0.38	2.61 ± 0.21	3.45 ± 0.29	4.05 ± 0.39	0.89 ± 0.18	0.59 ± 0.14
L2.5	2.46 ± 0.33	...	4.57 ± 0.31	5.52 ± 0.23	6.14 ± 0.29	2.67 ± 0.14	3.55 ± 0.16	4.17 ± 0.23	0.93 ± 0.14	0.61 ± 0.13
L3	2.42 ± 0.32	1.99 ± 0.21	4.64 ± 0.36	5.64 ± 0.32	6.27 ± 0.43	2.72 ± 0.19	3.65 ± 0.26	4.30 ± 0.33	0.96 ± 0.17	0.62 ± 0.17
L3.5	2.39 ± 0.64	2.07 ± 0.30	4.73 ± 0.47	5.75 ± 0.53	6.40 ± 0.57	2.77 ± 0.38	3.77 ± 0.48	4.44 ± 0.48	0.99 ± 0.23	0.64 ± 0.24
L4	2.35 ± 0.56	2.15 ± 0.19	4.81 ± 0.33	5.86 ± 0.40	6.52 ± 0.55	...	3.89 ± 0.30	4.59 ± 0.46	1.03 ± 0.28	0.66 ± 0.17
L4.5	2.31 ± 0.55	2.24 ± 0.35	4.91 ± 0.37	5.98 ± 0.21	6.64 ± 0.30	...	...	...	...	0.68 ± 0.21
L5	2.26 ± 0.53	2.33 ± 0.22	5.00 ± 0.14	6.09 ± 0.27	6.75 ± 0.32	...	...	...	...	0.70 ± 0.13
L5.5	2.22 ± 0.38	2.42 ± 0.07	5.11 ± 0.27	6.20 ± 0.37	6.86 ± 0.45	...	...	...	...	...
L6	2.17 ± 0.75	2.52 ± 0.34	5.21 ± 0.35	6.32 ± 0.51	6.97 ± 0.51	...	...	...	...	...
L6.5	2.12 ± 0.55	2.61 ± 0.24	5.33 ± 0.39	6.43 ± 0.43	7.08 ± 0.38	...	...	...	...	...
L7	2.07 ± 0.54	2.72 ± 0.44	5.45 ± 0.40	6.55 ± 0.42	7.19 ± 0.48	...	...	...	...	0.70 ± 0.27
L7.5	2.02 ± 0.93	2.82 ± 0.29	5.57 ± 0.54	6.66 ± 0.53	7.29 ± 0.55	...	3.91 ± 0.42	4.68 ± 0.53	...	0.65 ± 0.18
L8	1.97 ± 0.63	2.93 ± 0.37	5.70 ± 0.35	6.77 ± 0.45	7.39 ± 0.58	...	3.89 ± 0.17	4.61 ± 0.21	...	0.61 ± 0.13
L8.5[b]	1.91 ...	3.04 ...	5.84 ...	6.89 ...	7.48 ...	...	3.87 ...	4.55 ...	...	0.57 ...
L9[b]	1.86 ...	3.15 ...	5.98 ± 0.75	7.00 ± 0.53	7.57 ± 0.49	2.67 ± 0.27	3.85 ± 0.28	4.48 ± 0.27	...	0.52 ± 0.15
L9.5	1.80 ± 1.38	3.27 ± 0.62	6.13 ± 0.99	7.11 ± 1.15	7.66 ± 1.10	2.73 ± 0.18	3.83 ± 0.34	4.41 ± 0.24	...	0.48 ± 0.20
T0	1.74 ± 1.49	3.39 ± 0.71	6.28 ± 0.42	7.23 ± 0.28	7.75 ± 0.31	2.78 ± 0.29	3.81 ± 0.22	4.35 ± 0.15	1.24 ± 0.23	0.43 ± 0.14
T0.5	1.68 ± 0.65	3.51 ± 0.39	6.44 ± 0.57	7.34 ± 0.44	7.84 ± 0.53	2.84 ± 0.37	3.79 ± 0.25	4.28 ± 0.55	1.14 ± 0.37	0.39 ± 0.45
T1	1.61 ± 0.65	3.63 ± 0.80	6.60 ± 1.09	7.45 ± 0.84	7.92 ± 0.71	2.89 ± 0.30	3.77 ± 0.10	4.22 ± 0.08	1.03 ± 0.09	0.35 ± 0.20
T1.5	1.55 ± 0.42	3.76 ± 0.85	6.77 ± 0.92	7.57 ± 0.88	8.00 ± 0.72	2.94 ± 0.31	3.75 ± 0.31	4.15 ± 0.66	0.92 ± 0.13	0.30 ± 0.24
T2	1.48 ± 1.02	3.89 ± 0.64	6.95 ± 0.68	7.68 ± 0.79	8.07 ± 0.71	3.00 ± 0.10	3.73 ± 0.28	4.09 ± 0.33	0.81 ± 0.17	0.26 ± 0.53
T2.5[b]	1.41 ± 0.83	4.03 ± 0.85	7.13 ...	7.79 ...	8.15 ...	3.05 ...	3.71 ...	4.02 ...	0.70 ...	0.21 ...
T3	1.34 ± 2.19	4.16 ± 1.58	7.31 ± 1.51	7.91 ± 1.25	8.22 ± 1.19	3.11 ± 0.22	3.69 ± 0.36	3.96 ± 0.50	0.59 ± 0.25	0.17 ± 0.16
T3.5[b]	1.27 ...	4.30 ...	7.51 ...	8.02 ...	8.28 ...	3.16 ...	3.67 ...	3.89 ...	0.48 ...	0.13 ...
T4[b]	1.19 ...	4.44 ...	7.70 ...	8.13 ...	8.35 ...	3.21 ...	3.65 ...	3.83 ...	0.38 ...	0.08 ...
T4.5	1.11 ± 1.24	4.59 ± 0.85	7.90 ± 1.02	8.25 ± 0.93	8.41 ± 1.11	3.27 ± 0.11	3.63 ± 0.26	3.76 ± 0.81	0.27 ± 0.20	0.04 ± 0.51
T5	1.04 ± 0.83	4.74 ± 0.62	8.11 ± 0.57	8.36 ± 0.60	8.47 ± 0.79	3.32 ± 0.21	3.61 ± 0.10	3.70 ± 0.40	0.16 ± 0.19	−0.01 ± 0.27
T5.5	0.96 ± 1.45	...	...	...	...	3.38 ± 0.04	3.59 ± 0.16	3.63 ± 0.73	...	...
T6	0.87 ± 1.79	...	...	...	...	3.43 ± 0.26	3.57 ± 0.36	3.56 ± 0.83	...	...
T6.5[b]	0.79 ...	...	...	...	...	...	3.55 ± 0.20	3.50 ± 0.50	...	...
T7	0.71 ± 0.77	...	...	...	...	...	3.53[c] ...	3.43[c] ...	...	...
T7.5[b]	0.62 ...	...	...	...	...	...	3.51 ...	3.37 ...	...	...

Notes: Colors of different spectral types are calculated with our fitting equation (Eq. (9)). Standard errors are used; [a] for these colors, the spectral type-color relationships can be double valued. One can relay or indications from the other colors (*i-J, i-H* or *i-z*) to identify the correct value to use; [b] there is only one object available for colors of these subtypes without errors, we prefer to use 0.5 as their errors; [c] no object with this type has data of these colors.

Table 6. Proper motions constraints of SDSS L dwarfs that were also found in UKIDSS DR4.

SDSS Name	Proper motion[a] ($''$yr^{-1})	Proper motion Angle[a]	Proper motion[b] ($''$yr^{-1})	Proper motion Angle[e]	Proper motion[c] ($''$ yr^{-1})	Proper motion Angle[e]	Proper motion[d] ($''$yr^{-1})	Proper motion Angle[e]
SDSS J004759.59+135332.0	...[h]	...	0.13 ± 0.02	208 ± 10	0.13 ± 0.03	234 ± 14	0.47 ± 0.27	300 ± 36
SDSS J015141.04−005156.5	0.044 ± 0.012	274.8 ± 14.2	0.07 ± 0.06	285 ± 57	0.04 ± 0.03	257 ± 72	0.07 ± 0.15	150 ...
SDSS J022927.95−005328.5	0.068 ± 0.012	104.8 ± 25.1	0.02 ± 0.03	57 ...	0.04 ± 0.04	136 ...	0.10 ± 0.09	143 ± 63
SDSS J073241.77+264558.9	0.002 ...	30.3 ...	0.04 ± 0.02	359 ± 32	0.02 ± 0.03	230 ...	0.12 ± 0.06	206 ± 30
SDSS J074436.02+251330.5	0.033 ...	262.6 ...	0.04 ± 0.03	296 ± 50	0.06 ± 0.06	296 ...	0.05 ± 0.28	322 ...
SDSS J075754.16+221604.9	0.016 ...	74.6 ...	0.02 ± 0.04	63 ...	0.05 ± 0.04	116 ± 59	0.11 ± 0.07	124 ± 38
SDSS J081303.96+243355.9	0.066 ...	251.3 ...	0.06 ± 0.03	254 ± 30	0.08 ± 0.03	228 ± 25	0.09 ± 0.06	216 ± 42
SDSS J081409.45+260250.4	0.057 ...	278.5 ...	0.06 ± 0.03	304 ± 35	0.03 ± 0.03	217 ± 59	0.08 ± 0.05	170 ± 36
SDSS J083613.45+022106.2	0.096 ± 0.003	285.0 ± 1.6	0.07 ± 0.02	311 ± 17	0.11 ± 0.03	291 ± 14	0.36 ± 0.16	263 ± 26
SDSS J092745.81+010640.4	0.100 ± 0.001	274.1 ± 2.0	0.12 ± 0.02	272 ± 9	0.10 ± 0.03	302 ± 19	...[g]	37 ± 58
SDSS J094624.37+344639.8	0.083 ...	293.8 ...	0.09 ± 0.03	304 ± 22	0.07 ± 0.04	298 ± 33	0.05 ± 0.07	295 ...
SDSS J095941.47+114146.0	0.148 ...	254.1 ...	0.15 ± 0.03	259 ± 12	0.14 ± 0.04	257 ± 18	0.11 ± 0.10	252 ± 67
SDSS J121238.73+000721.6	0.037 ...	278.5 ...	0.03 ± 0.02	342 ± 38	0.04 ± 0.05	282 ...	0.13 ± 0.27[f]	20 ...
SDSS J133131.70+122531.4	0.182 ± 0.006	193.7 ± 1.4	0.16 ± 0.03	188 ± 11	0.12 ± 0.02	207 ± 8	0.12 ± 0.03	243 ± 14
SDSS J134531.43+001551.2	0.047 ± 0.006	95.2 ± 1.9	0.05 ± 0.02	77 ± 22	0.04 ± 0.05	124 ...	0.25 ± 0.27[f]	34 ...
SDSS J150153.00−013507.1	0.236 ± 0.002	255.3 ± 0.7	0.26 ± 0.03	264 ± 6	0.24 ± 0.02	258 ± 5	0.21 ± 0.07	241 ± 19
SDSS J154236.26−004545.9	0.531 ± 0.001	258.5 ± 0.1	0.52 ± 0.02	259 ± 2	0.60 ± 0.05	252 ± 5	...[g]	40 ± 25
SDSS J154432.77+265551.2	0.141 ...	311.9 ...	0.16 ± 0.04	310 ± 15	0.15 ± 0.03	304 ± 11	0.18 ± 0.05	295 ± 16
SDSS J154740.16+053208.3	0.047 ± 0.006	293.1 ± 3.9	0.06 ± 0.05	327 ± 46	0.06 ± 0.05	243 ± 54	0.16 ± 0.11	209 ± 43
SDSS J161711.68+322249.5	0.099 ...	213.0 ...	0.04 ± 0.04	61 ...	0.02 ± 0.04	107 ...	0.02 ± 0.06	173 ...
SDSS J232715.71+151730.4	0.160 ± 0.001	202.4 ± 0.7	0.20 ± 0.02	216 ± 5	0.18 ± 0.02	211 ± 5	0.10 ± 0.04	210 ± 28
SDSS J234040.33−003337.2	0.028 ± 0.003	258.8 ± 6.4	0.05 ± 0.04	49 ± 57	0.01 ± 0.04	199 ...	0.05 ± 0.08	214 ...
SDSS J234513.85+002441.6	0.092 ± 0.001	200.1 ± 4.2	0.29 ± 0.03	189 ± 7	0.05 ± 0.05	221 ...	1.04 ± 0.26	4 ± 14

[a] SDSS-UKIDSS relative proper motions – found by specifically measuring the relative movement of the ultracool dwarfs with respect to nearby reference objects in the SDSS and UKIDSS images; [b] SDSS-UKIDSS data-base proper motions – found by dividing the difference between the SDSS and UKIDSS coordinates (from the respective databases) by the observational epoch difference. Standard errors are calculated using the major axes of the position error ellipses from SDSS and UKIDSS; [c] 2MASS-UKIDSS database proper motions – as for *b* except using 2MASS and UKIDSS; [d] 2MASS-SDSS database proper motions – as for *b* except using 2MASS and SDSS. We do not present the proper motions calculated with a baseline 10 months; [e] error ellipses of 2MASS and SDSS overlap for some objects for which position angle errors are not meaningful; [f] objects with a 2MASS-SDSS baseline <1 year; [g] we do not present their proper motions for they have a short 2MASS-SDSS baseline (<2 months); [h] We do not measure its proper motion for it is very faint in SDSS *z*-band image.

Table 7. SDSS and 2MASS photometry of 129 ultra-cool dwarf candidates.

SDSS Name	SDSS r	SDSS i	SDSS z	2MASS J	2MASS H	2MASS K	Proper motion ($''$ yr^{-1})	Proper motion Angle	Sp. Type by Colors
SDSS J073813.07+155304.7	23.76 ± 0.42	21.26 ± 0.08	19.25 ± 0.06	16.89 ± 0.20	16.07 ± 0.21	15.37 ± 0.17	0.04 ± 0.04	184 ...	L1
SDSS J074151.17+275837.6	23.60 ± 0.56	21.51 ± 0.15	19.39 ± 0.07	17.31 ± 0.18	16.67 ± 0.21	15.95 ± 0.23	0.05 ± 0.08	315 ...	L0
SDSS J074838.61+174332.9	23.89 ± 0.46	21.35 ± 0.07	19.06 ± 0.05	16.27 ± 0.11	15.18 ± 0.09	14.42 ± 0.09	0.07 ± 0.02	264 ± 14	L7
SDSS J075635.25+363033.6	22.26 ± 0.20	19.85 ± 0.06	17.07 ± 0.01	15.24 ± 0.04	14.61 ± 0.05	14.09 ± 0.05	0.11 ± 0.11	149 ...	L2.5
SDSS J075752.70+091410.0	22.86 ± 0.27	20.62 ± 0.05	18.57 ± 0.03	15.86 ± 0.08	14.83 ± 0.07	14.09 ± 0.06	0.14 ± 0.02	249 ± 8	L4
SDSS J075923.05+462007.4	24.18 ± 0.66	21.44 ± 0.12	19.30 ± 0.06	17.00 ± 0.16	16.09 ± 0.13	15.86 ± 0.23	0.23 ± 0.25	297 ...	L2
SDSS J080020.39+360627.1	23.61 ± 0.43	21.24 ± 0.08	19.23 ± 0.06	16.64 ± 0.13	15.93 ± 0.16	15.62 ± 0.19	0.37 ± 0.25	141 ± 42	L2.5
SDSS J080138.61+372205.8	23.00 ± 0.23	20.59 ± 0.08	18.21 ± 0.02	16.83 ± 0.22	15.84 ± 0.22	15.45 ± 0.19	0.22 ± 0.13	254 ± 35	...
SDSS J080252.73+051058.3	23.59 ± 0.64	20.72 ± 0.09	18.67 ± 0.06	16.16 ± 0.11	15.30 ± 0.09	14.91 ± 0.14	0.06 ± 0.04	270 ± 44	L2
SDSS J081215.88+504758.3	23.15 ± 0.32	20.71 ± 0.05	18.69 ± 0.04	16.37 ± 0.13	15.70 ± 0.18	15.28 ± 0.17	0.24 ± 0.05	232 ± 12	L0.5
SDSS J081409.11+281909.6	24.25 ± 0.74	21.69 ± 0.18	19.58 ± 0.10	17.45 ± 0.23	16.47 ± 0.21	15.79 ± 0.18	0.17 ± 0.07	246 ± 23	L0.5
SDSS J081825.78+374103.1	23.32 ± 0.27	21.70 ± 0.10	19.43 ± 0.06	16.94 ± 0.20	16.01 ± 0.19	15.44 ± 0.18	0.19 ± 0.10	65 ± 32	L3.5
SDSS J081843.64+175645.7	23.14 ± 0.34	21.61 ± 0.15	19.44 ± 0.09	17.01 ± 0.19	16.02 ± 0.19	15.45 ± 0.17	0.07 ± 0.05	349 ± 47	L2.5
SDSS J081905.47+493118.5	23.75 ± 0.54	21.23 ± 0.09	19.19 ± 0.06	17.09 ± 0.23	16.51 ± 0.31	15.56 ± 0.21	...	...	L0
SDSS J081951.43+543155.1	23.71 ± 0.50	21.02 ± 0.08	18.97 ± 0.06	16.97 ± 0.19	15.91 ± 0.14	15.45 ± 0.20	0.13 ± 0.06	179 ± 30	L1
SDSS J082059.29+280648.0	23.22 ± 0.36	21.22 ± 0.09	19.12 ± 0.06	16.92 ± 0.21	15.89 ± 0.19	15.40 ± 0.16	0.08 ± 0.10	240 ...	L1
SDSS J082213.75+510120.2	23.46 ± 0.43	20.85 ± 0.07	18.81 ± 0.05	16.57 ± 0.12	15.66 ± 0.12	15.17 ± 0.12	...	...	L0.5
SDSS J083301.44+445107.6	23.45 ± 0.43	21.19 ± 0.08	19.12 ± 0.05	16.54 ± 0.14	15.96 ± 0.19	15.42 ± 0.20	0.56 ± 0.22	152 ± 23	L2
SDSS J084537.80+293137.2	23.74 ± 0.42	21.47 ± 0.11	19.42 ± 0.06	16.74 ± 0.12	15.97 ± 0.13	15.14 ± 0.12	0.07 ± 0.04	124 ± 33	L2.5
SDSS J084737.45+462443.8	23.16 ± 0.50	20.92 ± 0.09	18.87 ± 0.07	16.88 ± 0.17	16.03 ± 0.19	15.78 ± 0.23	0.02 ± 0.17	76 ...	...
SDSS J084750.21+510846.3	23.08 ± 0.44	20.83 ± 0.08	18.79 ± 0.04	16.66 ± 0.14	16.00 ± 0.15	15.24 ± 0.15	0.20 ± 0.20	312 ± 83	L0
SDSS J084838.93+484025.4	23.07 ± 0.27	21.04 ± 0.07	19.03 ± 0.05	16.59 ± 0.13	15.77 ± 0.13	15.29 ± 0.15	0.55 ± 0.10	106 ± 11	L2
SDSS J085048.96+173210.9	23.33 ± 0.30	20.89 ± 0.06	18.88 ± 0.05	16.57 ± 0.12	15.93 ± 0.15	15.23 ± 0.11	0.15 ± 0.03	354 ± 12	L0.5
SDSS J085117.58+583226.6	24.25 ± 0.76	21.59 ± 0.13	19.53 ± 0.09	17.07 ± 0.19	16.45 ± 0.23	15.84 ± 0.23	0.03 ± 0.07	257 ...	L1.5
SDSS J085119.69+104348.0	24.36 ± 0.65	21.79 ± 0.11	19.58 ± 0.05	16.79 ± 0.15	15.78 ± 0.15	15.09 ± 0.12	0.23 ± 0.03	309 ± 7	L5
SDSS J085711.43+415928.6	23.72 ± 0.53	21.46 ± 0.11	19.39 ± 0.07	17.37 ± 0.24	16.18 ± 0.20	15.73 ± 0.22	0.26 ± 0.10	129 ± 21	L2
SDSS J090308.17+165935.5	24.87 ± 0.59	21.61 ± 0.10	19.38 ± 0.07	16.49 ± 0.11	15.78 ± 0.16	15.49 ± 0.19	0.11 ± 0.04	129 ± 20	L6
SDSS J090435.90+322918.7	23.71 ± 0.52	21.05 ± 0.07	19.02 ± 0.05	16.97 ± 0.17	16.22 ± 0.20	15.45 ± 0.20	0.38 ± 0.06	294 ± 10	...
SDSS J090546.54+562311.9	23.01 ± 0.36	20.28 ± 0.05	18.24 ± 0.03	15.40 ± 0.05	14.28 ± 0.04	13.73 ± 0.04	...	...	L4
SDSS J091428.64+230541.2	24.66 ± 0.72	21.26 ± 0.08	19.14 ± 0.05	16.62 ± 0.10	15.53 ± 0.08	14.90 ± 0.08	0.05 ± 0.02	311 ± 22	L3
SDSS J091811.89+390216.7	23.77 ± 0.62	22.07 ± 0.21	19.65 ± 0.10	17.02 ± 0.21	16.15 ± 0.21	15.57 ± 0.22	0.07 ± 0.10	234 ...	L5.5
SDSS J091816.02+481300.4	23.02 ± 0.23	20.75 ± 0.05	18.74 ± 0.05	16.43 ± 0.12	15.52 ± 0.12	15.30 ± 0.14	0.14 ± 0.06	71 ± 27	L0.5
SDSS J092752.44+572932.5	23.90 ± 0.51	21.37 ± 0.09	19.36 ± 0.07	16.65 ± 0.15	15.46 ± 0.13	14.84 ± 0.11	...	...	L3.5
SDSS J092819.74+180510.8	23.64 ± 0.35	22.20 ± 0.15	19.98 ± 0.08	17.23 ± 0.21	16.65 ± 0.26	15.90 ± 0.21	0.25 ± 0.05	289 ± 11	L3.5
SDSS J093100.69+605539.6	23.64 ± 0.58	21.10 ± 0.10	19.00 ± 0.07	16.48 ± 0.11	15.69 ± 0.10	15.30 ± 0.13	0.44 ± 0.15	280 ± 20	L2.5
SDSS J093204.02+345937.0	25.18 ± 0.73	21.97 ± 0.22	19.92 ± 0.10	17.01 ± 0.18	16.22 ± 0.19	15.46 ± 0.21	0.23 ± 0.07	149 ± 16	L4.5
SDSS J093956.05+242658.7	24.85 ± 0.64	22.07 ± 0.23	19.69 ± 0.10	16.97 ± 0.22	15.93 ± 0.22	15.53 ± 0.21	0.36 ± 0.05	244 ± 8	L6.5
SDSS J094146.38+215843.5	25.07 ± 0.58	21.78 ± 0.11	19.67 ± 0.09	16.94 ± 0.18	15.92 ± 0.18	15.55 ± 0.17	0.09 ± 0.04	244 ± 26	L4
SDSS J094427.33+641037.3	22.96 ± 0.33	20.95 ± 0.08	18.93 ± 0.06	16.67 ± 0.16	15.88 ± 0.17	15.46 ± 0.18	0.09 ± 0.06	296 ± 38	L0
SDSS J094429.58+465254.7	22.84 ± 0.32	21.26 ± 0.11	19.16 ± 0.06	17.26 ± 0.21	16.58 ± 0.23	16.09 ± 0.25	0.06 ± 0.16	322 ...	...
SDSS J095154.19+282040.8	23.10 ± 0.30	21.22 ± 0.08	19.21 ± 0.06	16.56 ± 0.16	16.06 ± 0.15	15.52 ± 0.18	0.07 ± 0.05	298 ± 44	L2
SDSS J095932.74+452330.5	23.73 ± 0.51	21.04 ± 0.08	19.01 ± 0.05	15.88 ± 0.07	14.76 ± 0.07	13.67 ± 0.04	0.19 ± 0.05	221 ± 15	L7.5
SDSS J100132.26+492819.9	23.05 ± 0.25	20.74 ± 0.05	18.72 ± 0.04	16.68 ± 0.13	15.95 ± 0.14	15.56 ± 0.18	0.23 ± 0.09	276 ± 23	...
SDSS J100317.30+331922.0	24.32 ± 0.79	21.60 ± 0.15	19.23 ± 0.07	16.74 ± 0.14	15.73 ± 0.11	15.23 ± 0.14	0.05 ± 0.04	75 ± 56	L4
SDSS J100633.74+363919.5	23.89 ± 0.39	21.60 ± 0.08	19.49 ± 0.05	17.10 ± 0.22	15.98 ± 0.16	15.32 ± 0.19	0.12 ± 0.07	184 ± 32	L2.5
SDSS J101134.72+501400.7	23.79 ± 0.49	21.93 ± 0.15	19.90 ± 0.10	17.60 ± 0.29	16.28 ± 0.20	15.57 ± 0.17	0.70 ± 0.22	259 ± 18	L2
SDSS J101439.66+252511.3	24.45 ± 0.59	21.14 ± 0.07	19.10 ± 0.05	17.24 ± 0.23	16.19 ± 0.21	15.83 ± 0.24	0.09 ± 0.05	215 ± 35	L0
SDSS J101951.13+044944.1	24.10 ± 0.57	21.80 ± 0.15	19.48 ± 0.07	16.85 ± 0.18	16.18 ± 0.20	15.54 ± 0.23	0.57 ± 0.31	240 ± 33	L4
SDSS J102517.57+285113.6	23.64 ± 0.54	20.95 ± 0.07	18.92 ± 0.05	16.54 ± 0.10	15.83 ± 0.12	15.31 ± 0.12	0.11 ± 0.03	288 ± 16	L1.5
SDSS J102546.97+151126.3	24.29 ± 0.70	21.52 ± 0.15	19.47 ± 0.07	16.99 ± 0.15	16.06 ± 0.17	15.42 ± 0.15	0.17 ± 0.04	276 ± 13	L2
SDSS J102935.23+062029.6	24.51 ± 0.55	22.47 ± 0.19	19.37 ± 0.05	16.87 ± 0.22	16.09 ± 0.21	15.02 ± 0.16	0.15 ± 0.14	212 ± 75	L8
SDSS J102939.69+571544.3	24.35 ± 0.52	21.62 ± 0.10	19.17 ± 0.06	16.70 ± 0.13	15.46 ± 0.11	14.99 ± 0.09	0.82 ± 0.07	95 ± 5	L4.5
SDSS J103908.17+244044.1	23.58 ± 0.34	21.73 ± 0.11	19.41 ± 0.06	16.76 ± 0.14	15.72 ± 0.13	15.04 ± 0.11	0.22 ± 0.03	236 ± 7	L5
SDSS J104808.29+544715.1	23.50 ± 0.40	21.86 ± 0.14	19.46 ± 0.07	16.73 ± 0.19	15.86 ± 0.20	15.43 ± 0.19	0.38 ± 0.11	295 ± 17	L6.5
SDSS J104814.75+135833.3	23.78 ± 0.44	21.94 ± 0.15	19.43 ± 0.07	16.90 ± 0.13	16.01 ± 0.14	15.34 ± 0.14	0.17 ± 0.04	197 ± 14	L5.5
SDSS J105204.75+172241.2	23.14 ± 0.34	21.27 ± 0.10	19.21 ± 0.06	16.71 ± 0.11	16.04 ± 0.14	15.53 ± 0.16	0.31 ± 0.03	158 ± 6	L1.5
SDSS J105254.02+584951.2	23.96 ± 0.37	21.44 ± 0.08	19.26 ± 0.04	16.44 ± 0.12	15.44 ± 0.13	14.87 ± 0.10	0.09 ± 0.05	54 ± 37	L5
SDSS J110827.31+083801.8	23.74 ± 0.71	22.39 ± 0.34	19.26 ± 0.07	16.58 ± 0.16	15.50 ± 0.11	15.03 ± 0.16	0.34 ± 0.08	217 ± 14	L8.5

Table 7. continued.

SDSS Name	SDSS r	SDSS i	SDSS z	2MASS J	2MASS H	2MASS K	Proper motion ($''$ yr^{-1})	Proper motion Angle	Sp. Type by Colors
SDSS J111501.36+160701.5	22.94 ± 0.37	20.71 ± 0.07	18.59 ± 0.05	16.40 ± 0.12	15.22 ± 0.09	14.56 ± 0.11	0.34 ± 0.08	248 ± 14	L1
SDSS J111802.89+060703.6	24.09 ± 0.53	21.42 ± 0.10	19.35 ± 0.05	17.00 ± 0.18	16.27 ± 0.21	15.66 ± 0.26	0.28 ± 0.11	133 ± 23	L1.5
SDSS J111910.46+055248.4	23.39 ± 0.33	21.67 ± 0.11	19.60 ± 0.06	16.76 ± 0.16	15.48 ± 0.11	15.03 ± 0.15	0.07 ± 0.16	109 ...	L5
SDSS J112012.95+212520.4	23.50 ± 0.42	21.65 ± 0.11	19.53 ± 0.06	16.90 ± 0.17	15.79 ± 0.14	15.34 ± 0.14	0.13 ± 0.04	198 ± 16	L4
SDSS J112722.94−003714.4	23.53 ± 0.33	21.34 ± 0.08	19.24 ± 0.05	16.81 ± 0.18	16.12 ± 0.26	15.35 ± 0.20	...	...	L1.5
SDSS J113022.46+122751.6	23.49 ± 0.48	21.69 ± 0.13	19.64 ± 0.10	17.05 ± 0.18	16.47 ± 0.22	15.98 ± 0.24	0.16 ± 0.11	358 ± 41	L2
SDSS J113639.67+485240.3	23.54 ± 0.31	20.91 ± 0.05	18.86 ± 0.03	16.16 ± 0.10	15.27 ± 0.11	14.58 ± 0.08	0.20 ± 0.06	307 ± 17	L3.5
SDSS J114103.28+632805.9	23.57 ± 0.41	21.50 ± 0.12	19.46 ± 0.07	16.72 ± 0.13	15.94 ± 0.13	15.62 ± 0.23	0.45 ± 0.18	308 ± 23	L3
SDSS J114302.72+190541.9	24.77 ± 0.62	22.76 ± 0.26	19.77 ± 0.08	16.77 ± 0.18	15.80 ± 0.15	15.01 ± 0.14	0.26 ± 0.03	172 ± 8	L9
SDSS J114807.23+390106.9	24.12 ± 0.66	21.23 ± 0.08	19.19 ± 0.05	16.92 ± 0.18	15.96 ± 0.17	15.52 ± 0.17	0.20 ± 0.06	323 ± 18	L1.5
SDSS J115017.36+512502.4	24.28 ± 0.60	22.02 ± 0.18	19.98 ± 0.11	16.87 ± 0.20	16.03 ± 0.18	15.08 ± 0.12	0.15 ± 0.12	221 ± 51	L6
SDSS J115058.98+440917.2	24.06 ± 0.58	21.38 ± 0.09	19.37 ± 0.06	17.05 ± 0.19	16.15 ± 0.23	15.49 ± 0.15	0.14 ± 0.06	272 ± 26	L1
SDSS J115722.81+264119.6	23.71 ± 0.47	21.06 ± 0.07	18.89 ± 0.04	16.71 ± 0.12	15.91 ± 0.15	15.02 ± 0.11	0.06 ± 0.03	263 ± 25	L1
SDSS J115820.75+043501.7	22.00 ± 0.20	20.36 ± 0.07	17.95 ± 0.04	15.61 ± 0.06	14.68 ± 0.06	14.44 ± 0.06	0.86 ± 0.86	316 ...	L3
SDSS J120136.14+135005.9	22.76 ± 0.17	20.66 ± 0.05	18.63 ± 0.04	16.88 ± 0.13	16.14 ± 0.17	15.74 ± 0.16	0.03 ± 0.04	94 ...	...
SDSS J120337.00+445333.4	23.85 ± 0.45	21.74 ± 0.12	19.52 ± 0.06	17.43 ± 0.25	16.55 ± 0.25	15.56 ± 0.18	0.24 ± 0.08	281 ± 20	L0.5
SDSS J121846.56+410016.0	24.87 ± 0.71	21.74 ± 0.13	19.61 ± 0.07	16.74 ± 0.16	15.58 ± 0.13	15.13 ± 0.15	0.05 ± 0.05	118 ...	L5.5
SDSS J122218.47+364348.4	22.61 ± 0.17	20.21 ± 0.03	18.15 ± 0.03	15.97 ± 0.08	15.27 ± 0.10	14.85 ± 0.09	0.27 ± 0.04	92 ± 9	L0
SDSS J122449.44+502154.1	23.98 ± 0.45	21.62 ± 0.10	19.14 ± 0.06	16.53 ± 0.13	15.66 ± 0.11	14.86 ± 0.10	0.48 ± 0.05	204 ± 6	L6
SDSS J123256.67+484417.0	22.21 ± 0.18	20.54 ± 0.06	18.54 ± 0.03	16.47 ± 0.18	15.59 ± 0.14	15.32 ± 0.20	0.44 ± 0.11	254 ± 15	L0
SDSS J124151.85+561541.6	23.44 ± 0.42	20.86 ± 0.07	18.81 ± 0.04	16.42 ± 0.11	15.61 ± 0.12	14.95 ± 0.11	0.04 ± 0.04	314 ± 77	L2
SDSS J124609.07+294200.1	24.07 ± 0.48	21.30 ± 0.08	19.26 ± 0.05	16.97 ± 0.19	16.12 ± 0.21	15.65 ± 0.24	0.02 ± 0.06	331 ...	L1
SDSS J124655.54+535342.8	23.89 ± 0.47	21.31 ± 0.08	19.24 ± 0.05	16.37 ± 0.11	15.57 ± 0.12	14.98 ± 0.12	0.17 ± 0.09	160 ± 33	L4
SDSS J125002.99+484834.3	23.99 ± 0.47	21.93 ± 0.16	19.88 ± 0.09	17.30 ± 0.26	15.82 ± 0.14	15.25 ± 0.14	0.37 ± 0.15	263 ± 24	L4
SDSS J125137.76+462026.0	22.94 ± 0.21	20.59 ± 0.05	18.50 ± 0.03	15.83 ± 0.08	14.75 ± 0.07	14.48 ± 0.10	0.31 ± 0.02	172 ± 4	L4
SDSS J125410.69+382546.0	23.80 ± 0.46	21.48 ± 0.11	19.42 ± 0.06	16.88 ± 0.15	16.11 ± 0.18	15.65 ± 0.16	0.06 ± 0.04	239 ± 47	L2.5
SDSS J125438.50+434657.2	23.70 ± 0.48	22.22 ± 0.22	19.47 ± 0.07	16.81 ± 0.15	15.35 ± 0.10	14.81 ± 0.09	0.20 ± 0.04	257 ± 11	L8.5
SDSS J130449.88+010627.0	23.10 ± 0.31	21.37 ± 0.10	19.30 ± 0.06	16.69 ± 0.17	15.80 ± 0.17	15.12 ± 0.17	0.83 ± 0.24	125 ± 17	L3
SDSS J131142.11+362923.9	23.08 ± 0.23	20.49 ± 0.04	18.31 ± 0.03	15.55 ± 0.05	14.75 ± 0.06	14.14 ± 0.05	0.40 ± 0.02	279 ± 3	L4
SDSS J131218.20+284643.0	24.13 ± 0.57	21.36 ± 0.09	19.31 ± 0.06	17.27 ± 0.26	16.33 ± 0.32	15.72 ± 0.21	0.10 ± 0.09	219 ± 58	L0
SDSS J132535.68+504007.0	24.45 ± 0.54	21.56 ± 0.08	19.38 ± 0.05	16.93 ± 0.23	15.86 ± 0.23	15.46 ± 0.23	0.32 ± 0.15	288 ± 27	L3
SDSS J133316.06+374421.7	23.31 ± 0.29	21.01 ± 0.06	18.65 ± 0.03	15.89 ± 0.06	14.90 ± 0.05	14.30 ± 0.05	0.12 ± 0.04	76 ± 18	L6.5
SDSS J134210.11+414023.8	23.65 ± 0.35	21.63 ± 0.11	19.56 ± 0.07	16.86 ± 0.13	15.87 ± 0.12	15.47 ± 0.14	0.20 ± 0.04	229 ± 12	L4
SDSS J135640.46+140205.3	23.83 ± 0.35	20.96 ± 0.08	18.36 ± 0.03	16.62 ± 0.15	16.10 ± 0.22	15.28 ± 0.15	0.03 ± 0.06	317 ...	L1
SDSS J140058.03+234923.9	23.67 ± 0.39	21.51 ± 0.09	19.48 ± 0.06	16.73 ± 0.17	16.12 ± 0.23	15.38 ± 0.22	0.06 ± 0.06	261 ...	L3
SDSS J140318.98+243718.0	23.56 ± 0.33	21.55 ± 0.09	19.52 ± 0.07	17.18 ± 0.23	16.06 ± 0.22	15.50 ± 0.22	0.03 ± 0.06	194 ...	L1.5
SDSS J141118.49+294850.4	23.52 ± 0.37	21.07 ± 0.07	18.76 ± 0.04	16.20 ± 0.09	15.43 ± 0.11	15.09 ± 0.11	0.28 ± 0.05	164 ± 10	L3.5
SDSS J141405.84+010710.4	23.40 ± 0.38	21.77 ± 0.15	19.63 ± 0.09	16.74 ± 0.20	15.74 ± 0.19	15.25 ± 0.20	...	...	L5.5
SDSS J142110.77+472834.3	23.92 ± 0.39	20.40 ± 0.03	18.33 ± 0.02	16.16 ± 0.09	15.33 ± 0.10	14.98 ± 0.13	0.07 ± 0.03	240 ± 22	L0
SDSS J142404.53+184641.4	24.16 ± 0.50	21.41 ± 0.09	19.34 ± 0.06	17.08 ± 0.19	16.44 ± 0.26	15.50 ± 0.16	0.01 ± 0.07	175 ...	L0.5
SDSS J142527.14+300400.4	23.11 ± 0.25	20.78 ± 0.05	18.72 ± 0.03	16.39 ± 0.12	15.54 ± 0.13	15.03 ± 0.12	0.02 ± 0.04	292 ...	L1.5
SDSS J142612.86+313039.4	23.70 ± 0.42	21.39 ± 0.09	19.29 ± 0.05	16.62 ± 0.16	15.59 ± 0.13	14.72 ± 0.09	0.19 ± 0.04	224 ± 11	L4
SDSS J143412.02+271729.9	23.98 ± 0.62	21.41 ± 0.11	19.29 ± 0.07	17.38 ± 0.24	16.33 ± 0.21	15.70 ± 0.21	0.08 ± 0.07	96 ± 68	L0
SDSS J143636.98+465302.7	23.75 ± 0.38	21.92 ± 0.11	19.92 ± 0.08	16.99 ± 0.16	16.13 ± 0.15	15.81 ± 0.20	0.28 ± 0.07	268 ± 15	L4
SDSS J145052.71+462024.8	23.87 ± 0.45	21.68 ± 0.10	19.67 ± 0.09	16.77 ± 0.15	15.93 ± 0.17	15.26 ± 0.14	0.14 ± 0.07	305 ± 32	L4
SDSS J150651.27+553350.7	22.93 ± 0.32	21.10 ± 0.10	19.10 ± 0.08	16.69 ± 0.12	15.80 ± 0.13	15.30 ± 0.15	0.08 ± 0.11	206 ...	L2
SDSS J151110.91+434036.3	23.48 ± 0.33	21.59 ± 0.09	19.29 ± 0.05	16.60 ± 0.15	15.47 ± 0.13	14.70 ± 0.13	0.24 ± 0.04	152 ± 9	L5
SDSS J152427.98+024210.1	22.76 ± 0.29	21.21 ± 0.12	19.16 ± 0.06	16.98 ± 0.20	16.39 ± 0.24	15.35 ± 0.17	...	...	L0
SDSS J152802.91+013949.6	23.06 ± 0.33	21.38 ± 0.11	19.27 ± 0.12	16.65 ± 0.14	15.75 ± 0.15	15.26 ± 0.17	...	...	L3
SDSS J153607.12+203032.6	24.01 ± 0.53	21.81 ± 0.14	19.73 ± 0.10	17.26 ± 0.21	16.17 ± 0.20	15.77 ± 0.24	0.03 ± 0.07	243 ...	L2.5
SDSS J153848.19+360337.5	24.05 ± 0.44	21.68 ± 0.11	19.56 ± 0.05	16.64 ± 0.15	15.76 ± 0.13	15.29 ± 0.14	0.06 ± 0.07	286 ...	L5.5
SDSS J153941.94+531131.0	23.53 ± 0.44	21.44 ± 0.12	19.40 ± 0.07	16.86 ± 0.16	15.95 ± 0.17	15.19 ± 0.18	0.17 ± 0.09	204 ± 34	L2
SDSS J154038.76−001257.1	23.11 ± 0.28	21.60 ± 0.10	19.35 ± 0.06	16.80 ± 0.15	15.67 ± 0.12	15.05 ± 0.14	...	...	L4
SDSS J154455.20+330145.1	22.96 ± 0.23	20.54 ± 0.05	18.33 ± 0.02	15.55 ± 0.06	14.52 ± 0.06	13.94 ± 0.05	0.11 ± 0.03	25 ± 15	L5
SDSS J154623.27+333803.2	24.03 ± 0.50	21.13 ± 0.08	19.05 ± 0.05	16.49 ± 0.11	15.77 ± 0.13	15.33 ± 0.14	0.08 ± 0.07	228 ± 54	L2.5
SDSS J155151.04+174216.7	23.34 ± 0.24	21.10 ± 0.06	19.08 ± 0.06	16.70 ± 0.14	15.83 ± 0.15	15.13 ± 0.12	0.12 ± 0.05	320 ± 24	L1.5
SDSS J155702.82+121258.1	23.84 ± 0.55	21.25 ± 0.10	19.19 ± 0.08	17.12 ± 0.25	16.02 ± 0.19	15.51 ± 0.26	0.62 ± 0.05	243 ± 4	L0.5
SDSS J160022.86+484132.8	23.53 ± 0.44	21.20 ± 0.10	19.06 ± 0.05	16.27 ± 0.09	15.43 ± 0.12	15.01 ± 0.14	0.46 ± 0.09	102 ± 11	L4.5
SDSS J160835.64+120226.8	23.22 ± 0.26	20.56 ± 0.04	18.56 ± 0.03	16.37 ± 0.12	15.35 ± 0.11	15.00 ± 0.14	0.07 ± 0.03	301 ± 28	L0.5
SDSS J160911.45+211658.7	24.02 ± 0.64	21.53 ± 0.14	19.50 ± 0.08	16.96 ± 0.21	15.97 ± 0.20	14.87 ± 0.11	0.09 ± 0.03	30 ± 22	L2

Table 7. continued.

SDSS Name	SDSS r	SDSS i	SDSS z	2MASS J	2MASS H	2MASS K	Proper motion ($''$ yr^{-1})	Proper motion Angle	Sp. Type by Colors
SDSS J161231.01+483357.5	24.34 ± 0.68	21.27 ± 0.08	19.17 ± 0.06	16.20 ± 0.10	15.62 ± 0.12	14.83 ± 0.12	0.11 ± 0.06	320 ± 38	L5.5
SDSS J161459.98+400435.1	22.60 ± 0.19	20.95 ± 0.08	18.93 ± 0.04	16.57 ± 0.12	15.84 ± 0.15	15.01 ± 0.12	0.30 ± 0.04	296 ± 8	L1
SDSS J161655.06+190842.8	23.57 ± 0.42	21.46 ± 0.09	19.45 ± 0.07	17.18 ± 0.19	16.37 ± 0.22	15.90 ± 0.24	0.06 ± 0.05	305 ± 59	L0
SDSS J163021.84−001801.6	24.80 ± 0.69	22.58 ± 0.24	19.42 ± 0.06	16.25 ± 0.12	15.55 ± 0.15	15.24 ± 0.19	...	...	L9.5
SDSS J164939.25+425043.7	24.06 ± 0.46	21.71 ± 0.11	19.48 ± 0.07	16.79 ± 0.14	15.46 ± 0.10	14.79 ± 0.12	0.18 ± 0.05	320 ± 15	L5
SDSS J165914.44+172642.3	24.22 ± 0.48	21.73 ± 0.10	19.69 ± 0.06	16.69 ± 0.16	15.54 ± 0.13	15.15 ± 0.14	0.11 ± 0.06	107 ± 32	L6
SDSS J170418.24+744315.0	23.26 ± 0.30	21.32 ± 0.07	19.07 ± 0.05	16.09 ± 0.09	15.14 ± 0.09	14.27 ± 0.09	0.13 ± 0.04	217 ± 18	L7.5
SDSS J171201.36+324456.6	23.99 ± 0.44	21.29 ± 0.08	19.25 ± 0.07	17.14 ± 0.17	16.26 ± 0.18	15.96 ± 0.24	0.52 ± 0.10	272 ± 11	L0
SDSS J172545.59+640501.2	23.90 ± 0.81	21.90 ± 0.23	19.46 ± 0.09	16.81 ± 0.17	15.89 ± 0.17	15.35 ± 0.20	0.61 ± 0.33	12 ± 33	L6.5
SDSS J172746.49+572247.6	22.53 ± 0.21	20.21 ± 0.04	18.21 ± 0.03	15.83 ± 0.08	14.96 ± 0.09	14.69 ± 0.11	0.14 ± 0.10	33 ± 51	L1.5
SDSS J210515.30−003701.5	24.48 ± 0.60	21.33 ± 0.08	19.10 ± 0.05	16.97 ± 0.17	15.90 ± 0.17	14.91 ± 0.13	0.07 ± 0.07	81 ± 64	L1.5

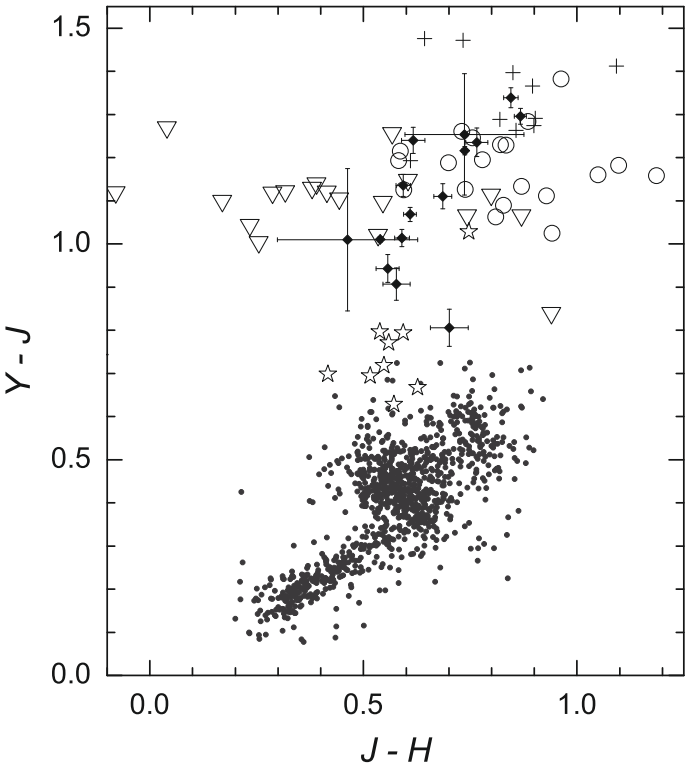

Fig. 7. $Y-J$ vs. $J-H$ diagram for known M, L and T dwarfs and 15 ultracool dwarf candidates (*diamonds*) which have Y band photometric data from UKIDSS, include 4 objects with SDSS spectra. M5.5-M8.5 (*open pentacles*), L0-L4.5 (*crosses*), L5-L9.5 (*open circles*), T0-T3.5 (*open triangles*) and 1024 sources from UKIDSS LAS in 1 deg^2 with $Y < 18.5$ (*gray points*). The J band photometric data of the two with the very large errors used here are transformed from 2MASS.

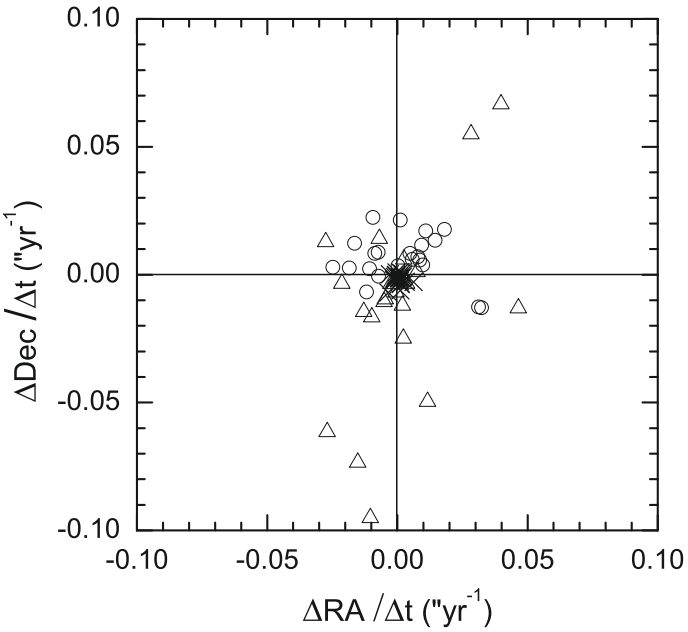

Fig. 8. Average proper motions of reference objects for ultracool dwarf candidates in Table 6. Different symbols indicated systematic coorections used for different survey combinations, 2MASS-SDSS (*open triangles*, 21 objects), SDSS-UKIDSS (*open circles*, 23 objects) and 2MASS-UKIDSS (*crosses*, 23 objects).

and are more likely to become i-band drop outs, precluding their selection in our sample. For our full sample, we reach fainter magnitudes and thus identify more later L dwarfs. The spectral type distribution of the candidates without spectra (i.e. based on the relationship between spectral type and colors) spans a range out to T3, with many candidates in the L0-L7 range.

Our spectral typing procedure makes use of numerous optical, near infrared and optical-infrared colors. Overall we find that the $i-z$, $i-J$, $i-H$ and $i-K$ colors are the most useful. For the objects in Table 1, the spectral types based on SDSS spectra and those based on colors generally agree with each other well. However, we caution against the use of $i-z$ for estimating spectral types earlier than L3, as Fig. 3 shows i-z does not correlate well in this range. In our analysis, if the i-J and i-H colors indicate a spectral type earlier than L3, then we do not include an estimated type based on the i-z color. The addition of UKIDSS photometry adds an additional means to constrain spectral type (e.g. using $Y-J$), particularly in and around the L-T transition (~L7-T3). With the increasing coverage of UKIDSS we can refine our selection techniques through additional color-spectral type relationships in the near future.

Of the 36 objects with SDSS spectra, 19 have 2σ detections of non-zero proper motions from SDSS-2MASS, 10 of which have proper motions above $0.2''$ yr^{-1} (see, Table 1). There are fewer 2σ proper motion detections for objects without spectra because they are, on average, further away. For SDSS-2MASS match, a matching radius of $6''$ might lead to the loss of a small number hight proper motion objects (e.g. proper motion larger than $1''$ yr^{-1} and baseline longer than 6 years). Some objects in Tables 1, 6 and 7 have larger proper motions (also with large errors) but usually have a shorter baseline (even less than a year) and these proper motions are not very reliable. The errors in our proper motion measurements are dominated by 2MASS

positional uncertainties (especially for objects with shorter baselines), however we have shown through a variety of comparisons that our 2MASS-SDSS database proper motions are of reasonable quality and can thus provide an additional tool to identify large samples of L dwarfs in the SDSS sky. In the future, a SDSS second epoch and surveys such as Pan-STARRS will offer an even more powerful means to efficiently select late M and L dwarfs through their proper motion.

It is clear that SDSS combined with 2MASS and now UKIDSS, offers a powerful means to select large populations of L dwarfs using spectroscopy, photometry and astrometry. As the sample of known L dwarfs grows we can expect to reveal a broader range of inherent properties (e.g. composition, mass, age, kinematics). Higher signal-to-noise and resolution spectroscopic observations could be used to study such interesting subpopulations e.g. by searching for the presence of lithium to directly assess age and mass (Pavlenko et al. 2007) and the use of higher resolution cross correlation techniques to measure radial velocities and space motions, yielding important kinematic information.

Acknowledgements. Funding for the SDSS and SDSS-II has been provided by the Alfred P. Sloan Foundation, the Participating Institutions, the National Science Foundation, the U.S. Department of Energy, the National Aeronautics and Space Administration, the Japanese Monbukagakusho, the Max Planck Society, and the Higher Education Funding Council for England. The SDSS Web Site is http://www.sdss.org/. The SDSS is managed by the Astrophysical Research Consortium for the Participating Institutions. The Participating Institutions are the American Museum of Natural History, Astrophysical Institute Potsdam, University of Basel, University of Cambridge, Case Western Reserve University, University of Chicago, Drexel University, Fermilab, the Institute for Advanced Study, the Japan Participation Group, Johns Hopkins University, the Joint Institute for Nuclear Astrophysics, the Kavli Institute for Particle Astrophysics and Cosmology, the Korean Scientist Group, the Chinese Academy of Sciences (LAMOST), Los Alamos National Laboratory, the Max-Planck-Institute for Astronomy (MPIA), the Max-Planck-Institute for Astrophysics (MPA), New Mexico State University, Ohio State University, University of Pittsburgh, University of Portsmouth, Princeton University, the United States Naval Observatory, and the University of Washington. This work is based in part on data obtained as part of the UKIRT Infrared Deep Sky Survey. This publication makes use of data products from the Two Micron All Sky Survey. This research has made use of the VizieR catalogue access tool, CDS, Strasbourg, France. Research has benefitted from the M, L, and T dwarf compendium housed at DwarfArchives.org and maintained by Chris Gelino, Davy Kirkpatrick, and Adam Burgasser. This work was part supported by the Natural Science Foundation of China under Grant Nos. 10521001, 10433030, 10503010 and the CAS Research Fellowship for International Young Researchers.

References

Adelman-McCarthy, J. K., Aguros, M. A., Allam, S. S., et al. 2007, ApJS, 172, 634
Adelman-McCarthy, J. K., Aguros, M. A., Allam, S. S., et al. 2008, ApJS, 175, 297
Baraffe, I., Chabrier, G., Baraman, T. S., et al. 2003, A&A, 402, 701
Becklin, E. E., & Zuckerman, B. 1988, Nature, 336, 656
Bessell, M. S. 1991, AJ, 101, 662
Bochanski, J. J., West, A. A., Hawley, S. L., & Covey, K. R. 2007, AJ, 133, 531
Burgasser, A. J., Kirkpatrick, J. D., Brown, M. E., et al. 1999, ApJ, 522, L65
Burgasser, A. J., Kirkpatrick, J. D., Brown, M. E., et al. 2002, ApJ, 564, 421
Burgasser, A. J., McElwain, M. W., Kirkpatrick, J. D., et al. 2004, AJ, 127, 2856
Burningham, B., Pinfield, D. J., Leggett, S. K., et al. 2008, MNRAS, accepted
Chiu, K., Fan, X., Leggett, S. K., et al. 2006, AJ, 131, 2722
Cruz, K. L., Reid, I. N., Liebert, J., Kirkpatrick, J. D., & Lowrance, P. J. 2003, AJ, 126, 2421
Cruz, K. L., Reid, I. N., Kirkpatrick, J. D., et al. 2007, AJ, 133, 439
Delfosse, X., Tinney, C. G., Forveille, T., et al. 1997, A&A, 327, L25
Epchtein, N., de Batz, B., Capoani, L., et al. 1997, The ESO Messeager, 87, 27
Fan, X., Knapp, G. R., Strauss, M. A., et al. 2000, AJ, 119, 928
Geballe, T. R., Knapp, G. R., Leggett, S. K., et al. 2002, ApJ, 564, 466
Gizis, J. E., Monet, D. G., Reid, I. N., et al. 2000, AJ, 120, 1085
Hawley, S. L., Covey, K. R., Knapp, G. R., et al. 2002, AJ, 123, 3409
Hewett, P. C., Warren, S. J., Leggett, S. K., & Hodgkin, S. T. 2006, MNRAS, 367, 454
Kendall, T. R., Mauron, N., Azzopardi, M., et al. 2003, A&A, 403, 929
Kendall, T. R., Jones, H. R. A., Pinfield, D. J., et al. 2007a, MNRAS, 374, 445
Kendall, T. R., Tamura, M., Tinney, C. G., et al. 2007b, A&A, 466, 1059
Kirkpatrick, J. D., Reid, I. N., Liebert, J., et al. 1999, ApJ, 519, 802
Kirkpatrick, J. D., Reid, I. N., Liebert, J., et al. 2000, AJ, 120, 447
Knapp, G. R., Leggett, S. K., Fan, X., et al. 2004, AJ, 127, 3553
Lawrence, A., Warren, S. J., Almaini, O., et al. 2007, MNRAS, 379, 1599
Lodieu, N., Pinfield, D. J., Leggett, S. K., et al. 2007, MNRAS, 379, 1423
Looper, D. L., Kirkpatrick, J. D., & Burgasser, A. J. 2007, AJ, 134, 1162
Nakajima, T., Oppenheimer, B. R., Kulkarni, S. R., et al. 1995, Nature, 378, 463
Pavlenko, Ya. V., Jones, H. R. A., Martín, E. L., et al. 2007, MNRAS, 380, 1285
Pinfield, D. J., Burningham, B., Tamura, M., et al. 2008, MNRAS, 390, 304
Reid, I. N., Cruz, K. L., Kirkpatrick, J. D., et al. 2008, AJ, 136, 1290
Schneider, D. P., Knapp, G. R., Hawley, S. L., et al. 2002, AJ, 123, 458
Schmidt, S. J., Cruz, K. L., Bongiorno, B. J., Liebert, J., & Reid, I. N. 2007, AJ, 133, 2258
Skrutskie, M. F., Cutri, R. M., Stiening, R., et al. 2006, AJ, 131, 1163
Stoughton, C., Lupton, R. H., Bernardi, M., et al. 2002, AJ, 123, 485
Warren, S. J., Mortlock, D. J., Leggett, S. K., et al. 2007, MNRAS, 381, 1400
York, D. G., Adelman, J., Anderson, J. E., Jr., et al. 2000, AJ, 120, 1579

Appendix II

"Discovery of the first wide L dwarf giant binary system and eight other ultracool dwarfs in wide binaries",
Zhang et al. 2010, MNRAS, 404, 1817-1834

Monthly Notices
of the
ROYAL ASTRONOMICAL SOCIETY

Mon. Not. R. Astron. Soc. **404,** 1817–1834 (2010) doi:10.1111/j.1365-2966.2010.16394.x

Discovery of the first wide L dwarf + giant binary system and eight other ultracool dwarfs in wide binaries

Z. H. Zhang,[1⋆] D. J. Pinfield,[1] A. C. Day-Jones,[1,2] B. Burningham,[1] H. R. A. Jones,[1] S. Yu,[3] J. S. Jenkins,[2] Z. Han,[4,5] M. C. Gálvez-Ortiz,[1] J. Gallardo,[2] A. E. García-Pérez,[1,6] D. Weights,[1] C. G. Tinney[7] and R. S. Pokorny[4,5]

[1]*Centre for Astrophysics Research, Science and Technology Research Institute, University of Hertfordshrie, Hatfield AL10 9AB*
[2]*Department of Astronomy, Universidad de Chile, Casilla Postal 36D, Santiago, Chile*
[3]*Armagh Observatory, College Hill, Armagh BT61 9DG*
[4]*National Astronomical Observatories/Yunnan Observatory, Chinese Academy of Sciences, Kunming 650011, China*
[5]*Key Laboratory for the Structure and Evolution of Celestial Objects, Chinese Academy of Sciences*
[6]*Department of Astronomy, University of Virginia, PO Box 400325, Charlottesville, VA 22904-4325, USA*
[7]*School of Physics, University of New South Wales, NSW 2050, Australia*

Accepted 2010 January 20. Received 2009 December 14; in original form 2009 October 4

ABSTRACT

We identify 806 ultracool dwarfs (of which 34 are newly discovered L dwarfs) from their Sloan Digital Sky Survey (SDSS) *riz* photometry and obtain proper motions through cross-matching with the United Kingdom Infrared Telescope Infrared Deep Sky Survey (UKIDSS) and Two-Micron All-Sky Survey (2MASS). Proper-motion and distance constraints show that nine of our ultracool dwarfs are members of widely separated binary systems: SDSS 0101 (K5V+M9.5V), SDSS 0207 (M1.5V+L3V), SDSS 0832 (K3III+L3.5V), SDSS 0858 (M4V+L0V), SDSS 0953 (M4V+M9.5V), SDSS 0956 (M2V+M9V), SDSS 1304 (M4.5V+L0V), SDSS 1631 (M5.5V+M8V) and SDSS 1638 (M4V+L0V). One of these (SDSS 0832) is shown to be a companion to the bright K3 giant η Cancri. Such primaries can provide age and metallicity constraints for any companion objects, yielding excellent benchmark objects. η Cancri AB is the first wide ultracool dwarf + giant binary system identified. We present new observations and analysis that constrain the metallicity of η Cancri A to be near-solar, and use recent evolutionary models to constrain the age of the giant to be 2.2–6.1 Gyr. If η Cancri B is a single object, we estimate its physical attributes to be mass = 63–82 $M_{\rm Jup}$, $T_{\rm eff} = 1800 \pm 150$ K, $\log g = 5.3$–5.5, [M/H] $= 0.0 \pm 0.1$. Its colours are non-typical when compared with other ultracool dwarfs, and we also assess the possibility that η Cancri B is itself an unresolved binary, showing that the combined light of an L4 + T4 system could provide a reasonable explanation for its colours.

Key words: binaries: general – brown dwarfs – stars: individual: η Cancri – stars: late-type – stars: low-mass.

1 INTRODUCTION

The number of discovered brown dwarfs is increasing rapidly (see e.g. http://dwarfarchives.org), benefitting from optical and near-infrared large-area surveys such as the Deep Near-Infrared Survey of the Southern Sky (DENIS: Epchtein et al. 1997), the Two-Micron All-Sky Survey (2MASS: Skrutskie et al. 2006), the Sloan Digital Sky Survey (SDSS: Abazajian et al. 2009) and the United Kingdom Infrared Telescope Infrared Deep Sky Survey (UKIDSS: Lawrence et al. 2007). Ultracool dwarfs have red optical–near-infrared colours due to their low effective temperature. Observable ultracool dwarfs are nearby because of their intrinsic faintness, and can therefore have relatively higher proper motion. It is very effective to select ultracool dwarfs by colour (Chiu et al. 2006; Cruz et al. 2007; Pinfield et al. 2008; Zhang et al. 2009b) or proper motion (Deacon et al. 2009; Sheppard & Cushing 2009). Proper motion is also a powerful tool for identifying ultracool dwarf companions to other stars, since such binary systems are common proper-motion pairs (Pinfield et al. 2006; Tokovinin et al. 2006; Luhman et al. 2007; Day-Jones et al. 2008; Burningham et al. 2009). We generically refer to such ultracool dwarfs as benchmark objects, for which

⋆E-mail: zenghuazhang@hotmail.com

optimal primaries include subgiant/giant stars and white dwarfs (Pinfield et al. 2006) along with the more common main-sequence primaries (Jenkins et al. 2009). Such systems are valuable, since ultracool dwarf properties may be constrained (at some level) by the primary star.

Current brown dwarf models have difficulty in reproducing observations accurately, and benchmark objects are thus needed to calibrate both atmospheric and evolutionary models. In order for a brown dwarf to be considered a benchmark it must have one or more properties (e.g. age, mass, distance, metallicity) that can be constrained relatively independently of ultracool dwarf models. The overall usefulness of an object as a benchmark is also dependent on the accuracy of the measured properties and the number of assumptions that have to be made if some degree of referencing to models is required.

The Galactic disc population provides a number of host environments that are useful for the discovery of such benchmarks. Many identified benchmarks are members of young clusters such as the Hyades, Pleiades and Praesepe (Rebolo, Zapatero Osorio & Martín 1995; Martín, Rebolo & Zapatero Osorio 1996; Cossburn et al. 1997; Magazzù et al. 1998; Martín et al. 1998; Zapatero Osorio et al. 1998; Chappelle et al. 2005; Bihain et al. 2006; Casewell et al. 2007; Bouvier et al. 2008; Hogan et al. 2008) and moving groups (e.g. LP 944−20: Tinney 1998; Ribas 2003; Clarke et al. 2009). These kinds of benchmarks provide accurate ages and metallicities that can be inferred from other cluster/group members. However, due to cluster evaporation (Bouvier et al. 2008) or disc-heating mechanisms (De Simone, Wu & Tremaine 2004), the spatial concentrations become dispersed and kinematic signatures diffused after ∼1 Gyr. Such benchmarks thus only populate the <1 Gyr age range, and are not fully applicable for studies of brown dwarf evolution across the full age extent of the Galactic disc. This is also the case for isolated field brown dwarfs that have lithium in their atmospheres, such as DENISp–J1228.2−1547 (Delfosse et al. 1997; Tinney, Delfosse & Forveille 1997), SDSS J0423−0414 (Burgasser, Kirkpatrick & Lowrance 2005), 2M0850 (Kirkpatrick et al. 1999) and Kelu1 (Ruiz, Leggett & Allard 1997), where the lithium test can be used to estimate age (Magazzù, Martín & Rebolo 1993).

More useful for this purpose are brown dwarfs as members of binaries, where the host star can provide age, distance and in some cases metallicity constraints. How useful these systems are is dependent on how well we understand the nature and physics of the primary stars. Main-sequence star ages can be largely uncertain due to the degeneracy of evolutionary models on the main sequence (Girardi et al. 2000; Yi et al. 2001). Tighter age constraints can be gained from more evolved stars, e.g. subgiants, giants and white dwarfs. Such primaries can constrain accurate ages, as well as metallicity in the case of subgiants and early-phase giant stars, via robust models. These types of binary systems can populate the full age range of the disc up to 10 Gyr (see Pinfield et al. 2006).

Benchmark brown dwarfs can also be in brown dwarf + brown dwarf binary pairs, where the dynamical mass of the components can be calculated. Liu, Dupuy & Ireland (2008a) suggest that these systems will yield good determinations of gravity and age. However they cannot, in general, provide accurate metallicity estimations, except for the rare examples that are found to be members of a cluster or components of a higher multiple system (where a higher mass component has known metallicity), as is the case for HD 10948BC (Dupuy, Liu & Ireland 2009).

In this paper we report the discovery of nine common-proper-motion binary systems with ultracool dwarf components. One is a benchmark L dwarf companion to the giant star η Cancri and the other eight are late M and early L dwarf companions to K–M dwarf stars. The photometric selection processes are presented in Section 2. The spectral types are presented in Section 3. Distances are presented in Section 4 and proper motions in Section 5. η Cancri AB is presented and discussed in Section 6, and Section 7 presents a summary.

2 PHOTOMETRIC SELECTION

2.1 SDSS identification

The SDSS uses a dedicated 2.5-m telescope equipped with a large-format mosaic CCD camera to image the sky in five optical bands (u, g, r, i, z), and two digital spectrographs to obtain the spectra of galaxies, quasars and late-type stars selected from the imaging data (York et al. 2000). The SDSS magnitude limits (95 per cent detection repeatability for point sources) for the u, g, r, i and z bands are 22.0, 22.2, 22.2, 21.3 and 20.5 respectively, where all magnitudes are in the SDSS AB system (Adelman-McCarthy et al. 2008).

The SDSS $i - z$ colour is particularly useful for L dwarf selection (Fan et al. 2000). We used $2 < i - z < 3.2$ in our previous ultracool proper-motion work (Zhang et al. 2009b) to select L dwarf candidates. In this work, we focus on a bluer sample to increase our sample size and increase the fraction of objects that have measured SDSS spectra. We used $1.5 < i - z < 2$ and $1.5 < r - i < 4.5$ for objects with SDSS spectra, leading to a total ultracool dwarf sample of 3154 objects. For objects without spectra we used a more constraining selection, requiring $1.7 < i - z < 2$, $2 < r - i < 3.3$, $r - i < 7(i - z) - 9.3$, $16 < z < 19.5$, and $17 < i < 21.2$. Fig. 1 shows the colour criteria for these selections.

We also made a deeper ultracool dwarf search towards the young open cluster Praesepe (M44: age = 0.79 Gyr, d = 181.5 pc; van Leeuwen 2009). The original motivation was to identify faint cluster members, however the most interesting discovery from this search

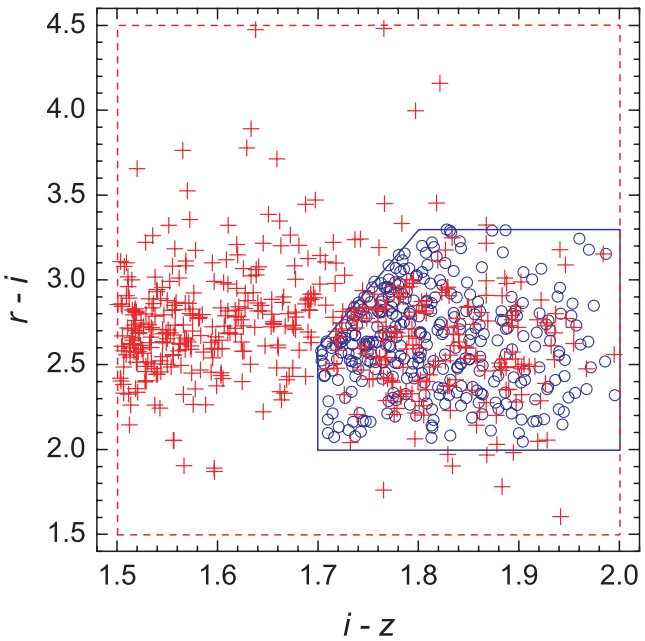

Figure 1. *riz* colour space for ultracool dwarfs with (crosses) and without (circles) SDSS spectra. The polygons show the $r - i$ and $i - z$ colour limits used to select ultracool dwarfs with (dashed lines) and without (solid lines) spectra.

was a foreground field object (see Section 5.2) so we have chosen to present the analysis of this deeper search here, along with that of our shallower search in the field. The Praesepe cluster has been surveyed by SDSS and UKIDSS (the Galactic Cluster Survey,within 3° of $08^h40^m06^s$, $+19^\circ41'06''$), and we used the same colour criteria as previously described for SDSS objects without spectra. However, the original aim to identify ultracool dwarfs at the distance of the cluster (van Leeuwen 2009; Taylor 2006) led us to limit this search to $19 < z < 20.5$ and $21 < i < 22.4$, corresponding to early L dwarfs ($i - z = 1.8$–2.1: Zhang et al. 2009b) at ∼100–200 pc (see the $M_i - (i - z)$ spectral type relationship: Hawley et al. 2002).

2.2 Near-infrared photometry

Near-infrared colours provide additional information useful for spectral-typing of ultracool dwarfs. SDSS-selected candidates were cross-matched with point sources in the 2MASS (Cutri et al. 2003) and UKIDSS (Lawrence et al. 2007) catalogues. We used a matching radius of 6 arcsec to ensure that ultracool dwarfs with high proper motion would generally be matched by this procedure, despite possible motion over a period of up to ∼8 yr (between SDSS–2MASS and SDSS–UKIDSS epochs). 563 objects with spectra were cross-matched in SDSS and 2MASS, of which 469 were also cross-matched in UKIDSS. 1761 objects without spectra were cross-matched in SDSS and 2MASS, of which 337 objects were cross-matched in UKIDSS. So 806 SDSS objects [see the online Table S1 (Supporting Information) for these ultracool dwarfs] were cross-matched in 2MASS and UKIDSS, of which 469 objects have SDSS spectra. For our ultracool dwarf sample towards Praesepe, we cross-matched candidates with the UKIDSS Galactic Cluster Survey (GCS), which covers 28 deg^2 of the cluster (radius ∼3°) in *ZYJHK*.

3 SPECTRAL TYPES

3.1 SDSS red optical spectroscopy

The SDSS imaging data are used to uniformly select different classes of objects, the spectra of which will be taken with the SDSS 2.5-m telescope (York et al. 2000). The target selection algorithms for spectroscopic follow-up are described by Stoughton et al. (2002). The wavelength coverage is from 3800–9200 Å with a resolving power $\lambda/(\Delta\lambda) = 1800$. The signal-to-noise ratio is better than 4 $pixel^{-1}$ at $g = 20.2$ (Adelman-McCarthy et al. 2008). SDSS spectra have been sky-subtracted and corrected for telluric absorption. The spectroscopic data are automatically reduced by the SDSS pipeline software. For 469 ultracool dwarf candidates with SDSS spectra, we assigned their spectral type with the HAMMER pipeline (Covey et al. 2007). The typical spectral-type error is ∼0.5–1.0 subtypes. A comparison between our analysis and the literature (Kirkpatrick et al. 2000; Hawley et al. 2002; Schneider et al. 2002; Cruz et al. 2003, 2007; Kendall et al. 2007; Reid et al. 2008; West, Hawley & Bochanski 2008) shows generally good agreement, with a small number of minor ambiguities. These are 79 L dwarfs with SDSS spectra in our sample: 11 objects are known L dwarfs (one of them is in a binary system), 42 objects are catalogued by West et al. (2008) as M9 or L0 dwarfs and 34 new L dwarfs are presented. Table 1 shows the SDSS, 2MASS and UKIDSS photometric data of the 34 new L dwarfs. Fig. 2 shows the SDSS spectra of 39 ultracool dwarfs. SDSS name and spectral types are labelled. The six ultracool dwarfs that we subsequently found to be wide binary companions (see Section 5.3) are labelled with both their original name and their new binary name.

Of these companion ultracool dwarfs, SDSS J020735.59+135556.2 (SDSS 0207) was characterized by Hawley et al. (2002) as an L3 dwarf using its SDSS spectrum, and SDSS J085836.97+271050.8 (SDSS 0858), SDSS J095613.13+014514.3 (SDSS 0956), SDSS 163817.31+321144.1 (SDSS 1638) and SDSS 163126.15+294836.9 (SDSS 1631) were catalogued by West et al. (2008) as L0, L0, M9 and M8 respectively. The spectra of these previously identified ultracool dwarfs are shown in blue. The spectra of SDSS 130433.16+090706.9 (SDSS 1304), a new L0 dwarf companion, and the other 33 new L dwarfs discovered in this work are shown in black.

3.2 Spectral types from colours

We used optical–near-infrared colour–spectral type relationships (Zhang et al. 2009a,b) to assign the spectral types of 337 objects without SDSS spectra. More specifically, we used three spectral type–colour ($i - J$, $i - H$, $i - K$) relationships, and took the average value of the three results. The typical error of the spectral type is about ±1.5 subtypes. Fig. 3 shows the spectral types of the ultracool dwarfs from both typing methods (as well as their distance estimates; see Section 4).

3.3 Near-infrared spectral type

Spectroscopy in the *J* band was obtained for ULAS 0832 using the Near InfraRed Imager and Spectrometer (NIRI: Hodapp et al. 2003) on the Gemini North Telescope on Mauna Kea (under programme GN-2009A-Q-16) on 2009 April 8 through thin cirrus cloud. All observations were made up of a set of sub-exposures in an ABBA jitter pattern to facilitate effective background subtraction, with a slit width of 1 arcsec. The length of the A–B jitter was 10 arcsec, and the integration consisted of 6 sub-exposures of 240 s.

The NIRI observations were reduced using standard IRAF Gemini packages. A comparison argon-arc frame was used to obtain a dispersion solution, which was applied to the pixel coordinates in the dispersion direction on the images. The resulting wavelength-calibrated subtracted AB pairs had a low level of residual sky emission removed by fitting and subtracting this emission with a set of polynomial functions fit to each pixel row perpendicular to the dispersion direction, and considering pixel data on either side of the target spectrum only. The spectra were then extracted using a linear aperture, and cosmic rays and bad pixels removed using a sigma-clipping algorithm.

Telluric correction was achieved by dividing the extracted target spectra by that of the F6V star HIP 41187, observed just before the target. Prior to division, hydrogen lines were removed from the standard star spectrum by interpolating the stellar continuum. Relative flux calibration was then achieved by multiplying through by a blackbody spectrum with $T_{\rm eff} = 6300$ K.

Fig. 4 shows this spectrum and three standard spectra (L0, L3 and L7). The spectrum is somewhat noisy, but it is consistent with early L spectral type, going by the near-infrared characterization scheme of Geballe et al. (2002).

4 DISTANCES

We used the M_J–spectral type relationship and M_i–$(i - J)$ relationship of Hawley et al. (2002) to estimate distances of ultracool dwarfs

Table 1. Photometric data of 34 new L dwarfs.

Name	SDSS i	SDSS z	2MASS J	2MASS H	2MASS K	UKIDSS Y	UKIDSS J	UKIDSS H	UKIDSS K	Sp. type
SDSS J000614.06+160454.5	20.74 ± 0.06	18.92 ± 0.05	16.59 ± 0.13	15.84 ± 0.11	15.09 ± 0.16	...	...	15.88 ± 0.02	15.32 ± 0.02	L0
SDSS J004058.92+152845.0	20.59 ± 0.06	18.85 ± 0.04	16.96 ± 0.21	15.58 ± 0.15	15.60 ± 0.23	...	...	15.96 ± 0.02	15.48 ± 0.02	L0
SDSS J084333.28+102443.5	19.30 ± 0.02	17.46 ± 0.01	14.87 ± 0.04	14.09 ± 0.04	13.67 ± 0.04	15.99 ± 0.01	14.78 ± 0.01	14.10 ± 0.01	13.55 ± 0.01	L2
SDSS J084407.00+284702.1	20.17 ± 0.04	18.25 ± 0.03	15.87 ± 0.06	14.82 ± 0.05	14.34 ± 0.06	...	15.76 ± 0.01	...	...	L2
SDSS J084610.73+030837.5	20.29 ± 0.04	18.39 ± 0.03	15.91 ± 0.09	15.17 ± 0.10	15.03 ± 0.17	16.95 ± 0.01	...	15.29 ± 0.01	14.76 ± 0.01	L0
SDSS J092142.51+084202.7	19.56 ± 0.04	17.82 ± 0.03	15.79 ± 0.08	14.89 ± 0.09	14.34 ± 0.07	16.80 ± 0.01	15.65 ± 0.01	15.00 ± 0.01	...	L1
SDSS J093215.45+345624.8	20.60 ± 0.04	18.81 ± 0.03	16.73 ± 0.15	15.70 ± 0.14	14.98 ± 0.14	...	16.34 ± 0.01	...	...	L2
SDSS J093242.84+042215.2	19.55 ± 0.02	17.87 ± 0.02	15.66 ± 0.08	14.91 ± 0.07	14.62 ± 0.09	...	...	15.00 ± 0.01	14.51 ± 0.01	L0
SDSS J093600.12+043147.9	20.86 ± 0.07	18.98 ± 0.04	16.12 ± 0.09	15.13 ± 0.06	14.48 ± 0.09	...	...	15.20 ± 0.01	14.44 ± 0.01	L3
SDSS J093858.87+044343.9	19.23 ± 0.02	17.50 ± 0.02	15.24 ± 0.05	14.50 ± 0.05	14.00 ± 0.07	...	...	14.59 ± 0.01	14.02 ± 0.01	L0
SDSS J094140.65−003215.8	20.60 ± 0.05	18.79 ± 0.04	16.77 ± 0.12	15.99 ± 0.14	15.59 ± 0.21	17.49 ± 0.02	16.69 ± 0.02	16.30 ± 0.02	15.86 ± 0.02	L0
SDSS J101304.34+071050.7	20.51 ± 0.04	18.62 ± 0.03	16.22 ± 0.14	15.47 ± 0.14	15.09 ± 0.18	17.22 ± 0.02	16.19 ± 0.01	15.60 ± 0.01	15.07 ± 0.01	L0
SDSS J121304.77+152922.2	20.69 ± 0.07	18.76 ± 0.05	16.33 ± 0.11	15.66 ± 0.12	15.42 ± 0.16	...	...	15.69 ± 0.02	15.18 ± 0.02	L4
SDSS J121917.86+151612.4	19.46 ± 0.02	17.88 ± 0.02	15.68 ± 0.07	15.09 ± 0.08	14.71 ± 0.11	...	...	15.08 ± 0.01	14.62 ± 0.01	L0
SDSS J124514.95+120442.0	20.53 ± 0.04	18.67 ± 0.03	16.05 ± 0.08	15.32 ± 0.11	14.73 ± 0.09	17.14 ± 0.02	16.06 ± 0.01	15.33 ± 0.01	14.67 ± 0.01	L1
SDSS J125214.08+142239.3	20.56 ± 0.04	18.76 ± 0.03	16.00 ± 0.07	15.16 ± 0.08	14.49 ± 0.07	17.28 ± 0.02	16.05 ± 0.01	15.24 ± 0.01	14.58 ± 0.01	L3
SDSS J125331.83+065933.4	20.20 ± 0.04	18.35 ± 0.03	16.19 ± 0.11	15.27 ± 0.10	15.07 ± 0.16	17.01 ± 0.01	16.07 ± 0.01	15.48 ± 0.01	14.96 ± 0.01	L0
SDSS J130433.16+090706.9[a]	19.11 ± 0.02	17.33 ± 0.02	15.29 ± 0.06	14.57 ± 0.07	13.95 ± 0.07	16.32 ± 0.01	15.28 ± 0.01	14.59 ± 0.01	14.03 ± 0.01	L0
SDSS J130831.02+081852.3	19.60 ± 0.02	17.82 ± 0.02	15.13 ± 0.05	14.35 ± 0.06	13.85 ± 0.07	16.31 ± 0.01	15.19 ± 0.01	14.37 ± 0.01	13.79 ± 0.01	L0
SDSS J132715.21+075937.5	19.17 ± 0.02	17.33 ± 0.01	14.60 ± 0.04	13.79 ± 0.04	13.24 ± 0.04	15.75 ± 0.01	14.58 ± 0.01	13.83 ± 0.01	13.20 ± 0.01	L1
SDSS J134607.41+084234.5	20.04 ± 0.03	18.16 ± 0.02	15.74 ± 0.07	14.79 ± 0.08	14.16 ± 0.07	16.74 ± 0.01	15.52 ± 0.01	14.75 ± 0.01	14.11 ± 0.01	L3
SDSS J142257.14+082752.1	19.37 ± 0.02	17.60 ± 0.02	15.10 ± 0.05	14.22 ± 0.03	13.65 ± 0.05	16.24 ± 0.01	15.01 ± 0.01	14.27 ± 0.01	13.61 ± 0.01	L3
SDSS J143911.87+082315.6	19.84 ± 0.03	17.93 ± 0.02	15.39 ± 0.04	14.65 ± 0.05	14.09 ± 0.07	16.54 ± 0.01	15.35 ± 0.01	14.69 ± 0.01	14.09 ± 0.01	L1
SDSS J144016.19+002638.9	20.43 ± 0.05	18.57 ± 0.03	16.07 ± 0.11	15.41 ± 0.12	14.82 ± 0.14	17.21 ± 0.02	16.01 ± 0.01	15.28 ± 0.01	14.69 ± 0.01	L4
SDSS J145201.33+093136.8	19.69 ± 0.02	17.79 ± 0.02	15.42 ± 0.07	14.77 ± 0.08	14.25 ± 0.09	16.35 ± 0.01	15.34 ± 0.01	14.81 ± 0.01	14.28 ± 0.01	L0
SDSS J145658.17+070104.7	20.55 ± 0.04	18.66 ± 0.03	16.28 ± 0.11	15.20 ± 0.09	14.60 ± 0.10	17.24 ± 0.01	15.97 ± 0.01	15.25 ± 0.01	14.59 ± 0.01	L4
SDSS J150309.53+115323.1	20.68 ± 0.04	18.74 ± 0.04	16.30 ± 0.10	15.40 ± 0.10	14.79 ± 0.09	17.32 ± 0.01	16.14 ± 0.01	15.42 ± 0.01	14.80 ± 0.01	L2
SDSS J152314.46+105258.9	20.53 ± 0.04	18.57 ± 0.03	16.09 ± 0.10	15.15 ± 0.08	14.82 ± 0.12	17.08 ± 0.01	15.94 ± 0.01	15.20 ± 0.01	14.62 ± 0.01	L0
SDSS J162307.37+290827.6	20.38 ± 0.05	18.50 ± 0.04	16.08 ± 0.09	15.50 ± 0.11	14.97 ± 0.10	...	16.13 ± 0.01	...	...	L4
SDSS J163748.64+275254.6	19.01 ± 0.02	17.29 ± 0.01	14.95 ± 0.04	14.16 ± 0.05	13.84 ± 0.05	...	14.89 ± 0.01	...	...	L0
SDSS J164911.16+300048.3	20.26 ± 0.03	18.38 ± 0.03	16.12 ± 0.09	15.38 ± 0.11	14.92 ± 0.09	...	16.09 ± 0.01	...	...	L1
SDSS J220517.48−003710.3	21.02 ± 0.06	19.13 ± 0.05	16.82 ± 0.14	16.24 ± 0.20	15.46 ± 0.19	17.79 ± 0.03	...	15.98 ± 0.02	15.52 ± 0.02	L0
SDSS J233615.99+004253.4	20.94 ± 0.07	19.05 ± 0.04	17.08 ± 0.20	15.71 ± 0.14	15.29 ± 0.16	17.59 ± 0.02	16.63 ± 0.02	15.98 ± 0.02	15.37 ± 0.02	L0
SDSS J234759.77−001546.9	20.86 ± 0.07	19.10 ± 0.06	16.40 ± 0.13	16.15 ± 0.20	15.46 ±	17.77 ± 0.02	16.90 ± 0.02	16.31 ± 0.03	15.88 ± 0.03	L0

Note: SDSS magnitude limits (95 per cent detection repeatability for point sources) for i and z bands are 21.3 and 20.5 respectively; UKIDSS magnitude limits for Y, J, H and K bands are 20.5, 20.0, 18.8 and 18.4 respectively.

[a]Companion to an M4.5 dwarf, SDSS J130432.93+090713.7, see Table 5.

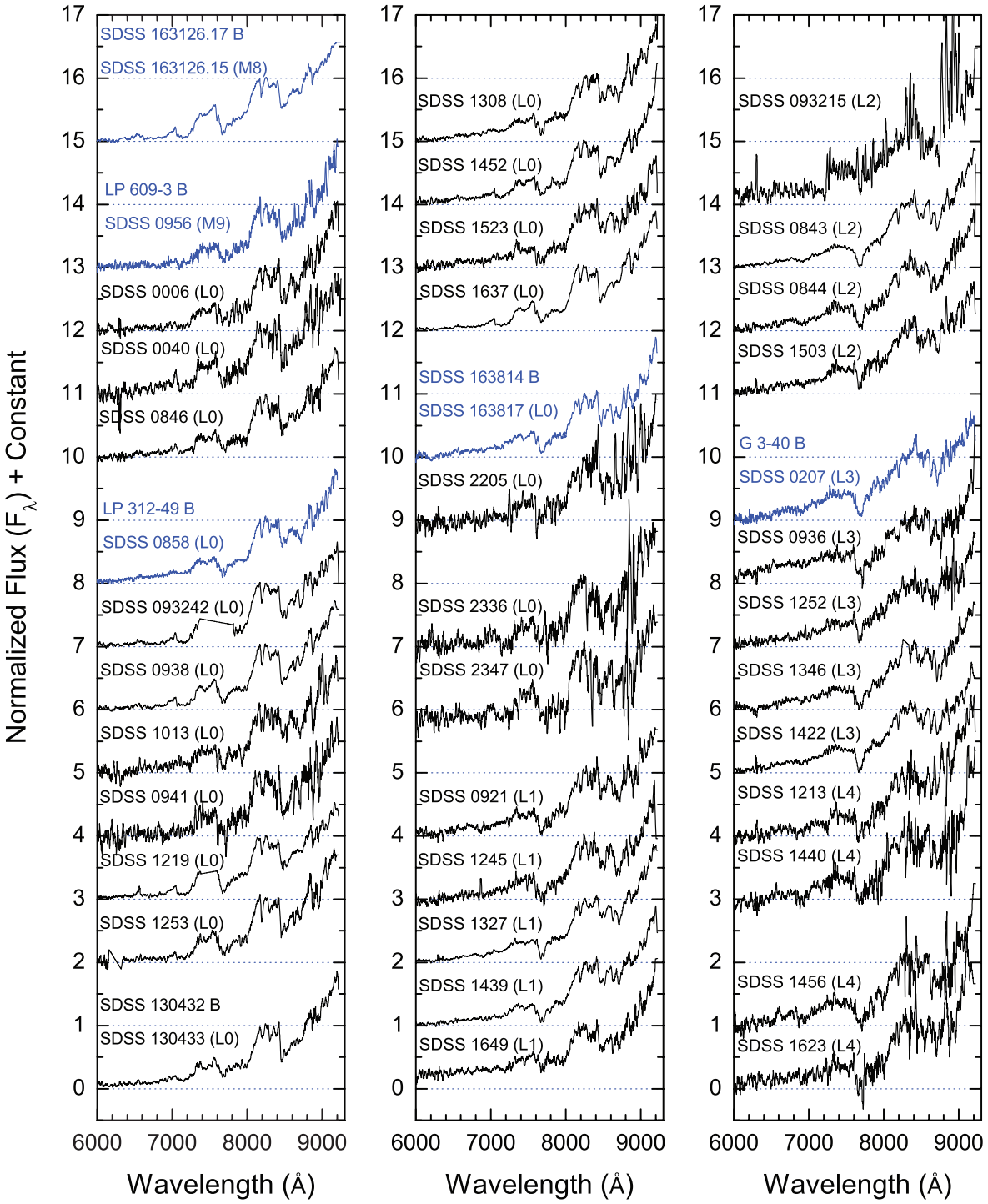

Figure 2. SDSS spectra of 39 ultracool dwarfs. Six objects in binary systems are those with two names (see Section 5.3), of which five are previously identified ultracool dwarfs (shaded/blue). The remaining 34 objects (black) are new L dwarfs discovered in this work, one of which is in a binary system. Note that two of the binaries we present in this paper do not have spectroscopy at this time. All spectra have been normalized to one at 8250 Å, smoothed by 11 pixels, and vertically offset for clarity. Dotted lines indicate zero-point offsets and also normalization levels to aid the visual examination of spectra.

with and without SDSS spectra respectively. We have assumed two limiting cases. First we assume that the ultracool dwarfs are single objects (these are the distances shown in Fig. 3 and referred to as 'Dist' in the subsequent tables). However, to provide conservative upper limits we also perform the calculations assuming that each candidate is an unresolved equal-mass binary, giving distances 41 per cent larger (referred to as Dist.b in subsequent tables). In each case the uncertainties were calculated to allow for spectral-type uncertainty and root-mean-square (RMS) scatter in the absolute magnitude–spectral type/colour relationships.

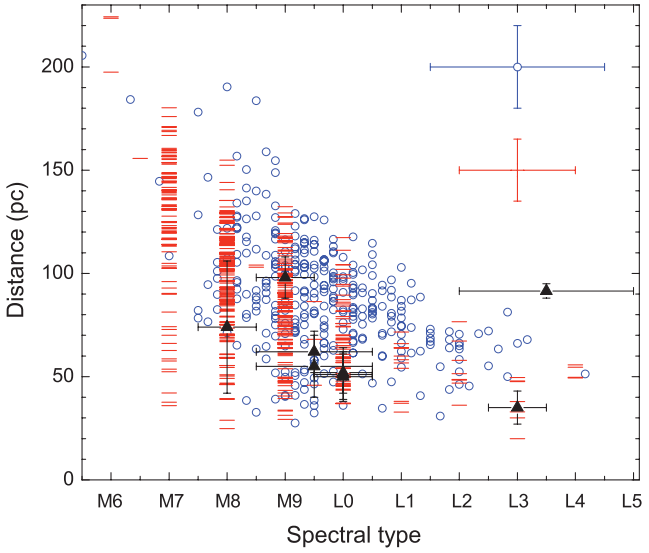

Figure 3. Plot of distance versus spectral type for ultracool dwarfs identified with SDSS spectra (bars) and optical–infrared colours (circles). Typical errors in spectral type and distance are shown in the top right. Black triangles and the black square (SDSS 0832) are the objects subsequently found to be in common-proper-motion binary systems (see Section 5.3). For these companions we assume their distances are the same as their primary stars (see Section 5.3).

5 PROPER MOTIONS

In previous work by our group we have measured proper motions using various combinations of survey data bases (Zhang et al. 2009b) and found that 2MASS and UKIDSS generally provide the most accurate proper motions, due to longer baselines (5–10 yr). The combinations of SDSS–2MASS and SDSS–UKIDSS only sometimes provide useful proper motions, when for example the baselines involved are relatively long ($\gtrsim$5 yr) or the measured objects have large proper motions (Deacon et al. 2009; Sheppard & Cushing 2009; Zhang et al. 2009b).

5.1 Ultracool dwarfs from our SDSS/2MASS/UKIDSS sample

806 of our objects matched in 2MASS and UKIDSS, so we calculated proper motions from their data base coordinates and epochs, following the method described in Section 3 (Zhang et al. 2009b). Fig. 5 shows the resulting 2MASS–UKIDSS proper motions of these 806 ultracool dwarfs. The 100 mas yr^{-1} ring shown in Fig. 5 acts as a guide to identify ultracool dwarfs with proper motions comparable with those in existing high-proper-motion catalogues ($>$100 mas yr^{-1}). This separation is useful when searching for possible companions (see Section 5.3). Table 2 shows the proper motions and distance estimates for the 34 new L dwarfs.

5.2 Ultracool dwarfs from our deeper search towards Praesepe

Due to the relatively short baselines between the SDSS and UKIDSS observations of our ultracool dwarfs towards Praesepe, and their low optical signal-to-noise ratio, we obtained additional epoch imaging for some of our candidates. z-band images were obtained for two candidates, SDSS J083823.69+164702.0 (SDSS 0838) and SDSS J083231.78+202700.0 (SDSS 0832), using the ESO Faint

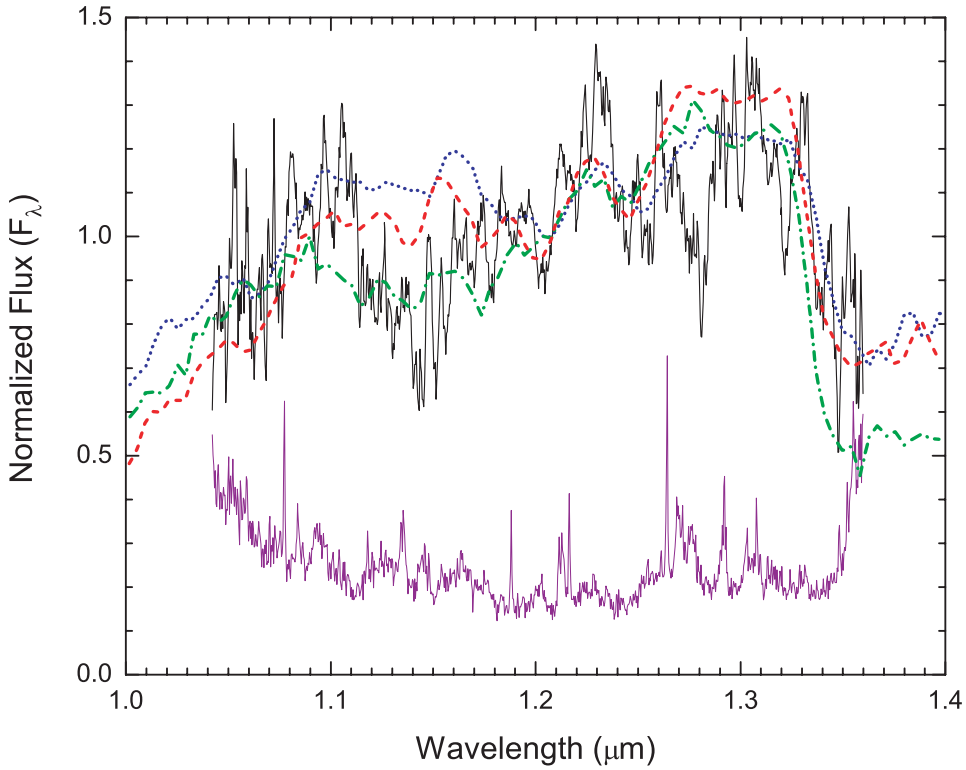

Figure 4. Gemini/NIRI spectrum of SDSS 0832. The spectrum (black) is normalized to one at 1.208 μm and smoothed by 11 pixels. The error spectrum is plotted below (shaded/purple). Three standard near-infrared spectra are overplotted, 2MASP J0345432+254023 (blue dot, L0 in optical, L1 in near-infrared: Burgasser & McElwain 2006; Kirkpatrick et al. 1999), 2MASSW J1146345+223053 (red dash, L3: Burgasser et al. 2010; Kirkpatrick et al. 1999; Knapp et al. 2004) and DENIS-P J0205.4−1159 (green dash dot, L7 in optical, L5.5 in near-infrared: Burgasser et al. 2010; Kirkpatrick et al. 1999).

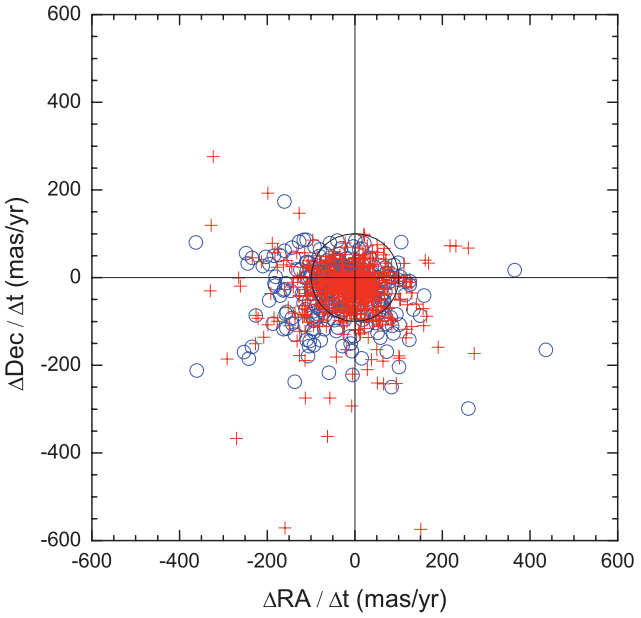

Figure 5. 2MASS–UKIDSS proper motions of ultracool dwarfs identified with (crosses) and without (circles) SDSS spectra. A ring indicates the 100 mas yr^{-1} proper-motion locus, which is a useful division when searching for common-proper-motion companions (see text).

Object Spectrograph and Camera (v.2) (EFOSC2: Buzzoni et al. 1984) on the New Technology Telescope (NTT) on La Silla, ESO (under programme 082.C-0399B) on 2008 December 25 with an exposure time of 500 s. The EFOSC2 observations were reduced using standard IRAF packages. We then used the IRAF task GEOMAP to derive spatial transformations from the SDSS z or UKIDSS GCS K-band images into the NTT z-band images. These transforms allowed for linear shifts and rotation. We then transformed the SDSS or GCS pixel coordinates of objects into the NTT images using GEOXYTRAN, and calculated the change in position (relative to the reference stars) between the two epochs.

We measured the proper motion of SDSS 0838 ($\mu_{\rm RA} = -21 \pm 15$ mas yr^{-1}, $\mu_{\rm Dec} = -19 \pm 15$ mas yr^{-1}; 2.2-yr baseline) based on GCS and NTT images with a baseline of 2.2 yr and using 14 reference stars. These data do not yield a proper motion that is greater than zero at a strongly significant level, although we note that the measurement is potentially consistent with the proper motion of Praesepe ($\mu_{\rm RA} = -35.81$ mas yr^{-1}, $\mu_{\rm Dec} = -12.85$ mas yr^{-1}: van Leeuwen 2009). The distance constraint for SDSS 0838 (see Section 4; 181 ± 62 pc if single or 256 ± 62 pc if an unresolved equal-mass binary) is also consistent with that of the cluster (181.5 pc: van Leeuwen 2009). A longer baseline is needed before cluster membership can be rigorously assessed, but this object could be a member of Praesepe. Table 3 shows the parameters of SDSS 0838.

We measured the proper motion of SDSS 0832 ($\mu_{\rm RA} = -46.6 \pm 8.2$ mas yr^{-1}, $\mu_{\rm Dec} = -37.0 \pm 8.2$ mas yr^{-1}) based on SDSS and NTT images with a baseline of 4.7 yr and using 16 reference stars. In addition, the combination of SDSS and UKIDSS GCS epochs provided a proper motion ($\mu_{\rm RA} = -52 \pm 46$ mas yr^{-1}, $\mu_{\rm Dec} = -50 \pm 46$ mas yr^{-1}) with a baseline of 2.6 yr (Zhang et al. 2009b) with significantly larger uncertainties. We combined these two measurements together, weighting by their reciprocal uncertainties, to give a final proper motion of $\mu_{\rm RA} = -47.4 \pm 8.2$ mas yr^{-1}, $\mu_{\rm Dec} = -38.9 \pm 8.2$ mas yr^{-1} for SDSS 0832. Both this proper motion and the distance constraint for SDSS 0832 (121 ± 33 pc) are

Table 2. Proper motions and distance estimates for the 34 new L dwarfs.

Name	$\mu_{\rm RA}$ [a] (mas yr^{-1})	$\mu_{\rm Dec}$ [a] (mas yr^{-1})	Distance[b] (pc)	Sp. type
SDSS 0006	-5 ± 19	-40 ± 19	94 ± 29	L0
SDSS 0040	121 ± 37	-62 ± 37	111 ± 39	L0
SDSS 0843	150 ± 10	-574 ± 10	32 ± 9	L2
SDSS 0844	40 ± 7	-98 ± 7	51 ± 15	L2
SDSS 0846	19 ± 19	-18 ± 19	69 ± 21	L0
SDSS 0921	-136 ± 15	-81 ± 15	57 ± 17	L1
SDSS 093215	40 ± 25	-74 ± 25	77 ± 15	L2
SDSS 093242	23 ± 11	12 ± 11	61 ± 18	L0
SDSS 0936	-49 ± 13	-38 ± 13	51 ± 15	L3
SDSS 0938	-12 ± 11	-38 ± 11	50 ± 15	L0
SDSS 0941	-63 ± 46	-362 ± 46	102 ± 32	L0
SDSS 1013	17 ± 32	28 ± 32	79 ± 25	L0
SDSS 1213	-292 ± 30	-186 ± 30	49 ± 8	L4
SDSS 1219	-32 ± 30	-13 ± 30	62 ± 18	L0
SDSS 1245	4 ± 18	-43 ± 18	64 ± 19	L1
SDSS 1252	-66 ± 23	-50 ± 23	48 ± 14	L3
SDSS 1253	-14 ± 21	-1 ± 21	78 ± 24	L0
SDSS 1304	-102 ± 19	14 ± 19	51 ± 14	L0
SDSS 1308	-234 ± 13	45 ± 13	48 ± 14	L0
SDSS 1327	-162 ± 22	29 ± 22	33 ± 9	L1
SDSS 1346	-221 ± 19	-93 ± 19	43 ± 13	L3
SDSS 1422	-159 ± 11	-571 ± 11	32 ± 9	L3
SDSS 1439	-130 ± 19	-3 ± 19	47 ± 14	L1
SDSS 1440	-26 ± 26	10 ± 26	43 ± 7	L4
SDSS 1452	65 ± 19	-191 ± 19	55 ± 16	L0
SDSS 1456	37 ± 17	-16 ± 17	48 ± 7	L4
SDSS 1503	22 ± 36	96 ± 36	63 ± 19	L2
SDSS 1523	0.4 ± 19	-19 ± 19	74 ± 22	L0
SDSS 1623	-265 ± 16	-1 ± 16	43 ± 7	L4
SDSS 1637	-226 ± 13	-86 ± 13	44 ± 13	L0
SDSS 1649	-27 ± 21	15 ± 21	66 ± 20	L1
SDSS 2205	51 ± 33	75 ± 33	104 ± 27	L0
SDSS 2336	-44 ± 45	-27 ± 45	117 ± 31	L0
SDSS 2347	13 ± 40	-6 ± 40	86 ± 23	L0

[a]2MASS–UKIDSS data base proper motions, found by dividing the difference between the 2MASS and SDSS coordinates (from the respective data bases) by the observational epoch difference. Standard errors are calculated using the major axes of the position error ellipses from 2MASS and SDSS.
[b]Distances based on M_J–spectral type relationship (Hawley et al. 2002).

Table 3. Parameters of SDSS 0838: a candidate Praesepe member.

Parameter	Value
RA (J2000)	08 38 23.69
Dec. (J2000)	16 47 02.0
Sp. Type	L0.5
Dist[a] (pc)	181 ± 62
Dist.b[a] (pc)	256 ± 62
$\mu_{\rm RA}$ (mas yr^{-1})	-21 ± 15
$\mu_{\rm Dec}$ (mas yr^{-1})	-19 ± 15
SDSS r	24.28 ± 0.53
SDSS i	22.32 ± 0.21
SDSS z	20.41 ± 0.18
UKIDSS Y	19.24 ± 0.08
UKIDSS J	18.29 ± 0.06
UKIDSS H	17.74 ± 0.07
UKIDSS K	17.02 ± 0.06

inconsistent with the Praesepe cluster, and this ultracool dwarf is thus seen to be a foreground object in the field.

5.3 Common-proper-motion systems

We searched for common-proper-motion companions to our ultracool dwarfs using three methods that combine efficacy with efficiency. Our searches are not fully complete, but are productive and effective in the identification of companions.

For our sample of 271 objects with proper motions larger than 100 mas yr^{-1}, we searched for common-proper-motion companions in high-proper-motion catalogues (Lépine & Shara 2005; Ivanov 2008) out to 3 arcmin separation, which corresponds to separation <9000 au for closer objects (50 pc) and <27 000 au for more distant objects (150 pc), and avoids an excess of contamination through chance alignments (see Section 5.4). Four of the ultracool dwarfs with proper motions greater than 100 mas yr^{-1} were found to have common-proper-motion companions (allowing for astrometric uncertainties), and the distance constraints for each pair were consistent with shared distance. Three of these four objects have SDSS spectra (SDSS 0207, SDSS 0858 and SDSS 0956) and one [SDSS J095324.54+052658.4 (SDSS 0953)] does not.

We also conducted a systematic search for companions to our lower-proper-motion (<100 mas yr^{-1}) objects. This search was conducted by visual inspection of the region of sky around each of our lower-proper-motion ultracool dwarfs using the SDSS Navigate Tool. We inspected images covering separations out to 2 arcmin on the sky, and looked for objects that could be mid-K to mid-M companions ($r-i\sim0.5$–2.0, $i-z\sim0.2$–1.0) with distances comparable to our sample (∼30–150 pc), and thus a magnitude of $i\sim9$–17. We then measured the proper motions of all such possible companions (as described in Section 5) to test for companionship. In this way, another four objects were found to have nearby common-proper-motion companions with reasonable distance agreement, three of which have SDSS spectra (SDSS 1304, SDSS 1631, SDSS 1638) and one of which [SDSS 010153.11+152819.4 (SDSS 0101)] does not.

In addition, we performed a wider angle visual search for bright companions to the two faint low-proper-motion ultracool dwarfs towards Praesepe, out to 3 arcmin separation. This resulted in the identification of a bright giant star (η Cancri) 164 arcsec away from SDSS 0832. The proper motion of η Cancri ($\mu_{\rm RA}=-46.33\pm0.43$ mas yr^{-1}, $\mu_{\rm Dec}=-44.31\pm0.24$ mas yr^{-1}) is taken from the updated *Hipparcos* catalogue (van Leeuwen 2007) and is consistent with SDSS 0832 to within the astrometric uncertainties. Fig. 6 shows the proper motion of SDSS 0832 and η Cancri (as well as SDSS 0838 and SDSS 1638). Fig. 7 shows a UKIDSS *JHK* false-colour image of SDSS 0832 and η Cancri.

We also obtained all available proper motions from the literature (VizieR/CDS data base) for comparison (summarized in Table 4), and note just one minor inconsistency. The literature proper motion of the companion (SDSS J163814.32+321133.5) to SDSS 1638 ($\mu_{\rm RA}=-61\pm10$, $\mu_{\rm Dec}=9\pm10$) was seen to be somewhat smaller than our initial data-base-measured proper motion ($\mu_{\rm RA}=-85\pm10$, $\mu_{\rm Dec}=2\pm10$). We therefore re-measured the proper motion of SDSS J163814.32+321133.5 and SDSS 1638 using a careful selection of fiducial reference stars and the IRAF routines GEOMAP and GEOXYTRAN. The results ($\mu_{\rm RA}=-68\pm15$, $\mu_{\rm Dec}=-4\pm12$ for SDSS J163814.32+321133.5; $\mu_{\rm RA}=-82\pm15$, $\mu_{\rm Dec}=9\pm12$ for SDSS 1638) show a good agreement with literature values, and we conclude that in this case the proper motion measured direct from the data-base coordinate/epoch information was not optimal.

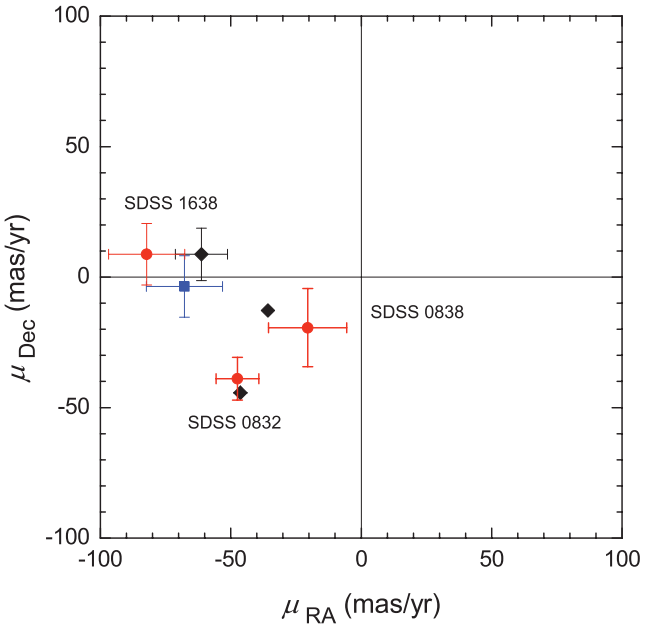

Figure 6. The proper motions of SDSS 0832 (L3.5), SDSS 0838 (M9.5), SDSS 1638 (L0) and their primary star or cluster (squares and a diamond respectively). The proper motions of these three ultracool dwarfs (circles) and the primary star of SDSS 1638 (square) are measured with the IRAF routines GEOMAP and GEOXYTRAN. The diamonds are proper motions from the literature. SDSS 0832 is the companion to the K3 giant η Cancri. SDSS 0838 is a Praesepe candidate member. SDSS 1638 is a companion to an M4 dwarf.

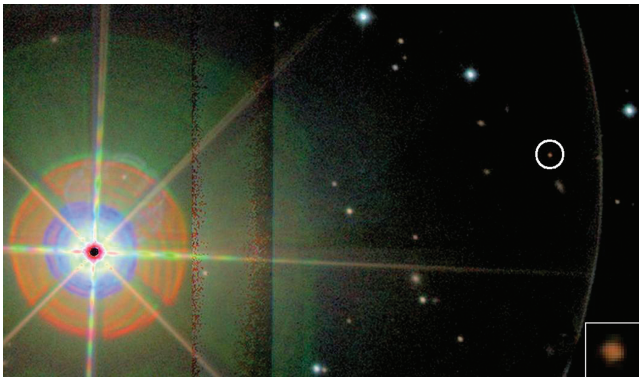

Figure 7. A UKIDSS ZYJ false colour image of η Cancri AB with a separation of 164 arcsec. η Cancri A is the brightest object in this field, η Cancri B is in the white circle and a five times enlarged image can be found in the bottom right corner.

Overall, we thus found nine star + ultracool dwarf common-proper-motion pairs. Proper motions of seven of these are shown in Fig. 8, and the proper motions of the other two (SDSS 0832 and SDSS 1638) are shown in Fig. 6 for clarity. Table 5 shows the parameters of the eight dwarf star + ultracool dwarf common-proper-motion pairs, and Fig. 9 shows UKIDSS *J*-band images of these systems. The η Cancri system is discussed further in Section 6.

5.4 Chance alignments?

To determine if the new binary systems are genuine, we carried out a statistical analysis of the probability that the pairs could be line-of-sight associations with photometry and proper motion consistent with binarity by random chance (using a similar method to

Table 4. Proper motions of companions of eight dwarf + ultracool dwarf binary systems.

Ref.[a]	μ_{RA} (mas yr^{-1})	μ_{Dec} (mas yr^{-1})	μ_{RA} (mas yr^{-1})	μ_{Dec} (mas yr^{-1})	μ_{RA} (mas yr^{-1})	μ_{Dec} (mas yr^{-1})	μ_{RA} (mas yr^{-1})	μ_{Dec} (mas yr^{-1})
Primary	TYC 1189−1216–1		G 3–40		LP 312–49		LP 548–50	
1	...	...	259 ...	−188 ...	...	...	...	...
2	...	...	...	...	113 ...	−196 ...	−184 ...	32 ...
3	20 ± 3	35 ± 3	...	...	...	...	...	...
4	21 ± 3	35 ± 3	261 ± 15	−165 ± 15	...	...	...	...
5	18 ...	34 ...	254 ± 4	−176 ± 1	80 ± 1	−198 ± 3	−182 ± 3	36 ± 2
6	...	...	261 ± 6	−185 ± 6	81 ± 6	−205 ± 6	...	...
7	20 ± 2	35 ± 2	263 ± 2	−180 ± 2	83 ± 4	−202 ± 5	−182 ± 3	36 ± 2
8	20 ± 2	33 ± 2	262 ...	−186 ...	82 ...	−201 ...	...	...
9	...	...	262 ...	−186 ...	82 ...	−201 ...	−186 ...	37 ...
10	22 ± 1	37 ± 1	265 ± 2	−181 ± 2	...	...	...	...
11	...	...	256 ± 3	−176 ± 3	81 ± 3	−200 ± 3	−191 ± 3	36 ± 3
12	20 ...	35 ...	264 ...	−180 ...	83 ...	−202 ...	...	...
13	21 ± 1	36 ± 1	264 ± 3	−179 ± 3	...	...	...	...
14	22 ± 16	54 ± 16	272 ± 15	−179 ± 15	107 ± 18	−183 ± 18	−188 ± 11	50 ± 11
Average[b]	20 ± 2	37 ± 2	262 ± 2	−179 ± 2	89 ± 6	−199 ± 3	−186 ± 3	38 ± 3
Secondary[c]	27 ± 17	43 ± 14	273 ± 19	−174 ± 17	104 ± 20	−184 ± 20	−203 ± 17	46 ± 17
Primary	LP 609-3		SDSS J130432.93+090713.7		SDSS J163126.17+294847.1		SDSS J163814.32+321133.5	
2	−105	−182	...	...	...	...	...	...
5	...	...	−126 ± 1	22 ± 3	−52 ± 20	6 ± 1	−60 ± 1	2 ...
7	...	...	−126 ± 1	22 ± 3	−52 ± 20	6 ± 1	−60 ± 1	2 ...
8	−107 ...	−189 ...	...	...	...	...	...	...
9	−107 ...	−189 ...	...	...	...	...	...	...
11	...	...	−132 ± 3	22 ± 3	−49 ± 3	1 ± 3	−66 ± 3	3 ± 3
14	−95 ± 19	−195 ± 19	−115 ± 22	7 ± 22	−53 ± 13	−7 ± 13	−85 ± 10	2 ± 10
15	...	...	...	...	...	...	−68 ± 15	−4 ± 12
Average[b]	−104 ± 14	−189 ± 19	−125 ± 3	18 ± 4	−52 ± 3	2 ± 4	−66 ± 6	6 ± 5
Secondary[c]	−113 ± 37	−190 ± 36	−102 ± 19	14 ± 19	−48 ± 11	5 ± 11	−82 ± 15	9 ± 12

[a]References: [1]Giclas, Burnham & Thomas (1971), [2]Luyten & Hughes (1980), [3]Hog et al. (2000), [4]Kharchenko (2001), [5]Monet et al. (2003), [6]Salim & Gould (2003), [7]Zacharias et al. (2004), [8]Zacharias et al. (2009), [9]Lépine & Shara (2005), [10]Ducourant et al. (2006), [11]Adelman-McCarthy et al. (2008), [12]Ivanov (2008), [13]Röser et al. (2008), [14]measured with data base information in this work, [15]measured with IRAF in this work.
[b]Average proper motions of primary stars.
[c]Proper motions of secondary ultracool dwarfs.

that used by Day-Jones et al. (2008)). As an example we discuss the case of η Cancri and SDSS 0832. To assess the probability of common proper motion, we searched the SuperCOSMOS Science Archive (Hambly et al. 2001) in a square degree of sky around the position of the L dwarf, and made a colour–magnitude selection (B versus $B - R$) consistent with a dwarf sequence in the ∼90–160 pc distance range. We found that seven out of 337 objects had common proper motion to within 2σ uncertainty, suggesting a probability of 2 per cent that such common proper motion could occur by random chance. Separations out to 164 arcsec from η Cancri and a distance range of 90–160 pc correspond to a space volume of 2.86 pc^3. Assuming a space density of 0.0106 pc^{-3} for ∼G–K stars ($M_V = 5.5$–8.5: Kroupa 1995) we thus estimate that we would expect 4.9×10^{-4} G or K stars to masquerade as common-proper-motion companions in the volume considered around the L dwarf SDSS 0832.

Our full ultracool dwarf sample contains 268 objects with proper motion >100 mas yr^{-1}, 283 with proper motion = 50–100 mas yr^{-1} and 258 with proper motion <50 mas yr^{-1}. η Cancri resides in our lowest proper-motion group, and companions to ultracool dwarfs in this group were searched for (in all but two cases) out to separations of 2 arcmin. Accounting for the typical volume searched around each ultracool dwarf, and the total number of ultracool dwarfs in this group, we estimate that we might have expected to find ∼0.05 apparent η Cancri-like common-proper-motion companions by random chance. We performed similar calculations for our other binary systems, using a K–M space density of 0.04 pc^{-3} (Kroupa 1995) and accounting for the significantly smaller separations and generally larger proper motions (see Table 5). We note that the expected numbers of random chance alignments for these other systems (0.000 02–0.0048) are much lower than for the η Cancri system. This analysis shows that overall we would not expect any random chance common-proper-motion companions to our full ultracool dwarf sample, and that our nine identified systems should be genuine binaries. However, we note that for the wide separation and lower proper motion of η Cancri B, the possibility of spurious companionship is larger (although still very small) than for the other binaries.

5.5 New binaries

Fig. 10 shows the distance constraints of the nine binary ultracool dwarfs plotted against the distance constraints for their respective primary stars. Distances of the seven brighter

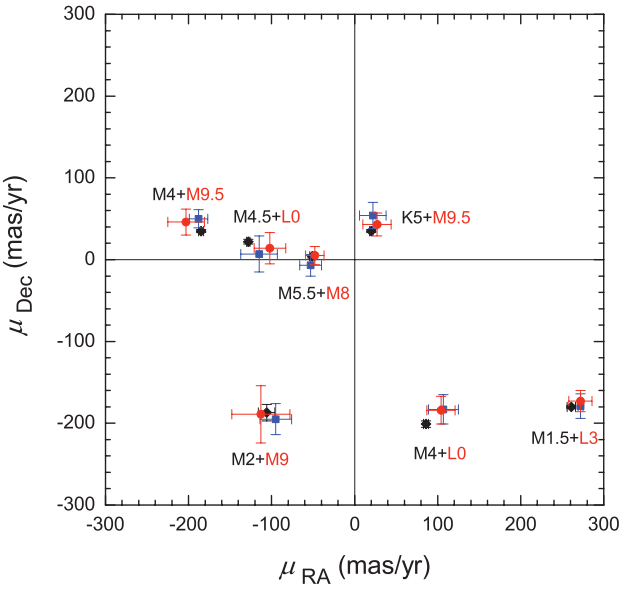

Figure 8. Seven dwarf star + ultracool dwarf common-proper-motion pairs. Proper motions of ultracool dwarfs (circles) and dwarf stars (squares) are measured in this work using 2MASS and UKIDSS data base coordinates and epochs. Dwarf star proper motions taken from the literature (diamonds) are also shown.

primary dwarfs are based on the relationship between the $V - J$ colour index and absolute magnitude M_V (Lépine 2005). However, SDSS J163126.17+294847.1 (M5.5V) is too faint and red to have a V-band magnitude available, so we constrained its distance using the same method that was used for the ultracool dwarfs (see Section 4). The distance of η Cancri is from *Hipparcos* (van Leeuwen 2007). This plot allows us to place constraints on possible unresolved binarity amongst our ultracool dwarf companions. It can be seen that six ultracool dwarfs could be equal-mass unresolved binaries by the distance constraints. We cannot, however, rule out the possibility of non-equal-mass unresolved binarity from this plot. If SDSS 0832 for example was an equal-mass binary, it would be too distant to be associated with η Cancri. However, a non-equal-mass binary (e.g. an unresolved L + T binary) would affect spectral type and distance estimates as well as absolute magnitude, and this is not ruled out by Fig. 10. This will be discussed further in Section 6.3.

Fig. 11 shows our new ultracool dwarf + star binaries in the context of the broader population of such wide systems (we plot known binaries with $a > 100$ au; see Rebolo et al. 1998; White et al. 1999; Burgasser et al. 2000; Gizis et al. 2000; Lowrance et al. 2000; Gizis, Kirkpatrick & Wilson 2001; Wilson et al. 2001; Bouy et al. 2003; Scholz et al. 2003; Golimowski et al. 2004; Neuhäuser & Guenther 2004; Scholz, Lodieu & McCaughrean 2004; Billères et al. 2005; Chauvin et al. 2005; Neuhäuser et al. 2005; Seifahrt, Guenther & Neuhäuser 2005a; Seifahrt et al. 2005b; Metchev & Hillenbrand 2006; Reid & Walkowicz 2006; Caballero 2007; Cruz et al. 2007; Luhman et al. 2007; Mugrauer, Seifahrt & Neuhäuser 2007; Phan-Bao et al. 2008; Radigan et al. 2008, 2009; Artigau et al. 2009; Burningham et al. 2009; Faherty et al. 2010). It is clear from this plot that the projected separation range <7000 au is well populated for binaries with a total mass $<1\,M_\odot$, with wider ultracool dwarf companions to such stars being rare. However, there is some indication that higher mass primaries are able to host wider ultracool dwarf companions, with the η Cancri system contributing to this trend.

6 η CANCRI AB

With a separation of 15 019 au, η Cancri AB is an extremely wide binary; however, as Section 5.4 explains, it is a statistically solid association, with the two components presumably having a common composition and age. Only five brown-dwarf-mass objects were previously known around (four) giant stars, all detected by the radial velocity method (Hatzes et al. 2005; Lovis & Mayor 2007; Liu et al. 2008b; Niedzielski et al. 2009). These objects all have $m \sin i$ in the range 10–20 $M_{\rm Jup}$ and are within 3 au of their primaries. They are thus unobservable with current technology, and their mass range overlaps that of the planetary regime. As such, their atmospheres may not share the same composition as the primary star, and without direct observation they are not useful benchmark objects for study.

6.1 The metallicity of η Cancri A

η Cancri A is a bright K3 giant with a V-band magnitude of 5.33, and its metallicity has been measured several times by various groups: [Fe/H] = 0.19 by Brown et al. (1989), [Fe/H] = 0.07 ± 0.21, [Fe/H] = 0.08, [Fe I/H] = 0.02, [Fe II/H] = 0.10 measured with different methods by Luck & Heiter (2007) and A(Fe) = 7.64 by Hekker & Meléndez (2007). These results are consistent with a metallicity of [Fe/H] = 0.10 ± 0.1 for η Cancri A. Given the importance of being able to infer a metallicity for the L dwarf companion, we have re-addressed the metallicity of this system with new data and analysis.

We obtained a high-resolution echelle spectrum of η Cancri A during an observing run from 2009 February 9–11, using the FIber fed Echelle Spectrograph (FIES) at the 2.56-m Nordic Optical Telescope located at the Observatorio del Roque de los Muchachos (La Palma, Spain). We used FIES with a 2048 × 2048 13.5-μm pixel EEV42-40 CCD detector. The wavelength range covered is from 3620–7360 Å in 80 orders. The reciprocal dispersion ranges from 0.02–0.04 Å pixel^{-1} and the spectral resolution (FWHM) is from 0.06–0.10 Å. We extracted the spectrum using standard reduction procedures in IRAF, including bias subtraction, flat-field division and optimal extraction of the spectra. We obtained the wavelength calibration by taking a spectrum of a Th–Ar lamp. Finally, we normalized the spectrum by a polynomial fit to the observed continuum.

Stellar iron abundances [A(Fe) = log N(Fe)/N(H) + 12] were estimated from the equivalent-width measurements of a set of 13 Fe I and two Fe II lines. The line list was provided by Jorge Meléndez (private communication), who has tested their use for F, G and K giant stars. Measurements were compared with equivalent widths computed under the assumption of local thermodynamical equilibrium (LTE) and spherical symmetry, which for stars of low surface gravity should be more appropriate than a plane-parallel description. Calculations were made using the Uppsala suite of codes and the new MARCS model atmospheres (Gustafsson, Edvardsson & Eriksson 2008). Stellar atmospheres are characterized by four fundamental parameters: $T_{\rm eff}$, log g, metallicity ([Fe/H] = A(Fe) − A(Fe)$_\odot$) and microturbulence ($\xi_{\rm t}$). For the values of interest here, a grid of model atmospheres of one solar mass and standard composition was linearly interpolated. The $T_{\rm eff}$ of η Cancri A was estimated from Johnson photometry in the blue ($V = 5.343$ and $B = 6.608$) and 2MASS in the red ($J = 3.489, H = 2.861$ and $K = 2.699$), using the Ramírez & Meléndez (2005) $T_{\rm eff}$ versus ($B - V$), ($V - H$), ($V - J$) and ($V - K$) calibrations. Estimates coming from the blue and the red were somewhat different, 4329 K versus 4520 K, so an average value of 4472 K with an assigned 107-K uncertainty was used in our computations. The interstellar extinction of this

Table 5. Parameters of eight ultracool dwarf binary systems.

Binary	A	B	A	B	A	B	A	B
Component	TYC 1189−1216–1	SDSS 0101	G 3–40	SDSS 0207	LP 312–49	SDSS 0858	LP 548–50	SDSS 0953
Sp. Type	K5	M9.5[g]	M1.5	L3[c]	M4	L0[d]	M4	M9.5[g]
SDSS RA	01 01 55.00	01 01 53.11	02 07 37.47	02 07 35.59	08 58 36.75	08 58 36.97	09 53 24.20	09 53 24.54
SDSS Dec	15 28 01.2	15 28 19.4	13 54 49.4	13 55 56.2	27 11 05.8	27 10 50.8	05 27 00.9	05 26 58.4
Dist (pc)	55 ± 15	60 ± 18	35[e] ± 8	37 ± 10	52 ± 10	46 ± 11	62 ± 10	65 ± 13
Dist.b[a] (pc)	...	85 ± 18	...	53 ± 10	...	65 ± 11	...	92 ± 13
μ_{RA} (mas yr^{-1})	20 ± 2	27 ± 17	262 ± 2	272 ± 14	88 ± 6	104 ± 17	−186 ± 3	−203 ± 22
μ_{Dec} (mas yr^{-1})	37 ± 2	43 ± 14	−179 ± 2	−173 ± 13	−199 ± 3	−184 ± 17	38 ± 3	47 ± 16
V	11.49 ± 0.15	...	12.50 ± 0.13	...	16.19	...	17.96	...
SDSS *i*	12.79 ± 0.01	19.57 ± 0.03	11.01 ± 0.01	19.75 ± 0.03	14.34 ± 0.01	19.44 ± 0.02	15.64 ± 0.01	19.70 ± 0.04
SDSS *z*	10.95 ± 0.01	17.74 ± 0.02	11.24 ± 0.01	17.99 ± 0.02	13.49 ± 0.01	17.64 ± 0.02	14.69 ± 0.01	17.83 ± 0.03
UKIDSS *Y*	...[f]	16.31 ± 0.01	...[f]	16.59 ± 0.01	...	...	...	...
UKIDSS *J*	...[f]	15.31 ± 0.01	...[f]	15.37 ± 0.01	11.92 ± 0.01	15.01 ± 0.01	13.12 ± 0.01	...
UKIDSS *H*	...[f]	14.68 ± 0.01	...[f]	14.53 ± 0.01	...	...	12.58 ± 0.01	15.05 ± 0.01
UKIDSS *K*	...[f]	14.15 ± 0.01	...[f]	13.83 ± 0.01	...	...	12.24 ± 0.01	14.47 ± 0.01
2MASS *J*	9.10 ± 0.02	15.49 ± 0.05	9.20 ± 0.02	15.46 ± 0.05	11.99 ± 0.02	15.05 ± 0.05	13.18 ± 0.03	15.67 ± 0.09
2MASS *H*	8.48 ± 0.03	14.70 ± 0.06	8.57 ± 0.06	14.47 ± 0.04	11.41 ± 0.02	14.23 ± 0.05	12.57 ± 0.03	14.96 ± 0.07
2MASS *K*	8.34 ± 0.02	14.21 ± 0.06	8.31 ± 0.02	13.81 ± 0.05	11.11 ± 0.02	13.66 ± 0.05	12.29 ± 0.03	14.39 ± 0.08
Separation	36″.6		72″.5		15″.4		5″.7	
Sep. (au)	2050 ± 571		2538 ± 580		801 ± 154		352 ± 57	
SP[b]	4.82×10^{-3}		1.75×10^{-3}		6.60×10^{-5}		1.62×10^{-5}	

Binary	A	B	A	B	A	B	A	B
Component	LP 609-3	SDSS 0956	SDSS 130432[h]	SDSS 130433[h]	SDSS 163126.17[h]	SDSS 163126.15[h]	SDSS 163814[h]	SDSS 163817[h]
Sp. Type	M2	M9[d]	M4.5	L0	M5.5	M8[d]	M4	L0[d]
SDSS RA	09 56 14.86	09 56 13.13	13 04 32.93	13 04 33.16	16 31 26.17	16 31 26.15	16 38 14.32	16 38 17.31
SDSS Dec	01 44 58.7	01 45 14.3	09 07 13.7	09 07 06.9	29 48 47.1	29 48 36.9	32 11 33.5	32 11 44.1
Dist (pc)	98 ± 10	91 ± 28	50 ± 11	51 ± 14	74 ± 32	75 ± 20	51 ± 13	54 ± 14
Dist.b[a] (pc)	...	128 ± 28	...	72 ± 14	...	106 ± 20	...	76 ± 14
μ_{RA} (mas yr^{-1})	−104 ± 14	−113 ± 35	−125 ± 3	−102 ± 19	−52 ± 3	−48 ± 11	−66 ± 6	−82 ± 15
μ_{Dec} (mas yr^{-1})	−189 ± 19	−189 ± 35	18 ± 4	14 ± 19	2 ± 4	5 ± 11	6 ± 3	9 ± 12
V	15.99	...	16.63 ± 0.34	...	...	...	14.89	...
SDSS *i*	14.12 ± 0.01	20.30 ± 0.04	14.45 ± 0.01	19.11 ± 0.02	17.07 ± 0.01	18.87 ± 0.01	13.39 ± 0.01	19.81 ± 0.03
SDSS *z*	13.50 ± 0.01	18.51 ± 0.04	13.52 ± 0.01	17.33 ± 0.02	15.86 ± 0.01	17.34 ± 0.02	12.37 ± 0.01	17.92 ± 0.02
UKIDSS *Y*	12.62 ± 0.01	17.20 ± 0.02	12.50 ± 0.01	16.32 ± 0.01	...	...	...	...
UKIDSS *J*	12.12 ± 0.01	16.36 ± 0.01	11.91 ± 0.01	15.28 ± 0.01	14.08 ± 0.01	15.39 ± 0.01	11.00 ± 0.01	15.35 ± 0.01
UKIDSS *H*	11.66 ± 0.01	15.92 ± 0.01	11.41 ± 0.01	14.59 ± 0.01	...	...	...	...
UKIDSS *K*	11.40 ± 0.01	15.48 ± 0.02	11.10 ± 0.01	14.03 ± 0.01	...	...	...	...
2MASS *J*	12.20 ± 0.02	16.24 ± 0.10	11.96 ± 0.02	15.29 ± 0.06	14.15 ± 0.03	15.53 ± 0.06	10.98 ± 0.02	15.39 ± 0.05
2MASS *H*	11.63 ± 0.03	15.77 ± 0.14	11.38 ± 0.03	14.57 ± 0.07	13.56 ± 0.04	14.85 ± 0.07	10.41 ± 0.02	14.64 ± 0.05
2MASS *K*	11.40 ± 0.02	15.28 ± 0.19	11.10 ± 0.03	13.95 ± 0.07	13.21 ± 0.04	14.59 ± 0.08	10.16 ± 0.02	14.16 ± 0.07
Separation	30″.4		7″.6		10″.1		46″.0	
Sep. (au)	2979 ± 304		374 ± 76		756 ± 200		2418 ± 664	
SP[b]	3.49×10^{-3}		2.23×10^{-4}		6.57×10^{-4}		8.75×10^{-4}	

[a]Distance calculation assumes unresolved equal-mass binaries.
[b]Statistical probability (SP) that the common proper motion could occur by random chance, see section 5.3 for details of the method.
[c]Characterized by Hawley et al. (2002) as an L3 dwarf.
[d]Catalogued by West et al. (2008) as L0, L0, M9 and M8 dwarfs.
[e]The distance given by Lépine & Shara (2005) is 32.5 ± 6.8.
[f]The star is too bright for UKIDSS, thus *JHK* magnitudes are not reliable.
[g]Based on optical–near-infrared colours.
[h]We used more digits in their names to distinguish the two components; SDSS 1304, SDSS 1631, SDSS 1638 refer to secondary ultracool dwarfs in this paper.

nearby star estimated from the models in Hakkila et al. (1997) is very low, $E(B-V) = 0.01 \pm 0.05$, and cannot explain the temperature discrepancy between these two estimates. We also tried the new $T_{\rm eff}$ versus colour calibrations in González Hernández & Bonifacio (2009), but the difference is even larger ($T_{\rm eff} = 4531 \pm 137$) with the blue estimate. Another concern is the precision of the surface-gravity determination, which in turns compromises the accuracy of the metallicity determinations. Our $\log g = 2.30$ estimate is based on the *Hipparcos* parallax of the star ($\pi = 10.93 \pm 0.43$: van Leeuwen 2007), and on a $M \sim 1.60\,{\rm M}_{\odot}$ stellar mass and

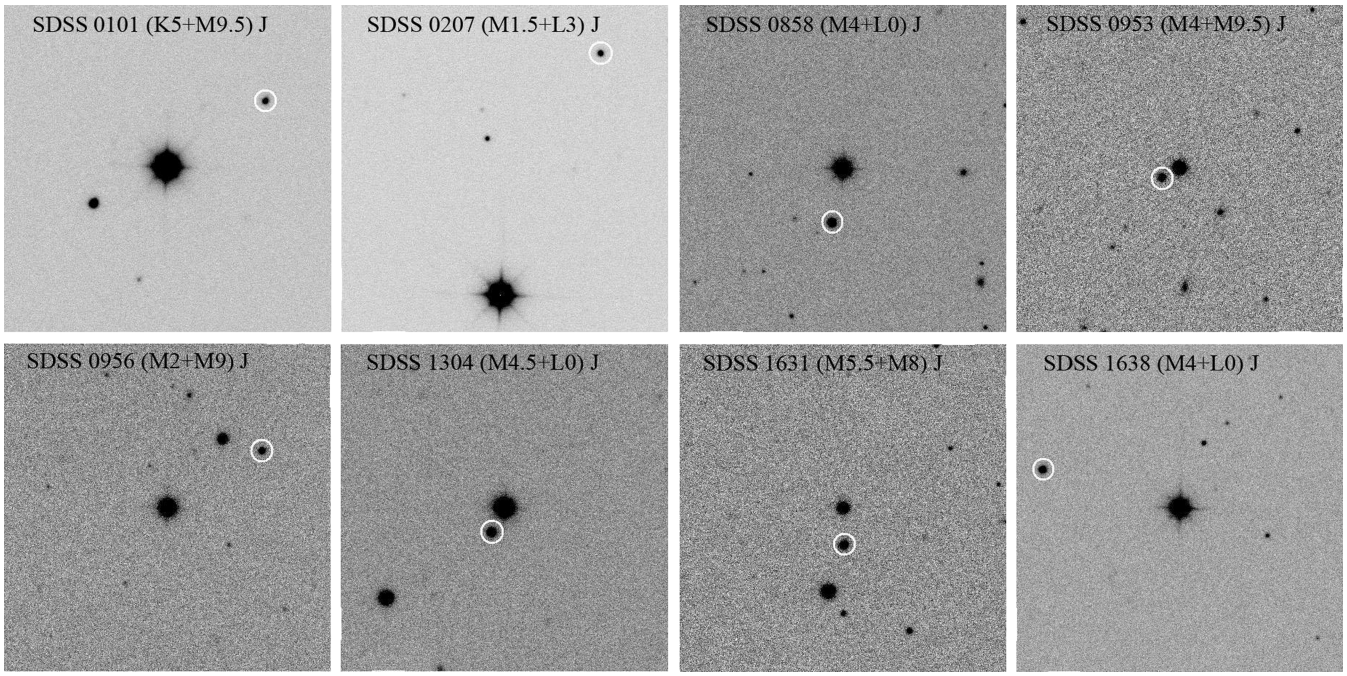

Figure 9. UKIDSS *J*-band images of eight ultracool dwarf binary systems. All the images have a size of 1.5 arcmin with north up and east left. The primary stars are generally in the centre of images, except the second one (SDSS 0207) in which the primary star is in the bottom of the field; the ultracool dwarfs are in white circles.

a $BC = -0.558$ bolometric correction for V. These two last values are estimated from isochrones and were taken from Luck & Heiter (2007) after checking they were appropriate for our stellar temperature and metallicity values (for details on the accuracy of these parameter determinations see Luck & Heiter 2007). Another way of estimating the surface gravity is the Fe ionization equilibrium; however, this method has the disadvantage of being sensitive to departures from LTE. In our case, our best estimate of $\log g$ (2.30) produces an abundance difference between Fe I and Fe II of $\Delta A(\mathrm{Fe}) = 0.15$ dex. The microturbulence value was changed until the trend in A(Fe) versus Fe I equivalent widths was minimized, which happened at $\xi_t = 1.62\,\mathrm{km\,s^{-1}}$.

The method employed here requires a priori knowledge of the metallicity, so that two iterations were necessary to obtain our best iron abundance value of 7.52 dex (an average value over the 15 Fe lines). Results based on the Fe II lines are sensitive to the uncertainties of the stellar parameters: abundance changes of -0.12 dex for $\Delta T_{\rm eff} \sim 100$ K, 0.08 dex for $\Delta \log g \sim 0.15$ (mass, parallax), 0.05 dex for Δ[Fe/H] ~ 0.10 dex. However, the average abundance based on the neutral lines is much less sensitive (abundance changes $\sim$0.02–0.03 dex). Changes in the microturbulence and the uncertainties in the measured equivalent widths have a more significant effect, 0.05 dex for 0.1 km s^{-1} microturbulence changes, and a similar effect for a typical $\Delta W_\lambda = 3$ mÅ uncertainty. We have adopted our total error budget to be $\pm$0.10 dex, the standard deviation associated with the 15 lines used, which will partially account for the sensitivity mentioned before. We also note that our abundances may suffer from other systematic errors, e.g. $T_{\rm eff}$ zero-points, isochrones uncertainties or departures from LTE. Our final metallicity value depends on the solar iron abundance that we assume: if the Sun was analysed in a similar way to η Cancri A (i.e. one-dimensional LTE but using the appropriate line list, e.g. García Pérez et al. 2006), then the metallicity (relative to solar) of η Cancri A would be -0.02 dex [$A(\mathrm{Fe})_\odot = 7.54$]. Solar abundances based on three-dimensional LTE analysis are much lower, 7.45 (Grevesse, Asplund & Sauval 2007), which leads to a higher metallicity value for η Cancri A of 0.07 dex. On balance we present a metallicity constraint (in Table 6) for η Cancri A of 0.0 ± 0.1.

6.2 The age of η Cancri A

The $T_{\rm eff}$ measurements of η Cancri A measured here and by Hekker & Meléndez (2007), Luck & Heiter (2007) and Allende Prieto & Lambert (1999) are all consistent with $T_{\rm eff} = 4450 \pm 100$ K. The radius of η Cancri A based on this temperature and $\log(L/\mathrm{L}_\odot) = 1.95 \pm 0.06$ (Luck & Heiter 2007) is $16.0^{+1.8}_{-1.6}\,\mathrm{R}_\odot$. Luck & Heiter (2007) estimated a mass for η Cancri A of $1.6 \pm 0.5\,\mathrm{M}_\odot$ (typical uncertainty $\sim$35 per cent), and Allende Prieto & Lambert (1999) estimate a mass of $1.36 \pm 0.67\,\mathrm{M}_\odot$. To provide additional refinement, we calculated the parameters of η Cancri A with PARAM (da Silva et al. 2006). PARAM is a web interface for the Bayesian estimation of stellar parameters. Table 7 shows our input and output values from PARAM. The [Fe/H], V magnitude, parallax and $B - V$ colour of η Cancri A are known, so we experimented with different $T_{\rm eff}$ input values until the model colour output was $B - V = 1.252$ (Perryman et al. 1997). The mass, gravity and radius output from PARAM are all consistent with other estimates, but provide a somewhat improved level of accuracy, and on balance we assumed a mass of $1.40 \pm 0.2\,\mathrm{M}_\odot$ for η Cancri A.

We have used these physical properties to constrain the age of η Cancri A by comparison with evolutionary tracks. Fig. 12 shows the $T_{\rm eff}$ and L evolutionary tracks (Girardi et al. 2000) as a function of time and on a Hertzsprung−Russell (HR) diagram for solar-metallicity stars with different masses (1.2 $\mathrm{M}_\odot$, 1.4 $\mathrm{M}_\odot$ and 1.6 $\mathrm{M}_\odot$). $T_{\rm eff}$ and $\log(L/\mathrm{L}_\odot)$ measurements from the literature are plotted in the HR diagram with different symbols (see caption).

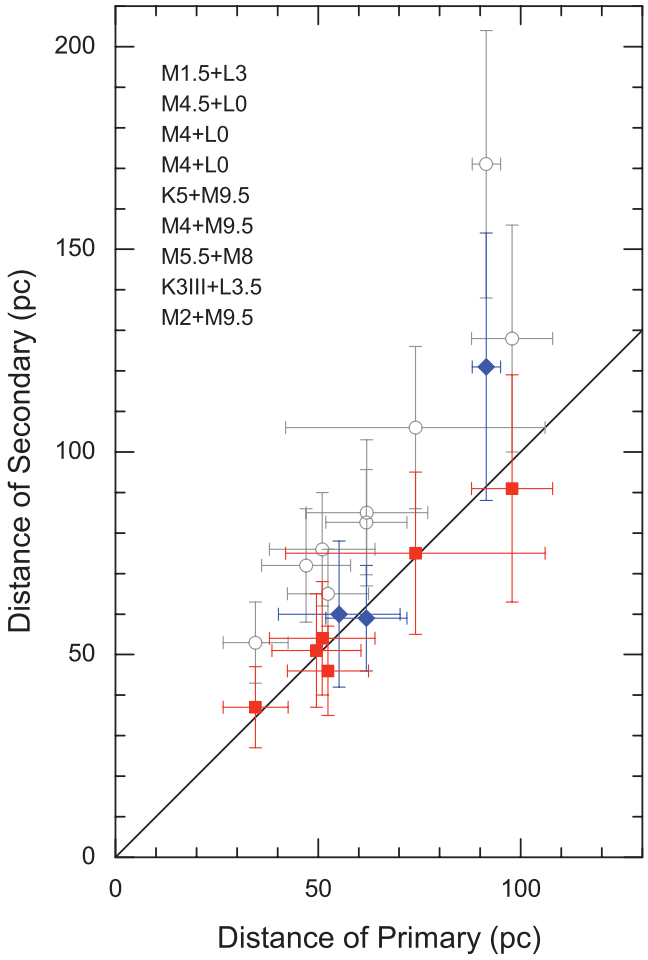

Figure 10. Distances of ultracool dwarfs (from left to right: SDSS 0207, 1304, 1638, 0858, 0953, 0101, 1631, 0832, 0956) and their primary stars. Spectral types of combinations are listed according to the distance of primaries in the top left of the plot. The squares and diamonds indicate the objects with and without SDSS spectra respectively. The open circles show the distances of ultracool dwarfs assumed to be unresolved equal-mass binaries.

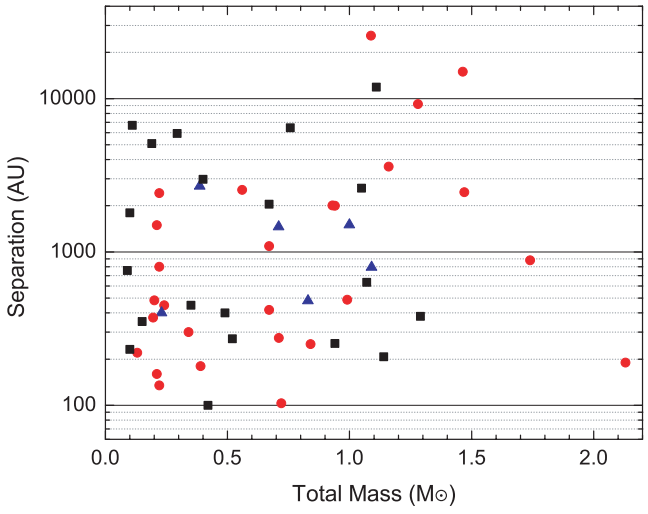

Figure 11. Total mass versus separation for binaries have projected separation larger than 100 au. Squares, circles and triangles are binaries with late M, L and T secondaries.

Table 6. Parameters of η Cancri AB.

Parameter	Adopted Value	Reference/Note
Separation (au)	15019^{+562}_{-522} (164″.16)	This paper
Distance (pc)	$91.5^{+3.5}_{-3.2}$	van Leeuwen (2007)
SP	0.05	This paper
η Cancri A		
Sp. Type	K3III	Perryman et al. (1997)
RA (J2000)	08 32 42.50	SDSS (2004)
Dec. (J2000)	20 26 27.7	SDSS (2004)
V	5.330 ± 0.004	Kharchenko et al. (2004)
$B-V$	1.252 ± 0.002	Perryman et al. (1997)
$V-I$	1.11 ± 0.04	Perryman et al. (1997)
J	3.49 ± 0.30	2MASS
H	2.86 ± 0.21	2MASS
K	2.70 ± 0.32	2MASS
Parallax (mas)	10.93 ± 0.40	van Leeuwen (2007)
μ_{RA} (mas yr^{-1})	-46.33 ± 0.43	van Leeuwen (2007)
μ_{Dec} (mas yr^{-1})	-44.31 ± 0.24	van Leeuwen (2007)
U (km s^{-1})	-27.1	Famaey et al. (2005)
V (km s^{-1})	-24.6	Famaey et al. (2005)
W (km s^{-1})	-10.7	Famaey et al. (2005)
$T_{\rm eff}$ (K)	$4446^{a} \pm 80$	Luck & Heiter (2007) Hekker & Meléndez (2007) Allende Prieto & Lambert (1999)
log (L/L$_\odot$)	1.95 ± 0.06	Luck & Heiter (2007)
Mass (M$_\odot$)	$1.4^{b} \pm 0.2$	Luck & Heiter (2007) Allende Prieto & Lambert (1999)
Radius (R$_\odot$)	$16.0^{c}\ ^{+1.8}_{-1.6}$	This paper
g (cm s^{-2})	2.24 ± 0.09 dex	Luck & Heiter (2007)
[Fe/H]	$0.0^{d} \pm 0.1$	This paper
Age (Gyr)	2.2–6.1	This paper
η Cancri B (SDSS 0832)		
Sp. Type	$L3.5 \pm 1.5^{e}$	This paper
RA (J2000)	08 32 31.87	SDSS (2004)
Dec. (J2000)	20 27 00.0	SDSS (2004)
Dist (pc)	121 ± 33	This paper
Dist.b (pc)	171 ± 33	This paper
μ_{RA} (mas yr^{-1})	-47.4 ± 8.2	This paper
μ_{Dec} (mas yr^{-1})	-38.9 ± 8.2	This paper
r	25.37 ± 0.63	SDSS
i	22.13 ± 0.17	SDSS
z	20.15 ± 0.12	SDSS
Z	19.69 ± 0.09	UKIDSS
Y	18.66 ± 0.05	UKIDSS
J	17.74 ± 0.04	UKIDSS
H	17.16 ± 0.04	UKIDSS
K	16.52 ± 0.04	UKIDSS
Mass ($M_{\rm Jup}$)	63–82	*e*
$T_{\rm eff}$ (K)	1800 ± 150	*e*
g (cm s^{-2})	5.3–5.5 dex	*e*

[a]This is the average $T_{\rm eff}$ of Luck & Heiter (2007), Hekker & Meléndez (2007) and Allende Prieto & Lambert (1999).
[b]This is the average mass of Luck & Heiter (2007) and Allende Prieto & Lambert (1999).
[c]Based on log (L/L$_\odot$) (Luck & Heiter 2007) and $T_{\rm eff}$ (4446 K). Note that the radius given in Allende Prieto & Lambert (1999) is $17.0^{+2.5}_{-2.2}$ R$_\odot$, along with a lower $T_{\rm eff}$ (4365 K).
[d]This is the medium value of Luck & Heiter (2007), Hekker & Meléndez (2007) and Brown et al. (1989).
[e]Based on the Lyon duty model (Chabrier et al. 2000) and Burrows et al. (2006), Burrows et al. (1997) model, assume as a single object at the same distance as η Cancri A.

Table 7. Input and output values from PARAM for η Cancri.

Input value		Output value	
$T_{\rm eff}$	$4388^{a} \pm 80$ K	Age	3.61 ± 1.86 Gyr
[Fe/H]^{b}	0.025 ± 0.100	Mass	1.36 ± 0.23 M$_{\odot}$
V^{b}	5.330 ± 0.004	g	2.16 ± 0.11 dex (cm s^{-2})
Parallax^{b}	10.93 ± 0.40 mas	R	15.4 ± 1.1 R$_{\odot}$
		$B-V$	$1.252^{c} \pm 0.038$

Note: PARAM is a web interface for the Bayesian estimation of stellar parameters, http://stev.oapd.inaf.it/cgi-bin/param (da Silva et al. 2006).
[a]This is an estimated value to obtain the correct $B-V$ value.
[b]Values are from the literature.
[c]This value is equal to the observed value.

In the left-hand plots we indicate with open symbols the locations where the measured values of luminosity and $T_{\rm eff}$ intersect with the evolutionary model tracks. In this way the Girardi et al. (2000) evolutionary models lead to an age constraint of 2.2–6.1 Gyr.

We have also used the Hurley, Pols & Tout (2000) stellar evolution sequence with initial masses 1.2–1.6 M$_{\odot}$ ($\Delta M = 0.05$ M$_{\odot}$) and metallicity [Fe/H] = 0.0 and 0.10. Using the same approach as in Fig. 12, these models give an age range of 2.4–6.6 Gyr for η Cancri A, which is very similar to the result from the Girardi et al. (2000) model. In addition we note that the age estimate from PARAM is also consistent with these values estimated directly from evolutionary tracks. A summary of the properties of η Cancri A is given in Table 6.

6.3 The properties of η Cancri B

6.3.1 As a single ultracool dwarf

We can assume that the distance of η Cancri B is essentially the same as that of η Cancri A. However, since this is a very wide binary system we have increased the uncertainty of the companion distance slightly to account for η Cancri B potentially being ~0.5 pc closer to or further away than the primary along the line of sight. This allows us to place reasonably tight constraints on the absolute brightness of this ultracool dwarf. η Cancri B must have $M_J = 12.93 \pm 0.09$, $M_H = 12.35 \pm 0.09$ and $M_K = 11.72 \pm 0.09$. Using the M_{JHK}–spectral-type relations of Liu et al. (2006), we thus estimate that its spectral type must be L3–4 if it is a single L dwarf. Combining these magnitudes and an age (inferred from η Cancri A), the evolutionary model of Chabrier et al. (2000) predicts that mass = 63–74 $M_{\rm Jup}$, $T_{\rm eff} = 1805 \pm 115$ K and $\log(g/{\rm cm\,s^{-2}}) = 5.31$–5.36. Using an alternative model set (Burrows, Sudarsky & Hubeny 2006) yields a slightly higher mass of 75–82 $M_{\rm Jup}$, and corresponding $T_{\rm eff} = 1800 \pm 150$ K, $\log\,(g/{\rm cm\,s^{-2}}) = 5.38$–5.48.

In Fig. 13 we compare the colour of η Cancri B with our large population of SDSS ultracool dwarfs, and it can be seen that its colours appear somewhat discrepant from those of other early L dwarfs. While it has similar $H-K$ to the bulk population, its $J-K$ colour is only similar to the bluer L dwarfs and its $Y-J$ and $J-H$ colours are significantly bluer than typical ultracool dwarfs of similar spectral type. Theoretical model colour trends suggest that L dwarfs with low metallicity or higher gravity could have bluer near-infrared colours (Burrows et al. 2006). However, the constraints we have placed on the properties of this benchmark object are not consistent with this interpretation, and the colours of η Cancri B are either at odds with the model trends or are indicative of unresolved multiplicity.

6.3.2 As an unresolved binary ultracool dwarf

We investigated the possibility that the colours of η Cancri B may result from unresolved binarity. T dwarfs have slightly bluer $Y-J$ and significantly bluer $J-H$ and $J-K$ than L dwarfs (Knapp et al. 2004; Pinfield et al. 2008). Combining the light of an L and

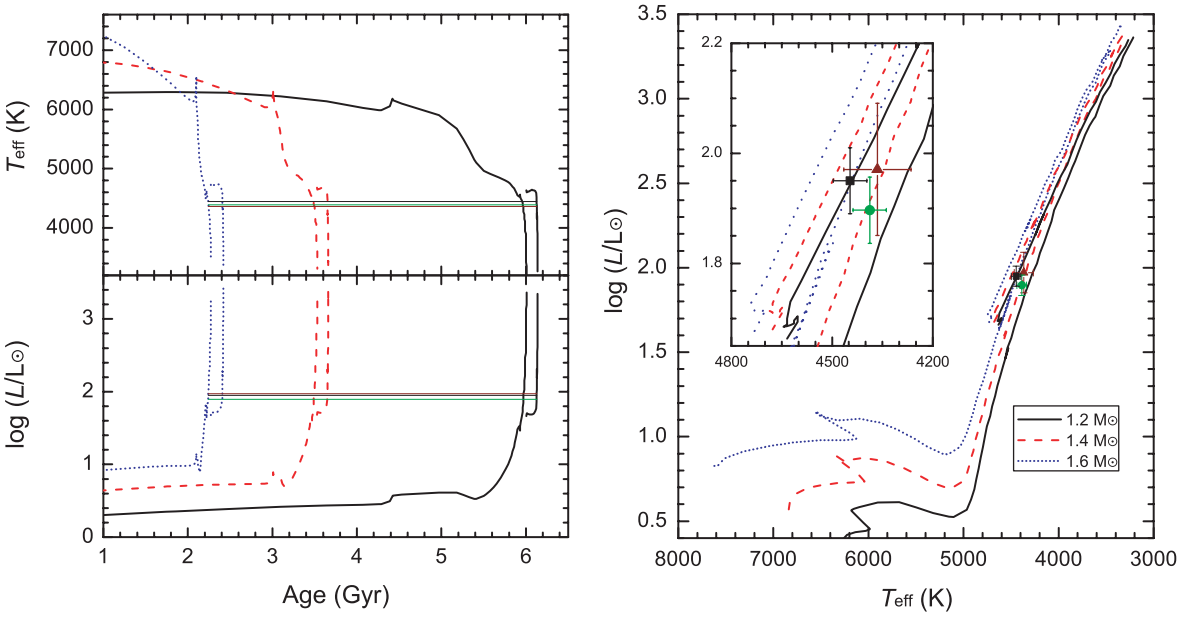

Figure 12. $T_{\rm eff}$ and L evolutionary tracks (Girardi et al. 2000) of solar-metallicity stars with different masses (1.2 M$_{\odot}$, black lines; 1.4 M$_{\odot}$, red dash lines; 1.6 M$_{\odot}$, blue dot lines). The filled square (4446, 1.95) in the right panel represents the average $T_{\rm eff}$ from the literature and L from Luck & Heiter (2007). The filled circle (4388, 1.90) represents the values from PARAM (da Silva et al. 2006). The filled triangle (4365, 1.97) represents the values from Allende Prieto & Lambert (1999). Horizontal lines in the left-hand panel indicate L and $T_{\rm eff}$ values in the same colours as the symbols in the right-hand panel.

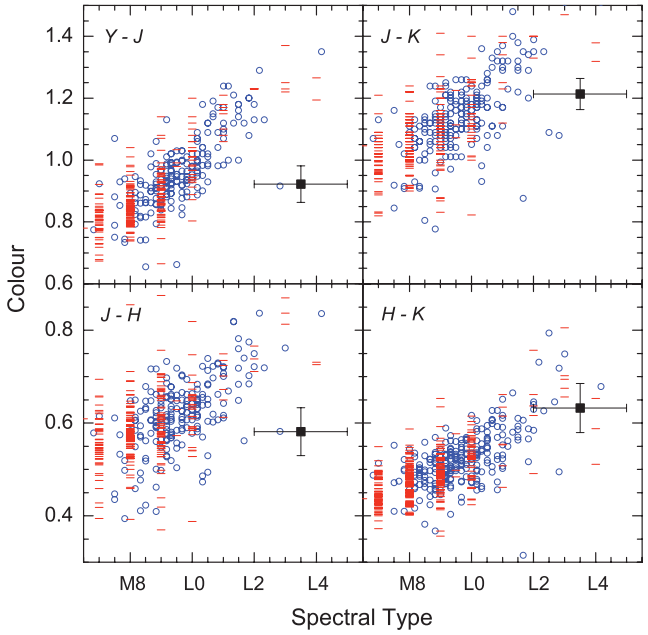

Figure 13. UKIDSS *YJHK* colours of η Cancri B (squares) and ultracool dwarfs with (bars) and without (circles) spectra, as a function of spectral type.

T dwarf could thus result in these colours being bluer than those of a single L dwarf. We experimented by combining the photometric brightnesses of a variety of L and T dwarf combinations, using the spectral type–M_{JHK} polynomial relations from Liu et al. (2006) to provide absolute magnitudes for flux combination. Fig. 14 shows the *JHK* absolute magnitudes and colours of the range of unresolved L–T binaries that we considered. The location of η Cancri B is indicated with its appropriate uncertainties. Considering the full range of colour and magnitude criteria, as well as the intrinsic scatter in the Liu et al. (2006) polynomial fits, we deduce that a combination of an L4 and T4 dwarf at the distance of η Cancri A would have colours and magnitudes reasonably consistent with those of η Cancri B. In this case, the physical parameters of these two unresolved objects (estimated from the same evolutionary models as before) are given in Table 8.

7 SUMMARY AND FUTURE WORK

We have identified 34 new L dwarfs and nine ultracool dwarf + star common proper motion binary systems (TYC 1189 − 1216–1 AB, G 3–40 AB, LP 312–49 AB, LP 548–50 AB, LP 609–3 AB, SDSS J130432.93+090713.7 AB, SDSS J163126.17+294847.1 AB, SDSS J163814.32+321133.5 AB and η Cancri AB). Further observations (parallax, activity and rotation rate) of the K–M dwarf primaries in these systems will provide age (e.g. Faherty et al. 2010) and metallicity (e.g. Johnson & Apps 2009) constraints. η Cancri AB is a K3III + early L system with a projected separation of 15 019 au. η Cancri A has a well-constrained parallax distance, and we use new observations and the latest theory to estimate an age of 2.2–6.1 Gyr and a composition of near-solar for the system. We thus estimate that η Cancri B (as a single object) has mass = 63–82 $M_{\rm Jup}$, $T_{\rm eff}$ = 1800 ± 150 K and $\log(g/{\rm cm\,s^{-2}})$ = 5.3–5.5, based on a range of evolutionary models.

It is unclear at this stage whether η Cancri B is a single L dwarf with unusual colour or an unresolved L + T binary, the components of which have fairly typical colours when compared with the bulk population. Quality optical–infrared spectroscopy would address this issue in more detail, and establish whether the binary explanation remains possible. In addition, adaptive optics observations could resolve the pair if their separation is >0.05–0. arcsec (e.g. LHS4009: Montagnier et al. 2006), corresponding to a separation >5–10 au. If the ultracool dwarf is shown to be single then this would provide a surprising result when compared with the models. We could also establish $T_{\rm eff}$ and log g more robustly by obtaining full optical-to-infrared measurements to constrain the bolometric flux and luminosity (e.g. Burningham et al. 2009). If η Cancri B is a closely separated ultracool dwarf binary system, it might be possible to derive dynamical masses for the components over a time-scale of several years, and thus improve the benchmark quality of this object still further through more direct constraints on its mass and log g. A more detailed examination of the spectral morphology and multiplicity of this benchmark ultracool dwarf will in any event provide rigorous tests for solar-metallicity dusty ultracool atmosphere models.

ACKNOWLEDGMENTS

Funding for the SDSS and SDSS-II has been provided by the Alfred P. Sloan Foundation, the Participating Institutions, the National Science Foundation, the US Department of Energy, the National Aeronautics and Space Administration, the Japanese Monbukagakusho, the Max Planck Society and the Higher Education Funding Council for England. The SDSS Web Site is http://www.sdss.org/. The SDSS is managed by the Astrophysical Research Consortium for the Participating Institutions. The Participating Institutions are the American Museum of Natural History, Astrophysical Institute Potsdam, University of Basel, University of Cambridge, Case Western Reserve University, University of Chicago, Drexel University, Fermilab, the Institute for Advanced Study, the Japan Participation Group, Johns Hopkins University, the Joint Institute for Nuclear Astrophysics, the Kavli Institute for Particle Astrophysics and Cosmology, the Korean Scientist Group, the Chinese Academy of Sciences (LAMOST), Los Alamos National Laboratory, the Max-Planck-Institute for Astronomy (MPIA), the Max-Planck-Institute for Astrophysics (MPA), New Mexico State University, Ohio State University, University of Pittsburgh, University of Portsmouth, Princeton University, the United States Naval Observatory and the University of Washington.

The UKIDSS project is defined in Lawrence et al. (2007). UKIDSS uses the UKIRT Wide Field Camera (WFCAM: Casali et al. 2007) and a photometric system described in Hewett et al. (2006). The pipeline processing and science archive are described in Irwin et al. (in preparation) and Hambly et al. (2008). We have used data from the fourth data release. This publication makes use of data products from the Two-Micron All-Sky Survey. This research has made use of data obtained from the SuperCOSMOS Science Archive, prepared and hosted by the Wide Field Astronomy Unit, Institute for Astronomy, University of Edinburgh, which is funded by the UK Science and Technology Facilities Council.

Based on observations obtained at the Gemini Observatory, which is operated by the Association of Universities for Research in Astronomy, Inc., under a cooperative agreement with the NSF on behalf of the Gemini partnership: the National Science Foundation (United States), the Science and Technology Facilities Council (United Kingdom), the National Research Council (Canada), CONICYT (Chile), the Australian Research Council (Australia), Ministério da Ciência Tecnologia (Brazil) and Ministério da

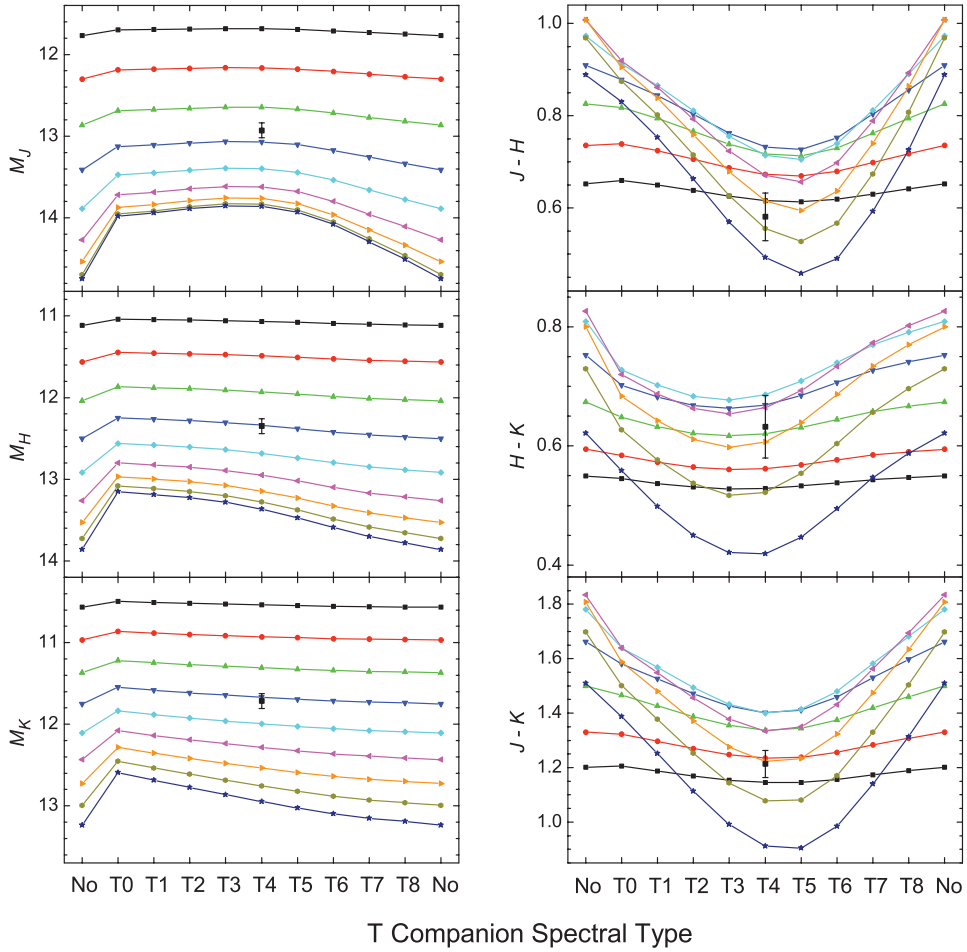

Figure 14. *JHK* absolute magnitudes and colours of unresolved L + T binaries. Different lines represent absolute magnitudes and colours of L dwarf primaries (L1–L9, from top to bottom in the left panel) without or with different T companions (T0–T8). If η Cancri B (square) is actually an unresolved binary, then the constituents would likely be made up of an L4 and a T4 dwarf.

Table 8. Parameters of an L4 and a T4 dwarf from the Lyon group and Burrows group models.

Spectral Type	L4[a]	T4[b]
M_J [c]	13.41 ± 0.37	14.49 ± 0.37
M_H [c]	12.50 ± 0.30	14.46 ± 0.30
M_K [c]	11.75 ± 0.34	14.52 ± 0.34
Mass[d] ($M_{\rm Jup}$)	59−80	40−70
$T_{\rm eff}$ [d] (K)	1675 ± 145	1140 ± 120
g[d] (cm s^{-2})	5.3−5.5 dex	5.1−5.4 dex

[a]Based on dusty model.
[b]Based on dust-free model.
[c]Based on the relationship between spectral types and absolute magnitudes (J and K band) of Liu et al. (2006).
[d]These parameters are for an L4 dwarf and a T4 dwarf at an age of 2.2–6.1 Gyr.

Ciencia, Tecnología e Innovación Productiva (Argentina). Based on observations carried out with the ESO New Technology Telescope (NTT). This paper has used observations made at the Nordic Optical Telescope (NOT), at the Spanish Observatory del Roque de los Muchachos of the Instituto de Astrofísica de Canarias.

This research has made use of the VizieR catalogue access tool, CDS, Strasbourg, France. Research has benefitted from the M, L and T dwarf compendium housed at DwarfArchives.org and maintained by Chris Gelino, Davy Kirkpatrick, and Adam Burgasser. IRAF is distributed by the National Optical Observatory, which is operated by the Association of Universities for Research in Astronomy, Inc., under contract with the National Science Foundation. This research has benefitted from the SpeX Prism Spectral Libraries, maintained by Adam Burgasser at http://www.browndwarfs.org/spexprism. ZengHua Zhang is supported by the University of Hertfordshire Research Studentship. Zhanwen Han is supported by NSFC (grant No. 10821061). CGT is supported by ARC grant DP774000.

REFERENCES

Abazajian K. N. et al., 2009, ApJS, 182, 543
Adelman-McCarthy J. K. et al., 2008, ApJS, 175, 297
Allende Prieto C., Lambert D. L., 1999, A&A, 352, 555
Artigau É., Lafrenière D., Loic A., Doyon R., 2009, ApJ, 692, 149
Bihain G., Rebolo R, Béjar V. J. S., Caballero J. A., Bailer-Jones C. A. L., Mundt R., Acosta-Pulido J. A., Manchado Torres A., 2006, A&A, 458, 805
Billères M., Delfosse X., Beuzit J.-L., Forveille T., Marchal L., Martín E. L., 2005, A&A, 440, L55
Bouvier J. et al., 2008, A&A, 481, 661
Bouy H., Brandner W., Martín E. L., Delfosse X., Allard F., Basri G., 2003, AJ, 126, 1526

Brown J. A., Sneden C., Lambert D. L., Dutchover E. J., 1989, ApJS, 71, 293
Burgasser A. J., McElwain M. W., 2006, AJ, 131, 1007
Burgasser A. J. et al., 2000, ApJ, 531, L57
Burgasser A. J., Kirkpatrick J. D., Lowrance P. J., 2005, AJ, 129, 2849
Burgasser A. J. et al., 2010, ApJ, submitted
Burningham B. et al., 2009, MNRAS, 395, 1237
Burrows A. et al., 1997, ApJ, 491, 856
Burrows A., Sudarsky D., Hubeny I., 2006, ApJ, 640, 1063
Buzzoni B. et al., 1984, ESO Messenger, 38, 9
Caballero J. A., 2007, ApJ, 667, 520
Casali M. et al., 2007, A&A, 467, 777
Casewell S. L., Dobbic P. D., Hodgkin S. T., Moraux E., Jameson R. F., Hambly N. C., Irwin J., Lodieu N., 2007, MNRAS, 378, 1131
Chabrier G., Baraffe I., Allard F., Hauschildt P., 2000, ApJ, 542, 464
Chappelle R. J., Pinfield D. J., Steele I. A., Dobbie P. D., Magazzù A., 2005, MNRAS, 361, 1323
Chauvin G. et al., 2005, A&A, 430, 1027
Chiu K., Fan X., Leggett S. K., Golimowski, D. A., Zheng W., Geballe T. R., Schneider D. P., Brinkmann J., 2006, AJ, 131, 2722
Clarke J. R. A. et al., 2009, MNRAS, 402, 575
Covey K. R. et al., 2007, AJ, 134, 2398
Cossburn M. R., Hodgkin S. T., Jameson R. F., Pinfield D. J., 1997, MNRAS, 288, L23
Cruz K. L., Reid I. N., Liebert J., Kirkpatrick J. D., Lowrance P. J., 2003, AJ, 126, 2421
Cruz K. L. et al., 2007, AJ, 133, 439
Cutri R. M. et al., 2003, The IRSA 2MASS All-Sky Catalog of Point Sources. NASA/IPAC, Pasadena
da Silva L. et al., 2006, A&A, 458, 609
Day-Jones A. C. et al., 2008, MNRAS, 388, 838
Deacon N. R., Hambly N. C., King R. R., McCaughrean M. J., 2009, MNRAS, 394, 857
Delfosse X. et al., 1997, A&A, 327, 25
De Simone R., Wu X., Tremaine S., 2004, MNRAS, 350, 627
Ducourant C. et al., 2006, A&A, 448, 1235
Dupuy T. J., Liu M. C., Ireland M. J., 2009, ApJ, 699, 168
Epchtein N. et al., 1997, ESO Messeager, 87, 27
Faherty J. K., Burgasser A. J., West A. A., Bochanski J. J., Cruz K. L., Shara M. M., Walter F. M., 2010, AJ, 139, 176
Famaey B., Jorissen A., Luri X., Mayor M., Udry S., Dejonghe H., Turon C., 2005, A&A, 430, 165
Fan X. et al., 2000, AJ, 119, 928
García Pérez A. E., Asplund M., Primas F., Nissen P. E., Gustafsson B., 2006, A&A, 451, 621
Geballe T. R. et al., 2002, ApJ, 564, 466
Giclas H. L., Burnham R., Thomas N. G., 1971, Lowell proper motion survey Northern Hemisphere. The G numbered stars. 8991 stars fainter than magnitude 8 with motions $> 0''.26$/year. Lowell Observatory, Flagstaff
Girardi L., Bressan A., Bertelli G., Chiosi C., 2000, A&AS, 141, 371
Gizis J. E., Monet D. G., Reid I. N., Kirkpatrick J. D., Burgasser A. J., 2000, MNRAS, 311, 385
Gizis J. E., Kirkpatrick J. D., Wilson J. C., 2001, AJ, 121, 2185
Golimowski D. A. et al., 2004, AJ, 128, 1733
González Hernández J. I., Bonifacio P., 2009, A&A, 497, 497
Grevesse N., Asplund M., Sauval A. J., 2007, Space Sci. Rev., 130, 105
Gustafsson B., Edvardsson B., Eriksson K., 2008, A&A, 486, 951
Hakkila J., Myers J. M., Stidham B. J., Hartmann D. H., 1997, AJ, 114, 2043
Hambly N. C. et al., 2001, MNRAS, 326, 1279
Hambly N. C. et al., 2008, MNRAS, 384, 637
Hatzes A. P., Guenther E. W., Endl M., Cochran W. D., Döllinger M. P., Bedalov A., 2005, A&A, 437, 743
Hawley S. L. et al., 2002, AJ, 123, 3409
Hekker S., Meléndez J., 2007, A&A, 475, 1003
Hewett P. C., Warren S. J., Leggett S. K., Hodgkin S. T., 2006, MNRAS, 367, 454
Hodapp K. W. et al., 2003, PASP, 115, 1388
Hog E. et al., 2000, A&A, 355, L27
Hogan E., Jameson R. F., Casewell S. L., Osbourne S. L., Hambly N. C., 2008, MNRAS, 388, 495
Hurley J. R., Pols O. R., Tout C. A., 2000, MNRAS, 315, 543
Ivanov G. A., 2008, Kinematika Fiz. Nebesnykh Tel, 24, 480
Jenkins J. et al., 2009, MNRAS, 398, 911
Johnson J. A., Apps K., 2009, ApJ, 699, 933
Kendall T. R., Jones H. R. A., Pinfield D. J., Pokorny R. S., Folkes S., Weights D., Jenkins J. S., Mauron N., 2007, MNRAS, 374, 445
Kharchenko N. V., 2001, Kinematika Fiz. Nebesnykh Tel, 17, 409
Kharchenko N. V. et al., 2004, AN, 325, 740
Kirkpatrick J. D. et al., 1999, ApJ, 519, 802
Kirkpatrick J. D. et al., 2000, AJ, 120, 447
Knapp G. R. et al., 2004, AJ, 127, 3553
Kroupa P., 1995, ApJ, 453, 350
Lawrence A. et al., 2007, MNRAS, 379, 1599
Lépine S., 2005, AJ, 130, 1680
Lépine S., Shara M. M., 2005, AJ, 129, 1483
Liu M. C., Leggett S. K., Golimowski D. A., Chiu K., Fan X., Geballe T. R., Schneider D. P., Brinkmann J., 2006, ApJ, 647, 1393
Liu M. C., Dupuy T. J., Ireland M. J., 2008a, ApJ, 689, 436
Liu Y.-J. et al., 2008b, ApJ, 672, 553
Lovis C., Mayor M., 2007, A&A, 472, 657
Lowrance P. J. et al., 2000, ApJ, 541, 390
Luck R. E., Heiter U., 2007, AJ, 133, 2464
Luhman K. L. et al., 2007, ApJ, 654, 570
Luyten W. J., Hughes H. S., 1980, Proper motion survey with the forty-eight inch Schmidt telescope. LV. First supplement to the NLTT catalogue. Univ. Minnesota, Mineapolis, NM
Magazzù A., Martín E. L., Rebolo R., 1993, ApJ, 404, L17
Magazzù A., Rebolo R., Zapatero Osorio M. R., Rebolo R., García López R. J., 1998, ApJ, 497, L47
Martín E. L., Rebolo R., Zapatero Osorio M. R., 1996, ApJ, 469, 706
Martín E. L., Basri G., Zapatero Osorio M. R., Rebolo R., García Lòpez R. J., 1998, ApJ, 507, L41
Metchev S. A., Hillenbrand L. A., 2006, ApJ, 651, 1166
Monet D. G. et al., 2003, AJ, 125, 984
Montagnier G. et al., 2006, A&A, 460, L19
Mugrauer M., Seifahrt A., Neuhäuser R., 2007, MNRAS, 378, 1328
Neuhäuser R., Guenther E. W., 2004, A&A, 420, 647
Neuhäuser R., Guenther E. W., Wuchterl G., Mugrauer M., Bedalov A., Hauschildt P. H., 2005, A&A, 435, L13
Niedzielski A., Nowak G., Adamów M., Wolszczan A., 2009, ApJ, 707, 768
Phan-Bao N. et al., 2008, MNRAS, 383, 831
Perryman M. A. C. et al., 1997, A&A, 323, L49
Pinfield D. J., Jones H. R. A., Lucas P. W., Kendall T. R., Folkes S. L., Day-Jones A. C., Chappelle R. J., Steele I. A., 2006, MNRAS, 368, 1281
Pinfield D. J. et al., 2008, MNRAS, 390, 304
Radigan J., Lafrenière D., Jayawardhana R., Doyon R., 2008, ApJ, 689, 471
Radigan J., Lafrenière D., Jayawardhana R., Doyon R., 2009, ApJ, 698, 405
Ramírez I., Meléndez J., 2005, ApJ, 626, 465
Rebolo R., Zapatero Osorio M. R. Z., Martín E. L., 1995, Nat, 377, 129
Rebolo R., Zapatero Osorio M. R., Madruga S., Bejar V. J. S., Arribas S., Licandro J., 1998, Sci., 282, 1309
Reid I. N., Walkowicz L. M., 2006, PASP, 118, 671
Reid I. N., Cruz K. L., Kirkpatrick J. D., Allen P. R., Mungall F., Liebert J., Lowrance P., Sweet A., 2008, AJ, 136, 1290
Ribas I., 2003, A&A, 400, 297
Röser S., Schilbach E., Schwan H., Kharchenko N. V., Piskunov A. E., Scholz R.-D., 2008, A&A, 488, 401
Ruiz M. T., Leggett S. K., Allard F., 1997, ApJ, 491, L107
Salim S., Gould A., 2003, ApJ, 582, 1011
Schneider D. P. et al., 2002, AJ, 123, 458
Scholz R. D., McCaughrean M. J., Lodieu N., Kuhlbrodt B., 2003, A&A, 398, L29

Scholz R. D., Lodieu N., McCaughrean M. J., 2004, A&A, 428, L25
Seifahrt A., Guenther E., Neuhäuser R., 2005a, A&A, 440, 967
Seifahrt A., Mugrauer M., Wiese M., Neuhäuser R., Guenther E. W., 2005b, Astron. Nachr., 326, 974
Sheppard S. S., Cushing M. C., 2009, AJ, 137, 304
Skrutskie M. F. et al., 2006, AJ, 131, 1163
Stoughton C. et al., 2002, AJ, 123, 485
Taylor B. J., 2006, AJ, 132, 2453
Tinney C. G., Delfosse X., Forveille T., 1997, ApJ, 490, L95
Tinney C. G., 1998, MNRAS, 296, L42
Tokovinin A., Thomas S., Sterzik M., Udry S., 2006, A&A, 450, 681
van Leeuwen F., 2007, A&A, 474, 653
van Leeuwen F., 2009, A&A, 497, 209
West A. A., Hawley S. L., Bochanski J. J., 2008, AJ, 135, 785
White R. J., Ghez A. M., Reid I. N., Schultz G., 1999, ApJ, 520, 811
Wilson J. C., Kirkpatrick J. D., Gizis J. E., Skrutskie M. F., Monet D. G., Houck J. R., 2001, AJ, 122, 1989
Yi S., Demarque P., Kim Y.-C., Lee Y.-W., Ree C. H., Lejeune T., Barnes S., 2001, ApJS, 136, 417
York D. G. et al., 2000, AJ, 120, 1579
Zacharias N., Monet D. G., Levine S. E., Urban S. E., Gaume R., Wycoff G. L., 2004, American Astron. Soc. Meeting, 205, 4815
Zacharias N. et al., 2009, VizieR Online Data Catalog, 1315
Zapatero Osorio M. R. et al., 1998, in Rebolo R., Martin E. L., Osorio M. R., eds, ASP Conf. Ser. Vol. 134, Brown Dwarfs and Extrasolar Planets. Astron. Soc. Pac., San Francisco, p. 51
Zhang Z. H., Jones H. R. A., Pinfield D. J., Pokorny R. S., Han Z., 2009a, in Zhang S.-N., Li Y., Yu Q., eds, Proc. 10th Asian-Pacific Regional IAU Meeting. China Science & Technology Press, Beijing, p. 191
Zhang Z. H. et al., 2009b, A&A, 497, 619

SUPPORTING INFORMATION

Additional Supporting Information may be found in the online version of this article:

Table S1. 806 ultracool dwarfs from SDSS, 2MASS and UKIDSS.

Please note: Wiley-Blackwell are not responsible for the content or functionality of any supporting materials supplied by the authors. Any queries (other than missing material) should be directed to the corresponding author for the article.

This paper has been typeset from a TEX/LATEX file prepared by the author.

Appendix III

"A spectroscopic and proper motion search of SDSS.
Red cool subdwarfs in binary systems",
Zhang et al. 2013, MNRAS, e-print: astro-ph/1306.3060

Mon. Not. R. Astron. Soc. **000**, 1–25 (2013) Printed 13 June 2013 (MN LATEX style file v2.2)

A spectroscopic and proper motion search of SDSS: Red subdwarfs in binary systems

Z. H. Zhang,[1,2,3⋆] D. J. Pinfield,[1] B. Burningham,[1] H. R. A. Jones,[1] M. C. Gálvez-Ortiz,[4,1] S. Catalán,[1] R. L. Smart,[3] S. Lépine,[5] J. R. A. Clarke,[1,6] Ya. V. Pavlenko,[7,1] D. N. Murray,[1] M. K. Kuznetsov,[7] A. C. Day-Jones,[1] J. Gomes,[1] F. Marocco[1] and B. Sipőcz[1]

[1] *Centre for Astrophysics Research, Science and Technology Research Institute, University of Hertfordshire, Hatfield AL10 9AB*
[2] *Shanghai Astronomical Observatory, Chinese Academy of Sciences, 80 Nandan Road, Shanghai 200030, China*
[3] *Istituto Nazionale di Astrofisica, Osservatorio Astronomico di Torino, Strada Osservatrio 20, 10025 Pino Torinese, Italy*
[4] *Centro de Astrobiología (CSIC-INTA), Ctra. Ajalvir km 4, E-28850 Torrejón de Ardoz, Madrid, Spain*
[5] *Department of Astrophysics, Division of Physical Sciences, American Museum of Natural History, New York, NY 10024, USA*
[6] *Departamento de Física y Astronomía, Universidad de Valparaíso, Av. Gran Bretaña 1111, Casilla 5030, Valparaíso, Chile*
[7] *Main Astronomical Observatory, Academy of Sciences of Ukraine, Golosiiv Woods, Kyiv-127, 03680, Ukraine*

Accepted 2013 June 06. Received 2013 May 15; in original form 2012 August 13

ABSTRACT

Red subdwarfs in binary systems are crucial for both model calibration and spectral classification. We search for red subdwarfs in binary systems from a sample of high proper motion objects with SDSS spectroscopy. We present here discoveries from this search, as well as highlighting several additional objects of interest. We find thirty red subdwarfs in wide binary systems including: two with spectral type of esdM5.5, six companions to white dwarfs and three carbon enhanced red subdwarfs with normal red subdwarf companions. Fifteen red subdwarfs in our sample are partially resolved close binary systems. With this binary sample, we estimate the low limit of the red subdwarf binary fraction of ~ 10 %. We find that the binary fraction goes down with decreasing masses and metallicities of red subdwarfs. A spectroscopic esdK7 subdwarf + white dwarf binary candidate is also reported. Thirty new M subdwarfs have spectral type of $\geqslant$M6 in our sample. We also derive relationships between spectral types and absolute magnitudes in the optical and near-infrared for M- and L- subdwarfs, and we present an M subdwarf sample with measured U, V, W space velocities.

Key words: binaries – subdwarfs – stars: late-type – stars: low-mass – brown dwarfs – stars: carbon – stars: Population II – Galaxy: halo.

1 INTRODUCTION

Dwarf stars with sub-solar metallicity are bluer than solar abundance dwarfs or main sequence stars of the equivalence mass. They lie below the main sequence in the Hertzsprung-Russell diagram and appear less luminous than main sequence stars. These objects were thus called "subdwarfs" by Kuiper (1939). Evolving subdwarfs are referred to as cool subdwarfs to provide distinction from hot subdwarfs, a different class of objects (e.g. Han, Podsiadlowski, & Lynas-Gray 2007). Cool dwarfs and cool subdwarfs are observationally and kinematically distinct, and were separated into Population I and II categories, respectively by Baade (1944). Population I and II are associated with the Galactic disk and spheroid respectively. Roman (1950, 1952, 1954) find that the old, high-velocity Population II stars were also metal deficient.

Red dwarfs are low-mass and relatively cool stars on the main sequence with spectral types of late-type K and M, masses between $\sim 0.6\ M_{\odot}$ and $\sim 0.08\ M_{\odot}$, and surface effective temperatures between ~ 4000 K and ~ 2300 K (Kaltenegger & Traub 2009). Red dwarfs are the most common type of star both in the Milky Way (Kirkpatrick et al. 2012) and other galaxies (van Dokkum & Conroy 2010). The spectra of red dwarfs are dominated by molecular absorption bands of metal oxides and hydrides. TiO and CaH near 7000 Å are the most prominent bands (Bessell 1982, 1991). Red subdwarfs (RSDs) are the subsolar counterparts

⋆ E-mail: zenghuazhang@gmail.com

of red dwarfs by chemical abundance. RSDs are significantly rarer than red dwarfs. The Kapteyn's Star (sdM1 type) is the only cool subdwarf among the sample of eight parsecs within the Sun which contains more than 244 known stars and brown dwarfs, including 157 M dwarfs (Kirkpatrick et al. 2012). The known sample of late-type M subdwarfs is significantly smaller than that of early-type M subdwarfs because they are fainter and have lower space density according to the halo mass function (e.g. Chabrier 2003). Late-type M subdwarfs have the most complex stellar atmospheres because they are ultracool cool and have large-scale variation of chemical abundance and gravity.

Although RSDs are less luminous than F, G and mid-K subdwarfs, they are numerous and have more notable spectral features caused by chemical abundance and gravity, thus they are better targets for observational and theoretical studies. It is difficult to distinguish F, G and mid-K subdwarfs from normal dwarf stars of the same spectral type using their optical spectra because they are featureless. Dwarfs and subdwarfs with spectral types of late-type K and M, however, have a number of very different spectral features. Model atmospheres also suggest that optical spectra of M subdwarfs are dramatically affected by metallicity variations. It is thus possible to use low-resolution spectroscopy for exploring effective temperature, metallicity and gravity effects on the spectra of these cool objects (Allard & Hauschildt 1995).

Classification and characterization of M subdwarfs is a rapidly evolving field (Gizis 1997; Lépine, Rich, & Shara 2007; Jao et al. 2008; Dhital et al. 2012). M subdwarfs are classified into three metal classes: subdwarf (sdM), extreme subdwarf (esdM) and ultra subdwarf (usdM) based on the ratio of TiO to CaH indices (Lépine, Rich, & Shara 2007). CaH and TiO indices are easy to measure and sensitive to temperature and metallicity. However, Jao et al. (2008) found that the CaH and TiO indices are affected in complicated ways by combinations of temperatures, metallicities and gravities of RSDs. Model spectra show that the TiO5 index is more sensitive to metallicity while the CaH2 and CaH3 indices are more sensitive to gravity. This suggests that the effect of gravity, which was previously ignored, should be considered in the classification of M subdwarfs. An ideal testbed for the impact of gravity on spectra of M subdwarfs is binary systems with two M subdwarfs which share the same age and metallicity. With the same effect on spectra from metallicity, it is possible to measure the difference of gravity on the broad indices of CaH2, CaH3 and TiO5.

M subdwarfs in binary systems are the key for both model calibration, and spectral classification and characterization. Discovery of a sample of RSD binary systems is therefore crucial. In this paper we present the discovery of 45 RSD binary systems from the Sloan Digital Sky Survey (SDSS, York et al. 2000) and the UKIRT Infrared Deep Sky Survey (UKIDSS, Lawrence et al. 2007). At least one companion in each system is confirmed as an RSD with SDSS spectra. The selection and classification processes of our RSD sample is presented in Section 2. The identification of RSD binary systems is presented in Section 3. Section 4 presents further discussion of RSD binary systems of particular interests. Summary & conclusions is described in Section 5.

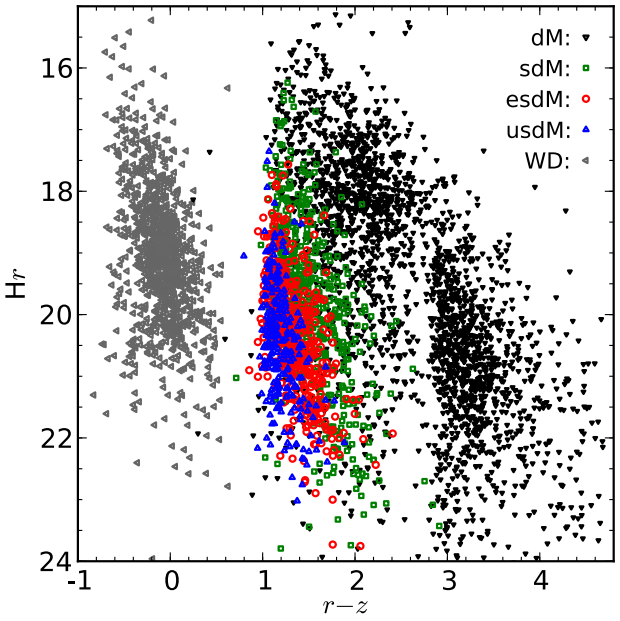

Figure 1. SDSS r band reduced PMs H_r and $r-z$ colour of our PM selected objects. Symbols in the figure are black down-pointing triangles: M dwarfs; green squares: sdMs; red circles: esdMs; blue up-pointing triangles: usdMs; grey left-pointing triangles: WDs.

2 THE SDSS SAMPLE

The eighth data release (DR8) of SDSS includes 14555 deg^2 of imaging data, and 9274 deg^2 of spectroscopic data. There are over 1.84 million spectra in total, including 0.6 million stars, 0.13 million quasars and 0.95 million galaxies (Aihara et al. 2011). The SDSS DR8 also includes proper motions (PMs) for objects derived by combining SDSS astrometry with USNO-B positions, re-calibrated against SDSS. The errors of PMs are typically less than 10 mas·yr^{-1} (Munn et al. 2004).

2.1 Selection

We selected our candidates using SDSS CasJobs by combining the spectroscopic and PM catalogues. We required PM greater than 100 mas·yr^{-1}. No photometric criteria were applied but spectral observations for red dwarfs in SDSS is limited to $r \sim 21.0, i \sim 20$ and $z \sim 19.5$. Most of RSDs in SDSS spectroscopic database are at distances of 200 $\sim$ 400 parsecs. Objects with tangential velocity of 200 km·s^{-1} at a distance of 400 parsecs (or 100 km·s^{-1} and 200 parsecs) will have PMs higher than 100 mas·yr^{-1}. A PM cut of 100 mas·yr^{-1} allows a good balance in order to select most late-type K, early-type M and almost all mid-late type M subdwarfs in the combined SDSS PM + spectroscopic catalogues while minimising the contamination by dwarf stars. Since not all spectra in DR7 are reproduced in DR8 we applied our search to both data releases finding 7499 and 8445 spectra respectively. There were 9146 spectra in total for 8236 objects (some objects had more than one spectrum).

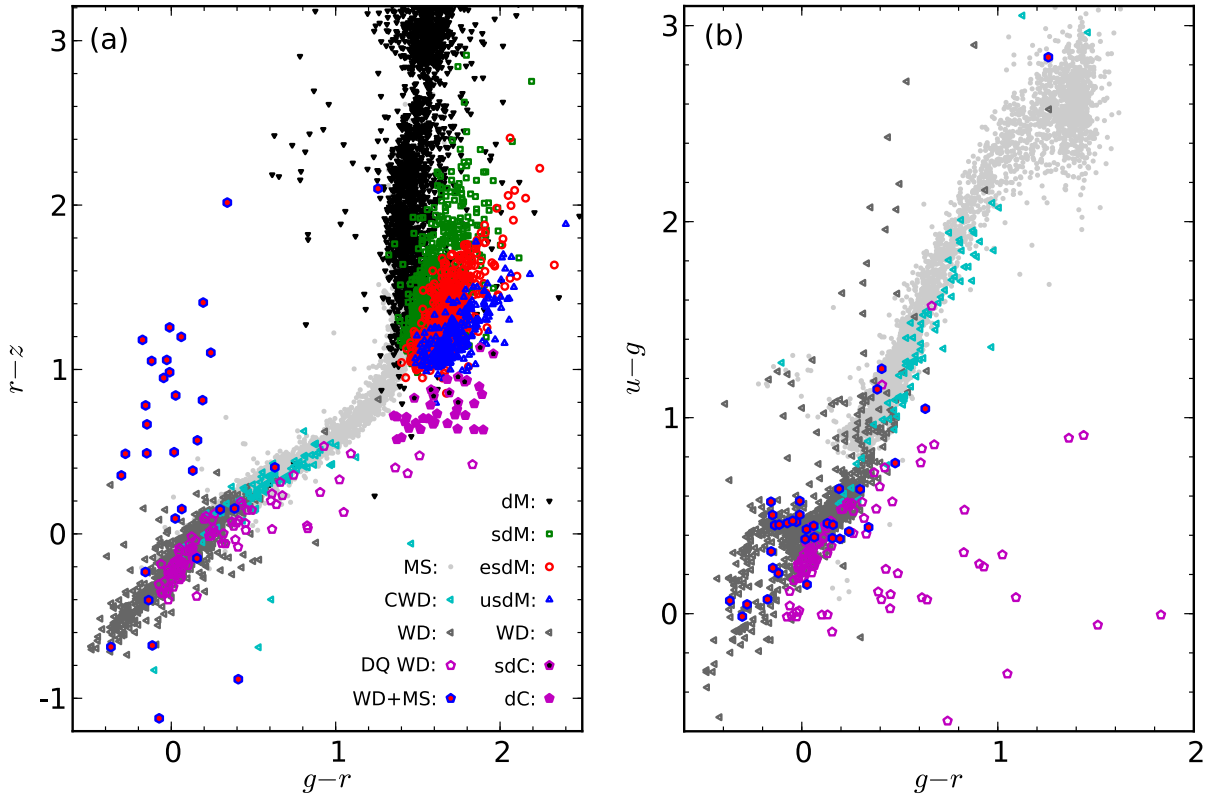

Figure 2. $g-r$ versus $r-z$ (left) and $g-r$ versus $r-z$ (right) colours of our PM selected sample. Symbols in the figure are black down-pointing triangles: dMs; green squares: sdMs; red circles: esdMs; blue up-pointing triangles: usdMs; filled magenta pentagons: carbon dwarfs (dC); magenta pentagons filled with black: carbon subdwarfs (sdC); open magenta pentagons: DQ WDs; blue hexagon filled with red: WD + MS binaries; dark grey left-pointing triangles: WDs; cyan left-pointing: cool WDs (CWD); light grey dots: 3028 point sources (MS) with $17 < r < 18$ selected from 10 square degrees of SDSS.

2.2 Spectral Classification

SDSS spectra were reduced and classified with the idlspec2d code by SDSS (Aihara et al. 2011). For 8236 objects in our sample, 5687 were classified as stars, 1558 as galaxies and 348 as QSOs, 643 of them were not classified. Not all objects in the sample are classified by SDSS. RSDs are generally classified as stars or galaxies in some cases.

To pick out and classify RSDs in our sample properly we used a K and M subdwarf classification code developed by Lépine, Rich, & Shara (2007). We ran the code on the spectra of all 8236 objects to identify subdwarfs and assign their spectral types. The code classified objects into nine groups: dM (2455), dK (80), sdM (689), sdK (326), esdM (483), esdK (189), usdM (256), usdK (189), and unclassified (3442). We found many objects, originally classified as galaxies by SDSS, that were re-classified as sdK, esdK or usdK.

We inspected the spectra by eye in each group to ensure the correct classification was applied in each case. We found 2004 galaxies with false PMs were selected into our sample: 383 of them were classified as stars (mostly late-type K subdwarfs). We found that 463 late-type K subdwarfs and 1363 M subdwarfs survived the eyeball check. Fifty four objects were classified as sdM but removed from our subdwarf sample because they do not have typical halo kinematics. Figure 1 shows reduced PMs and $r-z$ colour of these objects. Three sequences from left to right show the location of white dwarfs (WDs), M subdwarfs and M dwarfs. Figure 2 shows two colour diagrams of $g-r$ versus $r-z$ and $g-r$ versus $r-z$ of the sample. The whole RSD catalogue is available on line. The WD sample will be discussed in a future paper.

2.3 The M subdwarf sample

2.3.1 Spectroscopic distances

M, L and T dwarfs are known in relatively large numbers in the solar neighbourhood and have recently improved absolute magnitude versus spectral type relationships (e.g. Faherty et al. 2012; Dupuy & Liu 2012). M- and L- subdwarfs are much less numerous in nearby space and their absolute magnitude and spectral type relationships have not been well constrained. To estimate distances of our M subdwarfs we determined relationships between spectral types and absolute magnitudes ($M_{r,i,z,J,H,Ks}$) based on SDSS and

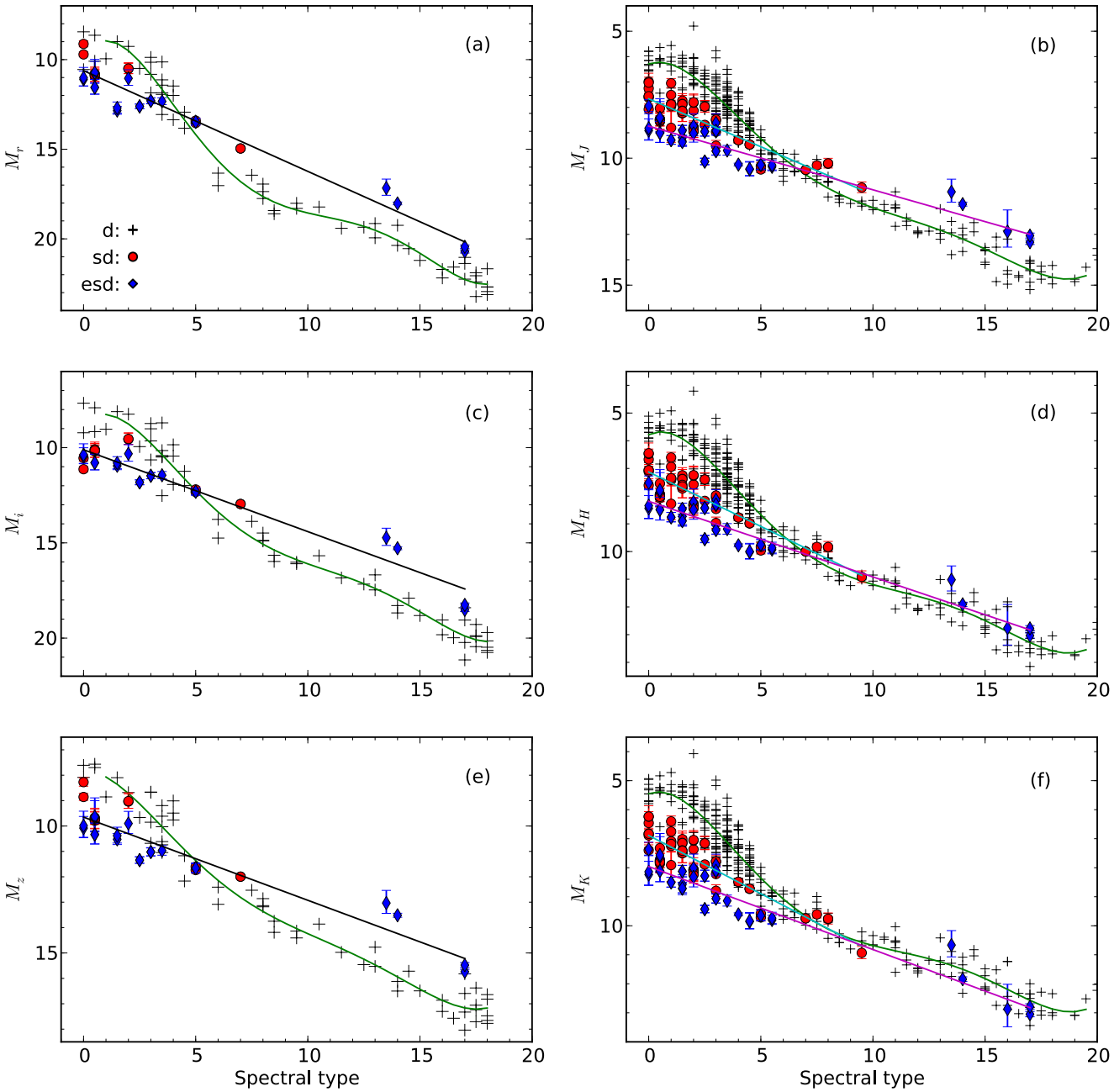

Figure 3. Spectral type and absolute magnitude relationships of dwarfs (black pluses), subdwarfs (red dots) and extreme subdwarfs (blue diamonds). M0 = 0, M5 = 5, L0 = 10, L5 = 15. Green and black lines on the left panels are best fits of dwarfs and all subdwarfs respectively. Green, cyan and magenta lines on the right panels are best fits of dwarfs, subdwarfs and extreme subdwarfs respectively. M- and L- subdwarfs with two independent parallax measurements are plotted twice.

2MASS filters. We collected a sample of M- and L- dwarfs[1] and subdwarfs[2] with parallax distances from the literature.

[1] References of parallax distances for M- and L- dwarfs: Gliese & Jahreiß (1991); Perryman et al. (1997); Gizis (1997); Dahn et al. (2002); Vrba et al. (2004); Costa et al. (2005, 2006); Jao et al. (2005, 2011); Henry et al. (2006); Lépine et al. (2009); Smart et al. (2010); Riedel et al. (2010); Andrei et al. (2011); Faherty et al. (2012).

[2] See table 1 for references of parallax distances of M- and L- subdwarfs.

Figure 3 shows spectral type - absolute magnitude relationships of M and L types of dwarfs and subdwarfs. The parallax sample of available M subdwarfs is classified under the system of Gizis (1997) which has three metal classes: dM, sdM and esdM. M subdwarfs with metal class of usdM (see Fig. 3 of Lépine, Rich, & Shara 2007) are included in the esdM metal class of Gizis (1997). Table 1 shows parallax measurements of M- and L- subdwarfs used in Figure 3. We fitted $M_{r,i,z}$ of M- and L- subdwarfs and extreme subdwarfs together with straight lines. We fitted $M_{J,H,Ks}$ of M

Table 1. K7, M and L subdwarfs with parallax measurements

Name	2MASS	SpT	Ref1	π (mas)	Ref2	π (mas)	Ref3
LP 406−47	J01002474+1711272	sdM5	13	15.7±1.2	8	15.7±1.1	15
G 003−036	J02025226+0542205	sdM0	8	35.9±3.1	8	32.38±5.09	16
LHS 164	J03014052−3457548	sdK7	11	19.16±1.55	11		
G 038−001	J03285302+3722579	sdK7	8	35.3±3.1	8	39.32±2.24	16
GJ 1062	J03381558−1129102	sdM2.5	8	64.8±2.5	8		
G 079−059	J03422933+1231368	sdM1.5	8	45.1±6.6	8	45.1±7.8	9
WT0135	J04112712−4418097	sdM3	11	39.04±2.42	11		
Kapteyn's	J05114046−4501051	sdM1	8	258.3±6.5	8	255.66±0.91	16
G 099−033	J05480018+0822142	sdM0	8	18.8±2.9	8	19.3±3.1	15
G 105−023	J06140146+1509570	sdM2	8	30.6±3.0	8	30.1±3.1	15
G 251−044	J07432434+7248500	sdK7	8	18.7±1.8	8	18.2±2.8	15
LHS 272	J09434633−1747066	sdM3	8	73.95±1.18	11		
SSSPM 1013−1356	J10130734−1356204	sdM9.5	6	20.28±1.96	14		
SCR1107−4135	J11075597−4135529	sdM0.5	11	14.79±1.18	11		
LHS 300AB	J11111376−4105326	sdM0:	11	33.03±1.36	11		
G 176−040	J11324528+4359444	sdM0.5	8	18.3±2.7	8	17.9±3.3	15
Ross 451	J11402025+6715349	sdM0	8	32.7±2.5	8	42.79±2.70	16
LHS 318	J11565479+2639586	sdM2:	11	18.76±2.32	11		
G 011−035	J12023365+0825505	sdM2	8	26.0±3.4	8	25.8±3.6	12
LHS 326	J12242688−0443361	sdM3	11	20.39±1.94	11		
LHS 2734A	J13251422−2127120	sdK7	11	3.94±1.19	11		
LHS 2734B	J13251572−2128176	sdM1	11	3.94±1.19	11		
LSR 1425+7102	J14250510+7102097	sdM8	3	12.19±1.07	14	12.27±0.45	
LP 440−52	J14390030+1839385	sdM7	8	28.4±0.8	8	28.4±0.7	15
G 137−008	J15281403+1643109	sdK7	8	18.7±3.4	8	10±5	10
LHS 406	J15431836−2015310	sdM2	11	46.73±1.17	11		
LP 803−27	J15454034−2036157	sdM5	8	31.5±2	8	33.5±2.0	15
G 138−059	J16420431+1025583	sdM2	8	26.1±4.7	8	26±6	10
LHS 440	J17182561−4326373	sdM1	11	36.40±1.22	11		
G 021−023	J18413636+0055145	sdK7	8	36.2±2	8	30.63±3.76	16
LP 141−1	J18455236+5227400	sdM4.5	8	50.1±1.3	8	50.1±2.5	9
SCR1916−3638	J19164658−3638040	sdM3	11	14.78±1.37	11		
LP 869−24	J19442199−2230534	sdM4	8	17.7±0.8	8	17.7±0.8	15
LP 753−21	J19451476−0917581	sdM2.5	8	6.7±0.7	8	6.7±0.7	15
G 142−052	J19464860+1204580	sdM1	8	22.4±2.3	8	21.7±2.7	15
Gl 781	J20050227+5426037	sdM1.5	8	60.3±1.7	8	63.17±3.82	16
G 210−019	J20272905+3559245	sdM1.5	8	21.1±3.6	8	20.4±4.2	15
LSR 2036+5059	J20362165+5100051	sdM7.5	3	21.60±1.26	14		
LHS 3620	J21042537−2752453	sdM2	11	12.88±1.40	11		
Wo 9722	J21075543+5943198	sdM1.5	8	41.9±2.2	8	40±3	10
LHS 518	J22202698−2421500	sdM1	11	15.92±1.31	11		
LHS 521	J22275918−3009324	sdM0.5	11	18.46±1.07	11		
G 128−034	J23082608+3140240	sdM0.5	8	22.7±2.5	8	22.4±3.0	15

subdwarfs and M0-L7 extreme subdwafs with straight lines separately. The differences in absolute magnitudes between esdM and usdM subdwarfs of the same subtype are smaller than the fitting errors.

Table 2 and 3 show the coefficients of polynomial fits of the SDSS and 2MASS magnitudes as a function of spectral type for the M- and L- subdwarfs and dwarfs plotted in Figure 3. Table 4 shows average absolute magnitudes in 2MASS J, H, Ks bands for K7 subdwarfs in Table 3 and 2. Early-type M subdwarfs are fainter than the same subtype dwarfs in optical bands and even more so in near-infrared bands. It is clear that esdMs are fainter than sdMs, and sdMs are fainter than dMs for $\leqslant$M5 types. However, late-type M- and L- subdwarfs appear to be brighter than normal dwarfs with the same subtypes for $M_{r,i,z,J}$, and similar to that of dwarfs for $M_{H,Ks}$. The H_2 collision-induced absorption (Saumon et al. 1994) becomes stronger as metallicity goes down and suppresses the H and Ks band flux, thus the near infrared spectra become bluer. While the dust cloud delays the suppressing of spectra below 1 μm (Witte, Helling, & Hauschildt 2009). From Figure 3 we can see ultracool subdwarfs may not be a suitable name for metal-deficient ultracool dwarfs because they are not less luminous than the same subtype ultracool dwarfs. "Purple dwarfs" might be a sensible name for such bluish and very-red ultracool dwarfs with subsolar abundance.

2.3.2 Space motions

We estimated distances of our M dwarf and subdwarf samples based on spectral type - absolute magnitude relationships derived in Section 2.3.1. For objects detected in 2MASS we used the mean value of distances estimated with

Table 1. continued.

Name	2MASS	SpT	Ref1	π (mas)	Ref2	π (mas)	Ref3
G 004−029	J02341234+1745527	esdM3	17	27.3±4.2	15		
G 075−047	J02524557+0155501	esdM2	17	25.3±5	15		
G 005−022	J03132412+1849390	esdK7	8	30.9±2.3	8		
G 095−059	J03501388+4325407	esdM0	8	23.4±2.5	8		
G 007−017	J04013654+1843423	esdM0.5	8	16.7±4.6	8	16.2±4.7	15
LP 302−31	J04305244+2812001	esdM1	8	10.2±0.8	8	10.2±0.8	15
LP 417−42	J05103896+1924078	esdM5.5	8	13.4±1.2	8	13.8±1.0	15
LP 417−44	J05195663+2010545	esdM4.5	8	10.4±1.3	8	10.3±1.3	15
2MASS 0532+8246	J05325346+8246465	esdL7	2,1	42.28±1.76	14	37.5±1.7	2
2MASS 0616−6407	J06164006−6407194	esdL6	4,1	19.85±6.45	7		
LSR0627+0616	J06273330+0616591	esdM1.5	11	16.43±1.25	11		
LP 484−6	J08012900+1043041	esdM2.5	8	12.9±0.8	8	12.9±0.7	15
SDSS J1256−0224	J12563716−0224522	esdL3.5	3,1	11.10±2.28	14		
G 165−047	J14065553+3836577	esdM1.5	8	37.4±3.7	8		
LP 857−48	J14313832−2525328	esdM4	8	41.7±1	15		
LP 502−32	J15202946+1434391	esdM5	8	8.9±0.8	8	8.9±0.7	15
2MASS 1626+3925	J16262034+3925190	esdL4	3,1	29.85±1.08	14		
LP 686−36	J16595712−0333136	esdM0.5	8	6.4±1.2	8	6.4±1.2	15
LP 139−14	J17395137+5127176	esdM3.5	8	10.3±0.9	8		
LP 24−219	J18215294+7709303	esdM2.5	8	10.4±0.9	8	10.4±0.9	15
LP 515−3	J20190458+1235056	esdM0	8	18.9±3.6	8	18.1±4.2	12
LP 695−96	J20253705−0612366	esdM3	8	8.3±0.6	8	8.4±0.6	15
LP 757−13	J21073416−1326557	esdM1.5	8	8.8±0.8	8	8.8±0.8	15
G 018−051	J22284904+0548128	esdK7	8	26.8±2.1	8	21±3	10
LSPM J2321+4704	J23212321+4704382	esdM2	18	10.34±1.77	19		

References. 1: Zhang et al. (2013); 2: Burgasser et al. (2008); 3: Burgasser et al. (2009); 4: Cushing et al. (2009); 5: Dahn et al. (2008); 6: Faherty et al. (2009); 7: Faherty et al. (2012); 8: Gizis (1997); 9: Gliese & Jahreiß (1991); 10: Harrington & Dahn (1980); 11: Jao et al. (2011); 12: Jenkins (1952); 13: Kirkpatrick et al. (2010); 14: Schilbach, Röser, & Scholz (2009); 15: van Altena, Lee, & Hoffleit (1995); 16: van Leeuwen (2007); 17: Woolf, Lépine, & Wallerstein (2009); 18: Lépine, Rich, & Shara (2003a); 19: Gatewood & Coban (2009).

Table 3. Coefficients of polynomial fits to magnitudes versus spectral types of M- and L- dwarfs

$M_{\rm abs}$	c_0	c_1	c_2	c_3	c_4	c_5	RMS (mag)
M_r	9.8326	-1.8452	1.1111	-1.5169E-1	8.4503E-3	-1.6751E-4	0.71
M_i	8.6772	-1.0400	7.1114E-1	-9.6139E-2	5.3482E-3	-1.0634E-4	0.70
M_z	7.8303	-4.7257E-2	3.3379E-1	-4.9888e-2	2.9652E-3	-6.2600E-5	0.60
M_J	6.2826	-2.9785E-1	3.6508E-1	-4.9840E-2	2.7283E-3	-5.3057E-5	0.52
M_H	5.7798	-3.9566E-1	4.0397E-1	-5.5512E-2	3.0343E-3	-5.8608E-5	0.54
M_{Ks}	5.4490	-3.0303E-1	3.7299E-1	-5.2136E-2	2.8626E-3	-5.5258E-5	0.53

Note. Coefficients of fifth-order polynomial fits of the SDSS, 2MASS absolute magnitudes as a function of spectral types for M0-L8 dwarfs in Figure 3. The fits are defined as

$$M_{\rm abs} = \sum_{i=0}^{5} c_i \times (SpT)^i$$

where SpT = 1 for M1, SpT = 5 for M5, SpT = 10 for L0, SpT = 15 for L5. Optical spectral types are applied to fits of SDSS r, i, z magnitudes. Near-infrared spectral types are applied to fits of 2MASS J, H, Ks magnitudes. RMS errors are indicated in the last column. The fits are applicable from M1 to L8 for $M_{r,i,z}$ and from M1 to L9 for $M_{J,H,Ks}$.

spectral type versus $M_{J,H,Ks}$ relationships, since they have smaller root-mean-square errors than the optical bands (usdMs are treated as esdMs). For objects not detected in 2MASS or which have no errors for J, H, Ks band magnitudes, we estimated their distances with spectral type versus $M_{r,i,z}$ relationships, and the mean value of three distances for each object is adopted as a final distance.

Stellar Doppler shifts are computed using the ELODIE library (Prugniel & Soubiran 2001) spectra as templates with the SDSS pipeline (Adelman-McCarthy et al. 2008; Aihara et al. 2011). These Doppler shifts represent the best estimate of the radial velocity of the star. Figure 4 shows the normalized radial velocity and error distribution of dMs, sdMs, esdMs and usdMs. The full width at half maximum (FWHM) of the best Gaussian fits for dMs, sdMs, esdMs and usdMs are 85.71, 257.54, 296.54 and 303.11 km·s^{-1} respectively. The M subdwarfs velocities are larger than that of M dwarfs, which is consistent with these M subdwarfs be-

Table 2. Coefficients of polynomial fits to magnitudes versus spectral types of M- and L- subdwarfs

$M_{\rm abs}$	c_0	c_1	RMS (mag)	SpT Range
M_r	10.6168	0.5619	0.66	e/sdM0-e/sdL7
M_i	10.1092	0.4300	0.62	e/sdM0-e/sdL7
M_z	9.6501	0.3275	0.60	e/sdM0-e/sdL7
M_J	7.6626	0.3773	0.45	sdM0-sdM9.5
M_J	8.7385	0.2507	0.42	esdM0-esdL7
M_H	7.1279	0.3928	0.46	sdM0-sdM9.5
M_H	8.1861	0.2731	0.43	esdM0-esdL7
M_{Ks}	6.8886	0.4013	0.45	sdM0-sdM9.5
M_{Ks}	7.9591	0.2860	0.47	esdM0-esdL7

Note. Coefficients of first-order polynomial fits of the SDSS, 2MASS absolute magnitudes ($M_{\rm abs}$) as a function of spectral types (SpT) for M0-L7 subdwarfs in Figure 3. The fits are defined as $M_{\rm abs} = c_0 + c_1 \times {\rm SpT}$ where SpT = 0 for M0, SpT = 5 for M5, SpT = 10 for L0, SpT = 15 for L5. RMS errors and applicable ranges of spectral types are indicated in the last two columns.

Table 4. Absolute magnitudes of K7 type subdwarfs

$M_{\rm abs}$	sdK7	esdK7
M_J	6.99±0.47	8.62±0.38
M_H	6.41±0.48	8.14±0.38
M_K	6.24±0.49	7.96±0.38

ing members of the Galactic halo; while the M dwarfs derive from the Galactic disk.

With PMs and radial velocities from SDSS and spectroscopic distances estimated from Session 2.3.1, we calculated the *U, V, W* space velocities of our M subdwarfs. Figure 5 shows the space velocities in *V* - *U* and *V* - *W* spaces. Figure 6 shows distributions of U, V, W Galactic velocities for dMs, sdMs, esdMs and usdMs. The lack of objects around $U \sim 0$ km·s^{-1} reflects the fact that only objects with PMs higher than 100 mas·yr^{-1} are selected in our sample, thus some distant early-type M subdwarfs are missed. The *V* space velocity distributions of dMs, sdMs, esdMs and usdMs have their maxima at −34.64, −168.09, −206.08 and −237.19 km·s^{-1}, and we find FWHM of 67.95, 172.43, 171.65 and 257.59 km·s^{-1} respectively, assuming a Gaussian distribution. The *V* velocity distribution of M dwarfs can not be fitted well with a single Gaussian line (Figure 6). It appears that some of the M dwarfs (∼18%) have halo-like velocities ($V < -100$ km·s^{-1}). A single Gaussian also can not fit the distribution of *W* velocity (17% have $W > 50$ km·s^{-1} or $W < -80$ km·s^{-1}). This means a fraction of M dwarfs have halo like kinematics. There are also some M subdwarfs which have disk kinematics in the original sample. The study by Spagna et al. (2010) based on FGK stars shows that the metallicity tail of the thick disk population goes down to [m/H]∼ −1.2. Halo and disk populations have overlaps in metallicity and kinematics. Thus if a star has either metallicity as low as [M/H] ∼ −1.2 or halo-like kinematics, this does not always mean it is belongs to the Population II.

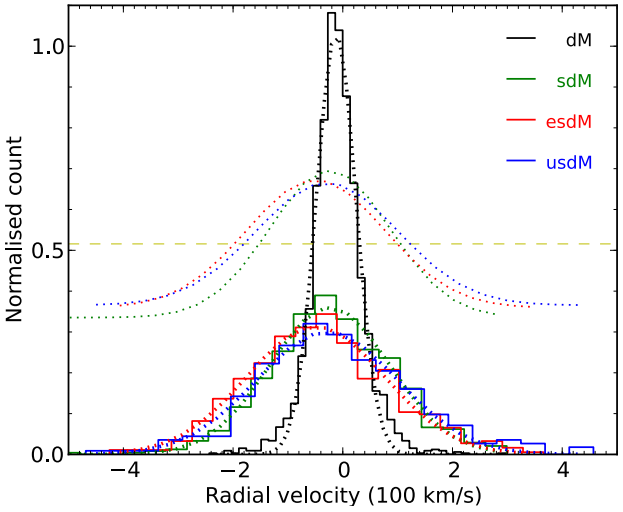

Figure 4. Radial velocity and error distribution of dMs (black), sdMs (green), esdMs (red) and usdMs (blue). All distributions are normalized so that the area, e.g. the sample for each class, is equal to one. Dotted lines are best Gaussian fits. A yellow dashed line shows the half maximum of dMs fit. Additional fit lines of sdMs, esdMs and usdMs are also plotted and shifted to the yellow line by their half maximum. Typical errors of radial velocities are 3-10 km·s^{-1}.

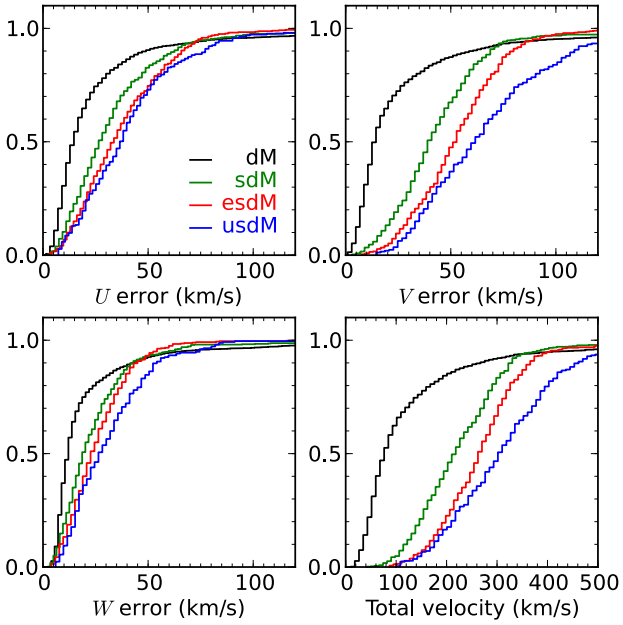

Figure 7. Cumulative histograms of errors of U, V, W Galactic velocities and total space velocity for dM, sdM, esdM and usdM dwarfs (from top left to bottom right).

2.3.3 New late-type M subdwarfs

Cool subdwarfs with spectral types of late-type M and L are referred to as ultracool subdwarfs (UCSD, e.g. Burgasser et al. 2009) following the definition of ultracool dwarfs (UCDs; e.g. Kirkpatrick, Henry, & Irwin 1997). UCSDs are important for our understanding of metal-poor ultracool atmospheres. UCSDs exhibit complex spectra domi-

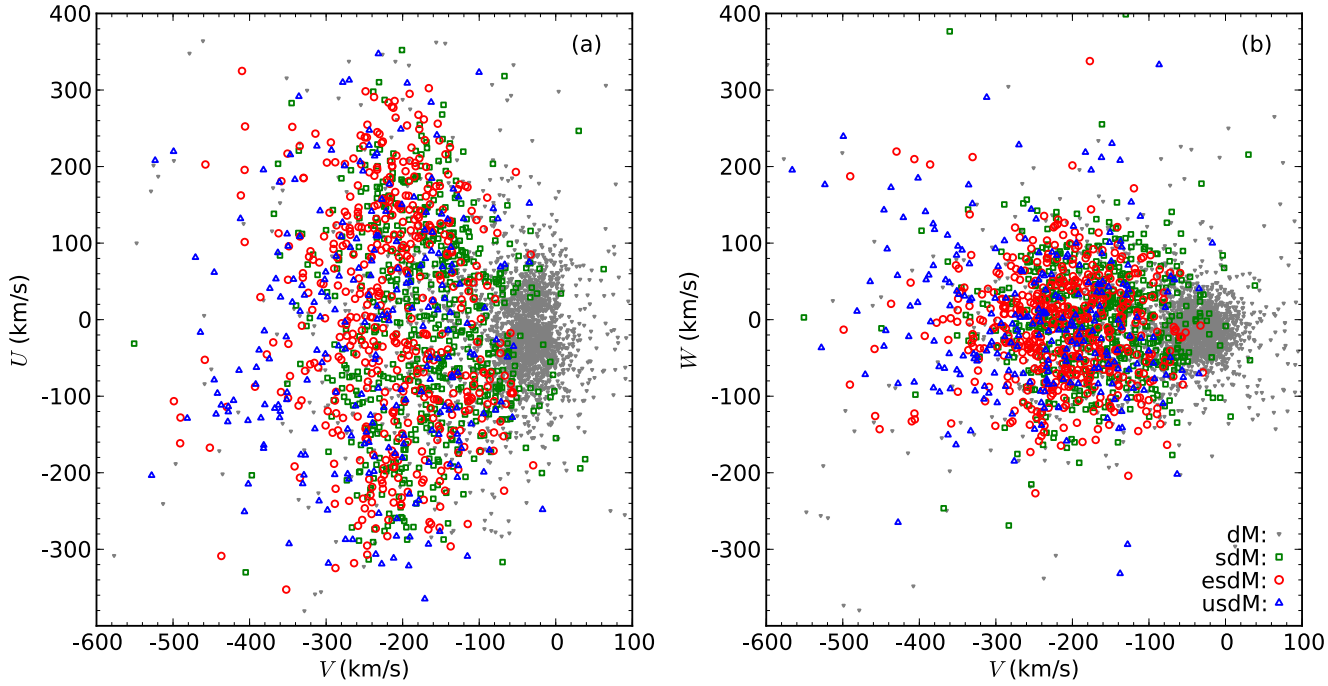

Figure 5. U, V, W Galactic velocities of dM (grey down-pointing triangles), sdM (green squares), esdM (red circles) and usdM (blue up-pointing triangles) dwarfs. Note that U is positive towards the Galactic anti centre.

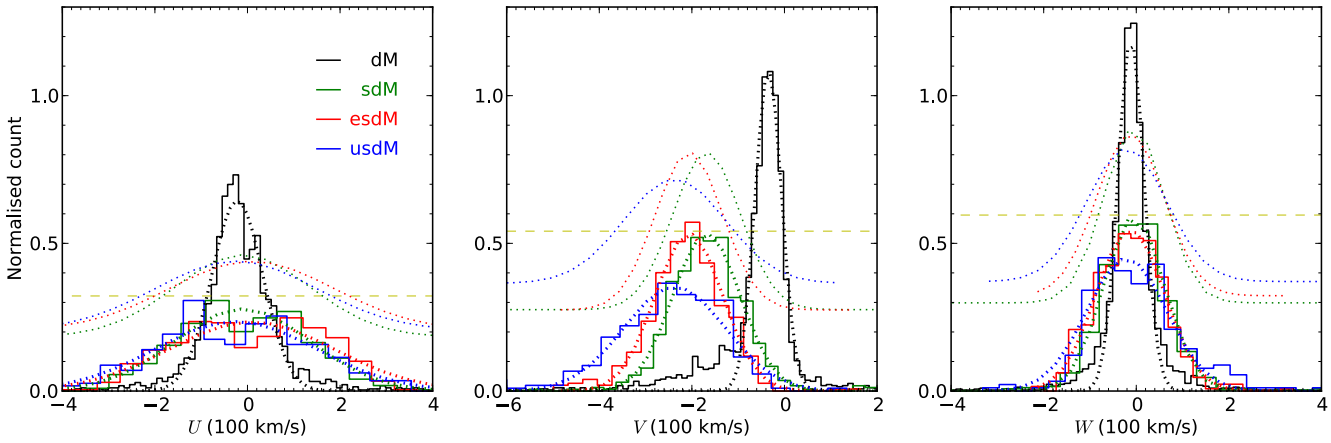

Figure 6. Histograms of U, V, W Galactic velocities for dM, sdM, esdM and usdM dwarfs. All distributions are normalized so that the area, e.g. the sample for each class, is equal to one. Dotted lines are best gaussian fits. A yellow dashed line show the half maximum of dMs fit. Additional fit lines of sdMs, esdMs and usdMs are also plotted and shifted to the yellow line by their half maximum.

nated by molecular absorption bands and metal lines. Spectra of UCSDs are affected by their low effective temperature, subsolar abundance and gravity in a complicated way. Current atmospheric models do not reproduce observed spectra of UCSDs (Burgasser, Cruz, & Kirkpatrick 2007). UCSDs with different properties ($T_{\rm eff}$, [M/H], gravity, multiplicity) are very useful to test and calibrate models of ultracool atmospheres (Burrows et al. 2001; Marley et al. 2002; Helling et al. 2008; Witte, Helling, & Hauschildt 2009) and low-mass stellar evolution scenarios (Baraffe et al. 1997, 2003; Montalbán, D'Antona, & Mazzitelli 2000).

To date, there have been only about 80 UCSDs discovered Gizis (1997); Gizis & Harvin (2006); Schweitzer et al. (1999); Lépine, Shara, & Rich (2003b); Lépine, Rich, & Shara (2003c); Lépine, Shara, & Rich (2004); Lépine, Rich, & Shara (2007); Lépine & Scholz (2008); Burgasser et al. (2003); Burgasser (2004); Burgasser & Kirkpatrick (2006); Burgasser, Cruz, & Kirkpatrick (2007); Scholz et al. (2004); Scholz, Lodieu, & McCaughrean (2004); Marshall (2008); Jao et al. (2008); Sivarani et al. (2009); Cushing et al. (2009); Lodieu et al. (2010, 2012); Kirkpatrick et al. (2010). Forty two subdwarfs in our sample have spectral types of $\geqslant$M6 , twelve of which are known $\geqslant$M7 (Lépine & Scholz 2008), 30 of which are new $\geqslant$M6 including nine M6.5-M7.5. Table 5 shows photometry and PMs of these 30 new $\geqslant$M6 subdwarfs. Figure 8 shows spec-

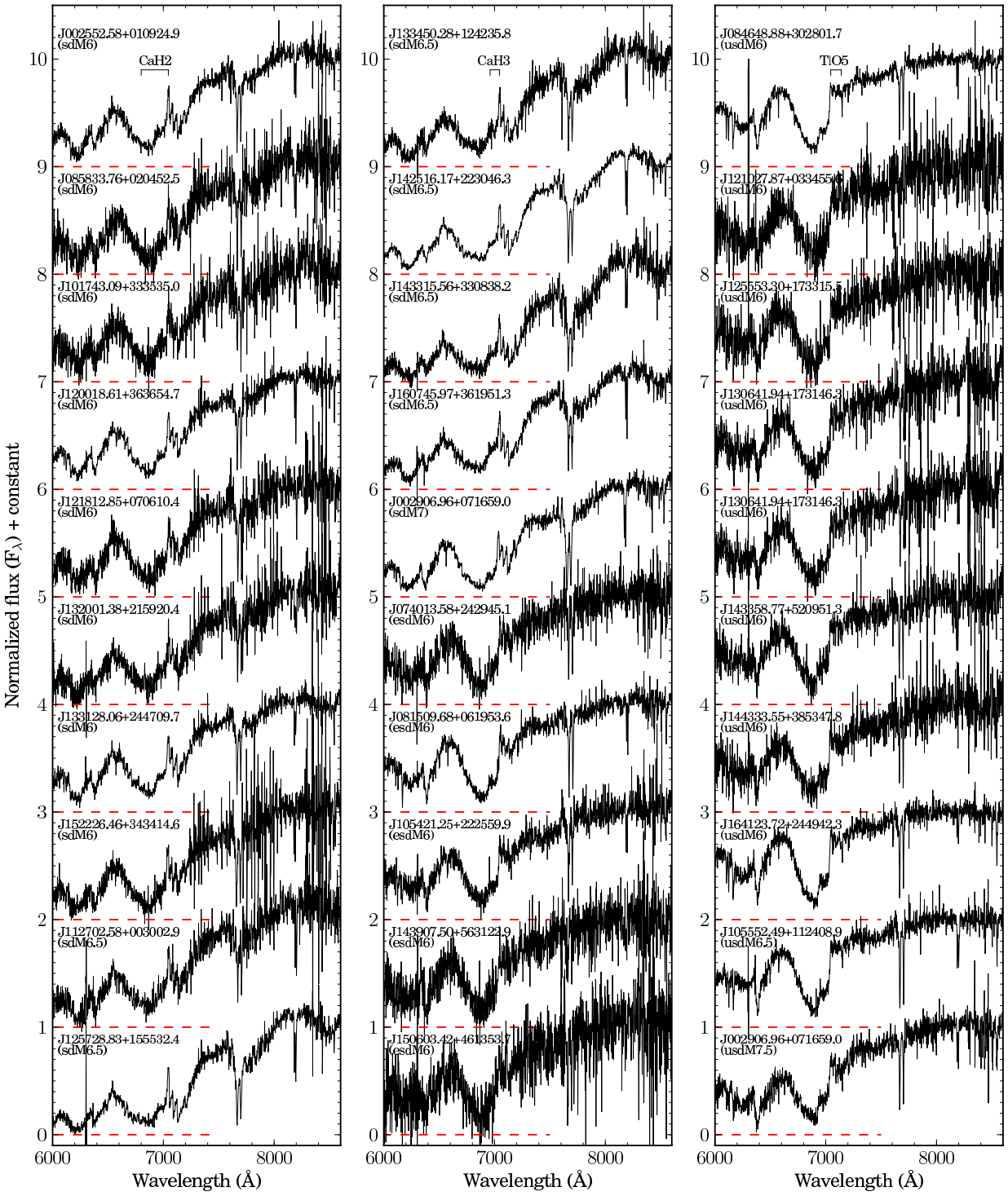

Figure 8. SDSS optical spectra of 30 RSDs with spectral types of ⩾sdM6, ⩾esdM6 and ⩾usdM6. The SDSS name and spectral type are indicated above each spectrum. Absorption bands of CaH2, CaH3 and TiO5 are also indicated above top spectra. All spectra are normalized at 8000 Å.

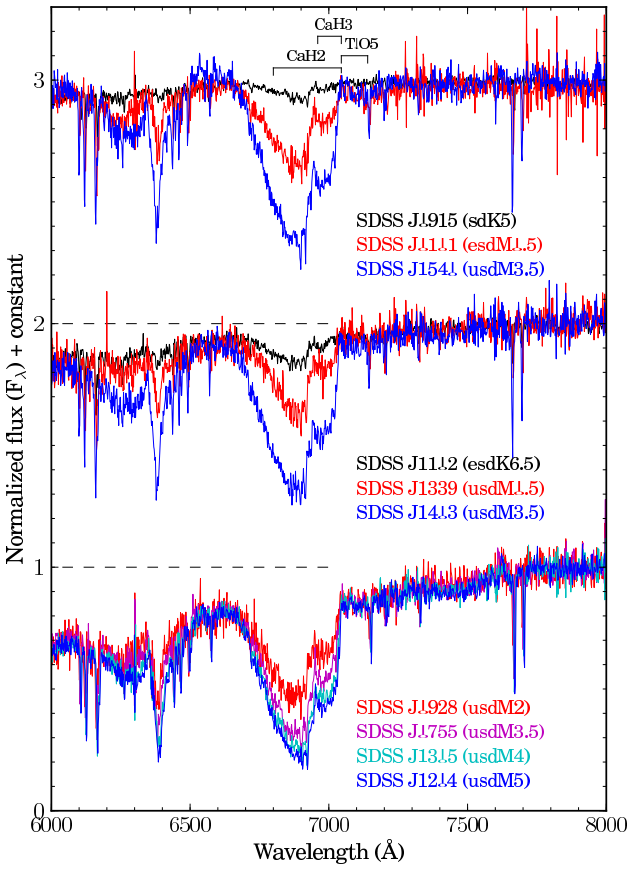

Figure 9. SDSS spectra of RSDs with different gravities. Subtypes indicated in the plot are flawed for high gravity subdwarfs. Small shifts between lines of different spectra along wavelength are due to different high radial velocities. All spectra are normalized at 8000 Å.

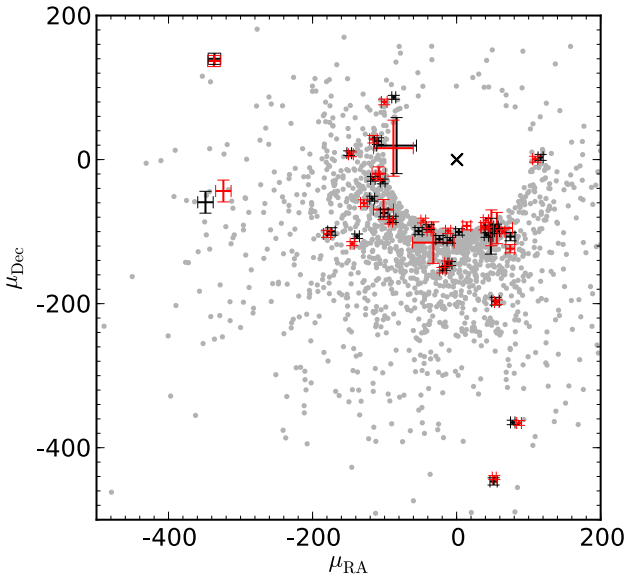

Figure 10. Thirty subdwarf common PM pairs. Companions in each binary are plotted in black and red error bars. A multiplication symbol indicates the location of (0, 0). Light grey dots are RSDs in our sample.

tral sequences of these ⩾sdM6, ⩾esdM6 and ⩾usdM6 subdwarfs. Spectral types are assigned according to a metallicity index $\zeta_{TiO/CaH}$ defined by absorption bands of CaH2, CaH3 and TiO5 (Lépine, Rich, & Shara 2007). From these spectra we can see that both CaH and TiO bands are sensitive to effective temperature, but that the TiO bands are more sensitive to metallicity compared to CaH bands. Spectral types of these late-type M subdwarfs have uncertainties of 0.5-1.0 because some spectra do not have a very high signal-to-noise ratio. The actual uncertainty of the spectral type classification could be larger because the effects of gravity are not included in the $\zeta_{TiO/CaH}$ index. In some extreme cases, gravity could changes the $\zeta_{TiO/CaH}$ index by an equivalent of three subtypes. We will discuss the impact of gravity on the spectra of M subdwarfs in Section 2.3.4.

2.3.4 High gravity M ultra subdwarfs

During our visual inspection of M subdwarf spectra we found some M subdwarfs that have very strong CaH bands, and appear up to three subtypes later than normal M subdwarfs with the same overall profile. The CaH and TiO indices are used to assign spectral types and metal class for M subdwarfs (Gizis 1997; Lépine, Rich, & Shara 2007). Gravity is not considered in the classification of M subdwarfs. The study by Jao et al. (2008) based on Gaia model grids (Brott & Hauschildt 2005) suggests that CaH and TiO absorption bands are both good indicators of effective temperature. The TiO is more sensitive to metallicity changes compared to CaH. The CaH is very sensitive to gravity changes but the TiO does not appear to be sensitive to gravity at all. Jao et al. (2008) also suggests that overall spectral profiles could be used as a major indicator of effective temperature. In this system, spectra with similar overall profiles and TiO indices would have similar effective temperatures and metallicities, and the variation of CaH indices would represents gravity changes.

We inspected all subdwarf spectra for unusual, relative CaH strength and found a large variation of the depth of CaH bands among M subdwarfs with the same overall profile and depth of TiO band. Figure 9 shows SDSS spectra of M subdwarfs with different gravity features. Spectra of M subdwarfs with normal gravity are over plotted for comparison: SDSS J091559.72+290817.4 (SDSS J0915; sdK5), SDSS J010131.32−002325.6 (SDSS J0101; esdM0.5), SDSS J110252.67+274203.7 (SDSS J1102; esdK6.5), SDSS J133945.66+134747.3 (SDSS J1339; usdM0.5), SDSS J092833.78+425428.8 (SDSS J0928; usdM2). Each set of spectra in Figure 9 have similar overall profile and depth of TiO band but have very different depths of CaH bands which are indicators of gravity. They are classified as different spectral types and metallicity classes according to the classification system of Lépine, Rich, & Shara (2007) as indicated in Figure 9. We note, however, that spectral types of these unusual M subdwarfs as they stand are flawed since they do not take account of the high-gravity of these sources. They should have similar subtypes as normal M subdwarf spectra (SDSS J0101, SDSS J1339, SDSS J0928) over plotted with them in Figure 9, e.g. spectral type of SDSS J1204 should be an usdM2 rather than usdM5. Table 6 shows SDSS

Table 5. 30 new sbudwarfs with spectral types of M6 and later

SDSS Name	SDSS g	SDSS r	SDSS i	SDSS z	$\mu_{\rm RA}$(mas/yr)	$\mu_{\rm Dec}$(mas/yr)	SpT
J002552.58+010924.9	21.06±0.03	19.30±0.02	17.83±0.02	17.06±0.02	159.34±5.13	-195.61±5.13	sdM6
J002906.96+071659.0	21.31±0.04	19.24±0.02	17.62±0.02	16.85±0.02	185.85±4.60	-176.32±4.60	sdM7
J013346.24+132822.4	20.82±0.04	18.96±0.02	17.82±0.02	17.19±0.02	80.02±4.70	-296.67±4.70	usdM7.5
J074013.58+242945.1	22.15±0.08	20.18±0.03	19.09±0.02	18.55±0.05	-119.28±5.29	-115.95±5.29	esdM6
J081509.68+061953.6	21.42±0.04	19.34±0.02	18.10±0.02	17.43±0.02	41.59±3.09	-251.88±3.09	esdM6
J084648.88+302801.7	20.52±0.03	18.51±0.02	17.48±0.01	16.83±0.02	-26.22±4.34	-375.02±4.34	usdM6
J085833.76+020452.5	22.02±0.09	20.40±0.03	19.03±0.02	18.20±0.03	96.82±3.90	-226.60±3.90	sdM6
J101743.09+333535.0	22.44±0.10	20.45±0.03	19.15±0.02	18.47±0.04	-109.52±5.29	-243.27±5.29	sdM6
J105421.25+222559.9	22.17±0.07	20.16±0.03	19.03±0.02	18.40±0.03	-201.90±17.37	-310.00±17.37	esdM6
J105552.49+112408.9	21.08±0.04	19.01±0.02	17.93±0.02	17.33±0.02	-232.08±4.53	-20.84±4.53	usdM6.5
J112702.58+003002.9	21.71±0.06	19.91±0.02	18.48±0.02	17.67±0.02	-67.31±8.09	-174.90±8.09	sdM6.5
J120018.61+363654.7	20.94±0.04	18.98±0.02	17.61±0.01	16.83±0.02	-314.66±3.28	-197.36±3.28	sdM6
J121027.87+033455.6	22.27±0.10	20.30±0.03	19.36±0.02	18.89±0.05	137.05±6.09	132.79±6.09	usdM6
J121812.85+070610.4	22.07±0.06	20.24±0.03	18.93±0.02	18.18±0.02	-343.08±5.20	-44.55±5.20	sdM6
J125553.30+173315.5	22.62±0.09	20.53±0.03	19.56±0.02	19.03±0.04	4.21±3.66	-153.31±3.66	usdM6
J125728.83+155532.4	21.45±0.05	19.65±0.02	17.75±0.01	16.74±0.02	157.97±13.22	-546.98±13.22	sdM6.5
J130641.94+173146.3	22.33±0.07	20.32±0.03	19.37±0.02	18.78±0.04	-177.61±4.51	-55.11±4.51	usdM6
J132001.38+215920.4	22.19±0.08	20.45±0.03	18.97±0.03	18.35±0.03	-157.81±5.39	-100.18±5.39	sdM6
J133128.06+244709.7	20.70±0.03	18.93±0.02	17.56±0.02	16.90±0.02	-489.51±13.24	-231.33±13.24	sdM6
J133450.28+124235.8	21.65±0.05	19.85±0.03	18.25±0.02	17.41±0.02	-79.76±4.86	-79.06±4.86	sdM6.5
J142516.17+223046.3	20.60±0.03	18.81±0.02	17.07±0.01	16.19±0.02	-243.34±3.14	-88.49±3.14	sdM6.5
J143315.56+330838.2	22.20±0.08	20.46±0.03	18.55±0.01	17.62±0.02	-73.11±4.96	-327.09±4.96	sdM6.5
J143358.77+520951.3	22.12±0.08	19.94±0.02	18.94±0.02	18.36±0.03	-157.79±5.31	-128.54±5.31	usdM6
J143907.50+563122.9	22.83±0.23	20.50±0.04	19.37±0.03	18.86±0.05	-97.47±5.77	-115.19±5.77	esdM6
J144333.55+385347.8	22.13±0.08	20.10±0.03	19.05±0.02	18.49±0.03	-153.15±4.65	-191.93±4.65	usdM6
J150603.42+461353.7	22.21±0.09	20.33±0.03	19.30±0.02	18.67±0.04	-120.98±5.68	-49.45±5.68	esdM6
J152226.46+343414.6	21.85±0.05	20.05±0.02	18.56±0.02	17.78±0.02	-166.36±4.76	-117.88±4.76	sdM6
J153647.08+025501.5	22.09±0.09	20.12±0.03	19.07±0.02	18.48±0.04	-192.88±5.33	-42.51±5.33	esdM6
J160745.97+361951.3	21.11±0.04	19.40±0.02	17.80±0.01	17.00±0.02	44.95±4.23	-136.49±4.23	sdM6.5
J164123.72+244942.3	20.33±0.02	18.31±0.01	17.23±0.02	16.61±0.02	-630.32±15.91	-177.37±15.91	usdM6

photometry, PMs and spectral types of these five high gravity M ultra subdwarfs.

We only found such large variation of CaH band in our usdM subdwarf sample. The TiO band in spectra of usdM subdwarfs is very weak and barely visible, thus has large measurement errors. If strengthening CaH bands in these five usdM subdwarfs does not represent high gravity, it probably indicates low metallicity beyond normal usdM subdwarfs.

2.3.5 Carbon subdwarfs

Dahn et al. (1977) identified the first dwarf carbon star G 77-61 (LHS 1555), and hypothesized that this object was in fact a double star. The primary ejected carbon material onto the surface of its lower mass companion during its giant branch phase, and then evolves to become a cool WD and is much fainter than the carbon dwarf secondary (e.g. Steinhardt & Sasselov 2005). Radial velocity variations proved this hypothesis of an unseen component in G 77-61 (Dearborn et al. 1986). The U, V, W space motion (Dahn et al. 1977) and spectrum fits (Gass, Wehrse, & Liebert 1988; Plez & Cohen 2005) of G 77-61 indicate that it is a low metallicity object of the Galactic halo.

Carbon dwarfs are rare objects compared to normal red dwarfs, with only about 120 published (e.g. Margon et al. 2002; Lowrance et al. 2003; Downes et al. 2004). The metal-poor carbon dwarfs have features of both carbon dwarfs and RSDs, and have not been distinguished from carbon dwarfs as a new population.

Five cool carbon dwarfs with strong CaH indices were noticed by Margon et al. (2002). They argue that CaH indices present in these stars may be an effective low-resolution luminosity indicator. However, it may be more natural to explain the presence of CaH indices with low metallicity. Strong CaH and weak TiO indices are main features of late-type K and M subdwarfs. These carbon-enriched metal-deficient objects could be called "carbon subdwarfs" because they have features of both cool subdwarfs and carbon dwarfs (see Section 4.3 for further discussion). Nine late-type K and M type carbon subdwarfs have been identified in our sample. Five mid K type carbon subdwarf candidates are also identified. A table of photometry and PMs of these carbon subdwarfs and 22 cool carbon dwarfs is available online.

3 NEW BINARY SYSTEMS

We used three different methods to identify subdwarf binary systems with different separations.

3.1 Wide common PM binaries

Common PM is one of the most useful indicators of wide binary systems (> 100 au). Many ultracool dwarf binary systems have been successfully identified by this method (e.g.

Table 6. Five M ultra subdwarfs with high gravity

SDSS Name	SDSS g	SDSS r	SDSS i	SDSS z	$\mu_{\rm RA}$(mas/yr)	$\mu_{\rm Dec}$(mas/yr)	SpT[a]
J075526.13+482837.3	19.71±0.02	17.86±0.02	17.11±0.02	16.62±0.02	244.13±3.25	−284.59±3.25	usdM3.5 (2.0)
J120426.90+132923.3	19.34±0.03	17.40±0.02	16.55±0.02	16.06±0.02	109.01±3.05	−384.54±3.05	usdM5.0 (2.0)
J130509.05+641753.2	19.75±0.02	17.83±0.02	16.95±0.01	16.48±0.02	−202.49±3.33	−251.65±3.33	usdM4.0 (2.0)
J140305.50+282424.4	19.48±0.02	17.63±0.02	16.77±0.01	16.33±0.02	−235.77±2.82	−328.94±2.82	usdM3.5 (0.5)
J154041.61+265812.0	18.60±0.02	16.78±0.01	15.95±0.01	15.48±0.01	−784.14±2.63	−120.55±2.63	usdM3.5 (0.0)

[a] Spectral types listed in the table are based on the classification system of Lépine, Rich, & Shara (2007) which has not consideration of gravity effects, thus are flawed for these high gravity objects. More practicable subtypes of these high gravity M subdwarfs are indicated in brackets after their spectral types.

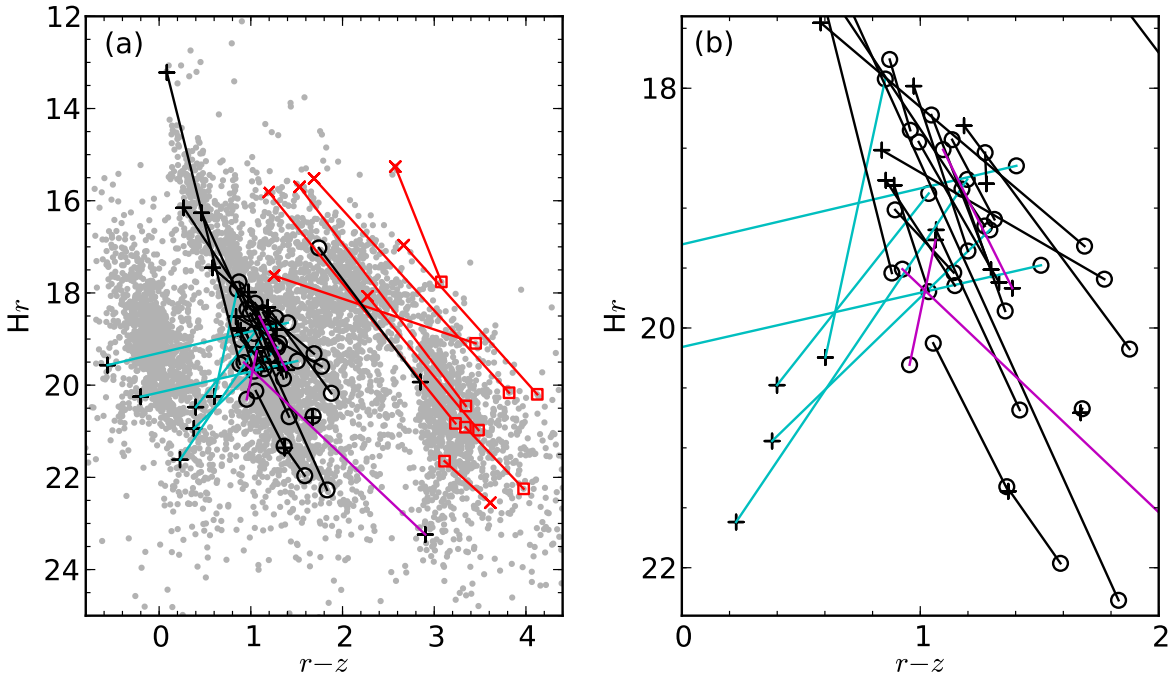

Figure 11. Reduced PMs and $r-z$ colour of our 30 RSDs binaries and nine binaries containing ⩾M6 dwarfs. Panel (b) on the right is a zoom in plot for panel (a) on the left. Our PM selected sample (known galaxies excluded) are also plotted on the left panel for reference. Black circles are spectroscopically confirmed RSDs, black pluses are their companions without spectra. RSD + RSD binaries are joined with black lines; RSD + WD binaries are joined with cyan lines. Red squares are spectroscopically confirmed ⩾M6 companions, red crosses **x** are companions without spectra, they are joined with red lines. Binaries with carbon subdwarf companions are joined with magenta lines.

Faherty et al. 2010; Zhang et al. 2010; Burningham et al. 2010; Day-Jones et al. 2011; Pinfield et al. 2012).

3.1.1 Cross match

The statistical probability that two objects with common PM higher than 100 mas·yr^{-1} and errors less than $\sim$ 15 mas·yr^{-1} within a few arcmins could occur by random is usually very small (e.g. $\ll$ 1%, Zhang et al. 2010). We obtained a sample of 1.81 million objects with PMs larger than 80 mas·yr^{-1} from SDSS DR8 and cross matched this sample with our PM and spectroscopy sample. To include some possible very wide binaries we used a separation limit of nine arcmins, and PM difference of 15 mas·yr^{-1} during this cross match. Objects in the SDSS PM catalogue generally have errors better than 15 mas·yr^{-1} for $r < 20$ (Figure 4 of Munn et al. 2004) . Objects with errors larger than 15 mas·yr^{-1} are not reliable.

We first estimate the expected number of random common PM pairs within our RSD sample and SDSS PM catalogue. The SDSS PM catalogue has 1.81 million objects with PM > 80 mas·yr^{-1}. For each of these 1.81 million objects, we counted the number of common PM pairs with PM differences of less than 15 mas·yr^{-1} in the PM sample of 1.81 million objects, without separation constraints. We then divided the total number of common PM pairs (1.642 billion) by the total number of objects (1.808 million) and the total coverage of the PM catalogue (14555 square arcmin) to get the average random common PM density of the whole sample. The possibility of finding common PM companions within 15 mas·yr^{-1} by random within a small area of radius of nine arcmins is 4.41×10^{-3}. Thus we would expect to find $1880 \times 4.41 \times 10^{-3} = 8.3$ random common PM pairs

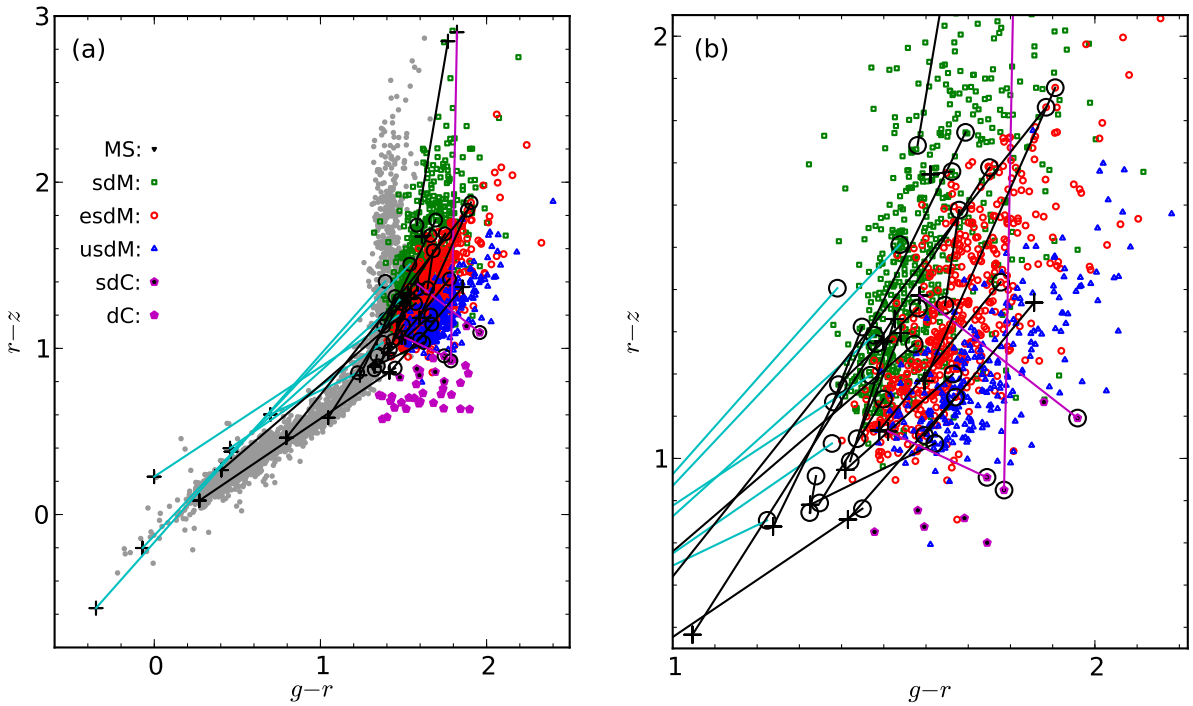

Figure 12. $g-r$ versus $r-z$ colours of our 30 RSD binaries. Green squares: sdMs; red circles: esdMs; blue up-pointing triangles: usdMs; filled magenta pentagons: carbon dwarfs; magenta pentagons filled with black: carbon subdwarfs; grey dots: 3028 point sources with $17 < r < 18$ selected from 10 square degrees of SDSS. Black circles are spectra confirmed RSDs, black pluses are their companions without spectra. RSD + RSD binaries are joined with black lines; RSD + WD binaries are joined with cyan lines. RSD + carbon subdwarf binaries are joined with magenta lines.

between our RSD sample and the PM catalogue with 1.81 million objects.

Fifty M subdwarf common PM pairs were found in our PM pair search. Figure 10 (a) shows PMs of 30 RSD binaries. Their PMs are listed in Table 7. To confirm the binary status of our common PM pairs, we did a colour consistency check of our common PM pairs according to three rules: (I) fainter companion should have redder colours; (II) companions of a binary should associate and line up on the same ridge in the reduced PM versus $r-z$ colour plot (Figure 11). (III) companions of a binary should associate and line up on the same metallicity sequences (Figure 12). Rule (I) is also applied when we use rule (II) or (III) for binarity checking. These three rules do not apply on binaries with WD companions. Thirty two survived rule (II), and 24 of them also survived rule (III). We thus believe these 24 common PM pairs are genuine binary systems.

Table 7 shows properties of the RSD binaries identified with common PMs. Of all our wide binaries identified with common PMs, at least one of the companions is a confirmed RSD with SDSS spectra. Colours and relative brightnesses of these RSD are consistent with their common PM companions. Figure 13 shows SDSS spectra of some of these companions. In five systems spectra of both components were taken by SDSS. Figure 11 shows the SDSS r band reduced PM and $r-z$ colours of these 30 RSD binaries and nine $\geqslant$M6 dwarf binaries (discovered as a by-product, see online table). Our sample (gray dots) are separated into three sequences: WD, RSD and M dwarfs from left to right. Figure 12 shows the $g-r$ and $r-z$ colours of 30 RSD binary systems. Four metal sequences of dwarfs, M subdwarfs, M extreme subdwarfs, and M ultra subdwarfs are plotted for comparison. A number of carbon dwarfs/subdwarfs are also over plotted. Three carbon subdwarfs look inconsistent in Figures 11 and 12, suggesting that only one companion in each system is a carbon subdwarf (see Section 4.3 for further discussion).

3.1.2 Visual inspection

We conducted a systematic search for companions to our M subdwarfs. This search was conducted by visual inspection of the region of sky around each of our M subdwarfs using the SDSS Navigate Tool. We inspected images covering separations out to one arcmin on the sky, and looked for objects that could be K or M subdwarf companions according to rule (I) (Section 3.1.1). Then we measured PMs of all such selected candidates following the method described in Section 5 of Zhang et al. (2009) to test their companionship. Images available from online databases of the SDSS, UKIDSS and POSS are used for our PM measurements. Five common PM pairs were found by this method.

We applied this method to a larger SDSS RSD sample without PM measurements to search for fainter companions. We select binary candidates by their colours, then measure their common PMs to confirm their binary status. SDSS J150015.11+473937.5 (SDSS J1500; usdM0.5) is found to has a fainter companion with spectral type of usdM3 accord-

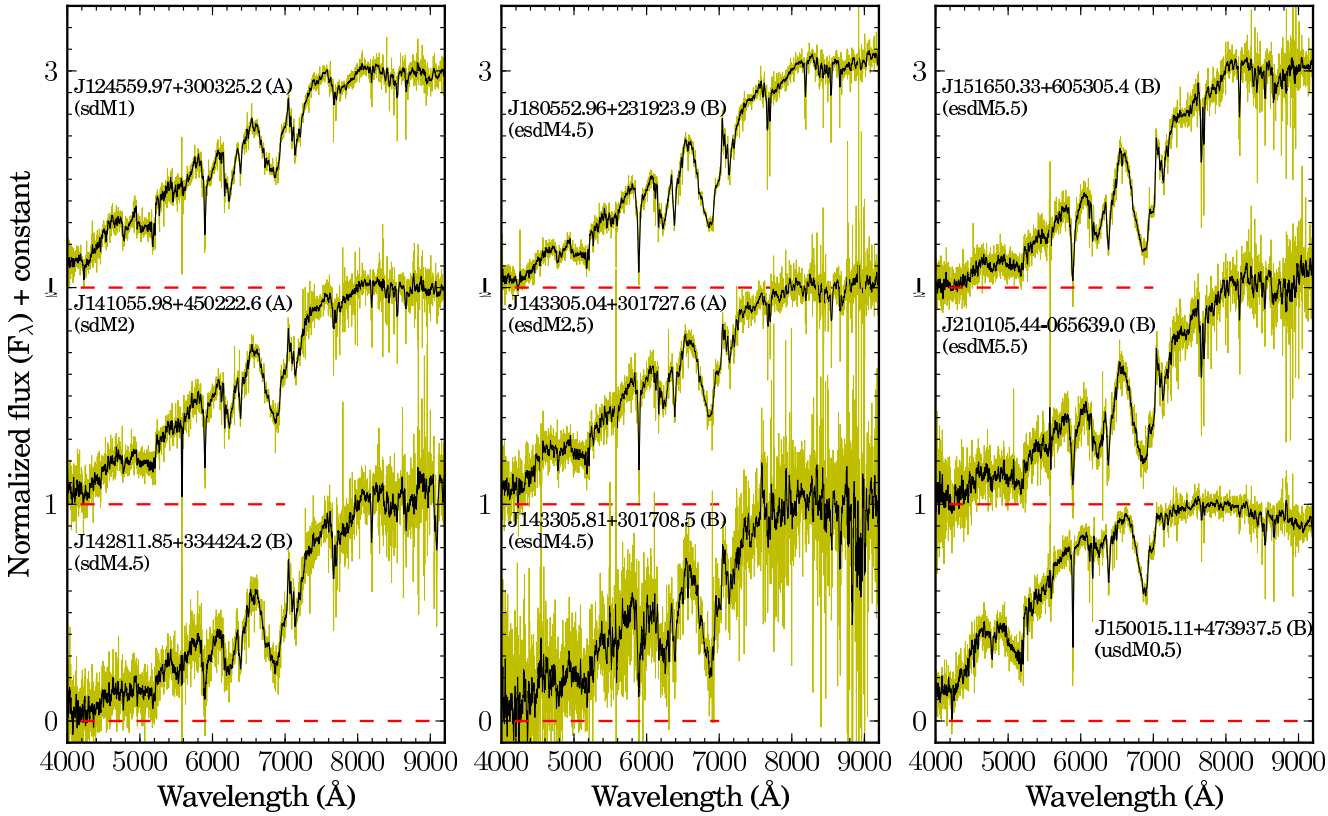

Figure 13. SDSS spectra of nine subdwarf companions in eight wide binary systems. All spectra are normalized at 8000 Å. Spectra are binned by 11 pixel, original spectra are plotted in yellow.

ing to Figure 3. We are following up more binary candidates from a colour + spectroscopy selected RSD sample.

3.2 Partially resolved binaries

Objects classified as galaxies by imaging data, but as stars by spectroscopy or PMs, are often in fact partially resolved binary systems. A binary system with relative small separation (e.g. 0.5″- 3″ for SDSS images) and similar luminosity for each companion (e.g. dM+dM, dM+WD or WD+WD) will be classified as an extended source, e.g. a galaxy.

Four spectroscopically confirmed M subdwarfs in our sample were classified as galaxies by the SDSS pipelines based on their imaging data. We found that they have a peanut-like configuration and double peaks in their images (SDSS J093517.25+242139.4, esdM1; SDSS J121502.52+271706.7, esdM0.5; SDSS J131304.72−033102.4, usdM1; SDSS J142259.37+144335.9, esdM0.5). These objects all have high PMs. To confirm that they are binaries, we checked their POSS1, POSS2 and UKIDSS images (Figure 14). These systems are all detected but not resolved in POSS1 r band images, and have substantially moved their positions in the SDSS images. They have elliptical shapes in POSS2 ir images (1.0″pixel^{-1}), and are consistent with their SDSS i and z band images (0.4″pixel^{-1}). SDSS J1215 and SDSS J1313 are also detected in the UKIDSS images (0.2″pixel^{-1}, 0.4″pixel^{-1}). These peaks in each pair generally the same separations and position angles in SDSS and UKIDSS images. As an example, Figure 14 (o) and (p) show that SDSS J1313 is passing by a background object to its western side from SDSS to UKIDSS epochs. Thus we conclude that these four objects are common PM binary systems.

Four late-type K subdwarf binary systems (SDSS J091956.86+324844.2, sdK7; SDSS J111523.79+270216.3, sdK7; SDSS J124951.09+324521.4, sdK6.5 and SDSS J152733.23+113853.2, sdK7.5) were found in the same way. Companions in these eight binary systems generally have similar magnitudes. To find close binary systems which contain fainter companions (and may not be classified as galaxies by SDSS) in our sample, we visually inspected all M subdwarfs in our sample in SDSS and UKIDSS, and found another seven close RSD binary systems. They all have double flux peaks and common PMs. In total we found 15 partially resolved binary systems from our RSD sample. Nearby stars around these binaries do not have double peaks.

Five M and two late-type K subdwarfs have faint companions detected nearby but there are not good enough second epoch images to confirm their common PMs. Table 8 shows photometry and PMs of 15 partially resolved RSD binaries and seven candidate systems. SDSS spectra of these RSD binaries can not be distinguished visually from that of single RSDs. A combined spectrum of two equal spectral type companions in a close RSD binary would looks similar to spectra of each companion. While a combined spectrum of two companions with more than 2-3 subtypes different would be dominated by the brighter companions.

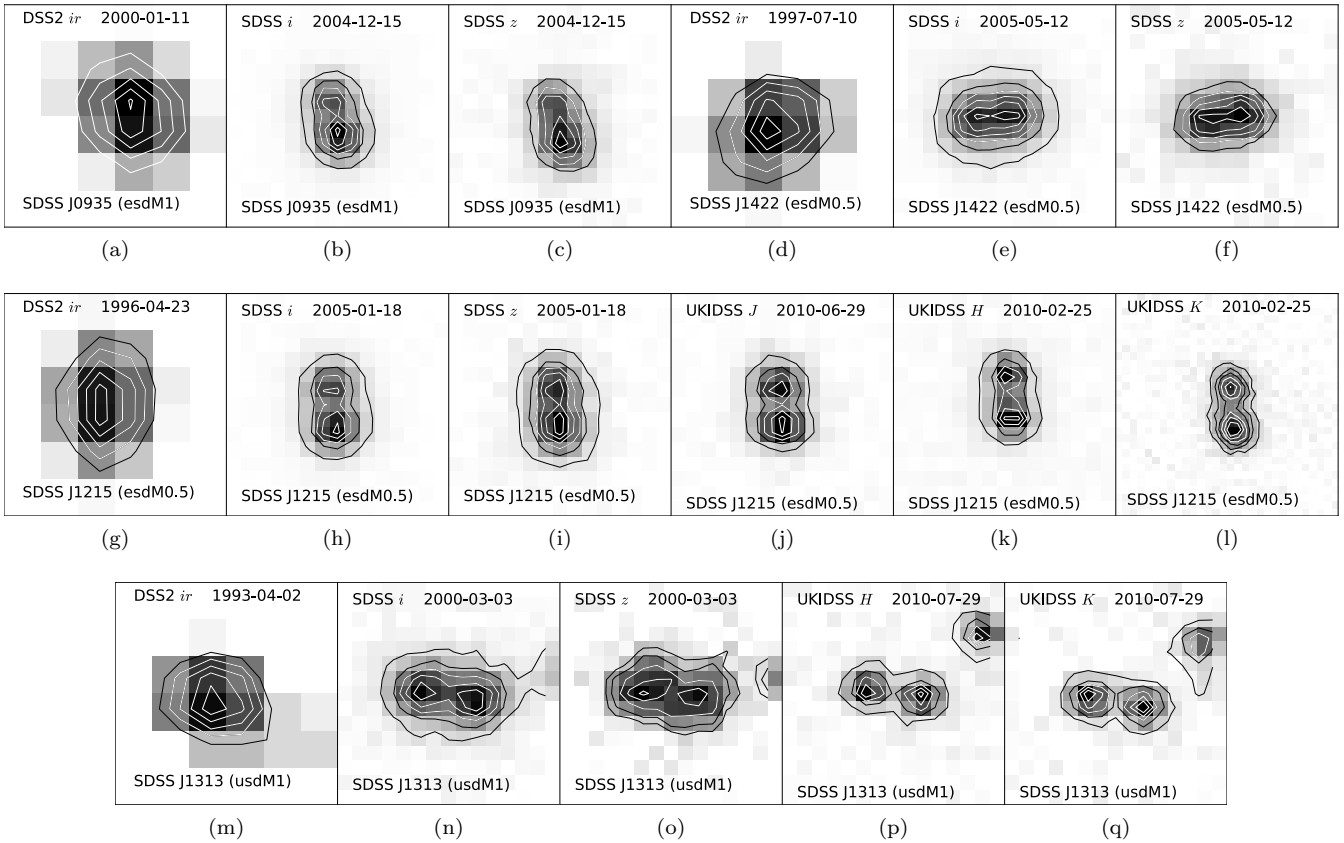

Figure 14. DSS2, SDSS and UKIDSS images of close binaries. All images have a size of $6'' \times 6''$ with north up and east left. Level differences between contour lines in images are equal and on a linear scale.

Table 7. 30 common proper motion confirmed RSD binaries.

Comp	SDSS Name	SDSS u	SDSS g	SDSS r	SDSS i	SDSS z	$\mu_{\rm RA}$ (mas/yr)	$\mu_{\rm Dec}$ (mas/yr)	Sep ($''$)	SpT[a]
01A	J000633.94−043511.2	21.46±0.14	19.01±0.03	17.60±0.02	17.01±0.02	16.63±0.02	64.24±2.66	−100.23±2.66	20.13	(esdK6)
01B	J000633.68−043531.0	22.90±0.47	20.74±0.04	19.07±0.02	18.37±0.02	17.87±0.03	56.14±3.35	−99.29±3.35		esdM1.5
02A	J000744.29−045418.1	22.67±0.43	19.89±0.02	18.43±0.01	17.64±0.02	17.23±0.02	116.61±3.54	3.06±4.15	5.23	sdM0
02B	J000744.56−045414.7	21.80±0.17	21.43±0.15	21.43±0.75	21.31±1.32	21.20±2.39	109.07±3.54	0.54±4.15		WD
03A	J041008.68−041234.7	22.36±0.24	19.11±0.02	17.62±0.02	16.93±0.01	16.55±0.02	55.72±3.19	−197.95±3.19	22.06	(esdM0)
03B	J041007.30−041242.6	22.99±0.46	20.91±0.04	19.14±0.02	18.21±0.02	17.72±0.03	54.08±5.39	−196.63±5.39		esdM3
04A	J092128.09+233235.5	22.38±0.18	20.07±0.02	18.68±0.02	17.96±0.01	17.50±0.02	54.65±3.16	−92.86±3.16	372.81	sdM0
04B	J092127.99+232622.7	24.36±0.82	21.23±0.04	19.65±0.02	18.76±0.02	18.29±0.03	55.88±21.71	−95.09±21.71		sdM2
05A	J093325.29+374940.5	22.54±0.26	20.14±0.03	18.82±0.02	18.28±0.02	17.93±0.03	−11.82±3.67	−98.87±3.67	152.75	(usdK7.5)
05B	J093320.38+374719.3	23.99±0.95	21.06±0.04	19.44±0.02	18.78±0.02	18.40±0.03	−9.28±3.95	−112.16±3.95		usdM0.5
06A	J095419.65+545136.9	22.70±0.29	20.33±0.03	18.91±0.02	18.36±0.02	18.06±0.02	40.65±3.67	−84.26±3.67	98.27	(esdM1)
06B	J095417.41+545000.6	24.18±0.78	21.18±0.04	19.51±0.02	18.75±0.02	18.37±0.03	45.15±5.32	−96.19±5.32		esdM2
07A	J101235.45+181945.5	21.95±0.27	20.01±0.03	18.53±0.02	17.75±0.02	17.25±0.04	3.15±4.52	−100.46±4.52	435.09	sdM0
07B	J101303.57+182236.0	23.02±0.36	20.45±0.03	18.95±0.02	18.14±0.02	17.67±0.04	14.10±5.56	−92.04±5.56		(sdM1)
08A	J104321.03+010436.5	23.85±0.58	20.74±0.03	19.12±0.02	18.06±0.02	17.45±0.02	−179.79±4.91	−103.20±4.91	8.89	(sdM3)
08B	J104320.47+010439.4	23.48±0.47	20.83±0.03	19.16±0.02	18.09±0.02	17.48±0.02	−173.83±5.23	−99.79±5.23		sdM3
09A	J104921.61+012044.4	21.65±0.12	19.31±0.02	17.89±0.01	17.18±0.01	16.90±0.02	−117.25±3.41	−54.22±3.41	12.91	sdK7.5
09B	J104922.06+012055.3	23.00±0.38	20.38±0.03	18.85±0.02	18.02±0.02	17.52±0.02	−128.73±4.73	−60.52±4.73		(sdM2.5)
10A	J110134.92+385614.5	21.87±0.18	19.16±0.02	17.84±0.02	17.25±0.02	16.97±0.03	−46.28±3.32	−84.65±3.32	234.96	sdK6.5
10B	J110140.89+385230.2	22.40±0.27	19.66±0.02	18.32±0.02	17.68±0.02	17.36±0.03	−38.63±3.44	−93.76±3.44		sdK7
11A	J113454.19+125242.7	17.18±0.02	16.11±0.03	15.70±0.03	15.50±0.02	15.44±0.02	−101.54±13.88	−69.38±13.88	531.17	(sdK4)
11B	J113433.88+124522.4	22.97±0.57	20.24±0.04	18.67±0.03	17.87±0.02	17.40±0.02	−100.53±5.32	−74.18±5.32		sdM1.5
12A	J120537.70+005747.5	21.80±0.17	18.94±0.02	17.36±0.01	16.25±0.01	15.62±0.02	−83.32±27.58	19.44±38.91	4.42	sdM3
12B	J120537.99+005748.2	23.13±0.53	21.95±0.08	20.18±0.03	18.31±0.02	17.33±0.02	−87.74±27.58	15.87±38.91		(sdM8)
13A	J121158.45+001450.9	22.61±0.21	20.39±0.02	18.92±0.01	18.08±0.02	17.62±0.02	−23.83±5.05	−110.46±5.05	245.48	sdM1
13B	J121155.81+001853.2	22.30±0.15	21.01±0.03	20.55±0.03	20.37±0.04	20.17±0.10	−32.33±28.81	−115.25±28.81		WD
14A	J124559.97+300325.2	22.08±0.18	19.71±0.06	18.32±0.03	17.40±0.02	16.91±0.02	47.57±2.83	−106.36±24.87	4.95	sdM1
14B	J124559.97+300330.1	19.42±0.03	19.08±0.03	19.43±0.08	19.70±0.25	20.00±0.10	48.33±2.83	−94.72±24.87		WD
15A	J124819.77+610930.9	14.23±0.02	13.38±0.00	13.10±0.00	13.96±0.00	13.02±0.03	−38.26±2.79	−98.25±2.79	221.30	(esdK1)
15B	J124758.27+610653.6	22.76±0.40	20.74±0.03	19.29±0.02	18.73±0.02	18.40±0.04	−52.83±4.99	−99.33±4.99		esdK6.5
16A	J124841.64−021538.7	22.45±0.31	19.87±0.02	18.49±0.02	17.92±0.03	17.46±0.02	−116.30±3.15	−26.78±3.15	429.59	sdK7
16B	J124823.55−022111.9	21.63±0.17	20.73±0.04	20.27±0.03	20.06±0.04	19.88±0.09	−108.02±9.39	−19.50±9.39		WD
17A	J141055.98+450222.6	23.23±0.57	20.14±0.03	18.61±0.02	17.70±0.02	17.10±0.02	−149.09±3.25	8.93±3.25	130.73	sdM2
17B	J141055.71+450011.9	19.80±0.04	19.34±0.02	19.41±0.02	19.53±0.03	19.62±0.09	−146.75±3.32	7.32±3.32		WD
18A	J142540.14+584045.6	22.88±0.31	20.11±0.03	18.76±0.01	18.18±0.02	17.87±0.03	−109.29±4.71	25.63±4.71	174.45	sdK6.5
18B	J142600.85+583939.8	22.93±0.33	20.66±0.03	19.16±0.01	18.42±0.02	18.02±0.03	−115.59±5.23	28.28±5.23		sdM0
19A	J142617.53+073749.2	21.44±0.11	18.89±0.03	17.66±0.01	17.13±0.01	16.81±0.02	41.44±3.11	−104.77±3.11	321.59	sdK6.5
19B	J142639.13+073731.8	22.15±0.20	20.94±0.04	20.24±0.03	19.89±0.03	19.64±0.08	38.62±5.21	−92.34±5.21		WD
20A	J142754.07+334736.7	22.09±0.14	19.51±0.03	18.28±0.01	17.73±0.02	17.44±0.03	−109.21±3.00	−23.18±3.00	293.65	(sdM3)
20B	J142811.85+334424.2	24.29±1.67	21.14±0.04	19.44±0.02	18.24±0.02	17.67±0.03	−102.66±3.29	−30.36±3.29		sdM4.5
21A	J143305.04+301727.6	22.65±0.30	20.11±0.02	18.46±0.02	17.58±0.01	17.10±0.02	77.93±3.11	−364.94±3.11	21.53	esdM2.5
21B	J143305.81+301708.5	23.12±0.45	20.77±0.03	19.09±0.02	18.06±0.01	17.50±0.02	86.68±3.28	−365.68±3.28		esdM4.5

Table 7. continued.

Comp	SDSS Name	SDSS u	SDSS g	SDSS r	SDSS i	SDSS z	$\mu_{\rm RA}$ (mas/yr)	$\mu_{\rm Dec}$ (mas/yr)	Sep ($''$)	SpT[a]
22A	J145725.85+234125.4[c]	21.38±0.09	18.55±0.02	16.77±0.02	16.12±0.02	15.84±0.02	−348.71±10.73	−59.22±15.17	3.96	sdK7
22B	J145726.02+234122.2	24.54±0.97	22.49±0.12	20.67±0.05	18.75±0.02	17.77±0.03	−323.85±10.73	−43.61±15.17		(esdM6.5)
23A	J150015.11+473937.5[b]	21.99±0.20	18.92±0.02	17.32±0.02	16.69±0.02	16.27±0.02	−336.22±8.72	139.96±7.77	4.36	usdM0.5
23B	J150014.95+473933.5[b]	23.69±0.94	20.42±0.05	18.56±0.09	17.69±0.08	17.19±0.07	−336.66±8.72	136.87±7.77		(usdM3)
24A	J151649.87+605437.6	15.56±0.02	13.82±0.02	13.02±0.00	12.72±0.00	12.56±0.02	52.25±2.73	−441.52±2.73	92.25	(esdK2)
24B	J151650.33+605305.4	24.57±0.34	20.89±0.03	19.01±0.02	17.84±0.02	17.18±0.02	51.33±5.02	−446.83±5.02		esdM5.5
25A	J153554.51+105328.0	24.32±0.85	20.27±0.02	18.76±0.01	18.11±0.01	17.70±0.02	−91.92±3.05	−86.20±3.05	6.17	(esdK5.5)
25B	J153554.81+105323.7[c]	25.20±0.77	21.63±0.05	19.89±0.02	19.27±0.02	18.93±0.04	−88.59±4.32	−82.95±4.32		esdK7
26A	J161454.33+145314.7[c]	22.56±0.32	19.56±0.02	17.60±0.01	16.92±0.01	16.50±0.02	−16.60±2.79	−151.41±2.79	437.85	esdK7.5
26B	J161519.36+145719.9	22.71±0.27	20.30±0.02	18.72±0.01	17.81±0.02	17.33±0.02	−19.71±3.78	−153.64±3.78		(esdM2.5)
27A	J173049.54+320123.9	21.68±0.13	19.21±0.02	17.78±0.01	17.13±0.01	16.73±0.02	−87.28±2.74	86.44±2.74	7.07	sdK7.5
27B	J173049.00+320122.5	23.11±0.43	20.51±0.11	18.97±0.08	18.12±0.06	17.67±0.05	−100.44±3.97	80.06±3.97		(sdM3)
28A	J180527.97+231935.9	19.69±0.04	17.15±0.03	16.11±0.03	15.73±0.02	15.52±0.02	−145.01±2.82	−116.68±2.82	344.34	(esdM1.5)
28B	J180552.96+231923.9	23.33±0.56	19.86±0.06	18.11±0.01	17.04±0.01	16.42±0.02	−138.20±3.17	−106.46±3.17		esdM4.5
29A	J210105.37−065633.0	21.87±0.18	19.11±0.01	17.51±0.01	16.80±0.01	16.33±0.01	74.49±6.21	−123.73±5.74	6.13	(esdM1.5)
29B	J210105.44−065639.0	22.77±0.40	21.50±0.06	19.60±0.02	18.40±0.01	17.72±0.02	74.78±6.21	−106.96±5.74		esdM5.5
30A	J221549.63+005732.0	21.88±0.14	19.01±0.02	17.63±0.01	16.91±0.01	16.50±0.01	−13.40±3.13	−143.78±3.13	7.36	sdK7.5
30B	J221549.22+005736.1	22.43±0.22	19.74±0.04	18.29±0.03	17.47±0.04	16.98±0.03	−9.26±2.78	−144.38±2.78		sdM0.5

[a] Spectral types in brackets are estimated from relationships of spectral types and r, i, z band absolute magnitudes (Figure 3).

[b] This binary system is not in the original PM search. [c] Objects have carbon lines and are classified as carbon subdwarfs.

Table 9. Statistics of binaries of late-type K and M subdwarfs

Group	Number	Binary	Fraction
sdK	204	11	5.39%
sdM	622	15	2.41%
esdK	175	4	2.29%
esdM	486	12	2.47%
usdK	84	0	—
usdM	255	2	0.78%
K	463	15	3.24%
M	1363	29	2.13%
sd	826	26	3.15%
esd	661	16	2.42%
usd	339	2	0.59%
Total	1826	44	2.41%

3.3 Binary fraction of red subdwarfs

The multiplicity fraction of dwarf stars decreases with mass, from 57% for nearby solar-type main-sequence stars (Duquennoy & Mayor 1991) to 42% for M dwarfs (Fischer & Marcy 1992). The M subdwarf multiplicity fraction is still not clear. Recent searches for M subdwarf binary systems (Riaz, Gizis, & Samaddar 2008; Lodieu, Zapatero Osorio, & Martín 2009) show a small binary fraction of $\sim 3\%$, and suggest a sharp cut-off in the multiplicity fraction from G to M subdwarfs. While a more extensive survey conducted by Jao et al. (2009) shows a multiplicity rate of 26±6% for K and M type cool subdwarfs.

Forty four RSDs from our original PM selected sample are found in binary systems with projected separation of > 100 au. Fainter companions are missed due to the survey depth and the incompleteness of the PM catalogue used for the companion search. Although our binary search is not complete, this binary sample does however indicate a changing trend of binary fraction by masses and metallicities. We find that the binary fraction of RSDs reduces with decreasing masses and metallicities. Table 9 shows the statistics of binary frequency of RSDs from our sample by spectra and metallicity classes.

Companions of wide binaries in Table 7 without SDSS spectra are not in our original sample. We group binaries by spectral types of companions in our original sample. Both companions of two sdK + sdM systems 18AB and 30AB in Table 7 are in our original sample, we count as one in both sdK and sdM groups.

This binary sample also allows us to put a lower limit on the binary fraction (> 100 au) of RSDs. 2.41% of our RSDs are confirmed in binary systems. As our search of binaries is not complete the binary fraction will be higher than 2.41%. There are another seven binary candidates listed in Table 8 to be confirmed with second epoch imaging. The completeness of SDSS+USNO PM catalogue is 0.7 for SDSS $i = 19$, and 0.3 for SDSS $i = 20$ (Munn et al. 2004). RSDs in our sample are at distances of 100-500 parsecs. Faint UCSD companions of these RSDs would be missed due to the survey depth. Massive ($M/M_{\odot} > 1$) companions of RSDs would have evolved (e.g. cool WDs, neutron stars and black holes) and are too faint to be detected by SDSS and UKIDSS. Thus the RSD binary fraction at > 100 au should be $\gtrsim 5\%$. The binary fractions of K- and M- subdwarfs at > 100 au and > 100 au measured by Jao et al. (2009) are 14% and 12% respectively. Assuming RSD binary fractions are comparable, the total RSD binary fraction would be $\gtrsim 10\%$ according to our sample. More complete and deeper PM catalogues (e.g. Gaia) and deep imaging surveys are needed to find wide and cooler companions of our RSDs. High spatial resolution imaging is needed to search for close binaries (< 100 au). These new searches will allow us to put a tighter constraint on the binary fraction of RSDs.

4 BINARY SYSTEMS OF NOTE

In this section we discuss in more detail systems of particular interest, including those where the secondary is a relatively nearby late-type star, and also those where a companion has somewhat unusual properties.

4.1 G 224-58 AB (esdK2 + esdM5.5)

The spectrum of SDSS J151650.33+605305.4 (SDSS J1516) is shown in Figure 13. It has been spectroscopically classified as an esdM5.5 subdwarf, and is a wide companion to the esdK2 subdwarf G 224-58 (22A in Table 7). With a separation of 93″, this system is one of our widest binaries. An optical spectrum of G224-58 was observed with the Intermediate Dispersion Spectrograph mounted on the Isaac Newton Telescope on 24 December 2010. The data were reduced and the spectrum extracted using standard software packages, and we measured the radial velocity of G 224-58 by cross-correlation with a radial velocity standard over several wavelength ranges. We avoided regions contaminated with telluric lines, and also avoided possible emission lines, and any lines that appeared to be broadened. When we cross-correlated with the reference star HD3765, which has a radial velocity of -63.30 km·s^{-1} (Udry, Mayor, & Queloz 1999), we derived a radial velocity of -189.07±0.15 km·s^{-1} for G 224-58. We also measured the radial velocity using a different reference star; HD10780 ($+2.70$ km·s^{-1}), and measured a consistent value. The radial velocity of G 224-58 is consistent with that of SDSS J1516 or G 224-58 B, -185.02±3.20 km·s^{-1} measured from the SDSS spectrum. This is consistent with expectations for a physically associated system. G 224-58 AB has the highest PM (449.77±7.10 mas·yr^{-1}) amongst our binary sample. It is at a distance of 137±28 parsecs, estimated using the relationship between absolute magnitudes and spectral type (Figure 3), and has clear halo space velocities ($U = 278$ km·s^{-1}, $V = -202$ km·s^{-1}, $W = -39$ km·s^{-1}).

Precise metallicity measurements of M dwarfs for calibration have become popular in the last few years (e.g. Rojas-Ayala et al. 2010, 2012; Terrien et al. 2012; Önehag et al. 2012; Neves et al. 2013). These works are based on M dwarfs in binary systems with FGK dwarfs primaries. Precise metallicities are measured from high resolution spectra of early-type primaries adopted to the M dwarf secondaries to calibrate metallicity features in their spectra. The lowest M dwarf metallicity calibrations are currently [M/H] ~ -0.5 due to the lack of binaries of M + FGK subdwarfs. With an early-type esdK subdwarf and a late-type esdM subdwarf,

Table 8. 15 partially resolved RSD binaries and seven candidate systems.

SDSS Name	SDSS i	$\mu_{\rm RA}$ (mas/yr)	$\mu_{\rm Dec}$ (mas/yr)	SpT	Dis (pc)	Sep ($''$)	Sep (au)	Binarity
J012958.44+073745.0	15.48±0.02	104.69±2.55	−1.54±2.55	sdM2	86-121	1.20	103-145	yes
J091956.86+324844.2	16.12±0.01	−56.01±2.77	−125.24±2.77	sdK7	201-285	0.85	171-242	yes
J093339.18+303908.5	17.58±0.03	53.40±2.88	−109.90±2.88	esdM0.5	294-416	1.69	497-703	yes
J093517.25+242139.4	17.72±0.03	8.51±2.78	−114.72±2.78	esdM1	276-390	1.06	292-414	yes
J111523.79+270216.3	17.78±0.02	22.28±2.86	−100.29±2.86	sdK7	435-615	0.90	391-553	yes
J120640.46+391543.8	16.70±0.02	16.74±2.83	−100.19±2.83	sdK6.5	290-410	1.84	533-754	yes
J120936.28+040806.6	15.81±0.02	−228.60±3.12	−127.11±3.12	sdM1.5	109-154	1.38	150-212	yes
J121502.52+271706.7	17.52±0.02	−133.15±3.03	10.20±3.03	esdM0.5	277-392	1.07	297-420	yes
J122322.55−010349.5	17.48±0.02	−265.08±3.72	43.70±3.72	esdM1.5	228-322	1.34	305-432	yes
J124951.09+324521.4	16.45±0.03	−99.36±2.46	−60.54±2.46	sdK6.5	260-367	1.39	361-510	yes
J131304.72−033102.4	18.43±0.03	−95.13±4.49	−108.82±4.49	usdM1	378-535	1.61	609-861	yes
J142259.37+144335.9	17.45±0.02	−33.32±3.04	−142.30±3.04	esdM0.5	277-392	0.84	233-329	yes
J142417.10+075530.6	18.60±0.02	−48.37±4.46	−93.16±4.46	sdM0.5	468-662	1.53	716-1013	yes
J152733.23+113853.2	18.01±0.21	−157.85±3.52	61.44±3.52	sdK7.5	435-615	0.50	218-308	yes
J214607.39+741129.0	17.61±0.02	49.51±3.97	152.23±3.97	sdM1	272-384	2.35	638-902	yes
J032805.96+001928.2	17.18±0.01	85.74±2.80	−106.72±2.80	esdK6.5	364-514	1.86	676-957	cand
J083345.49+233515.0	18.60±0.02	−424.25±4.74	−102.77±4.74	usdM1	425-601	1.96	832-1177	cand
J121850.48+053530.2	18.66±0.02	−131.25±5.49	−58.18±5.49	usdM2	362-512	2.00	724-1024	cand
J123754.58+185229.9	19.21±0.02	−150.13±4.62	−140.24±4.62	usdM1.5	505-715	1.60	808-1143	cand
J132237.29+665826.0	17.67±0.02	42.50±3.64	−110.26±3.64	esdM0.5	310-438	3.25	1006-1423	cand
J134040.52+190217.8	16.03±0.02	−454.75±2.79	−792.05±2.79	esdM4	72-101	1.40	100-142	cand
J234212.45+091037.2	14.81±0.01	107.27±2.35	1.13±2.35	sdK7	110-155	2.40	263-373	cand

G 224-58 AB is an ideal benchmark for subsolar metallicity calibration of M subdwarfs down to $= -1.5 <$ [M/H] < -1.2.

UCDs in wide binary systems have been identified (e.g. Luhman et al. 2007; Burningham et al. 2009, 2011; Zhang et al. 2010; Faherty et al. 2010; Pinfield et al. 2012) and used to calibrate spectral analysis techniques (e.g. Burgasser, Burrows, & Kirkpatrick 2006), and test atmospheric and evolutionary models (e.g. Dupuy, Liu, & Ireland 2009; Leggett et al. 2008). Yet among metal-poor ultracool dwarfs, only one benchmark has been discovered, the d/sdM9 ([Fe/H] $= -0.7$) HD 114762B (Bowler, Liu, & Cushing 2009), the proximity to its sdF9 primary has made it a challenge to observe. No L- and T- subdwarf benchmark has been found so far. Although there are a few mild metal-poor T dwarf benchmarks (with [M/H] $\sim -0.3 \pm 0.1$) that have been found: SDSS J1416AB (Burningham et al. 2010); HIP 73786B (Murray et al. 2011); BD+01° 2920B (Pinfield et al. 2012). G 224-58B is a very cool extreme subdwarf and could provide a precise metallicity constraint from its early-type primary, it is thus a benchmark object that could be used for testing and calibration of atmospheric and evolutionary models of metal-poor low-mass stars.

4.2 SDSS J210105.37−065633.0AB (esdM1+esdM5.5)

The spectrum of SDSS J210105.44−065639.0 (SDSS J2101 B) is shown in Figure 13, and is classified as an esdM5.5 subdwarf. It is a companion to the esdM1 subdwarf SDSS J210105.37−065633.0 (SDSS J2101A). This binary has an angular separation of $6''$, and it is at a distance of 183±37 parsec, derived using our relationship between absolute magnitudes and spectral type (Figure 3). The system has halo space velocities ($U = -90$ km·s^{-1}, $V = -310$ km·s^{-1}, $W = -49$ km·s^{-1}). This system is of particular use as a test for the M subdwarf classification methods which is still in debate (e.g. Lépine, Rich, & Shara 2007; Jao et al. 2008).

4.3 Three carbon subdwarfs in binary systems

Three of the companion objects have features that are characteristic of RSDs and also have features that are characteristic of carbon dwarfs. We have examined these objects closely in the SDSS i and z band images ($0.4''$/pixel), and they show no evidence for being partially resolved multiple systems. Figure 15 shows the relative location of each component with respect to the dM, sdM, esdM and usdM sequences in grz colour-space. The companions to these three objects appear to be normal RSDs occupying typical colour space in the $g-r$ versus $r-z$ diagram. This indicates that the carbon in subdwarfs did not originate in their formation environment, but has presumably comes from the progenitors of unseen WD companions.

SDSS J145725.85+234125.4 (SDSS J1457 A) was classified as an usdK6.5 subdwarf according to the metallicity index $\zeta_{\rm TiO/CaH}$ defined by Lépine, Rich, & Shara (2007). It has a high PM of $\mu_{\rm RA} = -348.71 \pm 10.73$ mas·yr^{-1}, $\mu_{\rm Dec} = -59.22 \pm 15.17$ mas·yr^{-1}. SDSS J1457AB is a robust genuine binary with separation of $3.96''$. The top panel of Figure 16 shows the spectrum of SDSS J1457A plotted along with a best-fit carbon dwarf spectrum (also from SDSS) and an esdK7 type subdwarf spectrum. We can see that the spectrum of the carbon dwarf is very similar to that of SDSS J1457A, apart from the CaH region around 6700-7000 Å. However, the spectrum of the esdK7 subdwarf SDSS J092302.40+301919.7 (SDSS J0923) compares well with the spectrum of SDSS J1457A in this 6400-7900 Å range. Features of both RSDs (CaH, TiO bands) as well as carbon dwarfs (e.g. the C_2 swan bands) are clear in the spectrum of SDSS J1457A. Thus we think SDSS J1457A is a K7 type carbon subdwarf.

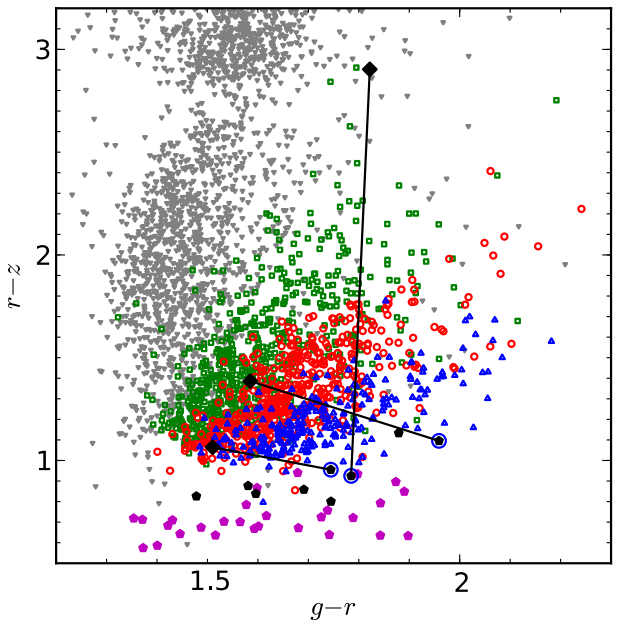

Figure 15. $g-r$ versus $r-z$ colours of the three carbon subdwarf binaries. Grey down-pointing triangles: dMs; Green squares: sdMs; red circles: esdMs; blue up-pointing triangles: usdMs; filled magenta pentagons: carbon dwarfs; black pentagons: carbon subdwarfs. Blue circles with black pentagons inside are spectroscopically confirmed carbon subdwarfs in binaries (SDSS J1535B, SDSS J1457A and SDSS J1614A, from left to right), and black diamonds are their companions which do not have measured spectra. Companions in confirmed binaries are joined with black lines.

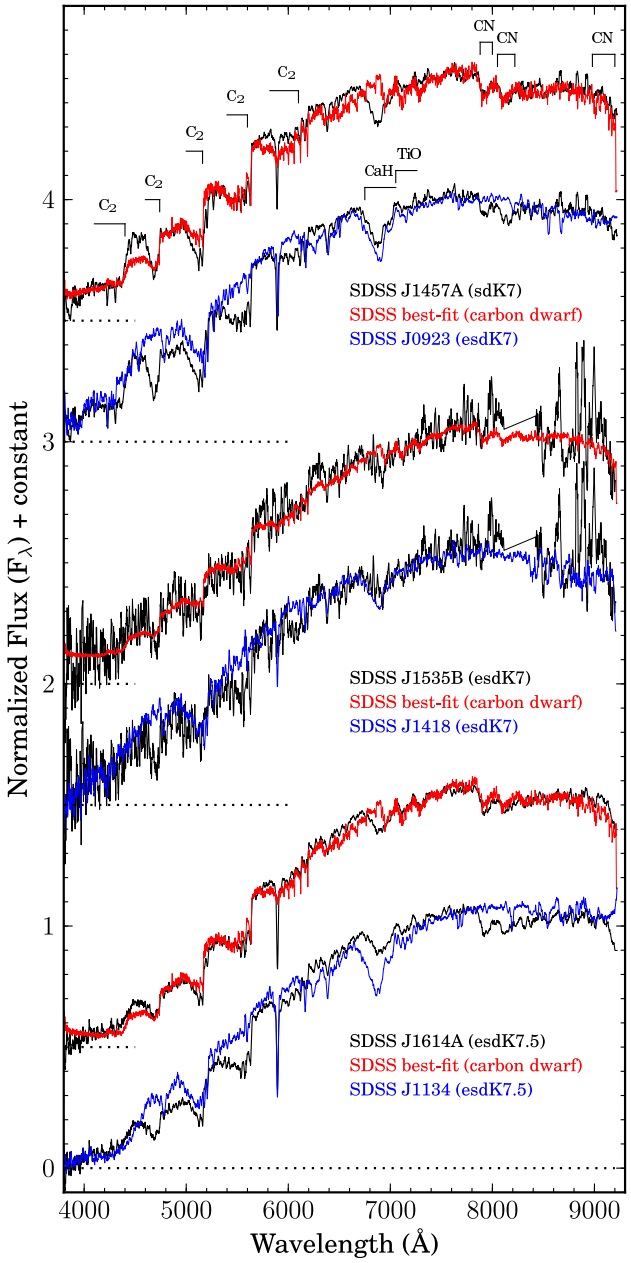

Figure 16. SDSS spectra of three carbon subdwarf SDSS J1457A, SDSS J1535B and J1614A. SDSS best-fit spectra (red, carbon dwarf) and spectrum of SDSS J0923 (top panel, blue, esdM7), SDSS J1448 (middle panel, blue, esdM7) and SDSS J1134 (bottom panel, blue, esdM7.5) are over plotted for comparison. Spectra are normalized at 7500 Å and binned by 11 pixels except SDSS best-fit carbon dwarf spectra.

Although the CaH and TiO indices match well with that of an esdK7 subdwarf, but SDSS J1457A is actually an sdK7 subdwarf. The reason why the SDSS J1457A appears like a esdK7 is because the TiO index is sensitive to both metallicity and carbon abundance. When the C/O ratio is greater than one, all of the oxygen is bound in CO, and none is left to bond with titanium to form TiO (Chapter 2, Reid & Hawley 2005). Thus it is not possible to measure the correct metallicity of carbon subdwarfs by their CaH and TiO indices without consideration of carbon abundance. In the case of SDSS J457A, we can measure the metallicity from its binary companion. SDSS J145726.02+234122.2 (SDSS J1457B) is an M6.5 type subdwarf according to the $M_{r,i,z}$ - spectral type relationships shown in Figure 3. Figure 15 shows that SDSS J1457B is an sdM subdwarf, as it is located at the sdM sequence and very close to the dM sequence. SDSS J1457A should share the same metallicity as SDSS J1457B. Thus we conclude that SDSS J1457AB is an sdK7+sdM6.5 carbon subdwarf system.

SDSS J153554.81+105323.7 (SDSS J1535B) was classified as an usdK6.5 subdwarf according to the metallicity index $\zeta_{\rm TiO/CaH}$ defined by Lépine, Rich, & Shara (2007). The spectrum of SDSS J1535B shown in the middle of Figure 16 is similar to that of SDSS J1457A but with shallower CaH indices and C_2 swan bands. The best fit carbon dwarf spectrum does not provide a good fit for the CaH indices at 6700-7000 Å. SDSS J1535B compares well with an esdK7 type subdwarf SDSS J144819.31+363400.4 (SDSS J1448) in the spectral range 6400-7900 Å. The carbon dwarf emission index at 6750-6950 Å explains why the CaH indices of SDSS J1535A are slightly shallower than those of the esdK7 subdwarf. We classify SDSS J1535B as a K7 type carbon subdwarf. SDSS J1535A is a K5.5 subdwarf according to Figure 3. SDSS J1535AB is an esdK5.5 + esdK7 carbon subdwarf system according to its CaH and TiO indices. They may have higher metallicity than a typical esdK because the TiO strength will also be affected by a higher carbon abundance.

Figure 15 shows that SDSS J1535A probably has metallicity between esdK7 and sdK7.

SDSS J161454.33+145314.7 (SDSS J1614A) was classified as an usdK7 subdwarf according to the metallicity index $\zeta_{\rm TiO/CaH}$ defined by Lépine, Rich, & Shara (2007). The spectrum of SDSS J1614A is shown at the bottom of Figure 16. The best fit SDSS spectrum of SDSS J1614A is a carbon dwarf. The spectrum of the carbon dwarf does not provide a good fit for the CaH indices at 6700-7000 Å which is the major spectroscopic feature of an RSD. The spectrum of SDSS J1614A compares well with that of an esdK7.5 subdwarf SDSS J113419.66+345807.8 (SDSS J1134), and we thus classify it as a K7.5 type carbon subdwarf. Its fainter companion, SDSS J161519.36+145719.9 which is 437.85″ away, has a spectral type of esdM2.5 according to Figure 3. We also note that the colours of SDSS J1614B are consistent with an esdM2.5 subdwarf (Figure 15).

The classification system for dwarf carbon stars has not been established. Spectral types assigned to these three carbon subdwarfs are equivalents of red subdwarfs, do not have information of carbon abundance. The C_2 swan bands in these carbon subdwarf spectra are somewhat weaker than in normal carbon dwarf spectra, suggesting that they have lower carbon abundance than normal carbon dwarfs. This could explains why the CaH indices of these late-type K subdwarfs are not as strong as we might expect. There are three possibilities to explain why these carbon subdwarfs have less carbon abundance than carbon dwarfs. (1) The progenitors of their WD companions had lower mass leading to a lower level of carbon accretion onto the secondary. Subdwarfs are older than dwarfs and thus have enough time for solar-mass companions to evolve through the red giant, AGB and WD stages. (2) These carbon subdwarfs have wider separation from their unseen WD companions than younger carbon dwarfs, again leading to lower levels of accretion. (3) The metal-poor WD progenitors have a lower carbon abundance.

4.4 Six red subdwarfs companion to white dwarfs

WDs provide important constraints on Galactic time scales (Schmidt 1959) because their age can be well estimated from WD cooling time scales combined with the evolutionary life-times of their progenitors. Binary systems containing old WDs and subsolar metallicity RSD components could provide a link between age and chemical abundance. Two old WD companions to early type K dwarfs with low metallicity ([M/H]~ -0.5) have been identified (Jao et al. 2003, 2005). Monteiro et al. (2006) measured the age of these WDs to be 6-9 Gyr, concluding that they were not likely to be members of the halo because they are younger than the canonical halo age of 12-14 Gyr (Gilmore, Wyse, & Kuijken 1989).

The ratio between the strength of TiO and CaH bands near 7000 Å for RSDs is a metallicity diagnostic (Bessell 1982; Allard & Hauschildt 1995). Thus WDs with RSD companions have advantages for the study of chemical enhancement and the early formation history of the Galaxy. Four M and two late-type K subdwarfs in our sample are found to be companions to probable WDs (see Table 7). Figure 13 shows spectra of two RSD companions to WDs (SDSS J124559.97+300325.2 and SDSS J141055.98+450222.6). WD companions are identified using reduced PMs (Figure 11) and SDSS colours (Figure 12). The reduced PMs and $r-z$ colour of these six binaries are plotted in Figure 11 and joined with cyan lines. These six WD companions are associated with confirmed WDs on the left of the plot. The RSD companions are located on the sequence of RSDs in Figure 11. The $g-r$ versus $r-z$ plot in Figure 12 also suggests that these six binary systems contain WD and RSD components. WDs are located at the bottom left in the $g-r$ versus $r-z$ plot (see Figure 15), while cool WDs overlap with the hot tail of the main sequence. Most of RSDs in our sample are beyond 200 parsecs and therefore very cool WD companions will be missed by our search. These six RSDs with WD companions are classified as sdM or sdK could be members of either the thick disk or inner halo of the Galaxy.

4.5 An esdK7+WD spectroscopic binary

Figure 17 shows the spectrum of SDSS J163340.83+133417.0 (SDSS J1633), which is classified as an esdK7 subdwarf. It has a significant flux excess in the blue band when compared to the normal esdK7 subdwarf SDSS J100849.85+200923.4 (SDSS J1008). When we remove the spectrum of SDSS J1008 from that of SDSS J1633, a typical WD spectrum remained. So SDSS J1633 is actually a WD+esdK7 spectroscopic binary system. It has a PM of $\mu_{\rm RA} = -107.63 \pm 3.61$ mas·yr^{-1}; $\mu_{\rm Dec} = -68.73 \pm 3.61$ mas·yr^{-1} and a radial velocity of -135.47 ± 7.45 km·s^{-1}. SDSS r, i and z band absolute magnitudes of K7 subdwarfs are $9.53 < {\rm M}_r < 12.23$, $8.97 < {\rm M}_i < 10.42$ and $8.68 < {\rm M}_z < 10.08$ respectively, based on sdK7 and esdK7 subdwarfs with parallax measurements. The distance of SDSS J1633 has been estimated (by averaging the absolute magnitudes in $\rm M_i$ and $\rm M_z$) as 592^{+229}_{-165} parsecs. Its tangential velocity is 356^{+138}_{-100} km·s, and the resulting space velocity is $U = -66.1^{+22.3}_{-18.4}$ km·s^{-1}, $V = -245.4^{+72.6}_{-78.0}$ km·s^{-1} and $W = 14.8^{+45.3}_{-41.0}$ km·s^{-1}.

We checked the SDSS images of SDSS J1633, to see if any companion was resolved. Figure 18 shows the SDSS *u, g, r, i* band images of SDSS J1633. It is less likely to be resolved in the SDSS u, i and z bands because WDs are too faint in i, z bands and RSDs are relatively faint in u band. There is no evidence that the system is resolved in the *urz* bands. The SDSS g band image shows a slightly elliptical profile, however, all stars around SDSS J1633 in this g band image show elliptical profiles so this must be a characteristic of this particular SDSS image. Thus we conclude that the WD+esdK7 binary is not resolved in the SDSS images, and that the separation of this binary is less than $\sim 0.4''$ ($\sim$ 171-328 au).

The atmospheric parameters ($T_{\rm eff}$ and $\log g$) of the WD component were derived by performing a fit of the observed Balmer lines to hydrogen-rich WD models (D. Koester, private communication), following the procedure described in Garcés, Catalán, & Ribas (2011). The Balmer lines in such WD models were calculated with the modified Stark broadening profiles of Tremblay & Bergeron (2009). For the line fitting we used the code fitsb2 (Napiwotzki et al. 2004), which follows a procedure based on χ^2 minimization. Hα was not included in the fit, since it was not clearly visible in the spectrum, probably due to the contribution of the subdwarf companion. The atmospheric parameters obtained

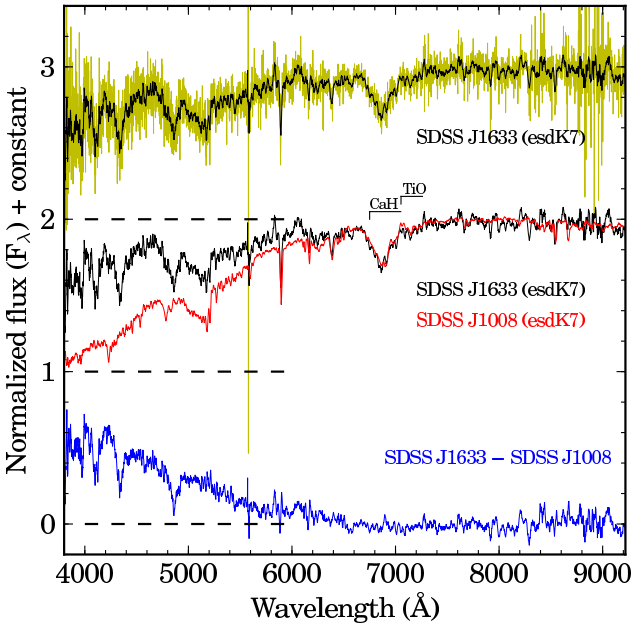

Figure 17. The spectrum of SDSS J1633. Black: spectrum of SDSS J1633 smoothed by 11 pixels. Red: SDSS J1008. Blue: the difference between SDSS J1613 and SDSS J1008. The spectra of SDSS J1633 and SDSS J1008 are normalized at 8000 Å.

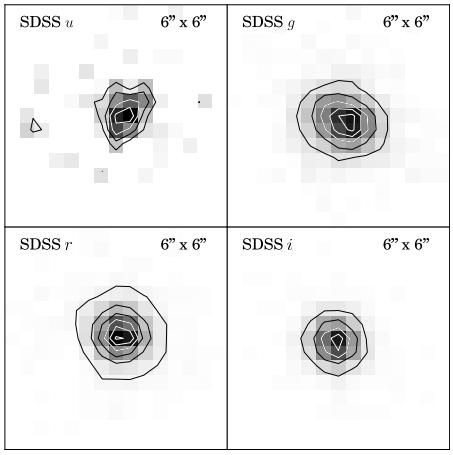

Figure 18. SDSS u,g,r,i images of SDSS J1633. All images are observed on 2004-06-12. Each image has a size of $6'' \times 6''$with North up and East left. The differences between contour levels in each image are equal.

were: $T_{\rm eff}$ = 12980±770 K and log g = 8.4±0.19 dex. As can be seen in Figure 19 the fit in Hβ is poor, which can also be due to the contribution of the companion. Considering these parameters and using the WD cooling sequences of Salaris et al. (2000) we determined the mass and cooling time of this WD, obtaining 0.86±0.08 $M_\odot$ and 0.53±0.12 Gyr, respectively. The total age of a WD is the WD cooling time plus its progenitor lifetime. When a WD is isolated we can calculate the progenitor mass by using an initial-final mass relationship (e.g. Catalán et al. 2008) and then determine the progenitor lifetime using stellar tracks. In this case the WD is in a close binary, so, we cannot follow this procedure since the two stars may have interacted in the past. It is

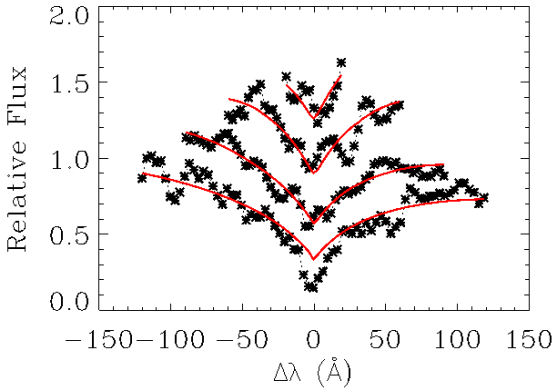

Figure 19. Fits of the observed Balmer lines for the WD companion of SDSS J1633. Dotted lines correspond to the observations and the red line corresponds to the best fit (WD models). Balmer lines range from Hβ (bottom) to Hϵ (top).

difficult then to obtain the total age for this WD since the progenitor lifetime could range from 0.2 to 6 Gyr if we consider progenitor masses from 4 to 1 $M_\odot$ and the stellar tracks of Dominguez et al. (1999) for Z=0.004. It is worth noting that the temperature obtained, 12980K, is also quite high for a halo WD with such a large mass. Typical halo WDs with $T_{\rm eff}$ >10000 K have an average mass of 0.45$M_\odot$(derived from the SPY project, Pauli et al. 2006). However, we note that the mass of the WD may have changed as a member of a close binary. Jao et al. (2005) discovered two WDs in systems with RSDs, LHS 193AB and LHS 300AB. These two systems have large tangential velocities and are likely members of the thick disk population of the Galaxy. Monteiro et al. (2006) estimated ages of these two WDs of 6-9 Gyr. If SDSS J1633 is a halo object, it should have an age of > 9 Gyr (Gilmore, Wyse, & Kuijken 1989). The age of the system estimated from its WD companion does not fit with that of a halo object.

There are however uncertainties about this system: (1) It could be a binary system formed when the Galactic disk had a lower metallicity; (2) It could be a member of a stream; (3) The spectrum of the WD companion (after subtraction of the RSD) has a low signal to noise; (4) Mass transfer between the two components could make the WD look younger. (5) The RSD could have been captured by the WD or its progenitor.

5 SUMMARY & CONCLUSIONS

We have selected ∼ 1800 RSDs from SDSS with PMs greater than 100 mas·yr^{-1}. Forty two of these objects are late-type M subdwarfs with spectral type of ⩾M6, thirty of them are new ones. We fitted an absolute magnitude - spectral type relationship (in the r, i, z, J, H, K bands) for M- and L- subdwarfs, showing that subdwarfs have different sequences to M- and L- dwarfs. Metal-poor cool dwarfs are sub-dwarfs only for spectral types of ⩽M5, and become "super" dwarfs for later types (>M5). We estimated distances of our M subdwarfs using the absolute magnitude - spectral type re-

lationships, and placed constraints on the U, V, W space velocities. Our sample shows that halo and disk populations have overlaps of metallicity and kinematics.

Five M ultra subdwarfs are found to have considerably higher gravity than normal M subdwarfs. Their CaH absorption features are significantly deeper than normal M subdwarfs (whose spectra are similar in other respects). These objects provide a good tests for how surface gravity effects the spectra of cool stars. These high gravity features are only found in M ultra subdwarfs which may reveal the role that metallicity plays in the formation and evolution history of low-mass stars. We also identify fourteen carbon rich RSDs which represent a new population of carbon subdwarfs. These objects can help us to study carbon star populations over a much greater age range.

We have presented 45 red subdwarfs in wide binary systems (> 100 au) containing sources with SDSS spectroscopy, confirming associations through common PMs. Their separations range from $0.4''$ to $9'$, and the secondaries have spectral types ranging from late-type K to late-type M. Thirty are wide and fifteen are partially resolved binary systems. G 224-58AB is one of our widest binary systems, and contains an esdK2 and an esdM5.5 type subdwarf. SDSS J210105.37–065633.0AB is a closer binary system that contains an esdM1 and an esdK5.5 type subdwarf. We found one spectroscopic and six wide WD + RSD binary systems. With age constraints from the WD companions in these systems, we can study the chemical evolution of the Galaxy. Three metal-poor carbon dwarfs are found in binary systems with subdwarf companions. Kinematics and radial velocity follow up would be very useful to better understand the physics of carbon subdwarfs. Although our binary search is not complete, our sample shows that the binary fraction of RSDs goes down with decreasing mass and metallicity, and we estimate a red subdwarf binary fraction of $\gtrsim 5\%$ for separation > 100 au and $\gtrsim 10\%$ for all separation distances.

In the future it will be possible to use UCSD binary systems (e.g. G 224-58AB) as benchmarks to test metal-poor ultracool atmospheric models. It will also be possible to use M subdwarf binaries systems (e.g. SDSS J2101AB, SDSS J143305.04+301727.6AB) to test M subdwarf classification methods, particularly gravity effects. We can also measure the metallicity of carbon subdwarfs most effectively if we are able to study their subdwarf companions (which do not suffer from carbon pollution). A larger sample of carbon dwarfs/subdwarfs in wide binaries is expected in the future, from surveys/facilities such as Pan-STARRS, LAMOST, Gaia and LSST, providing the potential to identify large numbers of new nearby M, L and T subdwarf multiple systems.

ACKNOWLEDGMENTS

Funding for the SDSS and SDSS-II has been provided by the Alfred P. Sloan Foundation, the Participating Institutions, the National Science Foundation, the U.S. Department of Energy, the National Aeronautics and Space Administration, the Japanese Monbukagakusho, the Max Planck Society, and the Higher Education Funding Council for England. The SDSS Web Site is http://www.sdss.org/. Funding for SDSS-III has been provided by the Alfred P. Sloan Foundation, the Participating Institutions, the National Science Foundation, and the U.S. Department of Energy Office of Science. The SDSS-III web site is http://www.sdss3.org/. This work is based in part on data obtained as part of the UKIRT Infrared Deep Sky Survey. This publication makes use of data products from the Two Micron All Sky Survey, the Palomar Observatory Sky Atlas (POSS-I) and The Second Palomar Observatory Sky Survey (POSS-II). The Isaac Newton Telescope is operated on the island of La Palma by the Isaac Newton Group in the Spanish Observatorio del Roque de los Muchachos of the Instituto de Astrofísica de Canarias. This research has made use of the VizieR catalogue access tool, CDS, Strasbourg, France. IRAF is distributed by the National Optical Observatory, which is operated by the Association of Universities for Research in Astronomy, Inc., under contract with the National Science Foundation.

ZHZ thank Kieran Forde and Roberto Raddi for the help with data analysis, thank Paul Steele for useful discussion about ages of WDs. ZHZ has received support from the Royal Astronomical Society during this research. ZHZ, BB, HRAJ and RLS have received support form the Marie Curie 7th European Community Framework Programme grant n.247593 Interpretation and Parameterization of Extremely Red COOL dwarfs (IPERCOOL) International Research Staff Exchange Scheme. ZHZ, DJP, HRAJ, MCGO, SC and YVP have received support from RoPACS during this research, a Marie Curie Initial Training Network funded by the European Commission's Seventh Framework Programme. MKK and JG were supported by RoPACS. MCGO acknowledges the support of a JAE-Doc CSIC fellowship co-funded with the European Social Fund under the program *"Junta para la Ampliación de Estudios"*. SC acknowledges financial support from the European Commission in the form of a Marie Curie Intra European Fellowship (PIEF-GA-2009-237718). The authors thank the referee, Dr Nigel Hambly for the useful and constructive comments.

REFERENCES

Abazajian K. N., et al., 2009, ApJS, 182, 543
Adelman-McCarthy J. K., et al., 2008, ApJS, 175, 297
Aihara H., et al., 2011, ApJS, 193, 29
Allard F., Hauschildt P. H., 1995, ApJ, 445, 433
Andrei A. H., et al., 2011, AJ, 141, 54
Baade W., 1944, ApJ, 100, 137
Baraffe I., Chabrier G., Allard F., Hauschildt P. H., 1997, A&A, 327, 1054
Baraffe I., Chabrier G., Barman T. S., Allard F., Hauschildt P. H., 2003, A&A, 402, 701
Bessell M. S., 1982, PASAu, 4, 417
Bessell M. S., 1991, AJ, 101, 662
Bowler B. P., Liu M. C., Cushing M. C., 2009, ApJ, 706, 1114
Brott I., Hauschildt P. H., 2005, ESASP, 576, 565
Burgasser A. J., et al., 2003, ApJ, 592, 1186
Burgasser A. J., 2004, ApJ, 614, L73
Burgasser A. J., Burrows A., Kirkpatrick J. D., 2006a, ApJ, 639, 1095
Burgasser A. J., Kirkpatrick J. D., 2006, ApJ, 645, 1485

Burgasser A. J., Cruz K. L., Kirkpatrick J. D., 2007, ApJ, 657, 494
Burgasser A. J., Vrba F. J., Lépine S., Munn J. A., Luginbuhl C. B., Henden A. A., Guetter H. H., Canzian B. C., 2008, ApJ, 672, 1159
Burgasser A. J., Witte S., Helling C., Sanderson R. E., Bochanski J. J., Hauschildt P. H., 2009, ApJ, 697, 148
Burgasser A. J., Lépine S., Lodieu N., Scholz R.-D., Delorme P., Jao W.-C., Swift B. J., Cushing M. C., 2009, AIPC, 1094, 242
Burningham B., et al., 2009, MNRAS, 395, 1237
Burningham B., et al., 2010, MNRAS, 404, 1952
Burningham B., et al., 2011, MNRAS, 414, 3590
Burrows A., Hubbard W. B., Lunine J. I., Liebert J., 2001, RvMP, 73, 719
Catalán S., Isern J., García-Berro E., Ribas I., 2008, MNRAS, 387, 1693
Chabrier G., 2003, PASP, 115, 763
Costa E., Méndez R. A., Jao W.-C., Henry T. J., Subasavage J. P., Brown M. A., Ianna P. A., Bartlett J., 2005, AJ, 130, 337
Costa E., Méndez R. A., Jao W.-C., Henry T. J., Subasavage J. P., Ianna P. A., 2006, AJ, 132, 1234
Cushing M. C., Looper D., Burgasser A. J., Kirkpatrick J. D., Faherty J., Cruz K. L., Sweet A., Sanderson R. E., 2009, ApJ, 696, 986
Dahn C. C., Liebert J., Kron R. G., Spinrad H., Hintzen P. M., 1977, ApJ, 216, 757
Dahn C. C., et al., 2002, AJ, 124, 1170
Dahn C. C., et al., 2008, ApJ, 686, 548
Day-Jones A. C., et al., 2011, MNRAS, 410, 705
Dearborn D. S. P., Liebert J., Aaronson M., Dahn C. C., Harrington R., Mould J., Greenstein J. L., 1986, ApJ, 300, 314
Dhital S., West A. A., Stassun K. G., Bochanski J. J., Massey A. P., Bastien F. A., 2012, AJ, 143, 67
Dominguez I., Chieffi A., Limongi M., Straniero O., 1999, ApJ, 524, 226
Downes R. A., et al., 2004, AJ, 127, 2838
Dupuy T. J., Liu M. C., Ireland M. J., 2009, ApJ, 692, 729
Dupuy T. J., Liu M. C., 2012, ApJS, 201, 19
Duquennoy A., Mayor M., 1991, A&A, 248, 485
Faherty J. K., Burgasser A. J., Cruz K. L., Shara M. M., Walter F. M., Gelino C. R., 2009, AJ, 137, 1
Faherty J. K., Burgasser A. J., West A. A., Bochanski J. J., Cruz K. L., Shara M. M., Walter F. M., 2010, AJ, 139, 176
Faherty J. K., et al., 2012, ApJ, 752, 56
Fischer D. A., Marcy G. W., 1992, ApJ, 396, 178
Garcés A., Catalán S., Ribas I., 2011, A&A, 531, A7
Gass H., Wehrse R., Liebert J., 1988, A&A, 189, 194
Gatewood G., Coban L., 2009, AJ, 137, 402
Gilmore G., Wyse R. F. G., Kuijken K., 1989, ARA&A, 27, 555
Gizis J. E., 1997, AJ, 113, 806
Gizis J. E., Harvin J., 2006, AJ, 132, 2372
Gliese W., Jahreiß H., 1991, adc..rept,
Gould A., 2003, ApJ, 583, 765
Han Z., Podsiadlowski P., Lynas-Gray A. E., 2007, MNRAS, 380, 1098
Harrington R. S., Dahn C. C., 1980, AJ, 85, 454
Helling C., et al., 2008, MNRAS, 391, 1854
Henry T. J., Jao W.-C., Subasavage J. P., Beaulieu T. D., Ianna P. A., Costa E., Méndez R. A., 2006, AJ, 132, 2360
Jao W.-C., Henry T. J., Subasavage J. P., Bean J. L., Costa E., Ianna P. A., Méndez R. A., 2003, AJ, 125, 332
Jao W.-C., Henry T. J., Subasavage J. P., Brown M. A., Ianna P. A., Bartlett J. L., Costa E., Méndez R. A., 2005, AJ, 129, 1954
Jao W.-C., Henry T. J., Beaulieu T. D., Subasavage J. P., 2008, AJ, 136, 840
Jao W.-C., Mason B. D., Hartkopf W. I., Henry T. J., Ramos S. N., 2009, AJ, 137, 3800
Jao W.-C., Henry T. J., Subasavage J. P., Winters J. G., Riedel A. R., Ianna P. A., 2011, AJ, 141, 117
Jenkins L. F., 1952, QB813,
Kaltenegger L., Traub W. A., 2009, ApJ, 698, 519
Kirkpatrick J. D., Henry T. J., Irwin M. J., 1997, AJ, 113, 1421
Kirkpatrick J. D., et al., 2010, ApJS, 190, 100
Kirkpatrick J. D., et al., 2012, ApJ, 753, 156
Kuiper G. P., 1939, ApJ, 89, 548
Lawrence A., et al., 2007, MNRAS, 379, 1599
Leggett S. K., et al., 2008, ApJ, 682, 1256
Lépine S., Rich R. M., Shara M. M., 2003a, AJ, 125, 1598
Lépine S., Shara M. M., Rich R. M., 2003b, ApJ, 585, L69
Lépine S., Rich R. M., Shara M. M., 2003c, ApJ, 591, L49
Lépine S., Shara M. M., Rich R. M., 2004, ApJ, 602, L125
Lépine S., Rich R. M., Shara M. M., 2007, ApJ, 669, 1235
Lépine S., Scholz R.-D., 2008, ApJ, 681, L33
Lépine S., Thorstensen J. R., Shara M. M., Rich R. M., 2009, AJ, 137, 4109
Lodieu N., Zapatero Osorio M. R., Martín E. L., 2009, A&A, 499, 729
Lodieu N., Zapatero Osorio M. R., Martín E. L., Solano E., Aberasturi M., 2010, ApJ, 708, L107
Lodieu N., Espinoza Contreras M., Zapatero Osorio M. R., Solano E., Aberasturi M., Martín E. L., 2012, A&A, 542, A105
Lowrance P. J., Kirkpatrick J. D., Reid I. N., Cruz K. L., Liebert J., 2003, ApJ, 584, L95
Luhman K. L., et al., 2007, ApJ, 654, 570
Margon B., et al., 2002, AJ, 124, 1651
Marley M. S., Seager S., Saumon D., Lodders K., Ackerman A. S., Freedman R. S., Fan X., 2002, ApJ, 568, 335
Marshall J. L., 2008, AJ, 135, 1000
Montalbán J., D'Antona F., Mazzitelli I., 2000, A&A, 360, 935
Monteiro H., Jao W.-C., Henry T., Subasavage J., Beaulieu T., 2006, ApJ, 638, 446
Munn J. A., et al., 2004, AJ, 127, 3034
Murray D. N., et al., 2011, MNRAS, 414, 575
Napiwotzki R., et al., 2004, ASPC, 318, 402
Neves V., Bonfils X., Santos N. C., Delfosse X., Forveille T., Allard F., Udry S., 2013, A&A, 551, A36
Önehag A., Heiter U., Gustafsson B., Piskunov N., Plez B., Reiners A., 2012, A&A, 542, A33
Pauli E.-M., Napiwotzki R., Heber U., Altmann M., Odenkirchen M., 2006, A&A, 447, 173
Perryman M. A. C., et al., 1997, A&A, 323, L49
Pinfield D. J., et al., 2012, MNRAS, 2821
Plez B., Cohen J. G., 2005, A&A, 434, 1117
Prugniel P., Soubiran C., 2001, A&A, 369, 1048
Reid I. N., Hawley S. L., 2005, nlds.book,

Riaz B., Gizis J. E., Samaddar D., 2008, ApJ, 672, 1153
Riedel A. R., et al., 2010, AJ, 140, 897
Rojas-Ayala B., Covey K. R., Muirhead P. S., Lloyd J. P., 2010, ApJ, 720, L113
Rojas-Ayala B., Covey K. R., Muirhead P. S., Lloyd J. P., 2012, ApJ, 748, 93
Roman N. G., 1950, ApJ, 112, 554
Roman N. G., 1952, ApJ, 116, 122
Roman N. G., 1954, AJ, 59, 307
Salaris M., García-Berro E., Hernanz M., Isern J., Saumon D., 2000, ApJ, 544, 1036
Saumon D., Bergeron P., Lunine J. I., Hubbard W. B., Burrows A., 1994, ApJ, 424, 333
Schilbach E., Röser S., Scholz R.-D., 2009, A&A, 493, L27
Schmidt M., 1959, ApJ, 129, 243
Scholz R.-D., Lehmann I., Matute I., Zinnecker H., 2004, A&A, 425, 519
Scholz R.-D., Lodieu N., McCaughrean M. J., 2004, A&A, 428, L25
Schweitzer A., Scholz R.-D., Stauffer J., Irwin M., McCaughrean M. J., 1999, A&A, 350, L62
Sivarani T., Lépine S., Kembhavi A. K., Gupchup J., 2009, ApJ, 694, L140
Smart R. L., Ioannidis G., Jones H. R. A., Bucciarelli B., Lattanzi M. G., 2010, A&A, 514, A84
Spagna A., Lattanzi M. G., Re Fiorentin P., Smart R. L., 2010, A&A, 510, L4
Steinhardt C. L., Sasselov D. D., 2005, astro, arXiv:astro-ph/0502152
Terrien R. C., Mahadevan S., Bender C. F., Deshpande R., Ramsey L. W., Bochanski J. J., 2012, ApJ, 747, L38
Tremblay P.-E., Bergeron P., 2009, ApJ, 696, 1755
Udry S., Mayor M., Queloz D., 1999, ASPC, 185, 367
van Altena W. F., Lee J. T., Hoffleit E. D., 1995, gcts.book,
van Dokkum P. G., Conroy C., 2010, Natur, 468, 940
van Leeuwen F., 2007, A&A, 474, 653
Vrba F. J., et al., 2004, AJ, 127, 2948
Witte S., Helling C., Hauschildt P. H., 2009, A&A, 506, 1367
Woolf V. M., Lépine S., Wallerstein G., 2009, PASP, 121, 117
York D. G., et al., 2000, AJ, 120, 1579
Zhang Z. H., et al., 2010, MNRAS, 404, 1817
Zhang Z. H., et al., 2009, A&A, 497, 619
Zhang Z. H., Pinfield D. J., Burningham B., Jones H. R. A., Day-Jones A. C., Marocco F., Gomes J., Galvez-Ortiz M. C., 2013, EPJWC, 47, 6007

APPENDIX A: ONLINE DATA

This paper has been typeset from a TEX/ LATEX file prepared by the author.

Table A1. 37 carbon dwarfs and subdwarfs

SDSS Name	SDSS g	SDSS r	SDSS i	SDSS z	$\mu_{\rm RA}$(mas/yr)	$\mu_{\rm Dec}$(mas/yr)	SpT[a]
J012518.66−104448.2	17.90±0.02	16.42±0.02	15.89±0.02	15.60±0.02	−28.58±2.73	−127.96±2.73	sdC
J093619.49+374034.6	19.18±0.02	17.60±0.03	17.07±0.01	16.72±0.03	−139.67±3.08	−96.52±3.08	sdC
J121341.40+451919.9	20.47±0.03	18.59±0.02	17.85±0.02	17.46±0.03	−129.55±4.34	−218.48±4.34	sdC
J131639.62+121529.2	20.71±0.03	18.96±0.02	18.42±0.02	18.16±0.03	−106.82±4.32	−27.69±4.32	sdC
J145318.82+600421.4	19.20±0.02	17.60±0.02	17.00±0.02	16.76±0.02	−235.83±3.39	−6.25±3.39	sdC
J145703.10+363041.9	20.43±0.03	18.74±0.01	18.16±0.02	17.88±0.02	−101.29±3.62	60.83±3.62	sdC
J145725.85+234125.4	18.55±0.02	16.77±0.02	16.12±0.02	15.84±0.02	−360.44±2.60	−67.76±2.60	sdC
J153554.81+105323.7	21.63±0.05	19.89±0.02	19.27±0.02	18.93±0.04	−88.59±4.32	−82.95±4.32	sdC
J161454.33+145314.7	19.56±0.02	17.60±0.01	16.92±0.01	16.50±0.02	−16.60±2.79	−151.41±2.79	sdC
J004853.30−090435.8	21.06±0.04	19.46±0.02	18.87±0.02	18.59±0.04	−27.20±4.71	−117.35±4.71	dCf
J010717.91−091329.5	20.62±0.04	18.82±0.02	18.22±0.01	17.89±0.03	167.36±3.75	−60.07±3.75	dCf
J094352.09+362545.3	20.14±0.02	18.78±0.01	18.32±0.02	18.07±0.02	−72.40±3.52	−79.97±3.52	dCf
J144448.40+043944.2	21.41±0.05	19.62±0.02	19.10±0.02	18.90±0.05	−111.73±5.60	42.56±5.60	dCf
J163132.74+355328.9	19.09±0.02	17.41±0.01	16.89±0.01	16.73±0.02	−142.10±3.24	107.02±3.24	dCf
J012028.55−083630.8	18.72±0.02	17.00±0.02	16.45±0.01	16.27±0.02	145.82±3.01	−49.40±3.01	dC
J012150.11+011302.6	18.74±0.02	17.00±0.02	16.52±0.02	16.36±0.02	206.08±3.06	−132.26±3.06	dC
J074257.17+465918.1	17.64±0.02	15.77±0.02	15.15±0.02	14.87±0.02	−58.81±11.84	−142.40±11.84	dC
J074638.20+400403.4	21.40±0.05	19.50±0.02	19.00±0.02	18.86±0.05	−276.50±5.79	−173.34±5.79	dC
J081807.44+223427.5	17.15±0.01	15.56±0.01	15.09±0.01	14.89±0.02	46.63±2.70	−241.94±2.70	dC
J095005.05+584124.2	18.47±0.01	17.02±0.01	16.57±0.02	16.38±0.02	22.66±3.11	−97.64±3.11	dC
J095114.98+261207.5	21.24±0.04	19.35±0.02	18.80±0.02	18.50±0.03	−77.49±4.43	−79.51±4.43	dC
J100353.99+100807.2	18.50±0.02	17.13±0.02	16.66±0.02	16.42±0.03	−32.54±4.40	−113.36±4.40	dC
J105429.38+340225.0	18.59±0.02	17.19±0.02	16.78±0.02	16.60±0.02	−58.31±2.86	−116.22±2.86	dC
J111320.81+115234.9	20.38±0.03	18.81±0.02	18.34±0.02	18.11±0.03	−21.79±4.01	−112.77±4.01	dC
J111449.32+420252.9	19.52±0.02	18.09±0.02	17.60±0.01	17.38±0.02	−26.57±3.30	−101.59±3.30	dC
J114807.41+401008.9	19.91±0.02	18.17±0.02	17.64±0.01	17.41±0.02	−50.41±3.17	−101.35±3.17	dC
J115854.95+232234.6	21.35±0.05	19.51±0.03	18.94±0.04	18.72±0.04	19.13±4.45	−124.24±4.45	dC
J115929.27+640501.9	19.19±0.03	17.66±0.01	17.17±0.01	16.95±0.02	−98.94±3.17	−69.79±3.17	dC
J124358.58+183042.6	20.04±0.02	18.42±0.01	17.89±0.03	17.69±0.03	7.24±4.41	−133.08±4.41	dC
J130323.99+092543.6	19.24±0.02	17.64±0.01	17.15±0.02	16.96±0.02	−119.34±3.04	−3.44±3.04	dC
J133101.12+140613.1	21.14±0.04	19.30±0.02	18.81±0.02	18.66±0.04	4.83±5.49	−110.20±5.49	dC
J140325.56+202827.1	18.75±0.02	17.33±0.02	16.85±0.02	16.65±0.03	−139.35±2.58	5.18±2.58	dC
J151542.93+520145.9	18.77±0.02	17.39±0.01	16.98±0.02	16.82±0.02	−132.57±3.10	−15.71±3.10	dC
J154809.21+322724.9	18.08±0.01	16.51±0.01	15.99±0.01	15.72±0.02	−136.65±2.62	50.23±2.62	dC
J155237.29+292758.5	17.07±0.01	15.56±0.01	15.08±0.02	14.92±0.02	−218.51±2.45	−192.91±2.45	dC
J172843.18+270829.1	18.24±0.01	16.75±0.01	16.26±0.01	16.08±0.01	34.18±2.94	−113.35±2.94	dC
J223250.79−003437.0	21.07±0.04	19.39±0.02	18.79±0.02	18.45±0.03	4.03±3.32	−188.01±3.32	dC

[a] The sdC represents carbon subdwarfs, dC represents carbon dwarfs, dCf represents subdwarfs with weak carbon features.

Table A2. Nine common proper motion pairs of ultracool dwarfs.

Comp	SDSS Name	SDSS g	SDSS r	SDSS i	SDSS z	$\mu_{\rm RA}$(mas/yr)	$\mu_{\rm Dec}$(mas/yr)	Sep($'$)	SpT
01A	J042604.36+170714.3	16.52±0.03	14.99±0.02	13.33±0.00	12.41±0.02	109.24±2.52	−30.43±2.52	329.08	M5
01B	J042619.09+170301.9	19.23±0.02	17.64±0.03	15.66±0.02	14.56±0.02	101.69±2.83	−28.77±2.83		M6
02A	J120719.63+405349.9	16.80±0.01	15.39±0.02	14.38±0.02	13.86±0.02	−115.23±2.67	−2.43±2.67	13.98	
02B	J120718.57+405357.1	21.70±0.06	20.01±0.03	17.82±0.02	16.66±0.02	−122.59±4.91	3.76±4.91		M6
03A	J125945.65+195659.1	19.67±0.02	18.14±0.01	16.11±0.02	15.02±0.02	−480.80±3.15	151.47±3.15	39.93	M6
03B	J125948.18+195641.2	20.54±0.03	19.04±0.02	16.66±0.02	15.43±0.02	−477.93±4.44	156.55±4.44		
04A	J091244.25+560450.5	16.99±0.01	15.65±0.01	14.90±0.01	14.45±0.02	−53.74±2.82	−93.51±2.82	265.96	
04B	J091222.55+560136.3	22.19±0.09	20.76±0.04	18.62±0.03	17.53±0.02	−52.31±5.62	−88.92±5.62		M7
05A	J090215.19+033524.8	18.16±0.01	16.65±0.01	15.17±0.02	14.37±0.02	−107.63±2.95	160.27±2.95	165.29	
05B	J090226.21+033534.6	21.21±0.04	19.51±0.02	17.25±0.02	16.03±0.02	−110.16±4.97	162.28±4.97		M7
06A	J135208.56+502044.8	18.86±0.03	17.42±0.03	16.60±0.02	16.17±0.02	−23.34±3.14	−107.45±3.14	340.26	
06B	J135238.95+501748.7	20.69±0.02	19.06±0.02	16.82±0.01	15.61±0.02	−18.55±3.56	−99.93±3.56		M7
07A	J084909.03+560439.8	15.63±0.01	14.17±0.00	13.05±0.00	12.49±0.01	170.08±2.61	−73.97±2.61	90.51	
07B	J084918.85+560517.7	20.63±0.04	18.84±0.01	16.35±0.01	15.03±0.01	168.26±4.28	−74.28±4.28		M7.5
08A	J133619.15+615601.4	22.39±0.13	20.81±0.05	18.65±0.02	17.47±0.03	−35.93±5.61	−98.37±5.61	282.51	M6
08B	J133554.63+615944.7	23.60±0.32	21.98±0.11	19.39±0.02	18.00±0.03	−39.89±6.20	−105.94±6.20		M7.5
09A	J085147.11+413415.0	18.25±0.04	16.65±0.02	14.96±0.02	13.98±0.02	−113.94±2.88	18.69±2.88	32.66	
09B	J085148.19+413445.3	21.68±0.06	19.97±0.02	17.30±0.01	15.85±0.01	−109.39±4.96	18.78±4.96		M7.5